JAERI-M
86-125

REACTOR ENGINEERING DEPARTMENT ANNUAL REPORT

(April 1, 1985—March 31, 1986)

August 1986

Department of Reactor Engineering

日本原子力研究所
Japan Atomic Energy Research Institute

JAERI-Mレポートは、日本原子力研究所が不定期に公刊している研究報告書です。

入手の問合わせは、日本原子力研究所技術情報部情報資料課（〒319－11茨城県那珂郡東海村）あて、お申しこしください。なお、このほかに財団法人原子力弘済会資料センター（〒319-11茨城県那珂郡東海村日本原子力研究所内）で複写による実費頒布をおこなっております。

JAERI-M reports are issued irregularly.

Inquiries about availability of the reports should be addressed to Information Division, Department of Technical Information, Japan Atomic Energy Research Institute, Tokai-mura, Naka-gun, Ibaraki-ken 319-11, Japan.

編集兼発行　日本原子力研究所
印　　刷　日立高速印刷株式会社

JAERI-M 86-125

Reactor Engineering Department Annual Report (April 1, 1985 - March 31, 1986)

Department of Reactor Engineering,
Tokai Research Establishment
Japan Atomic Energy Research Institute
Tokai-mura, Naka-gun, Ibaraki-ken

(Received July 30, 1986)

Research and development activities in the Department of Reactor Engineering in fiscal 1985 are described.

The work of the Department is closely related to development of multipurpose Very High Temperature Gas Cooled Reactor, High Conversion Light Water Reactor and Fusion Reactor, and development of Liquid Metal Fast Breeder Reactor carried out by Power Reactor and Nuclear Fuel Development Corporation. Contents of the report are achievements in fields such as nuclear data and group constants, theoretical method and code development, reactor physics experiment and analysis, fusion neutronics, shielding, reactor and nuclear instrumentation, reactor control and diagnosis, reactor decommissioning technology, and activities of the Committee on Reactor Physics.

Keywords: Reactor Engineering, Very High Temperature Gas Cooled Reactor, High Conversion Light Water Reactor, Fusion Reactor Neutronics, Liquid Metal Fast Breeder Reactor, Group Constant, Theoretical Method, Code, Integral Experiment, Analysis, Shielding, Nuclear Instrumentation, Reactor Control, Diagnosis

---

JAERI－M 86－125

昭和60年度原子炉工学部年報

日本原子力研究所東海研究所原子炉工学部

（1986年7月30日受理）

昭和60年度における原子炉工学部の研究活動状況をとりまとめた。原子炉工学部の研究は，多目的高温ガス冷却炉の開発，高転換軽水炉の開発，核融合炉の開発及び動燃事業団による液体金属冷却高速増殖炉の開発と密接に関連するものが多い。核データと群定数，炉理論とコード開発，炉物理実験と解析，核融合ニュートロニクス，遮蔽，原子炉計装，炉制御と異常診断，原子炉解体技術及び炉物理に関する研究委員会活動の各分野にわたり当該年度に得た多くの成果を述べる。

東海研究所：〒319-11　茨城県那珂郡東海村白方字白根２－４

原子炉工学部年報編集委員会

金子義彦（委員長），篠原慶邦（副委員長），中川正幸，大部　誠，秋濃藤義，片桐正樹，島崎　潤也，大野秋男，大山幸夫，伊勢武治，山下哲行

Contents

Foreword

In the present report is given the annual research activity of Department of Reactor Engineering, Japan Atomic Energy Research Institute, during the period of April 1985 - March 1986, i.e. the FY 1985. The research activity of the Department extends to a broad area of reactor physics, fusion reactor physics, shielding, reactor instrumentation and control.

Total number of people working in the Department at the end of period was 96 of which regular members totalled to 84. Expenditure during the period amounted to about 0.82 billion yen, excluding nuclear fuel cost and personnel expenses. In addition, a considerable amount of expenditure was covered under research contracts with outside organizations: Science and Technology Agency(STA) for reactor decommissioning technology and non-destructive measurement technology of transuranic elements, and Power Reactor and Nuclear Fuel Development Corporation(PNC) for fast reactor physics, shielding and instrumentation.

The research activities were conducted in 7 Laboratories:

Reactor System Laboratory,
Fast Reactor Physics Laboratory,
Thermal Reactor Physics Laboratory,
Reactor Instrumentation Laboratory,
Reactor Control Laboratory,
Shielding Laboratory, and
Fusion Reactor Physics Laboratory

under the support of Reactor Physics Facility Operation Division and the Committee on Reactor Physics. The Safeguards Technology Laboratory was transferred to the Department of Fuel Safety Research as of April 1st, 1985.

The major research and development projects related closely to research programs in the Department are:

(1) Development of multipurpose very high temperature gas-cooled reactor(VHTR),
(2) Engineering research of fusion reactor,
(3) Development of liquid metal fast breeder reactor(LMFBR).

As concerns the R and D of multipurpose VHTR, efforts were continued in the fields of reactor physics, reactor instrumentation and reactor control. The reconstruction work of the SHE has been completed and the initial critical experiment was successfully performed in May 1985 on a new core, the first core of the Very High Temperature Reactor Critical Assembly(VHTRC-1), with 4% enriched uranium fuel elements. The criticality prediction by the SRAC code

agreed very accurately with the experimental result. Hereafter the assembly plays a role for validating nuclear calculation methods on the VHTR. The irradiation tests of fission counters and Pt-Mo thermo-couples have been carried out at the HFR(Petten, the Netherlands) and at the JMTR, respectively. They showed satisfactory results. In the study of reactor control, characteristics on load-following of the VHTR was investigated.

Concerning the fusion reactor physics, a set of neutronic benchmark data was expectedly obtained by the first stage FNS experiments under the collaboration research program between JAERI and US-DOE. The program has provided important experimental data for validating calculation methods of fusion blanket design. The second stage experiments will follow in the FY 1986.

As for the R and D of LMFBR, a series of experiments for three years has been completed using FCA on a model of an axially heterogeneous fast reactor. The measured items were reaction rate ratios, sample worth, control rod worth as well as power distributions. The obtained results are useful to extend understanding on the characteristics of a zoned core.

A new research activity on a high conversion light water reactor(HCLWR) has started in this fiscal year. The purpose of the research program is to investigate and to establish a possibility of the reactor concept as an advanced light water reactor for the next generation. Work at the initial stage includes a parametric survey of nuclear characteristics of tight lattices, preparation for FCA experiment and a survey of European research activities. The R and D activity on HCLWR looks expanding in following years.

In the R and D project for decommissioning nuclear reactor, most of all developments are approaching their final stages. Completed equipments are a prototype system for on-site non-destructive measurement of radio-activity in reactor pipe line and a light duty robot system. Their capabilities will be confirmed in the demonstration program of the next year.

In addition to the above mentioned activities, several significant achievements have been made. Examples are the development of a new radiation resistant optical fiber, successful start of in-site test of an in-vessel water level gauge for LWR, proposal of benchmark problem for radiation shielding of spent fuel cask, completion of a evaluated nuclear data storage and retrieval system, EDFSRS, and completion of all unit codes of the BERMUDA code system for shielding calculation.

Shojiro MATSUURA, Director
Department of Reactor Engineering

1. Nuclear Data and Group Constants

Continuous efforts have been devoted to development and improvement of the computer codes for use in reactor calculations. A nuclear data library production code system was developed for continuous energy Monte Carlo codes, such as the VIM code. This code system consisting of four main steps can treat the whole energy range of interest. Moreover, the group constant processing system PROF-GROUCH-G/B was furnished with a newly developed module to process the FILE 6 format of ENBF/B-V type. In addition, a computer aided tool, CATEX, for the evaluaters of neutron cross sections using sensitivity data in fast reactors has been improved to enhance its functions for practical use.

As concerns the group constant generation work, a validation study has been made for a cross section set based on the Joint Evaluated File (JEF-1) in order to assess its applicability to fast reactor analysis and it has been compared with that using the JENDL-2 for a series of benchmark problems. A new lumped group cross sections set, JFS-3-J2/FP2, for fission products (FPs) was produced using the JENDL-1 and ENDF/B-IV data for burn-up calculations of fast reactors.

Studies have been made on the effects of FPs on the characteristics of high conversion light water reactor (HCLWR). The burn-up reactivity loss was shown to be significantly reduced in HCLWR, when the resonance self-shielding of FPs is taken into account. Nuclear data of each FP nuclide were compared among four existing evaluated nuclear data files and shown to be largely scattered. The resulting discrepancies among burn-up reactivity changes in HCLWR were ,however, shown to be very small due to an accidental cancellation among FP nuclide data in each data file.

(Y. Ishiguro)

1.1 Development of Nuclear Data Library Production Code System for Continuous Energy Monte Carlo Codes

T. Mori and K. Kaneko*

Continuous effort has been devoted to the development of a code system to generate a nuclear data library for continuous energy Monte Carlo codes by processing the evaluated nuclear data files such as JENDL and/or ENDF/B. This code system has been designed to produce a data library for a general purpose Monte Carlo code like the VIM code. A flow chart of the system is shown in Fig. 1.1.1. This system consists of the following four steps:

(1) calculation of point cross sections and preparation of probability tables for angular and energy distributions : LINEAR, RECENT, SIGMA1 and ACER-J,
(2) production of cross section probability tables in the unresolved resonance energy range : U3R-J,
(3) processing of thermal scattering data : THERM-J, and
(4) edit of the processed data into a cross section library for a specific Monte Carlo code : LIBMAKE.

In the steps (1)~(3), the system converts all of neutron transport data given in the evaluated nuclear data file into the data with a relevant form to continuous energy Monte Carlo calculation (point cross sections and probability tables) and stores them in a Master PDS file. The LIBMAKE code used in the step (4) can produce a library only for the VIM code[2] in the energy range from 1.0×10^{-5} to 2.0×10^{7} eV at the present stage. This code is under development for the other Monte Carlo codes.

The LINEAR, RECENT and SIGMA1 codes were adapted in JAERI by Hasegawa[1]. The first versions of the ACER-J, U3R-J and LIBMAKE codes were developed in 1984. In this fiscal year, development of the THERM-J code and improvements of constituent codes (ACER-J and U3R-J) have been performed. Development and improvement effors are summarized as follows:

Developement of THERM-J : The THERM-J code has been developed from the FLANGE-II code[3] to process the thermal inelastic scattering data ($S(\alpha,\beta)$) and the thermal elastic scattering data in the ENDF/B thermal library. At first, both data at a specified temperature are calculated by temperature interpolation. Then the elastic data are processed by the same method as used in the ACER-J code[4] into the cross sections and angular distribution tables. As for thermal inelastic data, energy transfer matrices are calculated for 73 fixed energy grids from 1.0×10^{-5} to 4.5 eV from the $S(\alpha,\beta)$ data. The angular distribution in each energy transfer is represented by the double P_1 method used in the VIM code[2].

Improvement of ACER-J : The procedures to construct common energy grids and to prepare angular distribution tables of secondary neutrons have been modified to reproduce the original data in the evaluated data with sufficient accuracy for criticality analysis.

---

* Japan Information Service Co.,Ltd., Tokyo

Improvement of U3R-J : Subroutine DOPCRS (Doppler broadening calculation by solving the heat transfer equation) is vectorized by using the cyclic-reduction method[5]. A function of processing the unresolved resonance data for a material with natural isotope abundance is added to the U3R-J code.

References

1) Hasegawa A. : private communication (1984).
Detailed descriptions of original versions of the codes are given in UCRL-50400, Vol.17 Part A-C by D.E. Cullen (1979).
2) Blomquist R.N., Lell R.M. and Gelbard E.M. : "A Review of the Theory and Application of Monte Carlo Methods," ORNL/RSIC-44 31 (1980).
3) Honeck H.C. and Finch D.R.: "FLANGE II (Version 71-1): A Code to Process Thermal Neutron Data from an ENDF/B Tape," DP-1278 (ENDF-152) (1971).
4) Mori T., Kaneko K. and Ishiguro Y.: "Development of Cross Section Library Preparation Code System for a Continuous Energy Monte Carlo Code," unpublished (1986).
5) Ishiguro M. et al.: "Parallel Computation for Solving the Tridiagonal Linear System of Equations," JAERI-M 9703 (1981).

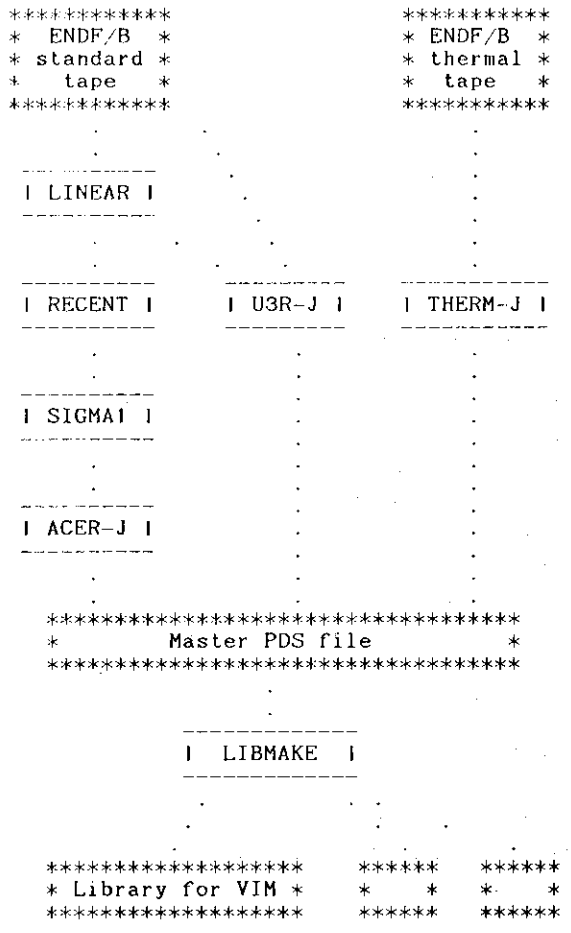

Fig. 1.1.1 Flow of nuclear data library production system

1.2 Comparison of Integral Tests on JENDL-2 and JEF-1 Nuclear Data Files

H.Takano

Applications of the Joint Evaluated File (JEF-1) to fast reactor analysis have been studied [1] for 20 fast critical assemblies and two infinite homogeneous media. The main discrepancies between the JENDL- 2 and JEF-1 for about twenty nuclides required for the fast reactor benchmarks are as follows:

(1) The U-235 data of JEF-1 were taken from the ENDF/B-V standard file and they differ in particular from the JENDL-2 data in the fission spectrum and cross sections.
(2) The Pu-239 data of JEF-1 contain newly evaluated information: the ν-value, the resonance and (n,2n) cross sections are different from the JENDL-2 data.
(3) The Cr, Fe and Ni structural material data of JEF-1 are taken from the KEDAK-3 file.

The group constants for U-235, Pu-239, Cr, Fe and Ni were calculated with the TIMS-PGG code [2] from the JEF-1 file. The group structure are based on the energy boundaries of the JFS-3-J2 set [3] . Benchmark calculations were performed by using both the JEF-1 group constants and JFS-3-J2 libraries.

The calculated results are shown in Figs. 1.2.1 - 1.2.4. In these figures, the different libraries are identified by the following symbols:

a) JFS-3-J2: 70 group constants library based on JENDL-2.
b) JEF1: The U-235, Pu-239, Cr, Fe and Ni data of JEF-1 are repaced in JFS-3-J2.
c) JEF1STR: The Cr, Fe and Ni data of JEF-1 are replaced in JFS-3-J2.

Figure 1.2.1 shows the comparison of the ratios of calculation to experiment (C/E) for k_{eff} as a function of core volumes. For large size cores, the JEF1 underpredicts k_{eff} , though the results of JEF1STR are similar to the ones of JFS-3-J2. However, remarkable discrepancies between JFS-3-J2 and JEF1 or JEF1STR are observed for the ZPR-3-54 assembly with the iron reflector. This difference may be caused by the discrepancy between data near 27 KeV resonance of iron. Figures 1.2.2 and 1.2.3 show the comparison of the reaction rate ratios of Pu-239 fission and U-238 capture to U-235 fission, respectively. The results for Pu-239(n,f)/U-235(n,f) obtained with JEF1 improve the underprediction observed for JFS-3-J2, though the results for JFS1STR are not so. For the U-238(n,γ)/ U-235(n,f) the results obtained with JEF1 are larger than the ones observed for JFS-3-J2.

Central sample worths(Δk/k) were calculated for many nuclides. The C/E -values for Cr and Fe obtained with JFS-3-J2 were closer to unity than those for JEF1 and JFS1STR, but these for Ni were not so as seen in Fig. 1.2.4.

References

1) Takano H. and Enrico S.:"Fast Reactor Benchmark Tests on the JEF-1 Evaluated Nuclear Data File,"JEF report 4 (1985).Unpublished report.
2) Takano H., Hasegawa A. and Kaneko K.:" TIMS-PGG : A Code System for Producing Group Constants in Fast Neutron Energy Region," JAERI-M 82-072 (1982).
3) Takano H. and Ishiguro Y.:"Production and Benchmark Tests of Fast Reactor Group Constants Set JFS-3-J2," JAERI-M 82-135 (1982).

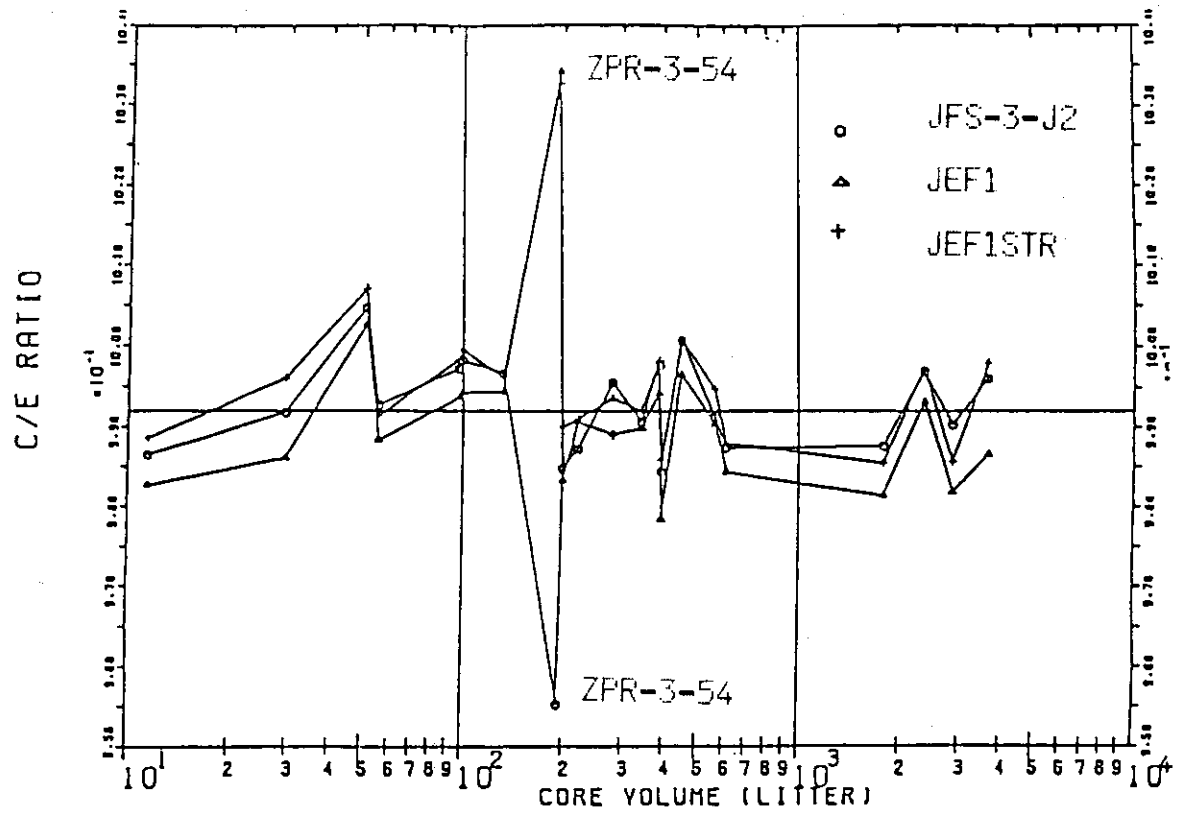

Fig.1.2.1 Comparison of Keff (C/E-values) calculated with JFS-3-J2, JEF1 and JEF1STR

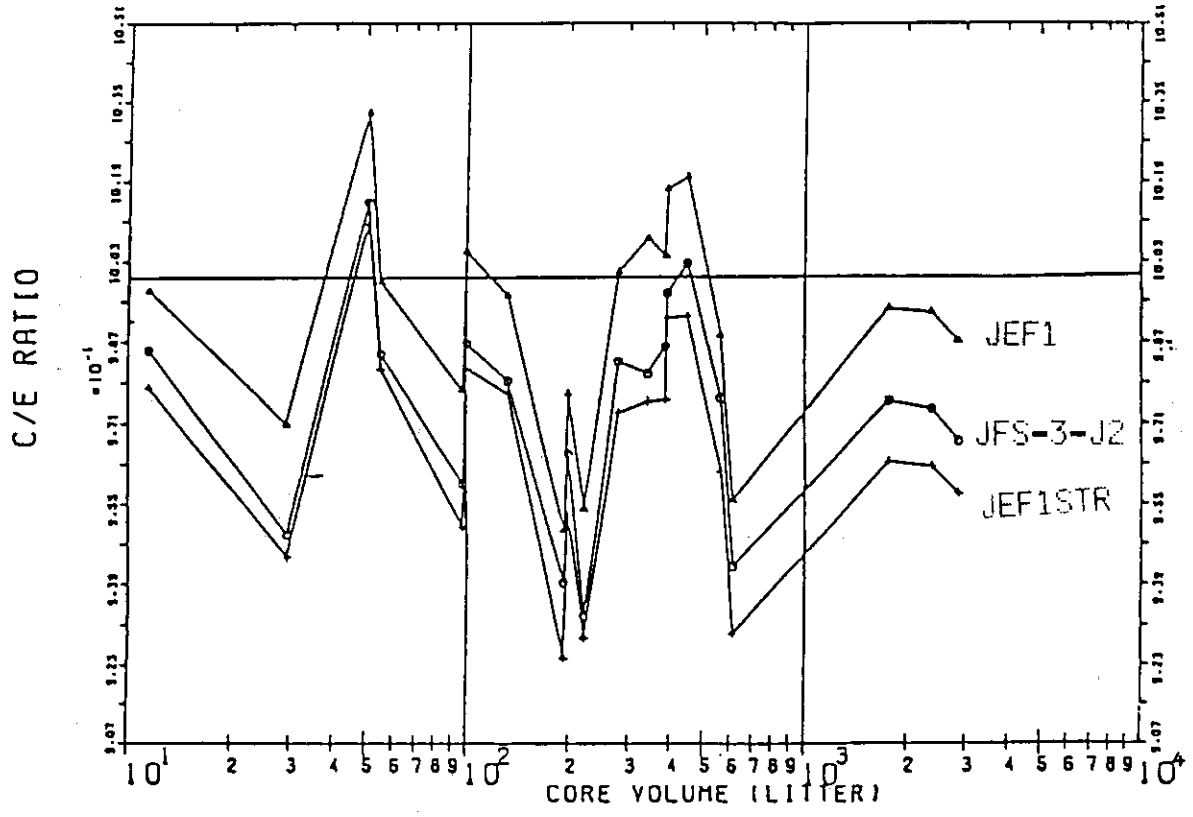

Fig.1.2.2 Comparison of central reaction rate ratios of Pu-239 fission to U-235 fission

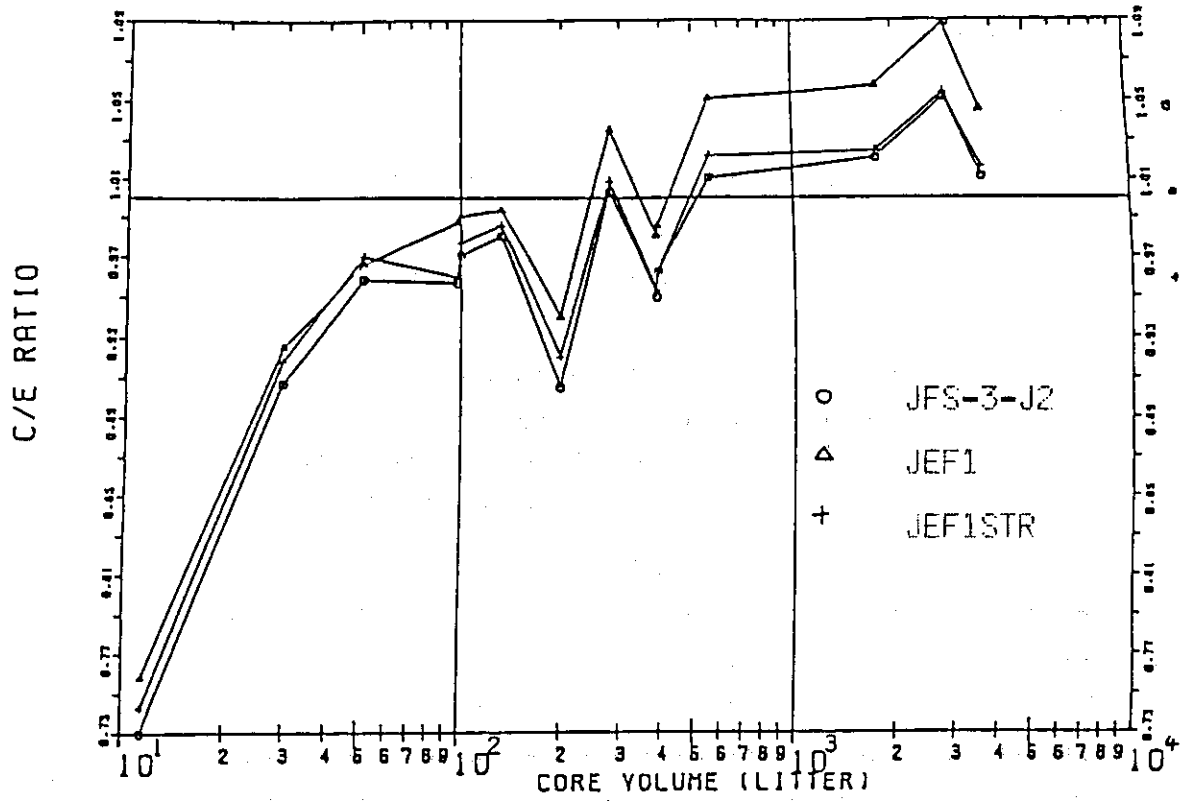

Fig.1.2.3 Comparison of central reaction rate ratios of U-238 capture to U-235 fission

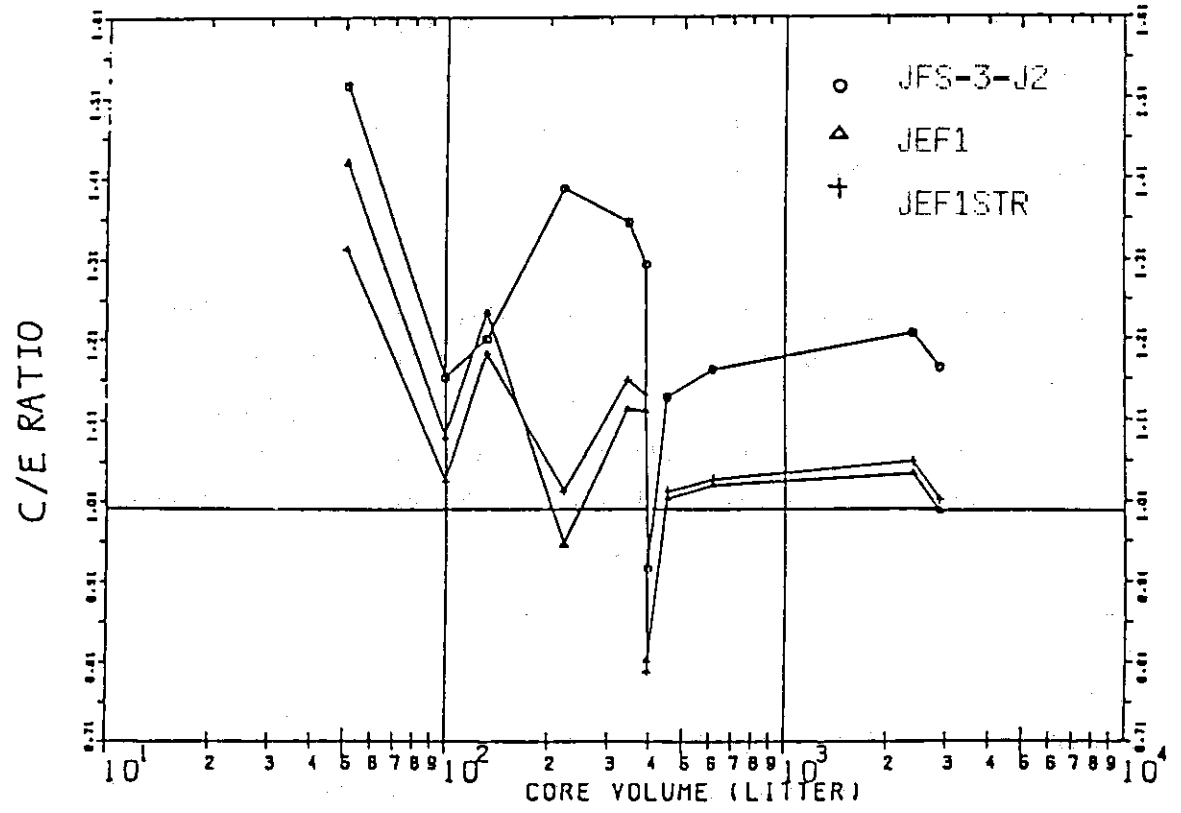

Fig.1.2.4 Comparison of central sample worths of nickel

1.3 Generation of Lumped Group Cross Sections of Fission Products : JFS-3-J2/FP2 Set

H. Takano and H. Ihara

Fission products have an important role in predicting burn-up characteristics of fast reactors. The JAERI-Fast Group Constant Sets JFS-2 and JFS-3-J2 include the lumped group cross sections [1),2)] for fission products based on the JENDL-1 and ENDF/B-IV data. The 100 fission product (FP) nuclides have been evaluated by the FP Working Group of Japanese Nuclear Data Committee and they have been adopted in the JENDL-2 file, recently. In this report, the lumped group cross sections are produced by using the FP data of JENDL-2 and ENDF/B-V.

To obtain the lumped group cross sections, group cross sections for each FP nuclide were required. They were calculated for the 100 and 55 nuclides of JENDL-2 and ENDF/B-V, respectively, with the MINX [3)] and TIMS-PGG [4)] codes. The energy structure was the 70-group one used in the JFS-3-J2 set[5)] .

Concentrations of the 155 nuclides are obtained by using the DCHAIN code[6)] which solves build up and decay chains for the 1170 nuclides. The summation of the fractional concentrations for the 155 nuclides is 99.95 percent to the total concentration at the burn-up time of 360 days. The DCHAIN code[6)] was modified so as to treat capture chains for the 155 nuclides with the 70-group capture cross sections. The calculations were performed on the basis of the following input parameters: the 70-group neutron spectrum obtained for a typical large fast reactor, constant flux of 3.5×10^{15} n/cm^2 /s and burn-up time of 30 - 1800 days (1.8 - 108 GWd/ton).

The lumped cross sections for capture, elastic scattering, inelastic scattering, (n,2n) and total reactions were generated corresponding to the fission products due to four mother nuclides of U-235, U-238, Pu-239 and Pu-241. These cross sections were calculated for the burn up time of 30, 60, 180, 360, 540, 720, 1080, 1440 and 1800 days.

The dependence of the lumped cross sections on burn-up was examined by calculating one group cross sections collapsed with the 70-group neutron spectrum. The burn-up time dependence of the one group cross sections calculated for the four mother nuclides are shown in Fig.1.3.1. The difference between the one group cross sections for

the burn-up of 400 and 1800 days is about 5 percent.

The burn-up time dependence of the one group cross sections calculated by taking account of various chain models are compared in Fig.1.3.2. The model $\sigma_c\varphi = 0$ shows the results calculated without considering capture chains for the 155 FP nuclides. This was the same model as th one used in Refs. (1) and (2). The one group capture cross sections obtained with this model increase with the burn-up time . The model (Xe=0) assumes that all the Xe gas are released at each burn-up stage. The model (Xe=0, Cs=0.5) assumes that all the Xe and the half of Cs gas are released at each burn-up stage. We can observe from this figure that accurate treatment for fission gas release should be considered for burn-up calculations.

References

1) Kikuchi Y., et al.:" Fission Product Fast Reactor Group Constant System of JNDC," JAERI 1248 (1976).
2) Takano H. and Sato W.:"Lumped Group Constants of Fission Products," JAERI-M 83-129, Reactor Engineering Department Annual Report, p15, (1983).
3) Weisbin C.R., et al.:" MINX, A Multigroup Interpretation of Nuclear X-sections from ENDF/B," LA-6486-MS (1976).
4) Takano H., Hasegawa A. and Kaneko K.:" TIMS-PGG : A Code System for Producing Group Constants in Fast Neutron Energy Region," JAERI-M 82-072 (1982).
5) Takano H. and Ishiguro Y.:"Production and Benchmark Tests of Fast Reactor Group Constants Set JFS-3-J2," JAERI-M 82-135 (1982).
6) Tasaka K.:" DCHAIN Code for Analysis of Build-up and Decay of Nuclides," JAERI 1250 (1977).

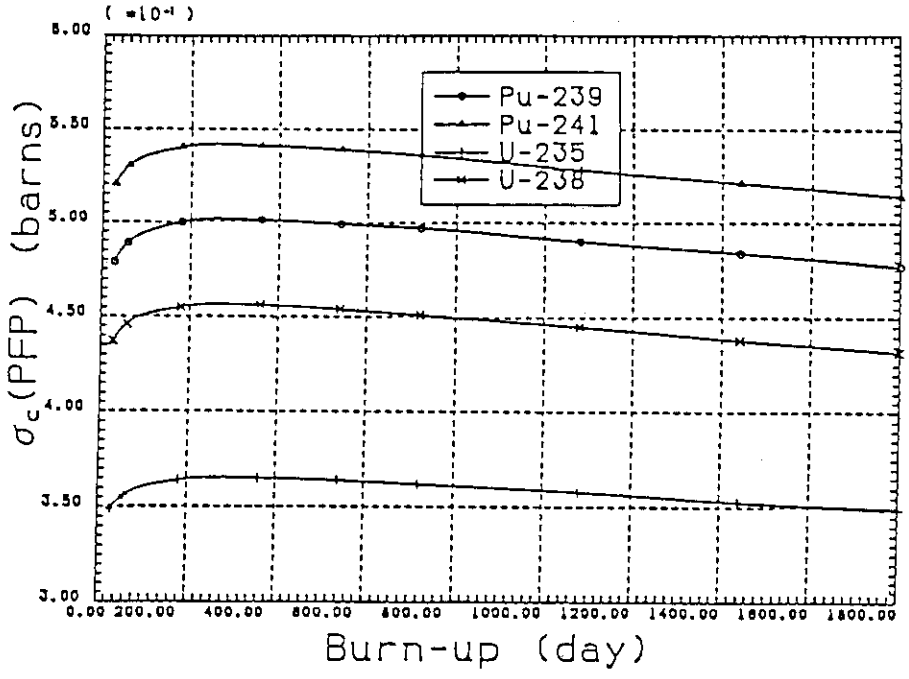

Fig.1.3.1 Burn-up time dependence of one-group capture cross sections

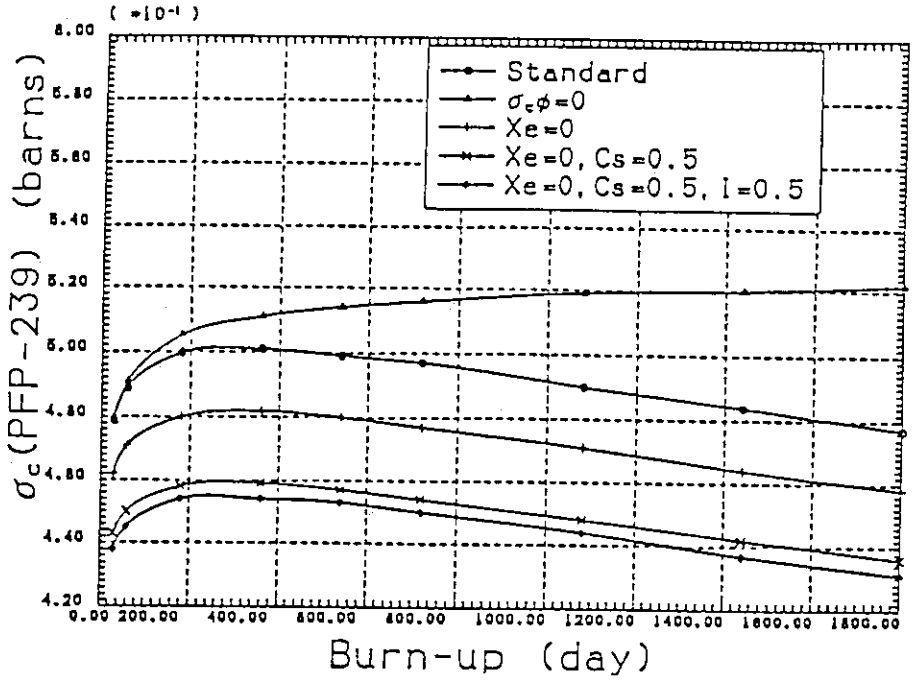

Fig.1.3.2 Comparison of burn-up dependence of one-group capture cross sections calculated with different chain models

1.4 Development of Processing Module for File 6: Energy-Angular Distribution Data of ENDF/B-V Format

A.Hasegawa

In the evaluated nuclear data files JENDL-2, -3 PR1 and -3 PR2 [1,2,3], the data representation in the FILE 6 format(energy- angular correlated distributions for secondary neutrons) of ENDF/B-V type [4] is activated for the first time in the world. Up to the release of JENDL-2 this FILE6 format had been discouraged and the code had few capability of processing.

Instead of the adoption of FILE 6, almost all nuclear data files in the world adopt the cross product representation using FILE4(angular distributions) and FILE5(energy distributions). But it is not possible to provide accurate representation by this way when trying to give a description of secondary neutrons resulting from certain neutron reactions with fairly light nuclei. Especially for the reactions with many body break-up process of light nuclei, such as Li-6 (n,2n), the File 6 representation is recommended for use.

Available data given in FILE 6 : energy-angular distributions in the evaluated data files in the world are shown in the Table 1.4.1. There are few obtainable data. But the nuclides listed in the table are very important for fusion neutronics.

As expressed previously, the FILE 6 format has the potential advantage over the combined FILEs 4 and 5. In order to use this more accurate FILE 6 data given in the JENDL files, we developed a processing module for this format. The module is written as a part of the group constants processing system : PROF-GROUCH-G/B code [5] so as to apply the processed data to either of the conventional Sn or BERMUDA codes (the direct integration method) [6] .

The FILE 6 in ENDF/B-V format is represented as follows: The secondary neutron energy-angle distributions are expressed as normalized probability distributions, $p(E \rightarrow E', \mu)$.

$$\int_0^{E'_{max}} dE' \int_{-1}^{+1} p(E \rightarrow E', \mu) d\mu = 1.$$

The differential cross section (barns/steradian/ev) is given by

$$\frac{d^2\sigma(E \rightarrow E', \mu)}{d\Omega dE'} = \frac{\sigma(E)}{2\pi} m \cdot p(E \rightarrow E', \mu).$$

The data are represented by one of the followings.

(1) LTT=1 : Legendre polynomial expansion

In this type, the probability distribution is expressed as a Legendre polynomial expansion. The lowest term of the expansion should be given explicitly.

$$p(E\rightarrow E',\mu)=\sum_{l=0}^{NL}\frac{2l+1}{2}\ a_l(E\rightarrow E')P_l(\mu).$$

$$\int a_0(E\rightarrow E')dE'=1.0.$$

(2) LTT=2 : the data are given as tabulation.

Secondary energy distributions are tabulated at a set of secondary angles and a set of incident neutron energies, i.e., at each anglular point, the probability distribution p(E-->E',μ) are given as energy distributions of FILE 5.

In a newly written module, both of the above described data can be processed. The processing flow is shown in Fig.1.4.1. The newly developed module is introduced to the PROF GROUCH-G/B code. The system is fully used in the production run stage for the preparation of the group cross-section library.

References

1) JAERI : "JENDL-2: Japanese Evaluated Nuclear Data Library, Version -2" (1983).
2) JAERI : "JENDL-3 PR1: Japanese Evaluated Nuclear Data Library, Version-3 preliminary 1" (1984).
3) JAERI : "JENDL-3 PR2: Japanese Evaluated Nuclear Data Library, Version-3 preliminary 2" (1985).
4) Kinsey R. (revised by) : "Data Formats and Procedures for the Evaluated Nuclear Data File," BNL-NCS-50496 (ENDF-102) (1975).
5) Hasegawa A., et al. : to be published.
6) Suzuki T., et al. : "BERMUDA-2DN : A Two-Dimensional Neutron Transport Code," JAERI-M 82-190 (1982)

Table 1.4.1 Available data given in FILE 6 : energy-angular distributions in the evaluated data files in the world

	Evaluated File	MAT	Z-A	MT	
1	ENDL-82	9003	1H2	16	(n,2n)
2	JENDL-2	2012	1H2	16	(n,2n)
3	JENDL-3 PR1	306	3Li6	16	(n,2n)
4	"	306	3Li6	91	(n,n')
5	"	307	3Li7	16	(n,2n)
6	"	307	3Li7	91	(n,n')
7	JENDL-3 PR2	306	3Li6	16	(n,2n)

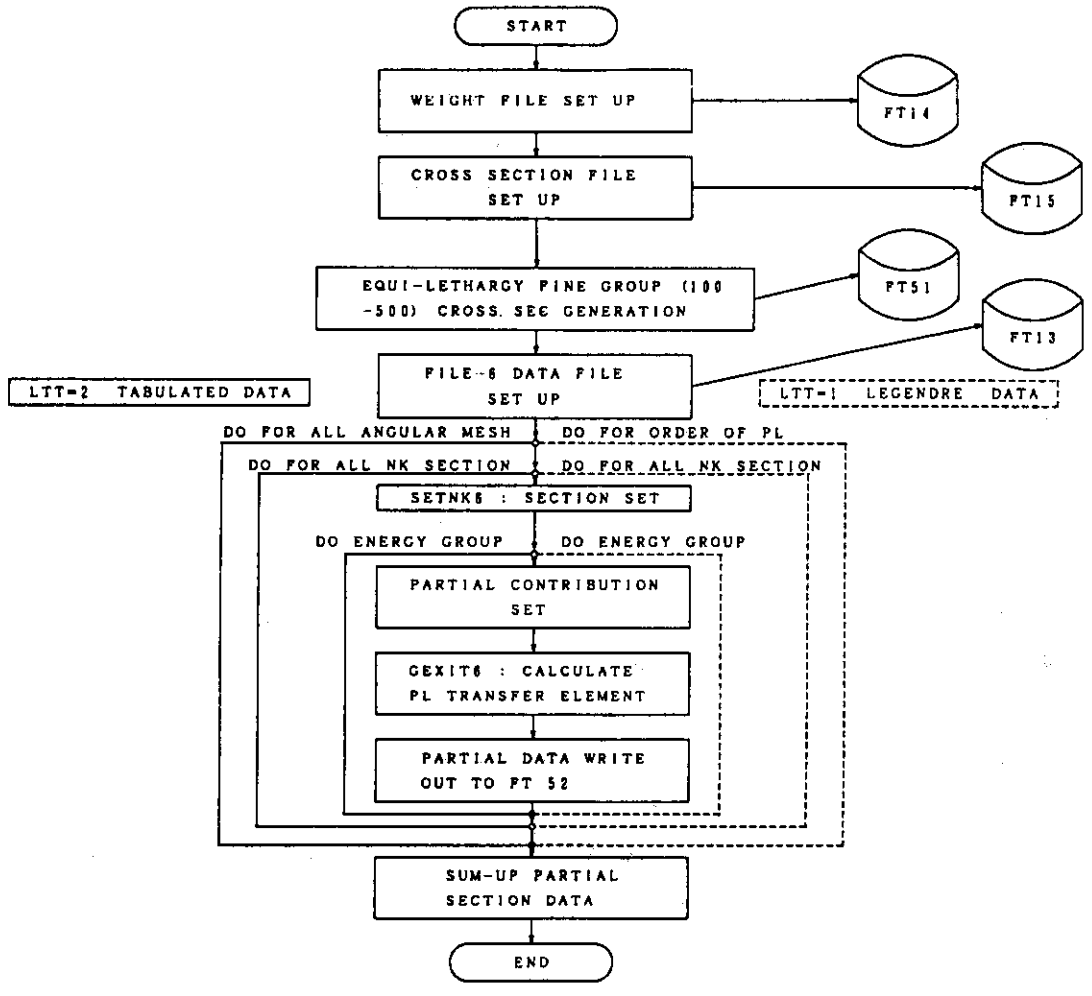

Fig. 1.4.1 Processing flow of FILE 6

1.5 Improvement of CATEX: A Computer Aided Tool for the Evaluators of Neutron Cross-Sections Using Sensitivity Data

A.Hasegawa and Y.Nakanishi *

The development of the first version of CATEX (a computer aided tool for the evaluators of neutron cross-sections) finished in 1984.[1] This system was intended for the evaluators of neutron cross-sections to supply the information about how newly evaluated nuclear data affect the calculational values of the integral quantities measured in reactor experiments in the FBR fields.

The system was opened to several users of the working group on Integral Test for JENDL of JNDC. Request for the possibility of direct calculation of the changes in the integral quantities due to the cross-section corrections was raised from the experience. To meet the request, some improvements have been made and the system is now re-opened to the users as CATEX-II.

In the first version the sensitivity profiles calculated by the SAGEP code [2] , which was based on the generalized perturbation theory using two dimensional diffusion model in 16 energy groups, were used to give the information. [3] However, the data loaded on the system were very limited to the numbers of adopted critical assemblies, integral quantities, nuclides and reactions.

We had some problems about the system. The first one was the change of the value in the integral quantities due to the change in the cross section value is calculated by the sensitivity profile on the system only whose sentivity profiles are given. Thus we could not get the value for some integral quantities originating from one reaction of some nuclide other than the loaded profiles. The second one was that we cannot obtain the information about the cross-effects emerging when the values of cross-sections of so many nuclides and reactions are considerably changed in a time, because the change of the value in the integral data reflects the change in the cross-section in a sense of perturbation in this system. The third one was the adopted cross-section representation in 16 group structure is not enough for users, especially for evaluators.

To overcome these situations we added a new function to the CATEX: Direct calculation of integral quantities due to the cross-section

---

* Nihon Software Kaihatsu Co.

correction can be carried out by updating the infinite cross-section part of the original 70 group JAERI-fast library , JFS-3 J-2 type. [4] The direct calculations are now performed by the EXPANDA- GENERAL(GS) and XPRTCS codes, in which a one-dimensional diffusion model is used.

By introducing this new function the first two problems can be resolved by using the direct calculation method. Thus the third one can be also solved by adopting the original 70 group library as input.

The change of the cross-section values in the original library is performed by the same way as that of the cross-section input panel of the CATEX system using full screen input terminals. Next the prefixed job of the direct calculation is submitted as the batch job. After the calculation the results are also displayed as the C/E (calculated to experimental value) values by this CATEX-II system.

Items of the FBR assemblies and integral quantities accepted as the objects for the direct calculation is shown in Tables 1.5.1 and 1.5.2. The nuclides and reactions able to be updated in the library for the direct calculations are summarized in Table 1.5.3 .

This work was performed according to the recommendation from the board of working group on Integral Test for JENDL of JNDC(Japanese Nuclear Data Committee).

References

1) Hasegawa A.:"Present Status of JNDC Sensitivity Analysis Code Systems,"Proceedings of the 1983 Seminar on Nuclear Data, JAERI-M 84-010 p 138- 147 (1984) (in Japanese). or JAERI-M 84-138 p 4- 7 (1984). Final report to be published.

2) Hara A., Takeda T. and Kikuchi Y.: "SAGEP: Two-Dimensional Sensitivity Analysis Code Based on General Perturbation Theory",JAERI-M 84 -027 (1984) (in Japanese).

3) Aoyama T., Suzuki T., Takeda T, Hasegawa A. and Kikuchi Y. : "Sensitivity Coefficients of Reactor Parameters in Fast Critical Assemblies and Uncertainty Analysis," JAERI-M 86-004 (1986) (in Japanese).

4) Takano H. and Ishiguro Y.:"Production and Benchmark Tests of Fast Reactor Group Constant Set JFS-3-J2," JAERI-M 82- 135 (1982).

Table 1.5.1 Items of FBR assemblies prepared for for the CATEX-II system

	Assembly	Fuel	Fer/Fiss	Vol(l)	Comments
1	VERA-11A	Pu	0.05	12.	Pu+C,No U in core
2	VERA-1B	U	0.07	30.	94% EU+C
3	ZPR-3-6F	U	1.1	50.	
4	ZEBRA-3	Pu	8.6	60.	Hard spectrum:80% E > 100keV
5	ZPR-3-12	U	3.8	100.	Soft spectrum. due to added C
6	SNEAK-7A	Pu	3.0	110.	
7	ZPR-3-11	U	7.5	140.	
8	ZPR-3-54	Pu	1.6	190.	Similar to 3-53 Fe reflector
9	ZPR-3-53	Pu	1.6	220.	U reflector
10	SNEAK-7B	Pu	7.0	310.	
11	ZPR-3-50	Pu	4.5	340.	(ZPR-3-48) with additional C
12	ZPR-3-48	Pu	4.5	410.	Soft spectrum due to added C
13	ZEBRA-2	U	6.2	430.	
14	ZPR-3-49	Pu	4.5	450.	(ZPR-3-48) without Na
15	ZPR-3-56B	Pu	4.6	610.	Ni reflector
16	ZPR-6-7(Ref)	Pu	6.5	3100.	L/D=0.9
17	ZPR-6-6A	U	5.0	4000.	L/D=0.8
18	ZPPR-2	Pu	5.1	2400.	L/D=0.5 2-zone equal vol.
19	MZA	Pu	3.9	570.	
20	MZB	Pu	5.2	1800.	
21	FCA-V-2	Pu+(U)	2.3	200.	Pu/EU=1/3

Table 1.5.2 Integral quantities prepared for the CATEX-II system

1. K-eff (effective multiplication factor) : All cores.
2. Reaction rate ratio: ALL cores.
   - F8/F5: U-238 fission/U-235 fission
   - F9/F5: Pu-239 fission/U-235 fission
   - F0/F5: Pu-240 fission/U-235 fission
   - C8/F5: U-238 capture/U-235 fission
   - C8/F9: U-238 capture/Pu-239 fission
3. Sample worth:

Table 1.5.3 Nuclides and reactions accepted as updatable in the CATEX-II system

No.	CODE	NUCLIDE	No.	CODE	NUCLIDE
1	105	B - 10	11	29	Cu
2	115	B - 11	12	42	Mo
3	6	C	13	924	U -234
4	8	O	14	925	U -235
5	11	Na	15	928	U -238
6	13	Al	16	949	Pu-239
7	24	Cr	17	940	Pu-240
8	25	Mn	18	941	Pu-241
9	26	Fe	19	14	Si
10	28	Ni	20	4	Be

Some other nuclides data are stored on the JFS-3-J2 type library. Only 20 nuclides described above can be treated as nuclides effective for benchmark calculation.

Note on reactions

1: Total 2: Nu 3: Fission 4:Capture 5:Elastic
7: Inelastic 8: N-2n 9: Elastic removal 10: Chi

1.6 Resonance Self-Shielding Effect of Fission Products on Burn-up Reactivity Loss in HCLWRs

H. Takano, K. Kaneko*, H. Akie and Y. Ishiguro

In high conversion light water reactors (HCLWRs), reactivity loss with burn-up is caused predominantly by fission product absorptions, with the relatively low consumption of fissile materials being of minor importance. Therefore, the fission product absorptions are very important for the burn-up calculations in HCLWRs. The fission product absorptions are calculated conventionally by using infinitely dilute capture cross sections without taking into account for resonance self-shielding effects, because atomic number densities of fission product nuclides are much less than those of fuel materials. However, a number of fission product nuclides have very large resonance capture cross sections in the intermediate neutron spectrum region where is important for HCLWR calculations. In the present work, the resonance self-shielding effect on the reactivity change with burn-up is studied for an undermoderated hexagonal fuel pin lattice: the diameter of fuel pin is 1.0 cm, the volume ratio of moderator to fuel regions is 0.8 and the enrichment of Pu fissile is 8.0 %.

The infinitely dilute cross sections and self-shielding factors for fission product nuclides were calculated with the TIMS-PGG code [1] using the evaluated nuclear data of JENDL-2. The lattice cell burn-up calculations were carried out by using the SRAC code [2]. The fission product chain model[3] which treats explicitly the 45 nuclides and one pseudo fission product was used in this calculations.

The dependence of the absorption fraction of fission products on burn-up was examined. Figure 1.6.1 shows the comparisons of the absorption fraction of Xe-131 and Cs-133 calculated with and without considering the self-shielding effects. It is observed from this figure that the absorption fraction is reduced significantly with burn-up by the self-shielding effect. On the other hand, the atomic number densities of Xe-131 increase with burn-up by considering the self-shielding effect as seen from Fig.1.6.2, because of the reduction of the effective capture rate.

The contribution of the individual fission product nuclide to the total reaction absorption rate is shown in Fig. 1.6.3, at the burn-up stage 50GWd/ton. It is observed from this figure that the self-shielding effects of Xe-131 and Cs-133 are remarkable in comparison with those of the other nuclides.

The dependence of the multiplication factors on burn-up is compared in Fig. 1.6.4. The reactivity loss by burn-up is reduced significantly by taking into account for the self-shielding effects of the fission products. The effect provides the difference of about 0.5 percent for the multiplication factor at the burn-up stage 50 GWd/ton. This difference is equivalent to the one of 10 % (5GWd/ton) in burn-up rate.

References

1) Takano H., Hasegawa A. and Kaneko K.: " TIMS-PGG : A Code System for Producing Group Constants in Fast Neutron Energy Region," JAERI-M 82-072 (1982).
2) Tsuchihashi K., et al.: " SRAC: JAERI Thermal Reactor Standard Code System for Reactor Design and Analysis," JAERI 1285 (1983).
3) Iijima S., et al.,: J.Nucl.Technol., Vol.19 (2), 96,(1982).

---

* Present address: Japan Information Service Co., Ltd., Tokyo

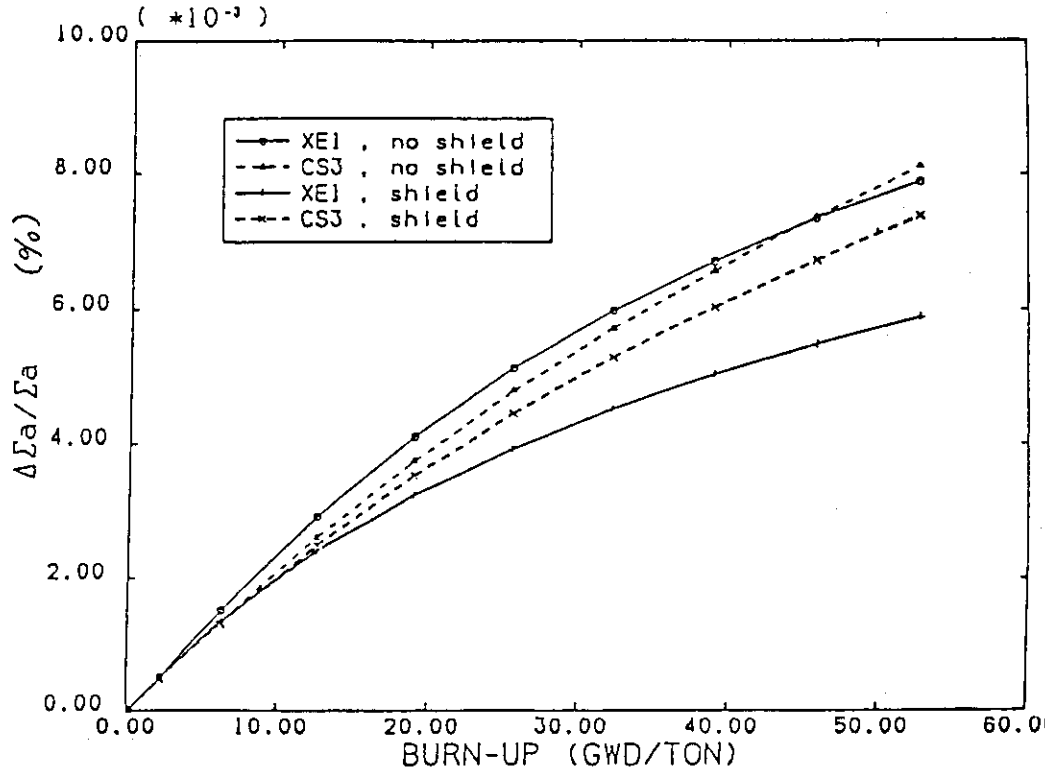

Fig.1.6.1 Dependence of absorption rate fraction on burn-up
$\Delta\Sigma_a$ is the absorption rate for each nuclide and Σ_a is the total absorption at the fuel region.

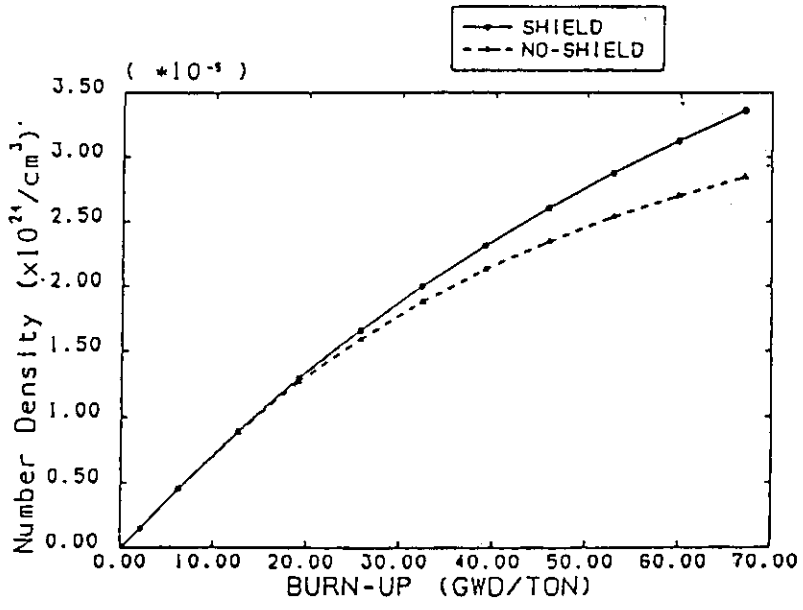

Fig.1.6.2 Dependence of atomic number density of Xe-131 on burn-up

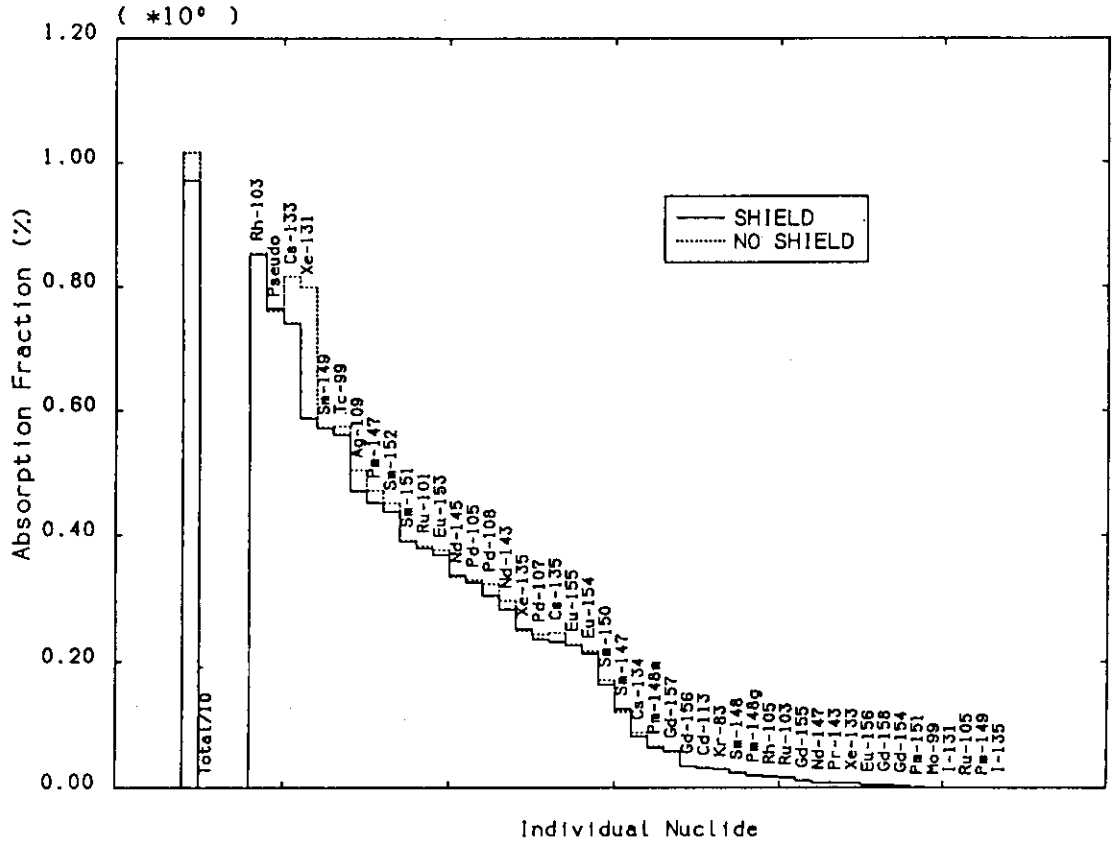

Fig.1.6.3 Contributions of the nuclides to the total absorption at 50 GWd/t.

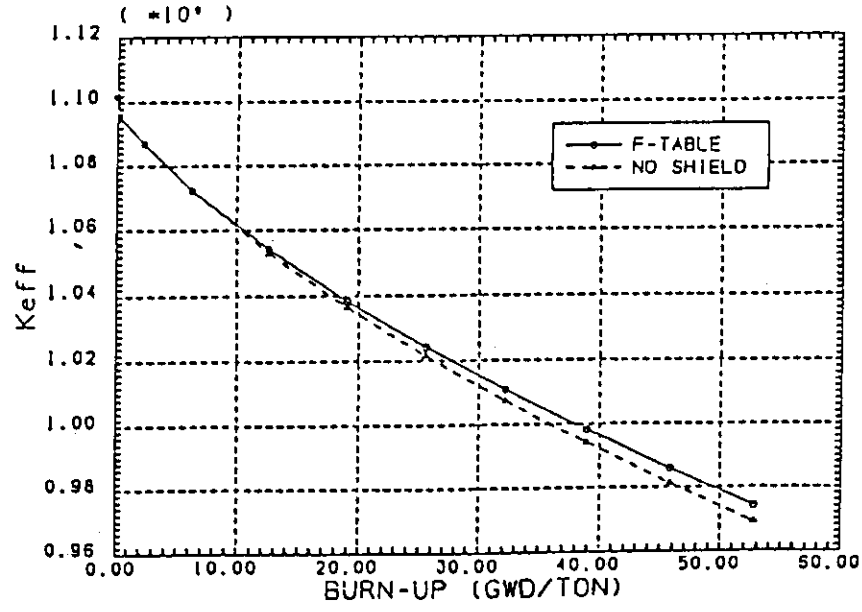

Fig.1.6.4 Comparison of reactivity changes due to burn-up

1.7 The Effect of Nuclear Data Uncertainty of Fission Product Nuclides on Burn-up Characteristics in HCLWRs

H. Takano, H. Akie and M. Nagatani*

Fission product absorptions play very important role for burn-up calculations in high conversion light water reactors (HCLWRs). Discrepancies between nuclear data of fission product nuclides are more remarkable than those for fuel materials. Table 1.7.1 shows the comparison of the primary data, the cross sections at 2200 m/s and resonance integrals for several fission product nuclides obtained from large evaluated nuclear data libraries, JENDL-2, JENDL-1, ENDF/B-V and JEF-1. Large discrepancies for these primary cross section data are observed from this table. Another example for the uncertainty of the fission product nuclides is resonance cross section data. As a typical example, the resonance cross sections for Pd-107 are compared for three evaluated files in Fig. 1.7.1. The resonance structure for Pd-107 is evaluated accurately in the JENDL-2 file.

In order to examine the effects of the nuclear data uncertainty for the fission products on burn-up reactivity change, cell burn-up calculations were performed with the SRAC code system [1] for a under-moderated hexagonal tight lattice: the diameter of fuel pin is 1.0 cm, the the volume ratio of the moderator to fuel region is 0.8 and the enrichment of Pu-fissile is 8.0 percent. The fission product chain model [2] which treats explicitly the 45 nuclides and one pseudo fission product was used in this calculations. The group constants for the 45 explicit nuclides were calculated with the TIMS-PGG code [3].

The fractional contributions of absorption rate of the individual fission product nuclide to the total one were calculated for the four evaluated files, JENDL-2, ENDF/B-IV, ENDF/B-V and JEF-1. They are compared with each other in Fig. 1.7.2. The differences between the absorption fractions are observed for several nuclides , in particular they are remarkable for Tc-99, Pd-107, Cs-133 and Ru-101.

The burn-up reactivity changes calculated for different evaluated files are shown in Fig.1.7.3. Significant discrepancy between the reactivity changes obtained with JENDL-2 and ENDF/B-V is observed. However, the discrepancies among those for JENDL-2, JEF-1 and ENDF/B-IV are small . This is due to an accidental cancelation as seen from Fig. 1.7.2.

References

1) Tsuchihashi K., et al.,:" SRAC: JAERI Thermal Reactor Standard Code System for Reactor Design and Analysis," JAERI 1285 (1983).
2) Iijima S., Yoshida T. and Yamamoto T.:" Fission Product Model for BWR Lattice Calculation Code," J. Nucl. Sci. Technol., Vol. 19 (2), 96, (1982).
3) Takano H., Hasegawa A. and Kaneko K.:" TIMS-PGG: A Code System for Producing Group Constants in Fast Neutron Energy Region," JAERI-M 82-072 (1982).

---

* Present address: I.S.L.,Inc.,Tokyo

Table 1.7.1 Comparison of thermal cross sections and resonance integrals (barns)

Nuclide		JENDL-2	JENDL-1	ENDF/B-V	JEF-1
Tc-99	2200m/s	19.8	17.7	19.5	19.0
	R.I	319.2	207.0	351.0	359.0
Ru-103	2200m/s	5.0		7.7	66.8
	R.I	92.0		70.0	595.0
Pd-107	2200m/s	1.9	10.0	10.0	1.9
	R.I	101.0	120.0	76.4	103.7
Pd-108	2200m/s	8.5		12.2	7.4
	R.I	252.4		226.0	188.0
Xe-131	2200m/s	85.0	88.0	90.1	85.5
	R.I	900.0	904.0	891.0	1015.0
Cs-133	2200m/s	29.0	29.0	29.6	29.0
	R.I	437.2	398.0	405.0	383.0
Nd-145	2200m/s	43.8	41.9	42.0	42.0
	R.I	204.0	268.0	233.0	233.0
Sm-152	2200m/s	206.0		207.0	206.0
	R.I	2766.0		3001.0	2982.0
Eu-155	2200m/s	4046.0	4040.0	4040.0	3647.0
	R.I	18840.0	3218.0	1857.0	2178.0
Gd-155	2200m/s	60890.0	61130.0	60930.0	61130.0
	R.I	1548.0	2589.0	1555.0	2589.0

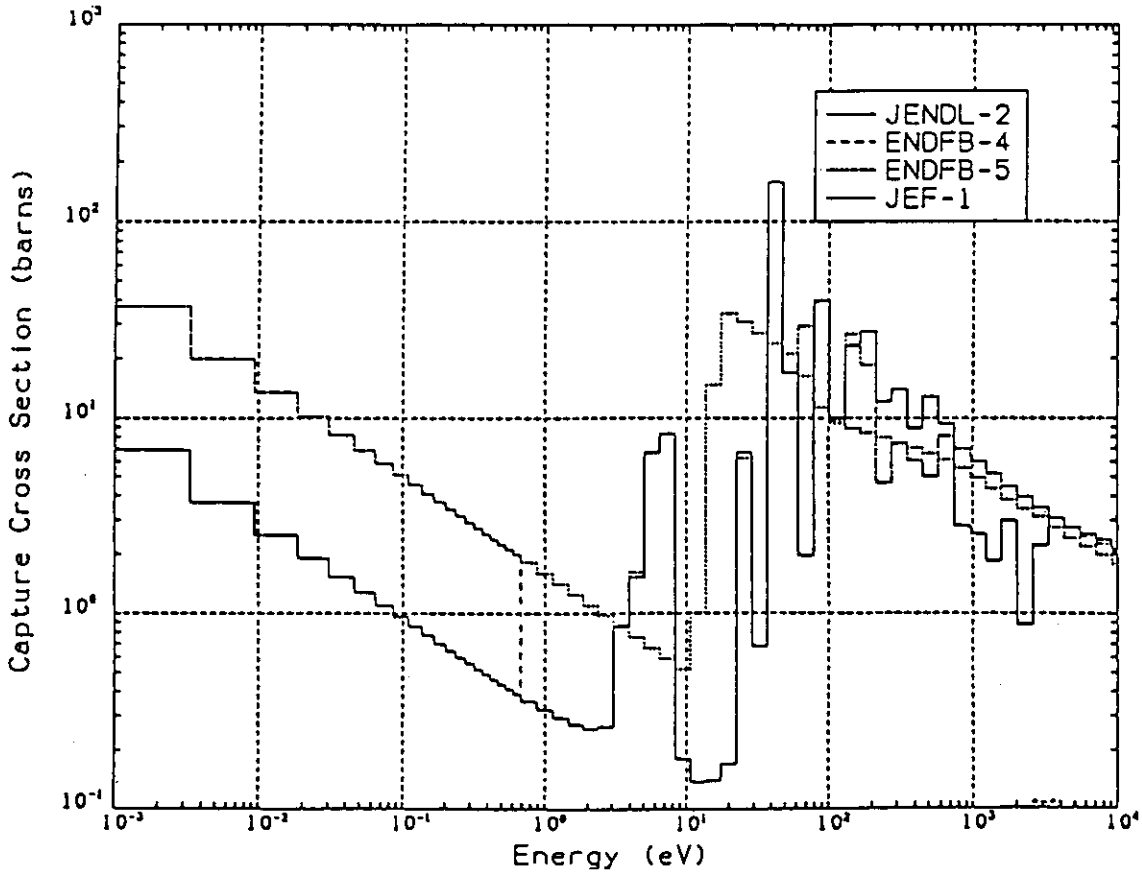

Fig. 1.7.1 Comparison of the capture cross sections of Pd-107

Fission Product Nuclides

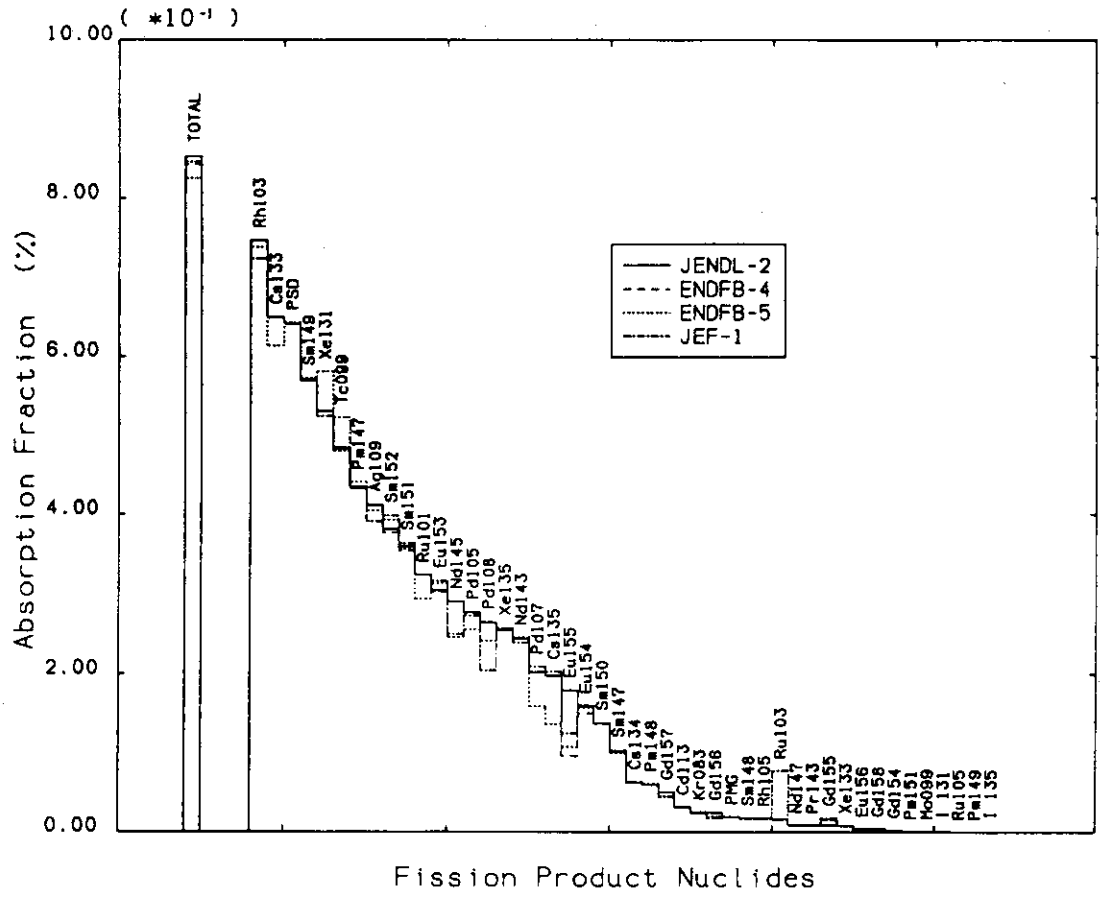

Fig.1.7.2 Contributions of individual nuclide to total absorption (42 GWd/t).

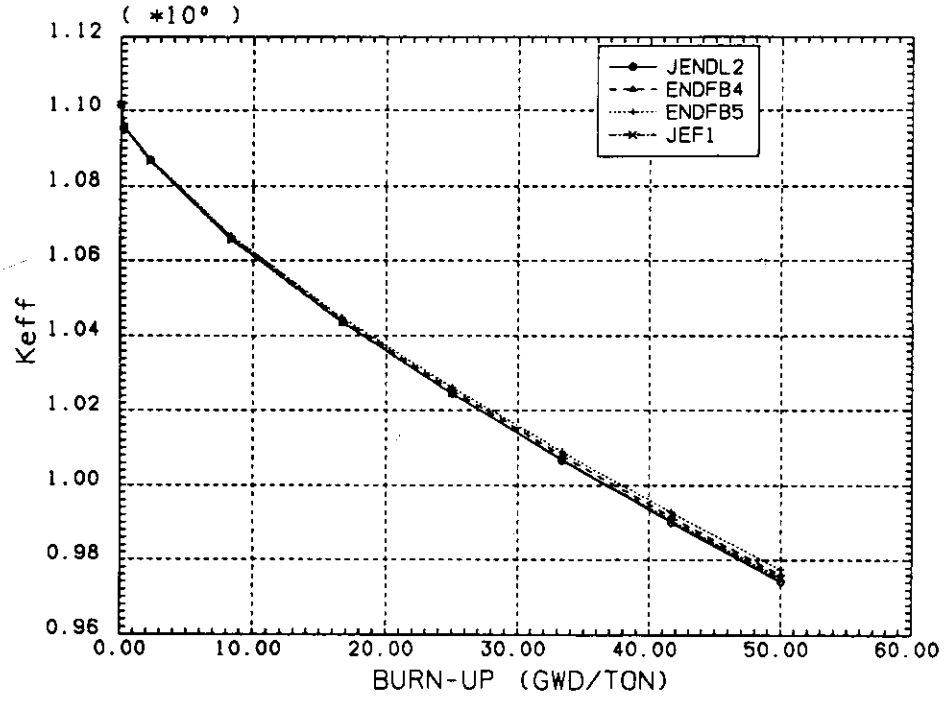

Fig.1.7.3 Comparison of reactivity changes due to burn-up

2. Theoretical Method and Code Development

As concerns the study of nuclear spallation reaction, the major portion of the effort is devoted to theoretical model, understanding of nuclear physical processes and improvement of analysis codes. The two step model proposed for the spallation reaction was improved to insert a preequilibrium decay step between the two steps. A preliminary analysis was made for the mass yield distribution of reaction products generated directly from proton spallation reaction to study target blanket characteristics of an accelerator driven breeder or transuranic waste transmuter. A study has been also made to obtain basic understanding of the transmutation of radioactive waste with various lifetime in the spallation process. A simulation code NUCLEUS has been developed to validate computational models for the nuclear spallation reaction. On the other hand, The Monte Carlo simulation code NMTC/JAERI was vectorized on FACOM VP-100 with a speed-up of about 1.5 times in computation time.

The development and improvement of computational codes continue to be carried out. The standard reactor analysis code (SRAC) system has been improved to extend its functions and to provide several new anxiliary codes. A three-dimensional neutron transport code DFEM based on the finite element method has been revised to apply two kinds of new angular bases; quadratic spline and piecewise constant function. The two-dimensional Sn transport code DOT was reconstructed so as to use the double differential form multigroup cross section (DDX) library. Furthermore, a simple thermo-hydraulic analysis code has been developed for parameter survey calculation of high conversion light water reactor (HCLWR) on a unit fuel cell base. A two-dimensional, time dependent diffusion code T2DK with delay neutrons has been extended to deal with the (R,Z) and(θ,R) geometries in addition to the original (X,Y) geometry.

The research on radiation damage using computer simulation has been performed in relation to the formation of an interstitial atom and to anisotropic threshold energies of atomic dispacement in a b.c.c. crystal. (Y.Ishiguro)

2.1 Monte Carlo Algorithm for Simulating Particle Emissions from Preequilibrium States during Nuclear Spallation Reactions

Y. Nakahara and T. Nishida

The spallation reaction has been treated usually as the two step process. The first step is the intra-nuclear cascades of nucleons initiated by an energetic incident particle. The second step is the competing decay of a residual nucleus in highly excited states by fissions and/or particle evaporations from the compound state. The spallation neutron spectra calculated by the two step model show remarkable underestimate in comparison with measured ones in the neutron energy range above 10 MeV.[1)]

In order to improve the computational accuracy we have generalized the two step model to a three step one. The preequilibrium decay step is inserted in between the two steps mentioned above, as shown in Fig. 2.1.1, since it is well known that neutrons emitted from the preequilibrium state have the spectra harder than those evaporated from the compound state. Investigations have been made on methods how to incorporate the preequilibrium decay process into the spallation simulation calculation and a Monte Carlo algorithm has been developed on the basis of the Griffin's exciton model for particle emissions from the preequilibrium state[2)].

In the exciton model an excited state of a nucleus is defined by numbers p and h of excited particle and hole degrees of freedom, respectively, above and below the Fermi surface. The sum n=p+h is referred to as the exciton number. Our problem is how to define the values of p and h at the end of the intra-nuclear cascades and at the transition from the preequilibrium state to the compound state.

In the simulation of intra-nuclear cascades a

Monte Carlo history of a nucleon participating in the cascade is no longer traced when its energy has fallen below a certain cutoff energy, which is taken to be one-half of the Coulomb potential energy at the surface of nucleus. Nucleons whose histories have been terminated have wave lengths too long for subsequent reactions to be treated as two body collisions. Their energies are, however, still well above the Fermi surface and contribute to the excitation of the residual nucleus. Considering these situations, we make a following proposal. The value of p at the end of the intra-nuclear cascades can be considered to be equal to the number of nucleons whose histories have been terminated during the cascades. The corresponding value of h can be assumed to be given by the relation $h=p-1$[3].

We have derived explicit expressions of probabilities for emissions of six kinds of particles, i.e., n, p, d, t, He-3 and He-4, from the given exciton state(p,h,E), where E is the excitation energy. Detailed descriptions are given in a forthcoming JAERI-M report.

As for the transition condition from the preequilibrium state to the compound state, we use an exciton number which can be defined as follows. In a picture of exciton representation of nuclear states, the number of excitons increases stepwise with $\Delta n=2$ as the internal transitions continue and the compound state is considered to be the one with infinite number of excitons, i.e., the continuum state. When n has become sufficiently large, larger than some n', the conventional evaporation model can be used instead of the preequilibrium model. For n' we can use the approximate expression derived by Gudima et al. from a condition of balance between the plus and minus internal transitions[4].

Programming of our Monte Carlo algorithm is to be performed in the fiscal year 1986.

References:

1) Tsukada T., Nakahara,Y.: Atomkernenergie Kerntech., 44,186(1984).
2) Griffin J.J.:Phys. Rev. Lett., 17,478(1966).
3) Kalbach C.: "PRECO-D2:Program for Calculating Pre-equilibrium and Direct Reaction Double Differential Cross Sections," LA-10248-MS(1985).
4) Gudima K.K., Mashnik S.G.and Toneev,V.D.: Nucl. Phys., A401,186(1984).

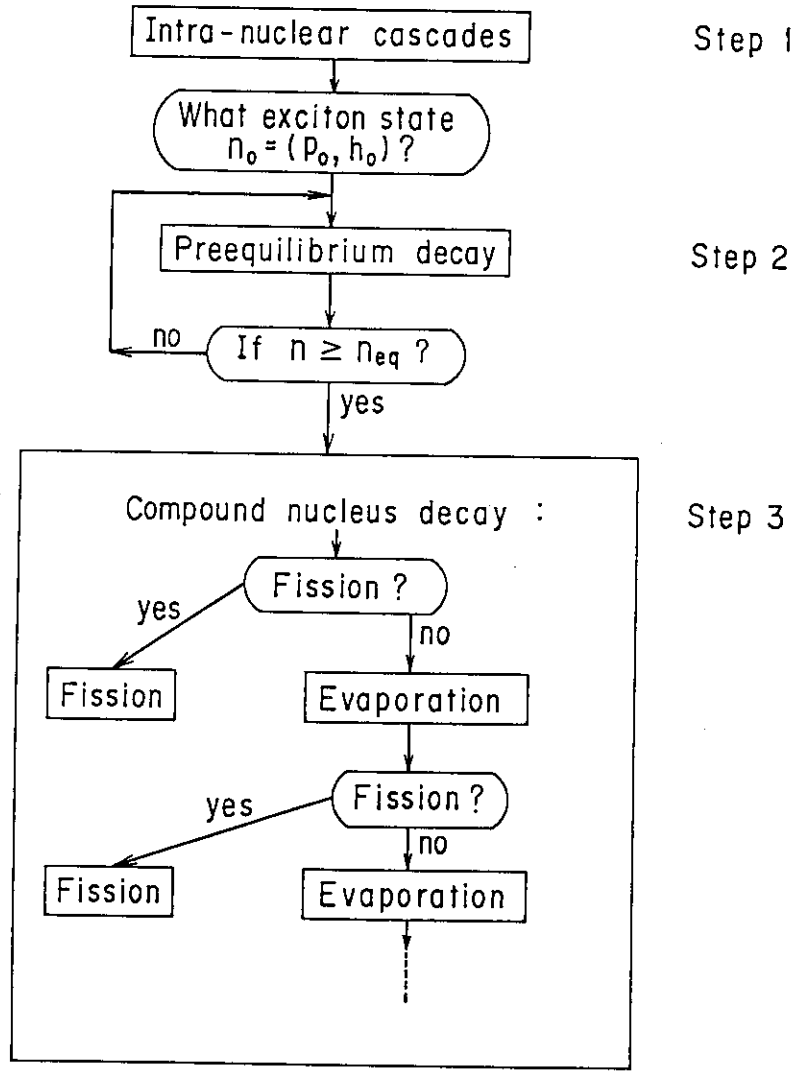

Fig.2.1.1 Scheme of the three step model

2.2 Analysis of Produced Nuclei and Emitted Particles in Nuclear Spallation Reactions

T. Nishida, Y. Nakahara and T. Tsutsui

Primary products generated from the proton spallation reaction of nucleus reflect details of nuclear physical processes essential for determining target-blanket characteristics of a accelerator fuel breeder or a transuranic waste transmuter. By "primary" we mean that internuclear cascades subsequent to the spallation are not taken into consideration in the present analysis.

In the preliminary study using the simulation code NUCLEUS [1], which has been developed at JAERI, we calculated all the residual nuclides and particles produced from a nucleus bombarded by protons with energies from 0.5 to 3.0 GeV. Figure 2.2.1 (a) shows the mass yield distribution of residual nuclei for the incident proton energy of 500 MeV. The peak and the plateau seen in the heavier mass region correspond to intranuclear cascade and non-fission evaporation products, and the spires in the light mass region to evaporated α and ^3He + t. A relatively flat distribution between them is due to the high energy fission. As the proton energy increases from 0.5 GeV to 1 GeV, the hill of non-fission product yield (A = 180 - 240) transforms to a mild slope. These results show that the distribution ceases to change its form as proton energy increases over about 2 GeV. Table 2.2.1 summarizes the number of emitted particles per incident proton and nucleus . This shows that the maximum yield of primary neutrons from an uranium nucleus is about 17 at 2 GeV, while it decreases also slightly over 2 GeV probably because of an increase of nuclear transparency for incident protons. Therefore, we should expect larger neutron yield due to a subsequent internuclear cascade in a target.

Spallation product yields with mass A = 125 -140 are plotted for the proton energy of 1 GeV in order to compare our simulation resluts with measured data [2] in Fig. 2.2.2. Both product distributions are in better agreement on the neutron deficient side than on the neutron-excess side (N/Z > 1.5).

References

1) Nishida T., Nakahara Y. and Tsutsui T. : " Development of a Nuclear Spallation Reaction Simulation Code and Calculations of Primary

Spallation Products," (to be published as JAERI-M).
2) Friedlander et.al. : Phys. Rev., 129, 1089 (1963).

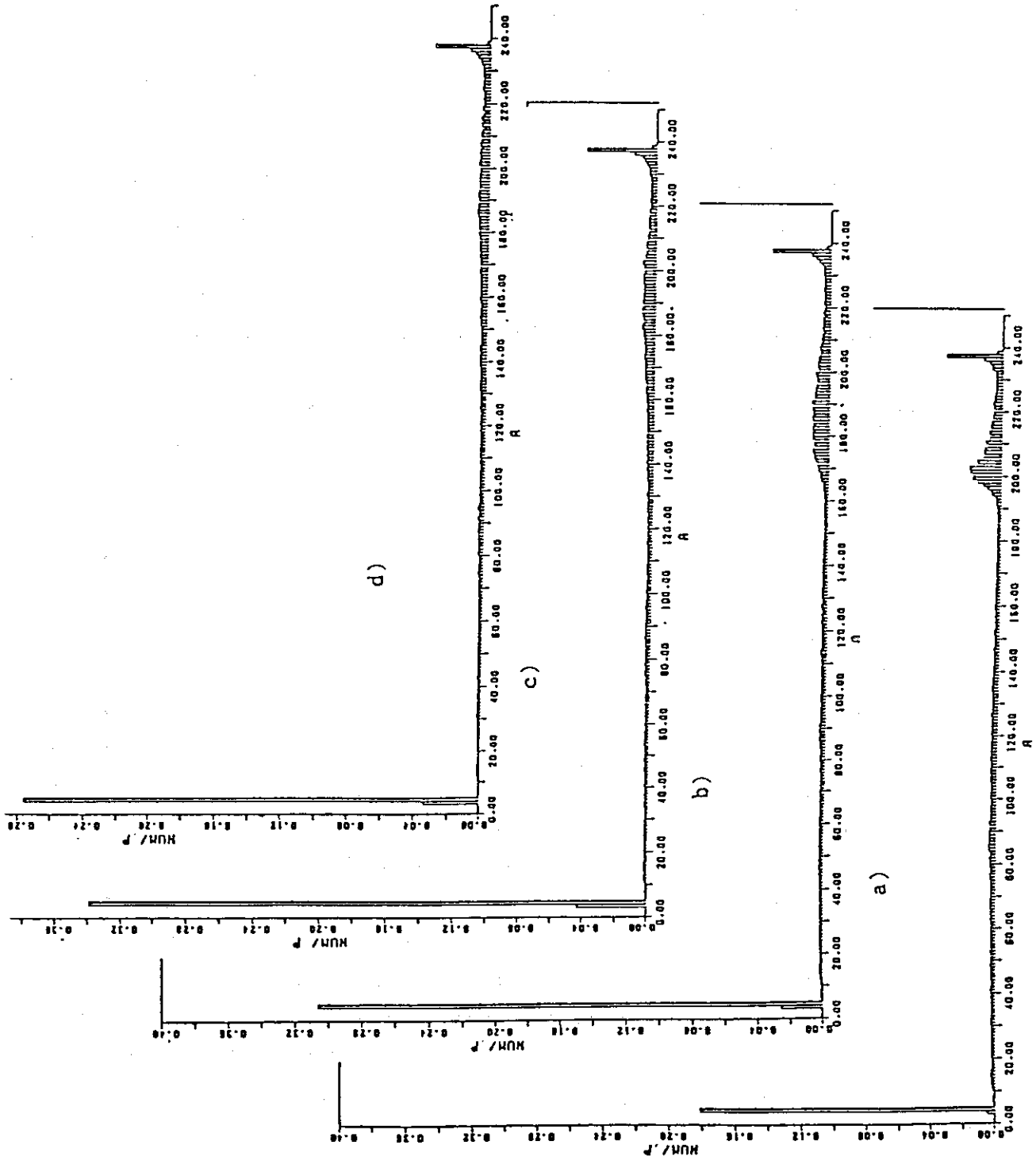

Fig. 2.2.1 Spallation product distributions (number of nuclei per incident proton) versus mass number A for an uranium nucleus. Proton energy is
(a) 0.5, (b) 1, (c) 2 and (d) 3 GeV.

Table 2.2.1 Particles emitted from an Uranium Nucleus

Energy of protons (MeV)	500	1000	2000	3000
Proton	1.612	3.126	3.750	3.228
Neutron	13.350	16.360	17.279	15.209
Deuteron	0.2678	0.7220	0.8740	0.7366
Triton	0.1076	0.2740	0.3226	0.2858
Helium 3	0.004	0.0242	0.0374	0.0298
Alpha	0.1576	0.2932	0.3014	0.2522
Emitted nucleons per Proton	16.463	22.998	25.063	21.800
Average mass number of non fission products	196	190	188	186

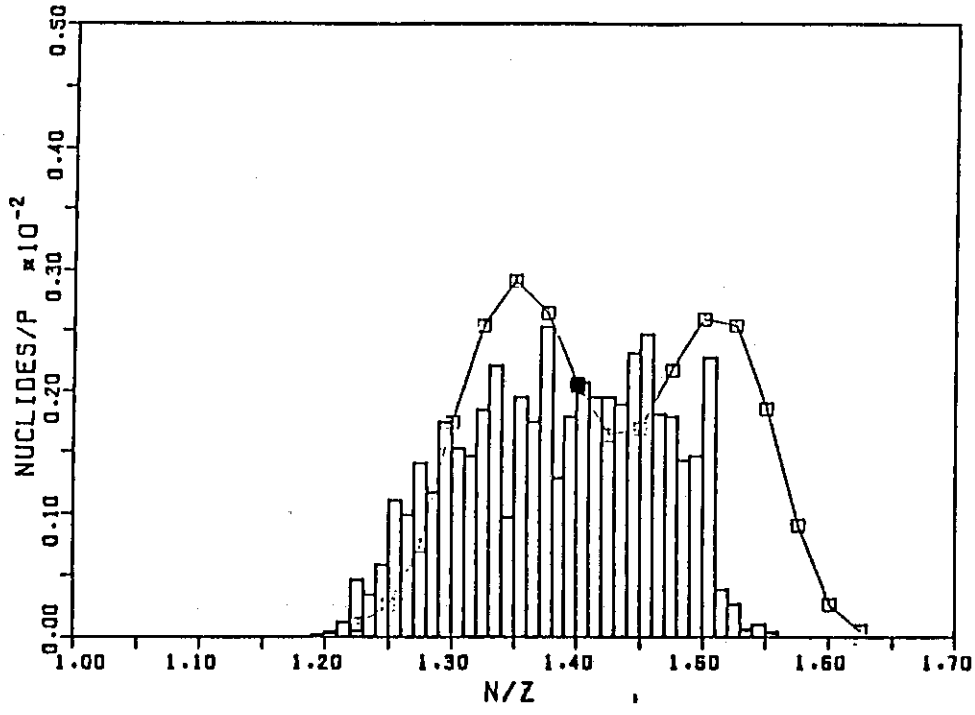

Fig. 2.2.2 Spallation products for A = 125 - 140 versus N/Z for a uranium nucleus bombarded by a 1 GeV proton
The curve shows the measured values from Friedlander et. al. and the blacked square at N/Z = 1.4 is for stable nuclides.

2.3 Analysis of Isotope Production in the Nuclear Spallation Reaction

T. Nishida, Y. Nakahara and T. Tsutsui

The present research has been made to obtain the basic knowledge concerning the transmutation of radioactive wastes with long lifetime, such as transuranic nuclides, to the ones with short lifetime or stable ones, using high enegry protons generated by a linear accelerator.

The computations by the new simulation code NUCLEUS [1] shows that after nuclear spallation reactions, a variety of nuclei, especially many neutron-deficient nuclides with nuclear charges nearly equal to the one of a target nucleus, are produced. In Fig. 2.3.1 mass distributions of isotope production in the nuclear spallation reaction by 1 GeV protons bombarding an uranium nucleus are shown for atomic numbers Z = 93 - 82. It is aparrent that the maximum in each distribution appears on the neutron deficient side on the A-axis except for Np, U (target nucleus) and Pa.

Heights of these maximum values alternate according to the even-oddness of the atomic numbers of products. Due to their short lifetime most of them will change to stable nuclides in due time.

Figure 2.3.2 shows isotope yields per incident proton and target nucleus versus N/Z for Sr, I, Cs and Eu, where the hatched, blacked and open rectangles denote stable nuclides and those with lifetime longer and shorter than 30 days, respectively. On the other hand, product yields on β decay chains leading to ^{90}Sr, ^{129}I, ^{137}Cs and ^{150}Eu are shown by blacked rectangles in Fig. 2.3.3. Most of them are produced mainly from the fission processes just after intranuclear cascades. These product yields are smaller by about an order of magnitude than those of non-fission products and the accumulations from the decay chains are seen also to be small. It is advantageous to the transuranic waste transmutation that the production of harmful FP nuclides such as ^{90}Sr is small.

Reference

1) Nishida T., Nakahara Y. and Tsutsui T. : " Development of a Nuclear Spallation Reaction Simulation Code and Calculations of Primary Spallation Products," (to be published as JAERI-M).

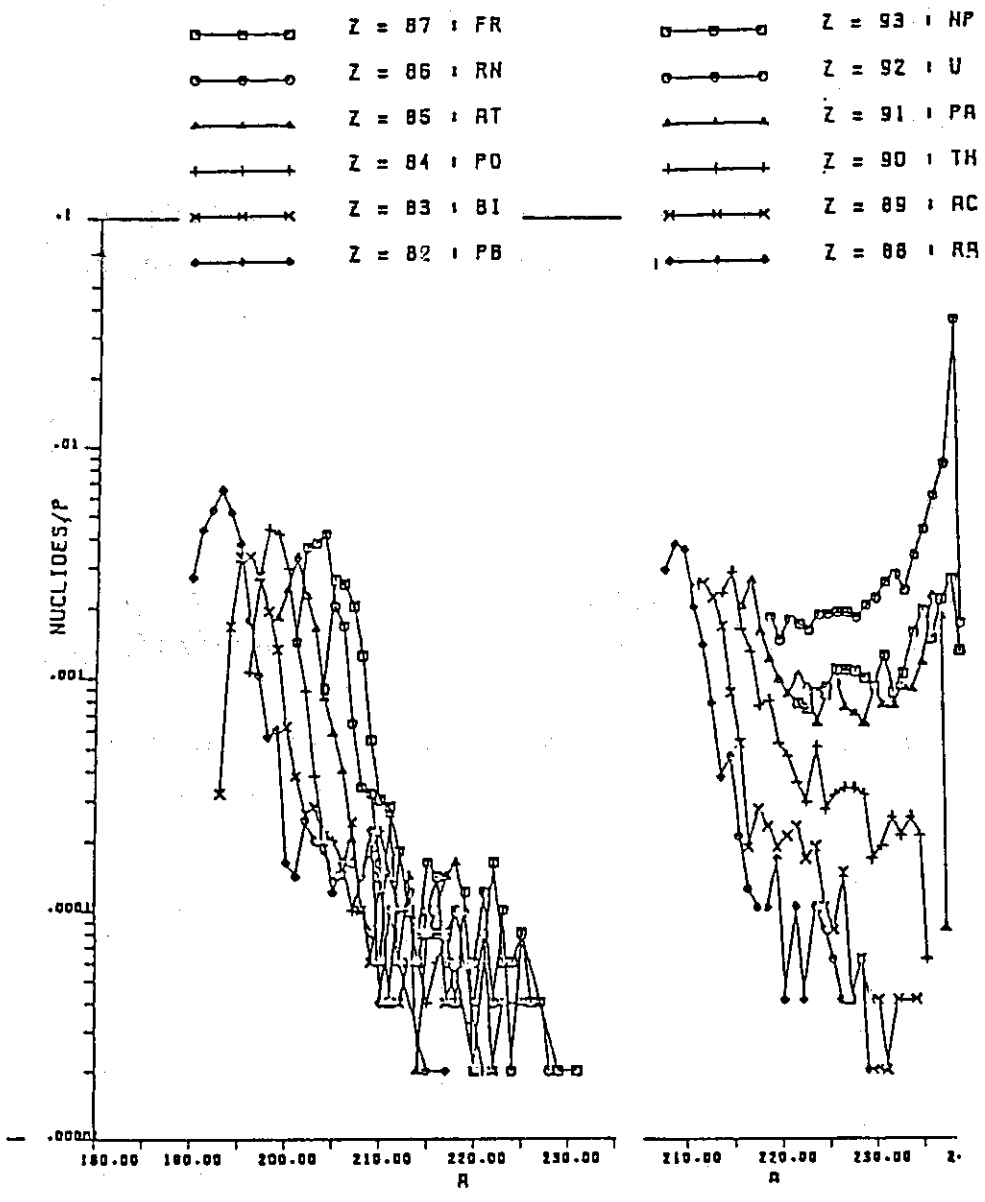

Fig. 2.3.1 Mass yield distributions of products with Z = 93 - 82 in the spallation nuclear reaction of an uranium nucleus with a 1 GeV proton

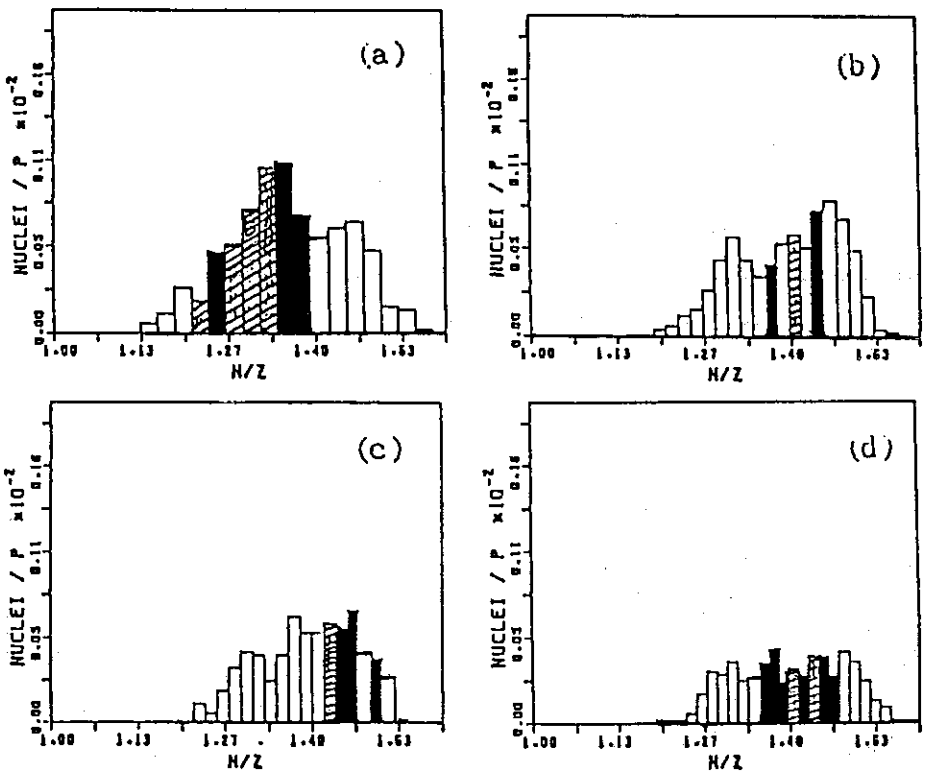

Fig. 2.3.2 Product yields of isotopes versus N /Z for a) Sr , b) I , c) Cs and d) Eu

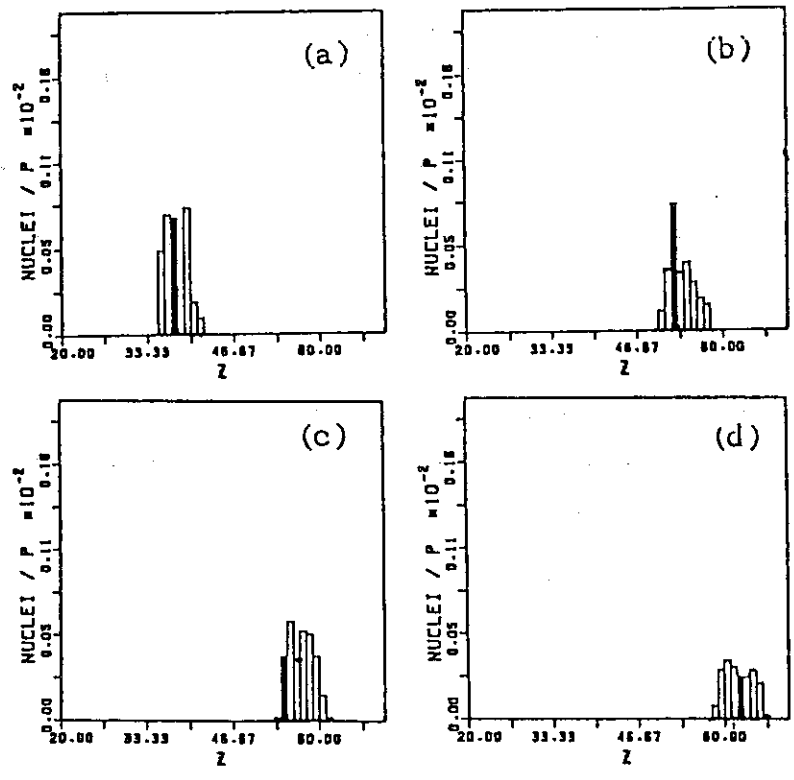

Fig. 2.3.3 Product yields on the β-decay chains leading to a) ^{90}Sr b) ^{129}I c) ^{137}Cs d) ^{150}Eu

2.4 Development of a Simulation Code NUCLEUS for Nuclear Spallation Reaction and Vectorization of NMTC/JAERI

T. Nishida and T. Tsutsui

In order to evaluate computational models for the nuclear spallation reaction from a nuclear physics point of view, a simulation code NUCLEUS [1] has been developed by modifying and combining the Monte Carlo codes NMTC/JAERI and NMTA/JAERI for calculating only the nuclear spallation reaction (intranuclear cascade + evaporation or fast fission) between a nucleus and a projectile without taking into consideration of the internuclear transport. The calculational models of the nuclear reactions are the same as those of NMTC/JAERI's. The nucleon pion transport code NMTC/JAERI connects with its statistical analysis code NMTA/JAERI by transferring Monte Carlo event data through a memory file, the size of which is limited in the actual computer system. However, NUCLEUS is free from that limitation because it has its own statistical process routines and the history memory file has been removed, which has made it possible to run as many histories as we want practically. New several plotting routines have been provided for the rapid process of much more event data.

Figure 2.4.1 shows the contour map (a) and the bird eye's view (b) representing the distribution of residual nuclides generated in the spallation reaction between an uranium nucleus and a 500 MeV proton, which were obtained by using the ARGUS plotting system. The figure is immediately printed out on a NLP printer. The results obtained by this code can be directly compared with measured nuclear data obtained by thin foil experiments, in which internuclear multiple collisions have little effects on the data, and will serve to upgrade the calculational methods and the values of nuclear parameters currently used in the calculations.

The Monte Carlo simulation code NMTC/JAERI with many "if option"s was converted to the vectorized one on FACOM VP-100 at JAERI. For the computational flows unsuitable for vectorization, some improvements have been made also. Total speed-up of only about 1.4 times in computation time was achieved in comparison with the original version.

Reference

1) Nishida T., Nakahara Y. and Tsutsui T. : " Development of a Nuclear Spallation Reaction Simulation Code and Calculations of Primary Spallation Products," (to be published as JAERI-M).

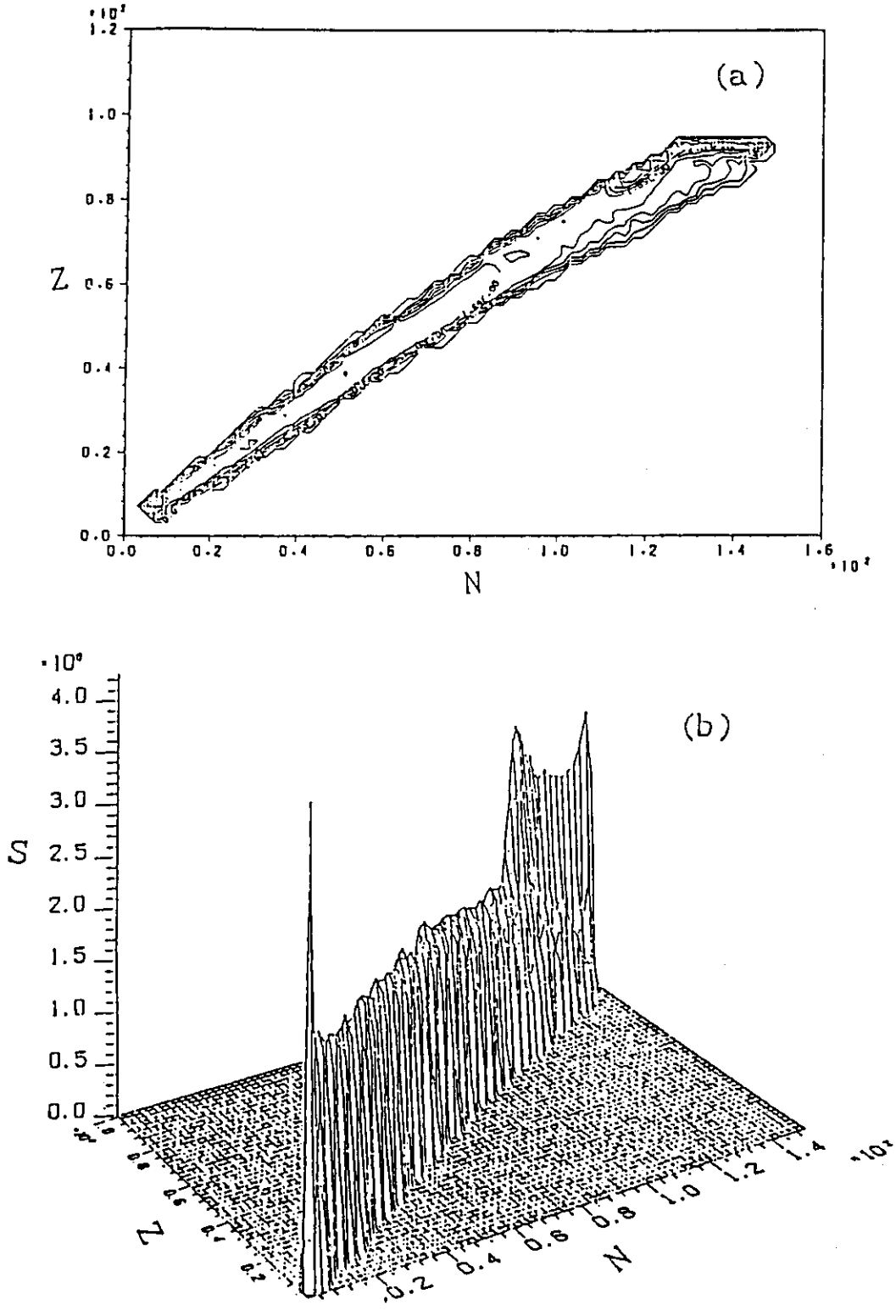

Fig. 2.4.1 Spallation product yield ; neutron number (N) versus proton number (Z) for a uranium nucleus bombarded by a 1 GeV proton as
(a) contour map and (b) bird eye's view
S indicates the logarithmic value of produced nuclei per proton.

2.5 Revised SRAC Code System

K. Tsuchihashi, Y. Ishiguro, K. Kaneko* and M. Ido**

The primary version of the SRAC code system[1] has been released in FY 1982 after the verification by extensive benchmark calculations[2]. After the release, a number of additions and changes have been made to the functions and several auxiliary codes are provided. The major points follow;

(1) The whole thermal scattering law data which were taken from ENDF/B-3 were recalculated in order to include the matrices on an additional temperature 325 K.

(2) The JENDL-2 version of data libraries are provided for an alternative of the ENDF/B-4 version[3].

(3) The treatment of resonance absorption in the doubly heterogeneous system as seen in VHTR with coated particle fuel is replaced by a direct method[4] based on the continuous energy cell calculation.

(4) A generalized Dancoff factor is introduced[5] for infinite arrays of multi-region cells containing several absorber lumps with different nuclide densities.

(5) A fixed boundary source problem can be solved in the cell calculation by the collision probability method. It can give a proper spectrum to an isolated cell which can not have its own spectrum.

(6) An edit function is added to calculate the reaction rate of the neutron detectors, the spectrum parameters, and the conversion rate.

(7) The self-shielded cross sections calculated for a particular composition and stored in a separate file which are used in the above reaction rate calculation.

(8) The reactivity caused by the change of cross section is calculated by using the first order perturbation theory.

(9) The assembler routine RWPDS to read/write the data from/to PDS files has been replaced by a new routine PDSFUTY in order to mount dynamically the directory of

---

Present address * Japan Information Service Co., Ltd.
** I. S. L. Inc., Tokyo

each PDS file on the core memory during the execution. This modification results in the decrease of I/O times into half and the elapsed time considerably.

(10) An auxiliary code COREBN for a core burn-up calculation has been developed. Through the data storage file, a fuel management is also available.

Parallel to the modification, further validation and application efforts have been continued as shown below.

An international RERTR (Reduction of Enrichment of Research and Test Reactor fuels) program has offered occasions to show the validity of the SRAC code system; such as the IAEA benchmark calculations for an idealized MTR[6] and for a DIDO type heavy water moderated reactor[7], an analysis of the initial LEU core of the Ford Nuclear Reactor[8], analyses for temperature and void coefficient of KUCA (Kyoto University Critical Assembly) MEU (medium enriched uranium) core[9,10], and a series of analyses for the critical experiments at JMTRC MEU core[11,12].

The SRAC code system has been successfully applied to the designs for the upgrading plan of the JRR-3[13] and for the reduction of uranium enrichment of JAERI research and test reactors[14]. Its application has been also extended to the reconstruction of the SHE[15] for neutronics study of the VHTR and to the design study of the Nuclear Fuel Cycle Safety Engineering Research Facility[16].

A good prediction accuracy of SRAC has been shown through the analyses of the initial critical approach of the VHTRC,[17], the reactivity worth of thorium plate and flux distribution in the test zone of the KINKI UTR (University Training Reactor)[18], and the reactivity worth of beryllium plate in the graphite zone of KUCA[19].

A fairly good agreement shown in the preliminary analysis[20] performed for high conversion LWR experiment in the Proteus reactor[21] encourages us to improve the SRAC code system to predict more accurately the reaction rates occurring in the intermediate energy range.

References

1) Tsuchihashi K., *et al.* : JAERI 1285 (1983).
2) Tsuchihashi K., Akino F., Nagaoka Y. and Ishiguro Y. : JAERI-M 9781 (1981).
3) Takano H., *et al.* : JAERI-M 83-202 (1983).
4) Tsuchihashi K., Ishiguro Y. and Kaneko K. : Nucl. Sci. Eng., 73,164 (1980).
5) Ishiguro Y.: Nucl. Sci. Technol. 22, 853 (1985).
6) Mori M. and Tsuchihashi K. : JAERI-M 84-230 (1984).
7) Physics Section IAEA (Ed.) : IAEA-TECDOC-324 (1985).
8) Arigane K. and Tsuchihashi K. : Proc. of the International Meeting on Reduced Enrichment for Research and Test Reactors, 24-27 Oct, 1983 Tokai, Japan, JAERI-M 84-073 (1984).
9) Mori T. and Tsuchihashi K. : Proc. of the International Meeting on Research and Test Reactor Core Conversion from HEU to LEU Fuels, 8-10 Nov, 1982 Argonne, ANL/RERTR/TM-4, CONF-821155 (1983);
Kanda K., *et al.* : Proc. of the International Meeting on Reduced Enrichment for Research and Test Reactors, October 14-16, 1985, Petten, The Netherlands, D. Reide Publishing Company (1986).
10) Senda Y., *et al.* : Nucl. Technol. 70, 318 (1985).
11) Nagaoka Y., *et al.* : Proc. of the International Meeting on Reduced Enrichment for Research and Test Reactors, October 24-27, 1983, Tokai, Japan, JAERI-M 84-073 (1984).
12) Shimakawa S., *et al.* : Proc. of the International Meeting on Reduced Enrichment for Research and Test Reactors, October 14-16, 1985, Petten, The Netherlands, D. Reide Publishing Company (1986).
13) Tsuruta H., Ichikawa H. and Iwasaki J. : JAERI-M 84-099 (1984);
Tsuruta H., Ichikawa H. and Iwasaki J. : Proc. of the International Meeting on Reduced Enrichment for Research and Test Reactors, Argonne National Laboratory, October 15-18, 1984, Argonne, USA, ANL-RERTR/TM-6 (1985).
14) Arigane K., *et al.* : JAERI-M 85-047 (1985).
15) Yasuda H. (Ed.) : private communication (1984).
16) Senuma I., *et al.* : JAERI-M 84-110 (1984).
17) Akino F. *et al.* : Section 3.3 in this report.
18) Itoh T., *et al.* : Annual Report of Kinki University Atomic Research Institute, 22, 15 (1985).
19) Misawa T. : private communication (1986).
20) Ishiguro Y., Tsuchihashi K. and Sasaki M. : JAERI-M 84-180 (1984).
21) Chawla R. : Atomkernenergie, 37, 303 (1981);
Chawla R. *et al.* : NUREG/CP-0034, 902 (1982).

2.6 Application of New Angular Basis Functions to the Double Finite Element Neutron Transport Code

T. Fujimura, Y. Nakahara and M. Obara*

The finite element method (FEM) is a powerful tool to solve the three-dimensional neutron transport problems in complicated geometries. The DFEM-SP3 is an original version of the double FEM code, in which a fixed number of cubic spline functions has been used as the angular basis functions[1]. In order to perform calculations with the required degree of accuracy, it is desirable for the number of angular bases to be given by an input option. Therefore, we tried to apply two kinds of new simple bases to the angular variable.

Quadratic Splines (SP2)

Let OX, OY and OZ be any three adjacent directions in the angular domain S, as shown in Fig. 2. 6. 1. The bases of the angular variable Ω are defined by using a skew coordinate system as

$$\chi_X(\Omega) = X^2 + 2YZ\cos\theta_{YZ},$$
$$\chi_Y(\Omega) = Y^2 + 2ZX\cos\theta_{ZX},$$
$$\chi_Z(\Omega) = Z^2 + 2XY\cos\theta_{XY}.$$

It is easier to prepare the coefficients of the system equation with these bases than with those of SP3[2].

Piecewise Constant Functions (PC)

Let S_j be a subspace of the domain S. Then, the bases are defined by

$$\chi_j(\Omega) = 1 \quad \Omega \in S_j, \qquad \chi_j(\Omega) = 0 \quad \Omega \in S_j.$$

*I. S. L. Inc., Tokyo

Since they satisfy the moment condition, the scheme may be interpreted as an S_n-like method in the FEM.

Sample calculations for the FCA-V-2 fast critical assembly have been performed to compare these results with those of the original version. Table 2. 6. 1 shows the convergence of k_{eff}'s obtained by the two group calculations when the spatial mesh width decreases. The value obtained by the S_8 fine mesh calculation with TWOTRAN-II[3] has been adopted for reference.

In the calculation by DFEM-SP2, the same number of the angular bases is chosen as in that by DFEM-SP3. The DFEM-PC(2) and DFEM-PC(4) mean the calculations by the DFEM-PC version with the angular elements comparable to the corresponding S_2 and S_4 calculations, respectively. As seen from the table, the SP3 gives the best value in the present results with the overestimate of 0.08% in comparison with the S_8 value. The values obtained by SP2 is slightly greater than those by SP3. Its value for the mesh width of 4.36 cm is greater by 0.15% than the S_8 value. These differences are mainly due to the truncation error for the equation of even parity flux. The error of this kind was larger for the PC version. In order to reduce this error, we have introduced a new remedy algorithm. The results by PC(4) were almost the same as those by PC(2). The PC version, however, still gives underestimates, i.e., the underestimate of 0.4% even in its best value. This subject must be studied further.

References

1) Fujimura T. : "Development of Three-Dimensional Transport Code by the Double Finite Element Method," Proc. of the Seminar on Software Development in Nuclear Energy Research, JAERI-M 85-017, 120 (1984) (in Japanese).
2) Lafore P. (private communication)
3) Lathrop K. D. and Brinkley F. W. : "TWOTRAN-II : An Interfaced, Exportable Version of the TWOTRAN Code for Two-Dimensional Transport," LA-4848-MS (1973).

Table 2. 6. 1 Comparison of the convergences of eigenvalue (k_{eff}) obtained by various methods with respect to the spatial mesh width

Code name	Spatial mesh width (cm)						
	15.25	10.17	7.63	6.10	5.08	4.36	1.53
DFEM							
SP3	1.0010	1.0219	1.0298	1.0335	1.0356	1.0367	
SP2	1.0014	1.0225	1.0305			1.0375	
PC(2)	0.9987	1.0185	1.0258	1.0291	1.0309	1.0317	
PC(4)	0.9988	1.0185	1.0255				
TWOTRAN-II							
S_8							1.0359

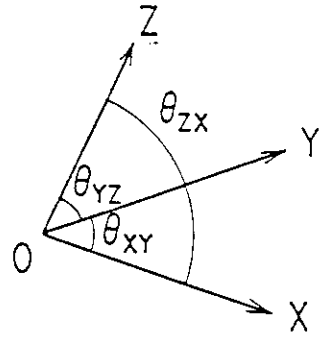

Fig. 2. 6. 1 Three adjacent angular directions and the angles between them

2.7 Development of a 2-D Sn Transport Code Using Double Differential Form Cross Section Library

T. Mori and M. Sasaki*

Sn transport codes are widely used for neutron transport calculations. However, inaccurate treatment of anisotropic scattering in the conventional multigroup method using the P_l expansion sometimes results in the significant misprediction of the neutron transport phenomena in the materials with highly anisotropic scattering cross sections. The double differential form multigroup cross section library (DDX library) has been developed to treat accurately the scattering anisotropy. The adequacy of this library was examined through the benchmark calculations with the Monte Carlo code MORSE-DD and the one-dimensional Sn code ANISN-DD in the previous works[1),2)]. At the present work, a two-dimensional Sn code DOT-DD, which can use the DDX library as well as the conventional multigroup library with the P_l expansion, has been developed on the basis of the DOT-3.5 code[3)]. At first, the cross section mixing is carried out in the same way as that in the MORSE-DD code.[1)] Then the elements of scattering matrices are rearranged into a group-independent form library. In addition to the DOT-DD code, developed is the UNCL-DD code which calculates a first collision source by using the DDX library. The newly developed DOT-DD code has the following functions:

(1) forward transport calculation in two-dimensional X-Y, R-Z and R-Θ geometries,
(2) adjoint transport calculation,
(3) transport calculation with external volume and/or shell sources or a first collision source calculated by the UNCL-DD code, and
(4) criticality search.

The scattering source is calculated by the following equation:

$$S(g,\bar{\Omega}_m) = \frac{1}{w_m}\int_{\Delta\bar{\Omega}_m} d\bar{\Omega} S(g,\bar{\Omega})$$

$$=\sum_{g'}\sum_{m'}\Phi(g',\bar{\Omega}_{m'})w_{m'}\sum_{k}\Sigma_{pr,g'}I(g'\to g,k)P(k,\bar{\Omega}_{m'}\to\bar{\Omega}_m),$$

where

$$P(k,\bar{\Omega}_{m'}\to\bar{\Omega}_m)=\frac{1}{2\pi\Delta\mu_k}\frac{1}{4\pi w_m w_{m'}}\int_{\Delta\bar{\Omega}_m} d\bar{\Omega}\int_{\Delta\bar{\Omega}_{m'}} d\bar{\Omega}'\,\delta_{\mu k}$$

$$\delta_{\mu k}=\begin{cases} 1 & \text{for } \mu_{k+1}<\bar{\Omega}\cdot\bar{\Omega}'<\mu_k \\ 0 & \text{otherwise,}\end{cases}$$

$\bar{\Omega}_m$, w_m : Sn constants (direction cosine and its weight),

$I(g'\to g,k)$: multigroup energy-angle distribution,

---

* Japan Information Service Co., Ltd., Tokyo

$P(k, \bar{\Omega}_m' \rightarrow \bar{\Omega}_m)$ is calculated by a utility code MONTA and has been stored on a file for S_4, S_8 and S_{16}. This quantity is normalized as

$$\sum_m P(\mu_k, \bar{\Omega}_m' \rightarrow \bar{\Omega}_m) = 1.$$

In order to examine an accuracy of the present code, the angle dependent leakage neutron energy spectrum from a Li_2O slab has been analyzed with the two DDX libraries (DDXLIB1 and DDXLIB3). Figure 2.7.1 compares them with that measured at FNS[4] and that calculated with the conventional P_5 library (JENGIX). In the energy range above 10 MeV, significant discrepancies are observed betweem the DDX and P_5 results. This fact shows the necessity of calculation with the DDX library for the assessment of cross section data. Below 10 MeV, on the other hand, the DDXLIB1 and JENGIX results show an agreement within a few percent. The observed discrepancy between the DDXLIB1 and DDXLIB3 results is ascribed to the different angular distributions of continuum inelastic scattering (DDXLIB1 : isotropic, DDXLIB3 : anisotropic).

References

1) Nakagawa M., Mori T. and Ishiguro Y.: "Benchmark Test of MORSE-DD Code using Double-Differential Form Cross Sections," JAERI-M 85-009 (1985).
2) Youssef M.Z. et al.: "U.S./JAERI Fusion Neutronics Calculational Benchmarks for Nuclear Data and Codes Intercomparison," JAERI-M 85-201 (1985).
3) Mynatt F.R. et al.: CTC-INF-952 (1969).
4) Oyama Y. and Maekawa H.: "Measurements of Angle-dependent Neutron Spectra from Lithium-Oxide Slab Assemblies by Time-of-Flight Method," JAERI-M 83-195 (1983).

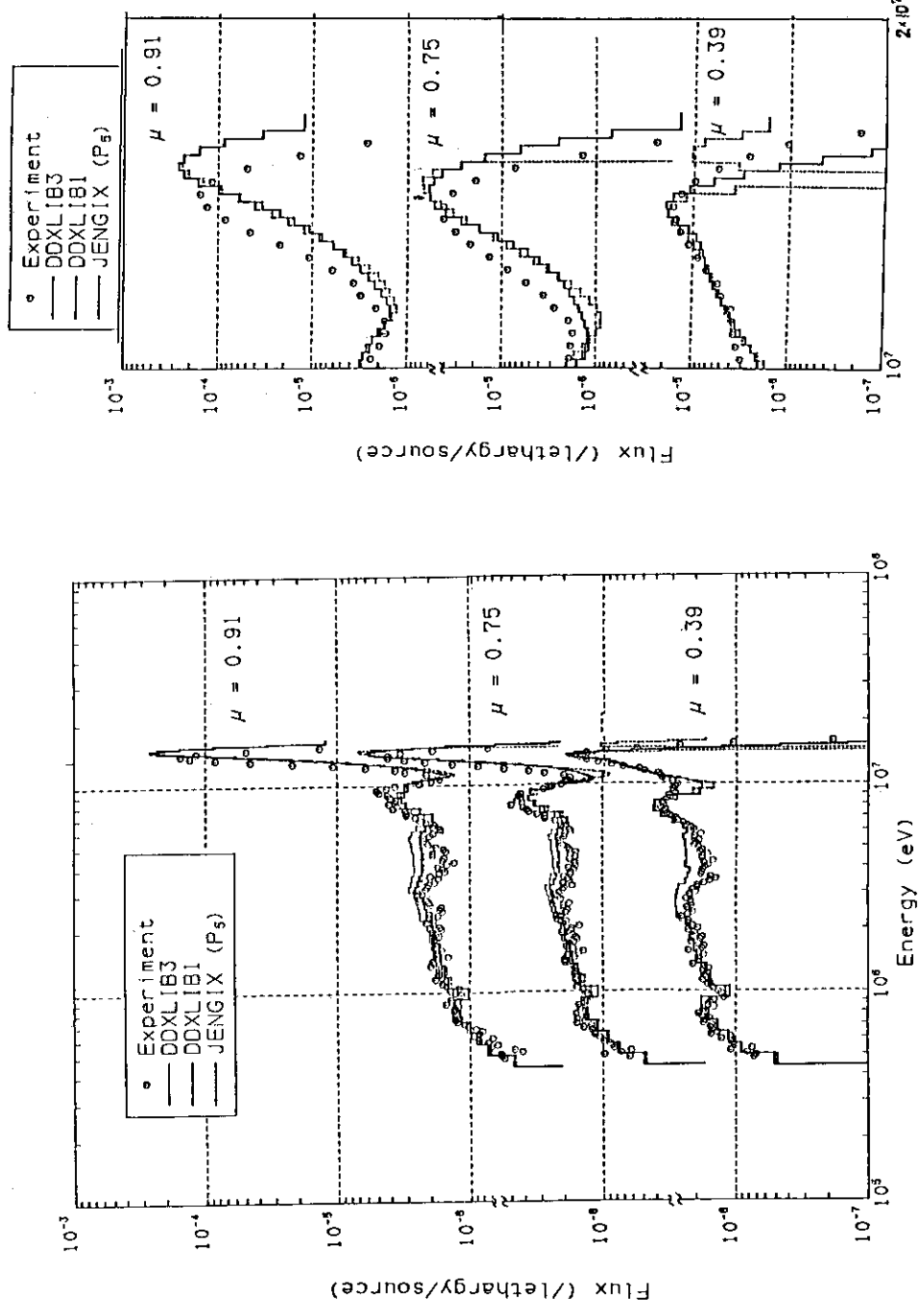

(a) Neutron spectra from 0.5 to 16 MeV (b) Neutron spectra above 10 MeV

Fig. 2.7.1 Angle dependent leakage neutron spectra from the Li_2O slab

2.8 Development of a Thermo-Hydraulic Analysis Code for a Unit Cell in an HCLWR

T. Mori

As the first stage of thermo-hydraulic design study of an HCLWR, a simple thermo-hydraulic analysis code has been developed for parameter survey calculation on a unit fuel cell of an HCLWR. The developed code is based on the MINCS-PIPE code[1]. This code has been modified to analyze a unit fuel cell of an HCLWR which is characterized by low water volume fraction, high velocity of coolant flow, high pressure drop in the axial direction and usage of mixed oxide fuel. The following correlations are adopted in the code.

Wall friction : Rehme's friction factor correlation[2] for a wire spacer and input assignment for a grid spacer.

Critical heat flux : B & W correlation[3] and KfK correlation[4].

Thermal conductivity of mixed oxide fuel : calculation by the MATPRO module in the MINCS-PIPE code[1] or input assignment.

These correlations can be replaced if more accurate ones are available.

Thermo-hydraulic behavior of coolant is analyzed by the 2V-2T model of the MINCS-PIPE code[1]. By using the developed code, the following quantities are obtained.

(1) Axial distribution of coolant temperature,
(2) Axial and radial distribution of temperature in a fuel rod,
(3) Axial distribution of pressure in a coolant : components of pressure drop (friction, grid spacer, acceleration and elevation),
(4) Axial distribution of void fraction in a coolant,
(5) Axial distribution of DNBR.

References

1) Akimoto M. et al.: "A Computer Code for Transient Thermo-Hydraulic Analysis in a Light Water Reactor System --- MINCS-PIPE: A Computer Code for Transient Two-Phase Flow Analysis in One-Dimensional Ducts ---," JAERI-M 84-202 (1984).

2) Rehme K.: Nucl. Technol., 17 , 15(1973).

3) Uofinen V.O. et al.: "Technical Feasibility of a Pressurized Water Reactor Design with a Low Water Volume Fraction Lattice," EPRI-NP-1833 (1981).

4) Donne M.D. and Hame W.: "A Critical Heat Flux Correlation for Advanced Pressurized Light Water Reactor Application," KfK-3279 (1982).

2.9 Development of Two-Dimensional Diffusion Kinetics Code

Y. Taji

A two dimensional diffusion kinetics code, T2DK has been extended to deal with the cylindrical geometry (R,Z) and the circular geometry (R,θ) in addition to the slab geometry (X,Y). Furthermore, development of a three-dimensional kinetics code started. Space-dependent kinetic analyses are important for the studies of transient or accident conditions and also the optimum designs of advanced nuclear reactors. However, because of the long computation time multi-dimensional kinetics codes do not yet prevail. Usually the one-point reactor model has been adopted by assuming the spatial distributions not to vary substantially in time. However, in these days high speed computers are available, hence two-dimensional calculations become practical.

In the T2DK code the time-dependent, two-dimensional diffusion equation with delayed neutrons is integrated over time by the Crank-Nicolson method. The implicit difference equation is solved by the successive overrelaxation iterative (S.O.R.) method. The T2DK code is applicable to problems of arbitrary number of neutron energy groups and of regions in the (X,Y), (R,Z) and (R,θ) geometries. The preliminary calculations were performed for a fast reactor model of two neutron energy groups with six delayed-neutron groups, in which the mesh points were set as 28 × 36 in (R,Z) geometry. When a neutron source was injected in the form of step function, the width of time step was needed to be less than 2×10^{-9} s in the initial stage. As the shape of neutron distribution approaches to a steady one the time step could be set as a longer interval $\sim 10^{-6}$ s. The computation time needed for a time step was 1.1 s in the initial stage and increased to 24.1 s in the later stage. This speed is quite unsatisfactory. A method of changing the time step automatically is proposed, which will be incorporated in the three dimensional code. The relaxation factor of the S.O.R. method has been changed as the computation proceeds; how to find the best factor is not clear. The vectoralization of the T2DK code is not yet enough, the conversion of which will be performed in near future. Other than the problem of delayed neutrons treated here more important problems of kinetics e.g. the effects of thermal feedbacks or nonlinearities remain, which will be taken into account in the future.

2.10 Molecular Dynamic Simulation of Defects in Reactor Materials

Y. Taji, T. Yokota[+], T. Iwata[+] and M. Fuse[++]

The research of radiation damages by the method of computer simulation has been performed in two directions; one is the precise simulation concerning with formation of an interstitial atom in graphite crystals[1] and another is the extensive simulation for investigating anisotropic threshold energies of atomic displacement in b.c.c. tantalum crystal. New results have been obtained in both the simulations.

The characteristic point in the simulation of graphite is that non-central force interactions have been taken into account to express the directional covalent bonds in the hexagonal lattices constituting layers. On the other hand, between atoms located on different layers the central force interaction of the van der Waals force has been adopted. Because the repulsive part of the central force can constitute well the compressibility in z-direction, it was applied to the interaction between the interstitial atom and other atoms lying on layers. It has been found that the interstitial atom rests at an asymmetric site in the hexagonal lattice, which is quite different from the symmetric site pronounced by the elastic membranes model representing approximately the lamellar structure of graphite. The reason why the asymmetric result is obtained is that the asymmetry of ABAB staggered stacking of the layers in graphite appears explicity through the non-central force intractions. The self-energy and the migration energy of an interstitial atom are obtained as 1.28 eV and 0.01 eV, respectively. The increase of crystal volume due to an interstitial atom amounts to 3.32 atomic volume, which coincides with the experimental value fairly well.

Systematic simulation for obtaining the anisotropic threshold energies of atomic displacement has been performed for b.c.c. tantalum crystal, which makes a series together with the former systematic simulation for Mo. We adopted an interatomic potential of central force interaction constructed by Johnson and Wilson on the basis of elastic constants. The contour of anisotropic displacement threshold energy is depicted in Fig. 2.10.1, which explains the experimental values fairly well. The most characteristic point in the present simulation is that the interstitial configuration was found

---

+ Department of Physics, JAERI ++ Energy Reseach Lab., Hitachi Ltd.

to be crowdion type along [100] and [111]. These results differ fundamentally from the [110] split dumb-bell type, which has been obtained for the b.c.c. Fe and Mo by Vineyard et al. and the present authors. The vacancy configuration was found to be more shrunk comparing with that in Fe and Mo. This computational result reflects well some experimental results concerning with the resistivity recovery following a low temperature irradiation and the Doppler broadening in the positron annihilation spectroscopy. In these experiments clearly different results are obtained between the group of Fe, Mo, W and that of Ta, Nb, V. The usual simple picture of damages for the b.c.c. metal seems to encounter with discrepancy. Now a new concept is needed for distinguishing these two types of damages in b.c.c. metal.

Reference

1) Taji Y., Yokota T. and Iwata T.: "Dynamic Simulation of Interstitial Atom in Graphite", to be published in J. Phys. Soc. Japan 55, No.8 (1986)

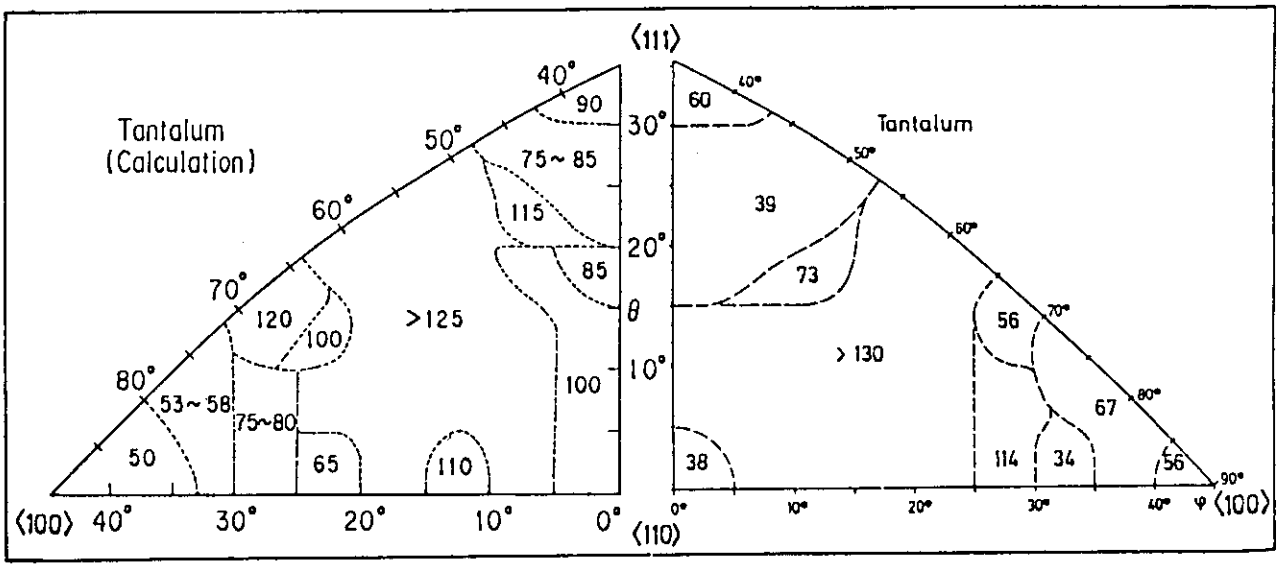

Fig.2.10.1 Comparison of displacement threshold-energy profiles simulated by the present authors and measured by Jung & Schilling (Phy. Rev. B5. 2046 (1972)). The figures give the average threshold energies in eV for the particular directions.

3. Reactor Physics Experiment and Analysis

A critical assembly VHTRC was constructed by modifying the SHE assembly and went critical with 282 fuel rods for the first time in May 1985. In the initial critical core, VHTRC-1, measured were critical mass, reaction rate distribution of $^{63}Cu(n,\gamma)^{64}Cu$, temperature coefficient of reactivity etc.. The measured results were in fairly good agreement with the predicted ones obtained by the SRAC code system. The delayed neutron data for thermal fission of ^{235}U was evaluated using the integral experiments in the various SHE cores. The study indicated that β_{eff} s of the SHE cores should be 4.0% higher than those calculated with Keepin's delayed neutron data set.

The physics experiment programme on the axially heterogeneous core LMFBR for three years was successfully completed at FCA in February 1986, after completing the experiments in the sector-type FCA XIII cores. As for the zone-type FCA XII cores built in the fisical year 1984, the remaining analyses were performed for the fuel slumping experiments and the effects of different internal blanket thickness on the physics characteristics. In the experiments in the FCA XIII cores, confirmed were flat radial distributions of reaction rate, fission power and sample worth. The measured results are now being analysed. An idea of subcriticality monitor was examined at FCA, where the subcriticality was evaluated by measuring a change in neutron spectrum with a paired detector.

Extensive efforts have been devoted to feasibility studies of HCLWR. A preliminary analysis was made to select adequate contents and dimensions of FCA XIV cores for simulating typical neutron spectra in HCLWR. Analyses of PROTEUS experiments and a benchmark calculation were performed using the SRAC code system to understand its predicted accuracy of HCLWR neutronics. A series of cell burnup calculations were made to obtain relation between physics parameters and burnup, aiming at selection of a reference core design of HCLWR.

Two types of PWR plant designs based on the inherent safety features were proposed, both of which have an integrated primary cooling system and a poison tank in the reactor pressure vessel. In addition, two types of HTGR designs were also developed : one for generating high temperature He gas and the other for electricity power production. The other design activity was physics study for designing neutron source and neutron guides to be installed in a new research reactor.

In addition to the above mentioned R&D activities, included in this section are operation, maintenance and thier related activities of VHTRC and FCA, which enabled successful experiments in both the critical facilities.

(H.Yoshida)

3.1 Initial Critical Experiments of VHTRC (I)
- Function Tests -

H. Yasuda, F. Yoshihara, T. Yamane, F. Akino, K. Kitadate, M. Takeuchi, T. Ono, H. Yoshifuji and Y. Kaneko

A critical assembly VHTRC (Very High Temperature Reactor Critical Assembly) was constructed by modifying the SHE assembly in order to verify the nuclear design of the experimental VHTR. The major specifications of the VHTRC are shown in the previous report.[1]

Preceding fuel loading, all elements of the facility were tested. The test results of fuel compacts and graphite blocks are shown in Tables 3.1.1 and 3.1.2.

Besides, was also performed the pulsed neutron experiment in which the neutron flux decay constant was measured to examine the assembly averaged graphite impurities. The measured value of, 184.3 ± 1.3 s^{-1} at 27 °C agreed fairly well with the theoretical value of 184.4 s^{-1} predicted using the chemical analysis data.

The items of uranium-235 enrichment, uranium contents and graphite impurities are very important from the view point of reactor physics. The test results are satisfactory as shown in the tables.

The assembly heating test was also performed where the uniformity of temperature distribution at 200 °C was confirmed and the performances of control, safety rods and movable half assembly driving systems were measured showing no significant differences from those at room temperature.

Reference

1) Kaneko Y. et al.: JAERI-M 85-116 p.50～ 51 (1985)

Table 3.1.1 Test results of BISO fuel compacts

Items		Results	
Type of fuel compact		B-2	B-4
Kernel	Enrichment (wt %) Diameter (μm) UO_2 density (g/cm^3)	2.00 6 02 10.42	4.00 5 99 10.35
Coated particle	Diameter (μm)	918	913
	Coating thickness (μm) 1st layer 2nd layer	 78.8 79.2	 79.2 77.8
	Carbon density (g/cm^3) 1st layer 2nd layer	 1.19 1.87	 1.18 1.87
Fuel compact	Uranium contents (g) Outer diameter (mm) Inner diameter (mm) Height (mm) Matrix density (g/cm^3)	21.00 36.0 18.0 36.0 1.71	20.95 36.0 18.0 36.0 1.69

Table 3.1.2 Test results of graphite blocks

Items	Results
Density (g/cm^3)	1.665
H_2 Contents (wt %) converted to H_2O form	0.011
Impurity contents in boron equivalent concentration (ppm)	0.07
Length of assembly (mm) Two blocks	2400.0
Height of assembly (mm) Eight blocks	2400.0
Compression strength of graphite material (MPa)	60.6

3.2 Initial Critical Experiments of VHTRC (II)
- Critical Approach -

T. Yamane, F. Akino, H. Yasuda, F. Yoshihara, K. Kitadate, M. Takeuchi, T. Ono , H. Yoshifuji and Y. Kaneko

Following the function test, VHTRC was brought critical for the first time. A fuel rod consisted of twenty fuel compacts inserted into a graphite sleeve. Each compact contains 4 % enriched uranium. The core was loaded step by step with the fuel rods keeping hexagonal symmetry.

The neutron multiplication was observed at each loading step by the source multiplication technique using six neutron detectors: two out-of-core BF_3 counters of 1 inch in diameter and four in-core BF_3 counters of 1/4 inch in diameter. At early four loading steps the effective multiplication factor, k_{eff}, and the prompt neutron decay constant, α, were measured by the pulsed neutron technique using the in-core detectors. The data were analyzed by means of an integral version of the Sjöstrand's area method[1] where responses of all detectors were simply summed up. The arrangement of the detectors was devised so that the contributions of spatial higher harmonics would be minimized by such summation. The measured values of k_{eff} agreed fairly well with those predicted by a three dimensional diffusion calculation, as shown in Fig.3.2.1. The measured α-values, shown in the same figure, are found to decrease linearly with the increasing number of fuel rods. These results confirmed at early loading steps that the neutron multiplication would increase as expected.

After the step-by-step loadings, the core reached criticality with 282 fuel rods at the ninth step. The pattern of this core, VHTRC-1, is shown in Fig.3.2.2. Figure 3.2.3 shows the inverse multiplication versus the number of fuel rods. The neutronic characteristics were measured to verify the safety of the core. The excess reactivity suppressed by partially inserted control rods was 28.4 cents. The reactivity worth of a fuel rod was measured with the calibrated control rods and found to be 7.1 cents. Using this fuel rod worth the loading of 282 fuel rods was corrected for the

excess reactivity, and the critical loading was estimated to be 278 fuel rods which gave the critical mass of 4.66 kg-^{235}U. Other corrections to the critical mass, required for comparison with calculation, were measured. The results are shown in Table 3.2.1.

Reference

(1) Kaneko Y. : J. Nucl. Sci. Technol. 12(7),402(1975)

Table 3.2.1 Corrections to critical mass

Item	Reactivity worth (Cents)
(1) Partial insertion of control rod ,i.e. excess reactivity	28.4
(2) Insertion holes of control and safety rods	46.1
(3) In-core portions of safety rods	5.4
(4) 14 thermocouples and a guide tube for start-up neutron source	1.6
(5) Four in-core detectors (1/4"Φ BF_3 detectors)	15.0
(6) Closing gap between two half assemblies	12.5

Note. 1) β_{eff}=0.0072456

2) Core temperature was 17.7℃ .

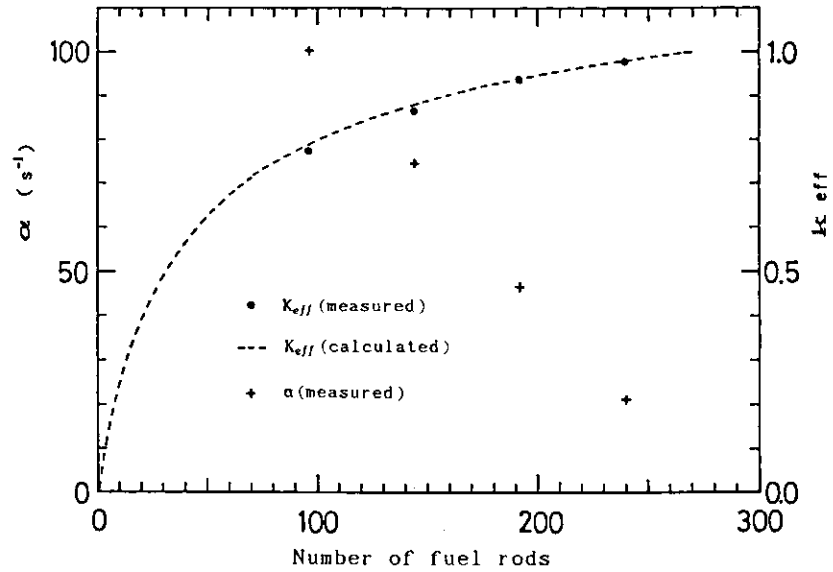

Fig.3.2.1 Effective multiplication factor (k_{eff}) and prompt neutron decay constant (α) versus number of fuel rods

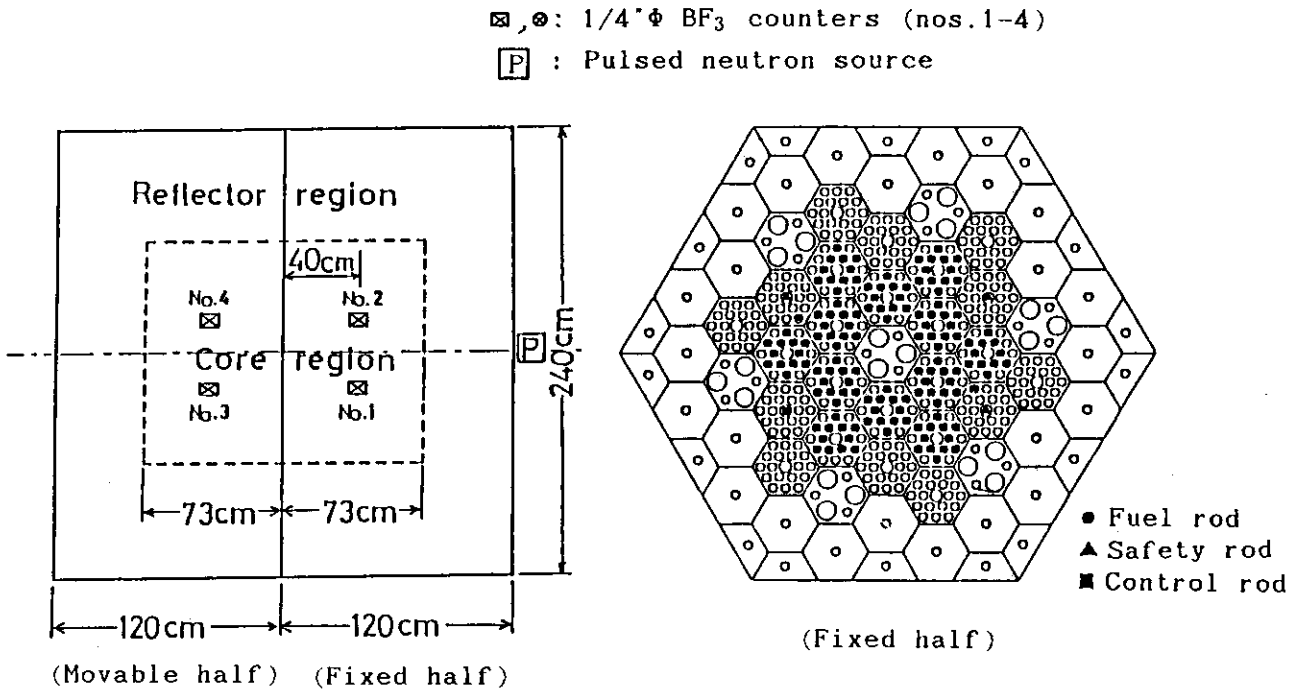

Fig.3.2.2 VHTRC-1 core pattern at initial critical

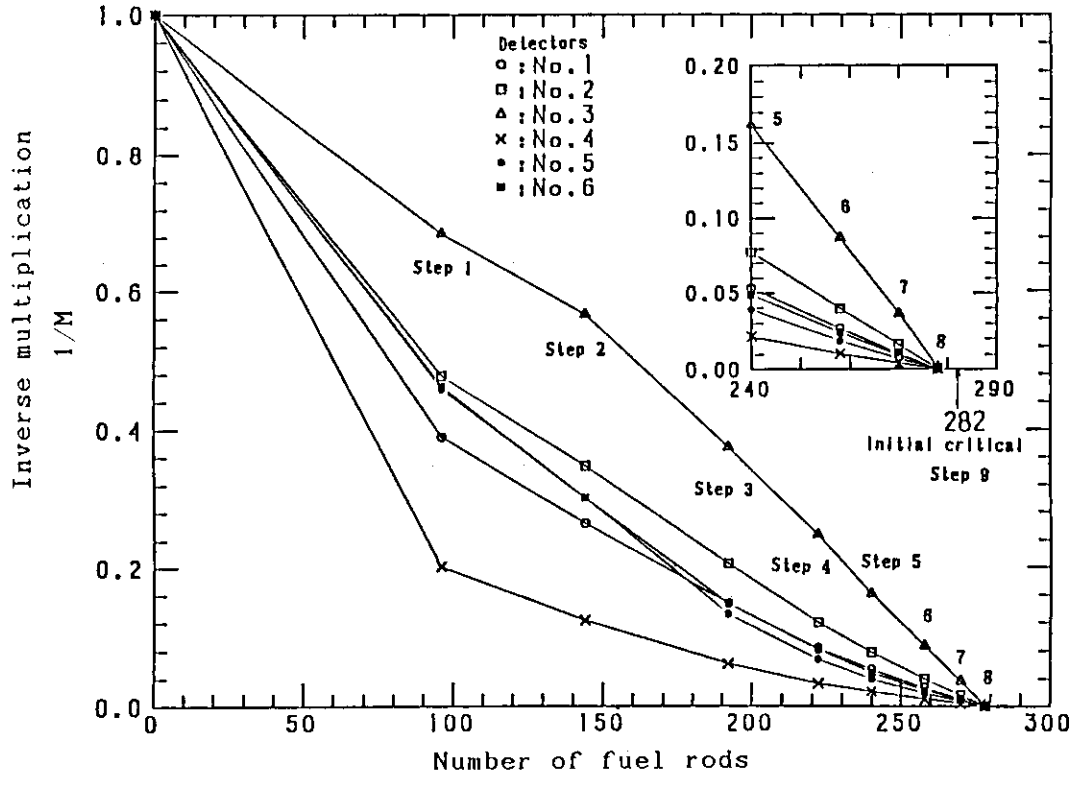

Fig.3.2.3 Inverse multiplication during initial approach-to-critical of VHTRC-1 core

3.3 Initial Critical Experiments of VHTRC (III)
- Analyses -

F. Akino, T. Yamane, H. Yasuda, F. Yoshihara, K. Kitadate, M. Takeuchi, T. Ono, H. Yoshifuji and Y. Kaneko

Initial critical experiments of VHTRC has been analyzed using the SRAC code system[1] . The modeling of the unit lattice of VHTRC-1 core is shown in Fig.3.3.1. Calculations of group constants for the lattice of VHTRC-1 core were made with use of the nuclear data of ENDF/B-IV, taking into account of the double heterogeneity with respect to fuel rod and coated particle, as precisely as possible.

The following conditions were adopted in lattice calculation:

1) Young-Koppel's model for the scattering kernel of graphite in the thermal energy region.
2) Isotropic reflective condition for outer boundary of the lattice.
3) Resonance absorptions in the energy region from 1.125 eV to 130.7eV were calculated by the PEACO[2] routine with the ultrafine energy groups of about 4000.
4) 300K for the temperature of lattice materials.

The thermal neutrons in the energy region from 0 eV to 1.125 eV were divided into 39 groups and the fast neutrons in the energy region from 1.125eV to 10 MeV were divided into 22 groups. Using the neutron spectra obtained by the lattice calculation, the 61 groups of cross section were condensed into the 24 groups (thermal group; 13, fast group; 11) for the three-dimensional core calculation by the diffusion code. On the other hand, 24 group cross sections for graphite reflector were obtained by averaging the 61 group cross sections with weights of the Maxwell distribution for thermal, and 1/E + fission spectra for fast groups, respectively.

Calculations of the effective multiplication factor, k_{eff} of the VHTRC-1 core were made by the three-dimensional diffusion code CITATION[3] , where the whole core was divided into triangular meshes. The calculated results of k_{eff} and critical

mass of ^{235}U are shown in Table 3.3.1 in comparison with the experimental ones, which are corrected for the reactivities of inserted materials in core, such as the safety rod insertion holes, gap between the fixed and movable half assemblies,etc., and also temperature difference between experiment and calculation.

Neutron decay constant, α of graphite assembly, preceding to the fuel loading, was calculated by the CITATION code, using the graphite reflector group constants.

As shown in Table 3.3.1, the discrepancies of k_{eff} between calculation and experiment were 0.4~2%Δk_{eff} in subcritical state and 0.4%Δk_{eff} at critical. The difference between experiment and calculation was 3% on critical mass of ^{235}U at room temperature. It was shown there that agreement between experiment and calculation was fairly good and satisfy the accuracy requirement for nuclear design in the experimental VHTR.

It is likely that the nuclear data and the calculation method are valid for the analyses of the graphite moderated core which is loaded with the coated particle fuels of low enriched uranium .

References

1) Tsuchihashi K.,et al.:JAERI-1285(1985)
2) Ishiguro Y.,et al.:JAERI-1219(1971)
3) Fowler T.B.,et al.:ORNL-TM-2496(1971)

Table 3.3.1 Measured and calculated effective multiplication factor and critical mass of VHTRC-1 core at room temperature

Items	Experiment	Calculation
Neutron decay constant of graphite assembly, α (s^{-1})	184.3	184.4
Effective multiplication factor, k_{eff}		
96 fuel rods loading	0.777	0.7930
144 fuel rods loading	0.869	0.8827
192 fuel rods loading	0.9410	0.9399
240 fuel rods loading	0.9817	0.9846
Critical mass of ^{235}U (kg)	4.520	4.386
(Number of fuel rods at critical)	(269.7)	(261.7)

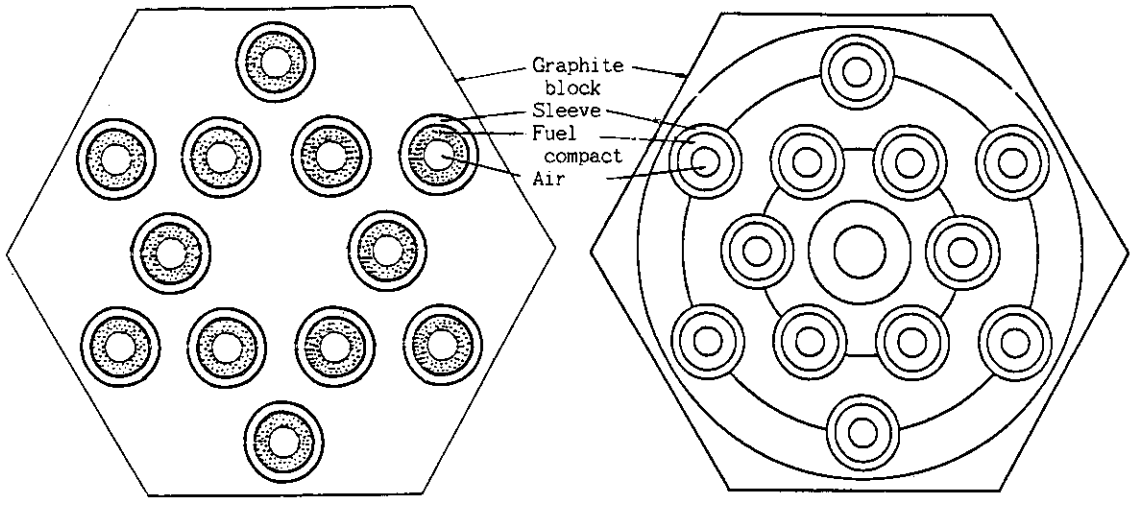

Fig.3.3.1 Simplification of unit lattice of VHTRC-1 core for calculation

3.4 Initial Critical Experiments of VHTRC (IV)
- Whole Core Heating Experiments -

H. Yasuda, F. Akino, T. Yamane, F. Yoshihara, K. Kitadate, M. Takeuchi, T. Ono, H. Yoshifuji and Y. Kaneko

The whole core including the reflector was heated up to 200 °C by electric heaters. The critical mass and the temperature coefficient of reactivity were measured.

The 40 cartridge type heaters were inserted in the radial reflector. The 17 K-type thermo-couples and 4 heat-resistant small BF_3 counters were placed in the core. After measuring the critical point at room temperature, the electric power of 30 kW was supplied to the heaters for about 50 hours until the core average temperature reached 200 °C. At the temperature, 200 °C, the number of fuel rods was increased stepwise to approach the criticality. (See Figs. 3.4.1 and 3.4.2)

The mass M of uranium 235 loaded in the core was given by

$$M = m \cdot N \quad . \qquad (1)$$

m : the uranium 235 contents in a fuel compact

N : the number of fuel compacts in the core

The critical mass Mc was obtained by

$$Mc = M - M_R \quad . \qquad (2)$$

M_R : the uranium 235 mass equivalent to the partially inserted control rods at critical state

The reactivity decrease $\Delta\rho$ due to the temperature rise was given by

$$\Delta\rho = \rho_f \cdot \Delta N - (\rho_{ex}^{RT} - \rho_{ex}^{200}) \quad . \qquad (3)$$

ρ_f : the reactivity worth of a fuel rod at 200 °C (measured by the pulsed neutron method)

ρ_{ex}^{RT} : the excess reactivity at room temperature

ρ_{ex}^{200} : the excess reactivity at 200 °C

ΔN : number of fuel rods added at 200 °C

The temperature coefficient of reactivity α_T was given by

$$\alpha_T = \Delta\rho/\Delta T \qquad (4)$$

ΔT : the temperature rise

An analysis was made using the SRAC code system. The calculated multiplication factor was corrected for heaters, thermo-couples, safety rod voids and the temperature difference between the experiment and calculation using the measured values.

The calculated results are given in Table 3.4.1 in comparison with experiment. Satisfactory agreements are obtained for both of the critical mass and the temperature coefficient of reactivity.

Table 3.4.1 Results of whole core heating experiments

Items		Room temperature	Elevated temperature
Core temperature (°C)		20.6	200.8
Number of fuel rods at critical	2% EU 4% EU	12 288	144 309
Reactivity worth of a fuel rod (¢)	2% EU 4% EU	2.13 7.12	1.88 6.96
Critical mass (g in U-235)	Expt. Calc.	4744± 57 4582	6366± 76 6365
Temperature coefficient of reactivity ($\delta k/k/°c$)	Expt. Calc.	$(-1.79 \pm 0.005) \times 10^{-4}$ -1.81×10^{-4}	

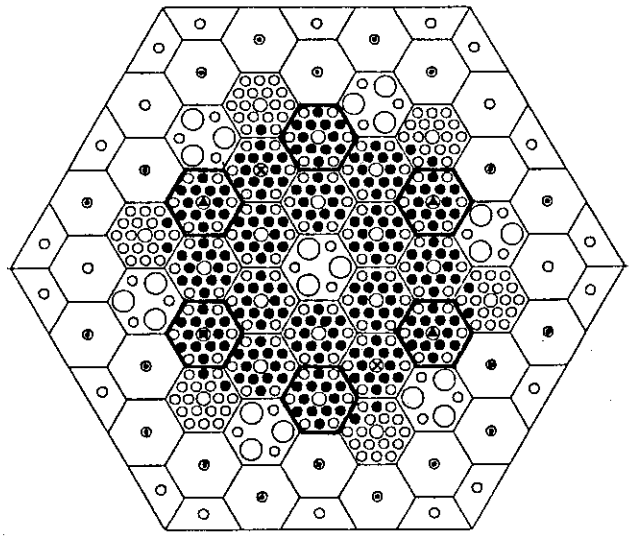

● Fuel rod 4% EU
● (in bold hex.) 2% EU
■ Control rod
▲ Safety rod
⊙ Heater
⊗ BF_3 counter

Fig. 3.4.1 Core cross section of VHTRC at 200 ℃

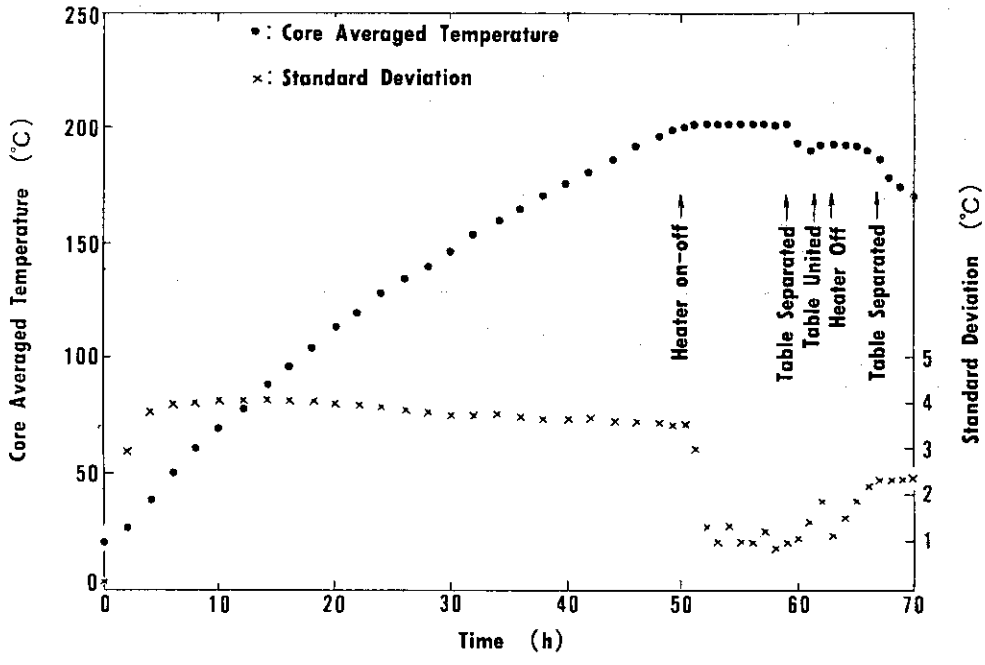

Fig. 3.4.2 Core averaged temperature and the standard deviation of its spatial distribution

3.5 Measurements of ^{63}Cu Reaction Rate Distributions in the VHTRC-1 Core

T. Yamane, F. Akino, H. Yasuda, M. Takeuchi,
M. Yoshizawa* and Y. Kaneko

The radial and axial distributions of ^{63}Cu(n,γ)^{64}Cu reaction rate in the VHTRC-1 core were measured by the activation technique to study the accuracy of neutronic design calculation on power distribution in the experimental VHTR.

Natural Cu foils and wires were prepared for activation samples. The foils were used for the measurement of the radial, i.e. rod-wise, reaction rate distribution. Each foil had a thickness of 0.1 mm and the inner and outer diameters, 18 and 36 mm, same as the fuel compacts and was put between compacts in every fuel rod of S-3 and C-6 blocks shown in Fig.3.5.1. The axial position was 113 mm from the mid-plane, in the fixed half assembly. The axial reaction rate distribution was measured using twenty five wires of 2 mm in diameter and 10 mm long, which were set on an aluminum wire at the intervals of 50 mm and were inserted at the position denoted by "A" in Fig.3.5.1. The activity of each sample due to β-decay of ^{64}Cu was measured by counting annihilation photons with Ge detector and gross β-rays with GM counter for the foils and the wires, respectively.

Calculations were performed with the SRAC code system[1] using mainly the nuclear data based on the ENDF/B-Ⅳ, except for the data of ^{63}Cu taken from the JENDL-2 The 61-group cell calculation was carried out to yield the homogenized 10-group constants. In this calculation, the collision probability method was employed and the heterogeneity in a fuel block, i.e. a unit of lattice-cell, was treated as precisely as possible. The neutron flux distribution in the core was calculated with a diffusion code, CITATION, available in the SRAC system, using three-dimensional triangular geometry. To consider the fine structure of the flux distribution in a fuel block, the calculated radial flux distribution was modified

---

* Department of Health Physics

with the relative ratio of the flux at the outer fuel rods to that at the inner in a unit cell, which was estimated from the results of the cell calculation. Reaction rate was obtained from the flux and the effective activation cross-section which was calculated with one dimensional approximation of slab and cylinder for the foil and the wire, respectively.

In the measured radial distribution of the reaction rate, a peaking of 33 % appeared at the fuel rod nearest to the core center. The block-average reaction rate was 20 % larger in the S-3 than in the C-6 block. The experimental error at each position was estimated to be 0.8 %. Comparison between measurement and calculation was made by normalizing the data to the average of all 24 fuel rods. Figure 3.5.2 shows the deviations of the calculated from the measured values and reveals, as a whole, a fairly good agreement. The values in parentheses in this figure are those without consideration of the fine structure in a fuel block. In this case the discrepancy increased by 1 % and the calculation resulted systematically in over- and under- estimation at the inner and outer fuel rods in each block, respectively. This means that the fine structure of the flux distribution in a fuel block should be taken into account on the calculation of radial power distribution in a pin-in-block type core.

The result of the measurement for the axial reaction rate distribution was compared with that of the calculation, where each was normalized to the integrated reaction rate over the axial length of the half assembly. The two results agreed with each other almost within 2 % in the fuel region, where the experimental error was estimated to be 1 %. Near the fuel-reflector boundary, however, the discrepancy became large, up to 5 %, and the measured reaction rate tended to change more smoothly. This may be attributed to the softening of the neutron spectrum caused by the reflector, which was disregarded in the calculation of the homogenized group constants and the effective activation cross-sections.

Reference

(1) Tsuchihashi K., et al. : JAERI 1285(1983)

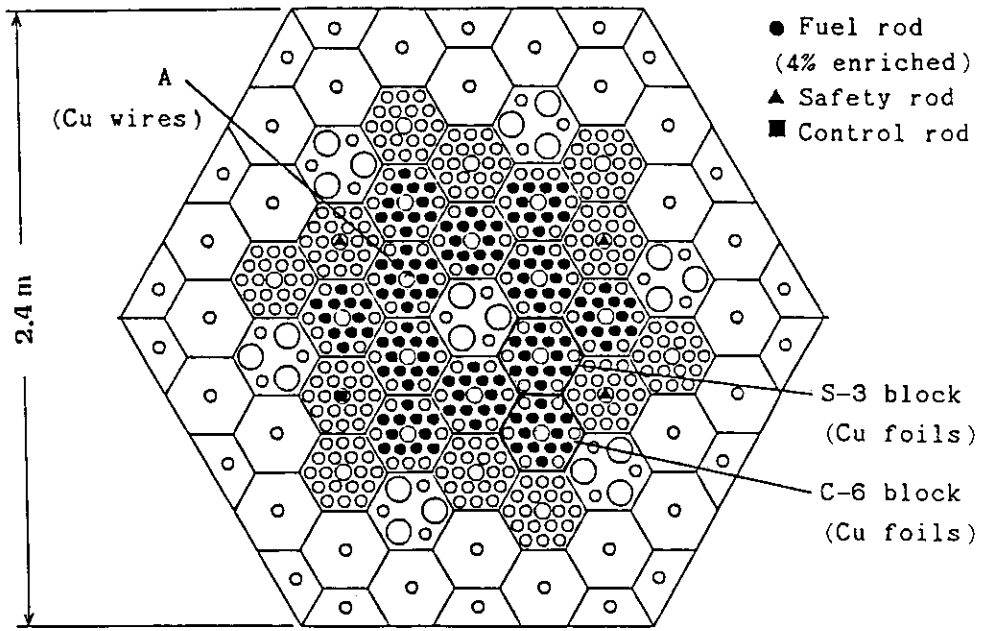

Fig.3.5.1 Arrangement of activation samples in the VHTRC-1 core

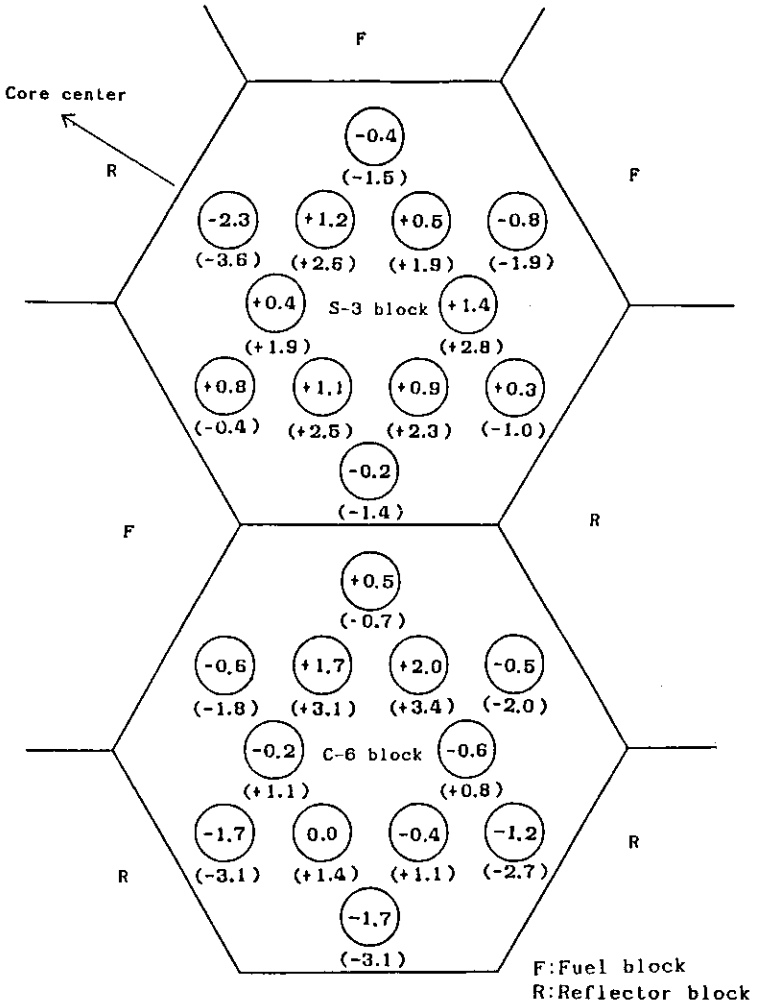

Fig.3.5.2 Comparison between the calculated and the measured distribution of the radial reaction rate in terms of (C/E-1)x100
The values in parentheses are those without consideration of the fine structure of the flux distribution in a fuel block

3.6 Evaluation of Delayed Neutron Data for Thermal Fission of ^{235}U Based on Integral Experiments Using SHE

Y. Kaneko, F. Akino and T. Yamane

Evaluation of the delayed neutron data for thermal fission of ^{235}U is attempted through an indirect measurement which is based on comparison between calculation and experiment on the following five integral quantities for Semi-Homogeneous Experiment (SHE):

Data 1 (Inverse kinetic parameter, Λ/β_{eff})

Data 2 (Central reactivity worth of Th, NU and EU rod, $\Delta k_{eff}/\beta_{eff}$)

Data 3 (Central reactivity worth of burnable poison rods, $\Delta k_{eff}/\beta_{eff}$)

Data 4 (Effective multiplication factor, k_{eff})

Data 5 (Increase of prompt neutron decay constant due to insertion of control rod, $\Delta\alpha$).

The SHE facility possesses particular advantages for the present purpose in that it is composed solely of 20% enriched UO_2 and graphite, both these components having nuclear data that are precisely known and also in that the geometrical simplicity of the cylindrical core shape provides for precise neutronic calculations.

Histogram of the percent deviations of the ratios of calculated to measured values from unity is shown in Fig. 3.6.1.

The ratios are obtained with use of the Keepin's delayed neutron data set. The plots for the Data 4 and 5 - not scaled on β_{eff} - are seen to present distributions around their own mean values which are close to zero. In contrast, for Data 1,2 and 3 - scaled on β_{eff} - their mean values are all definitely positive. The foregoing observations betake that the present nuclear data other than relevant to the delayed neutrons and also the methods adopted for the neutronic calculations are very accurate. Then, the least squares method for an indirect measurement was applied in order to find the most probable values of β_{eff} and decay constants of the precursors λs, assuming that disagreement beween calcula-

tion and experiment can wholly be attributed to the errors in the delayed neutron data used.

It is concluded that the most probable values of β_{eff} of the various SHE cores should be 4.0% higher than the values which are calculated with use of the Keepin's delayed neutron data set. This judgement leads to that Keepin's β value 0.0065 ± 0.0002 for thermal fission of ^{235}U should be corrected to 0.00676 ± 0.00011 under the assumption that Keepin's energy spectra $\chi(E)$s do not include so large uncertainties that resulting errors in β_{eff} are negligibly small. This corrected value is a little lower than both values of ENDF/B-IV and V. Experimental error of 1.7% estimated for the present indirect measurement of β_{eff} is comparable with that of ~ 3% which has often been estimated for the direct measurements. On the other hand, most probable values of λs obtained are not away from those for thermal fission filed in the Keepin's delayed neutron data set beyond their experimental uncertainties.

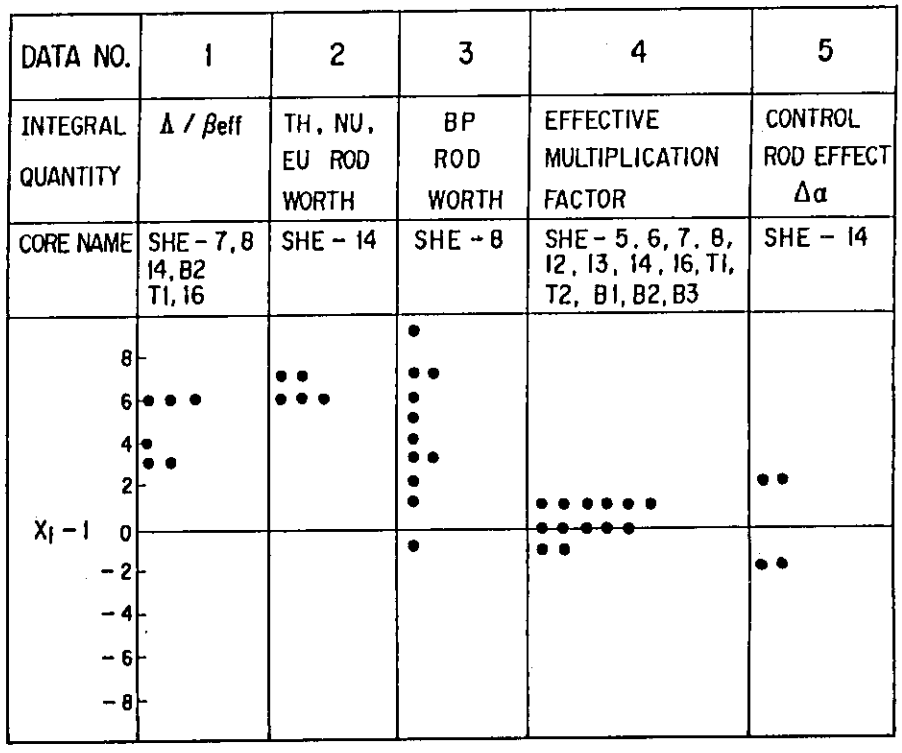

Fig. 3.6.1 Histogram of percent deviations of ratios of calculated to measured values for various integral quantities when use is made of Keepin's delayed neutron data.

3.7 Operation Report of VHTRC

K.Kitadate,H.Yoshifuji,M.Takeuchi,T.Ono, F.Yoshihara and
M.Nakano

Reconstruction work of the SHE to the VHTRC (Very High Temperature Reactor Critical Assembly), was completed in May this fiscal year. After the whole work of reconstruction was finished, the initial inspection by the Government for the new VHTRC core including initial critical approach, measurements of excess reactivity, control rod worth and reactivity temperature coefficient, have been done satisfactorily in June 1985.

After the inspection, the VHTRC was operated to perform the various reactor physics experiments. Operations were carried out for 846 hours during 98 days in this fiscal year. The total number of 178 critical operations has been recorded at the end of this fiscal year since the first critical approach on May 13, 1985. Much efforts were paid for reactor operation to measure the temperature coefficient of reactivity, because it takes about 100 hours to perform 200 ℃ experiments. The high temprature operation was carried four times without any trouble by using the whole core heating system.

Three kinds of fuel compacts used in the VHTRC have been fabricated by the end of this fiscal year. Details of the fuel compacts are given in Table 3.7.1. To improve the fuel management, a personal computer was introduced. The handling labour for the records on the fuel movement between the reactor and the fuel storage has been much saved by the computer.

The VHTRC operation data processing system was installed. The system compiles and analyses the data on reactor physics experiments as well as operation data using a 16-bit personal-computer. The systerm is equiped with many channels for analog and digital inputs, and can record not only neutron flux and control rod position data but also the other data such as core temperature and gap width between two half assemblies necessary for the reactor physics experiments. This work was done in cooperation with the Electronics Division of JAERI. The outline of the system is shown in Fig. 3.7.1

The other major activities relating to the maintenances were as

follows:

(1) Renewal of the rectifier of the battery of DC circuit, the indication panel of the puls neutron experimental instrument and the neutron source drive system, etc.

(2) Inspections of the control and the safety rod drive mechanism, the magnetic generator and the the automatic fire extinguishing system.

Table 3.7.1 Details of VHTRC fuel compacts

Fuel type	Compact		
	B - 2	B - 4	T - 6
Sort of coated fuel particles	Biso	Biso	Triso
Enrichment(%)	2	4	6
Number of compacts	3,090	6,180	3,090
Date of obtainment	Jan. 24,1985	Mar. 25,1985 Apr. 27,1985	Mar. 27,1986

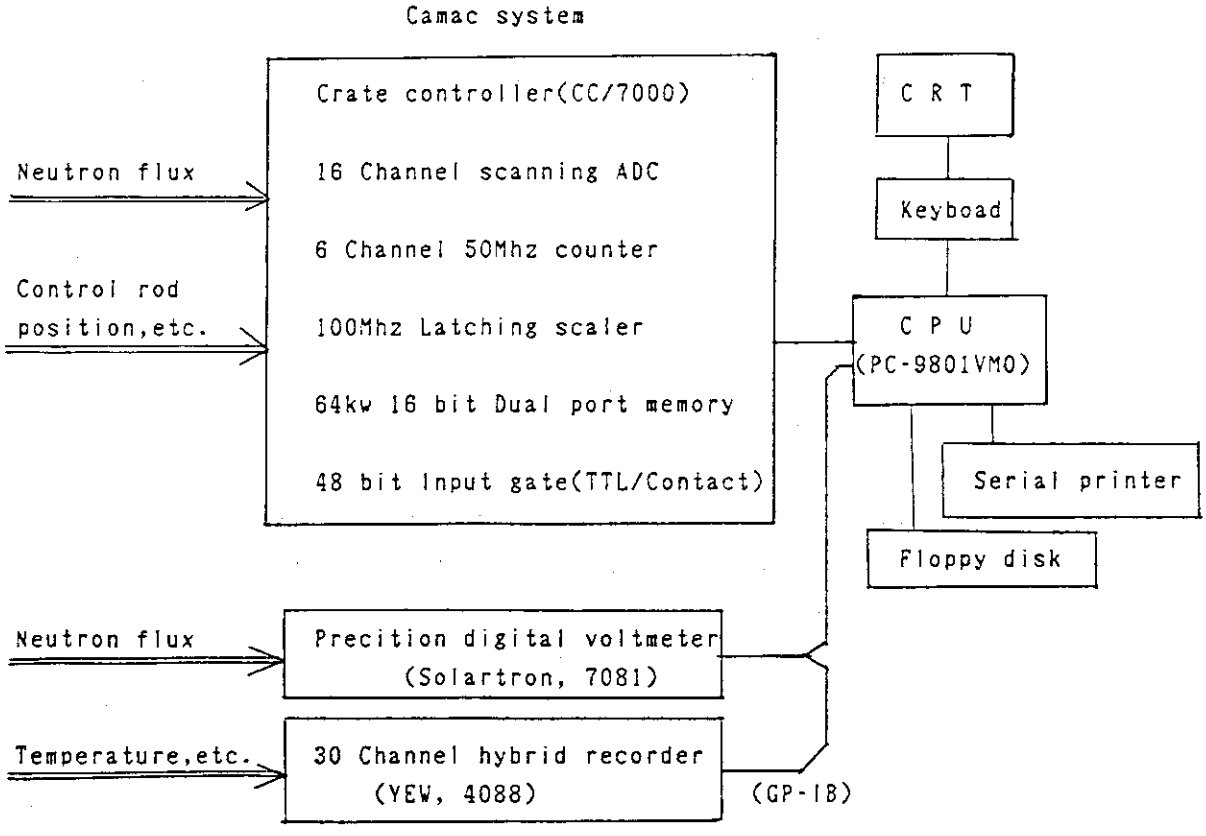

Fig.3.7.1 Outline of the VHTRC data processing system.

3.8 Preliminary Analysis for FCA XIV-1 Core

T. Osugi, H. Yoshida and S. Mashimo*

A neutronic analysis for the FCA XIV-1 core has been carried out to make it clear to what extent the core can simulate the HCLWR characteristics, especially of the neutron energy spectrum.[1] The cell calculation was made using the SRAC code system[2] with one-demensional slab model and 86 energy group cross-section file based on the Japanese Evaluated Nuclear Data Library Version 2 (JENDL-2).[3]

Figure 3.8.1 shows a two-dimensional cylinder model of the FCA XIV-1 core. The test zone with a diameter of 60 cm is surrounded by an annular buffer zone, the enriched uranium and plutonium driver zones, and the depleted uranium metal blanket region. Critical radius of the plutonium driver zone, Ro in Fig.3.8.1, was determined by a whole reactor calculation. An appropriate choice of the thickness and the material of the buffer zone are made so that the fast driver neutron spectrum is partially converted to the intermediate test zone spectrum and so that the central neutron spectrum is enabled to closely approximate that of a large single zone reactor.

To examine the effects of the buffer materials on the radial characteristics of the FCA XIV-1 core, whole reactor calculations were made using a 86-energy group diffusion approximation and 2RZ model shown in Fig.3.8.1. Three different materials of stainless steel block, carbon, and "Axial Blanket" were considered as a candidate for the buffer material, while EU08 cell with 50% polyethylene voidage for the test zone. This moderator voidage was assumed to get the appropriate value of infinite multiplication factor for the test zone cell, and to get the equivalent hydrogen atom density to that of pressurized water at operating condition.

The radial power distributions of the FCA XIV-1 core with various buffer materials are shown in Fig.3.8.2. It is found that the radial distortion of the power distribution is minimum in the case of the stainless steel buffer. The few group radial neutron flux distributions of the FCA XIV-1 core with the stainless steel buffer are shown in Fig.3.8.3. The few group fluxes were collapsed from those of the 86-group

---

* On leave from I.S.L Inc., Tokyo

calculations for convenience sake. It can be expected that the fundamental mode spectrum is well established in the inner test zone of the FCA XIV-1 core by selecting a stainless steel block as buffer material.

References

1) Osugi T. and Yoshida H. : "Experimental Program and Results of Preanalysis for a High Conversion Light Water Reactor (HCLWR) at FCA," NEACRP-A-729 (1985).
2) Tsuchihashi K., et al. : "SRAC : JAERI Thermal Reactor Standard Code System for Reactor Design and Analysis, "JAERI 1285 (1983).
3) Nakagawa T. (Ed.) : "Summary of JENDL-2 General Purpose File," JAERI-M 84-103 (1984).

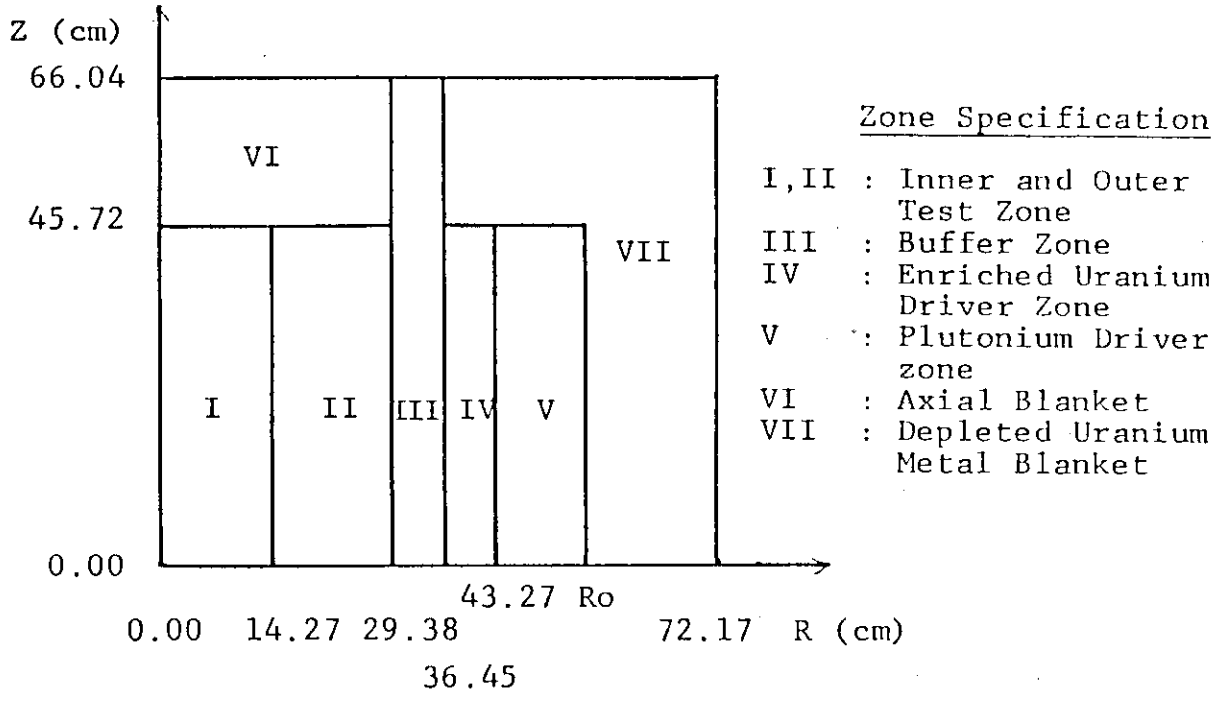

Fig.3.8.1 Two-dimensional cylinder model of the FCA-XIV core

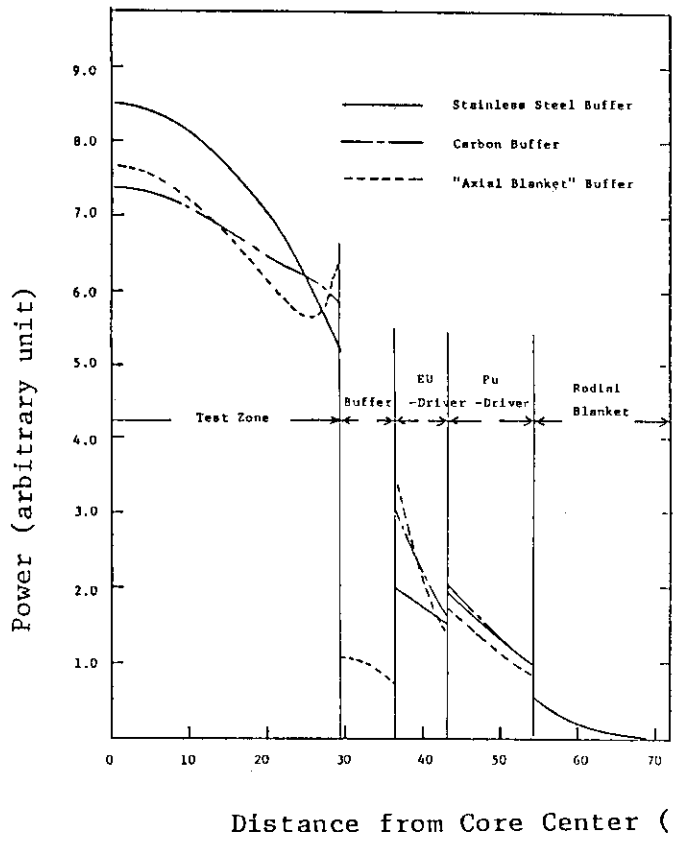

Fig.3.8.2 Radial power distributions for the FCA-XIV core with EU08 test zone and various buffer material

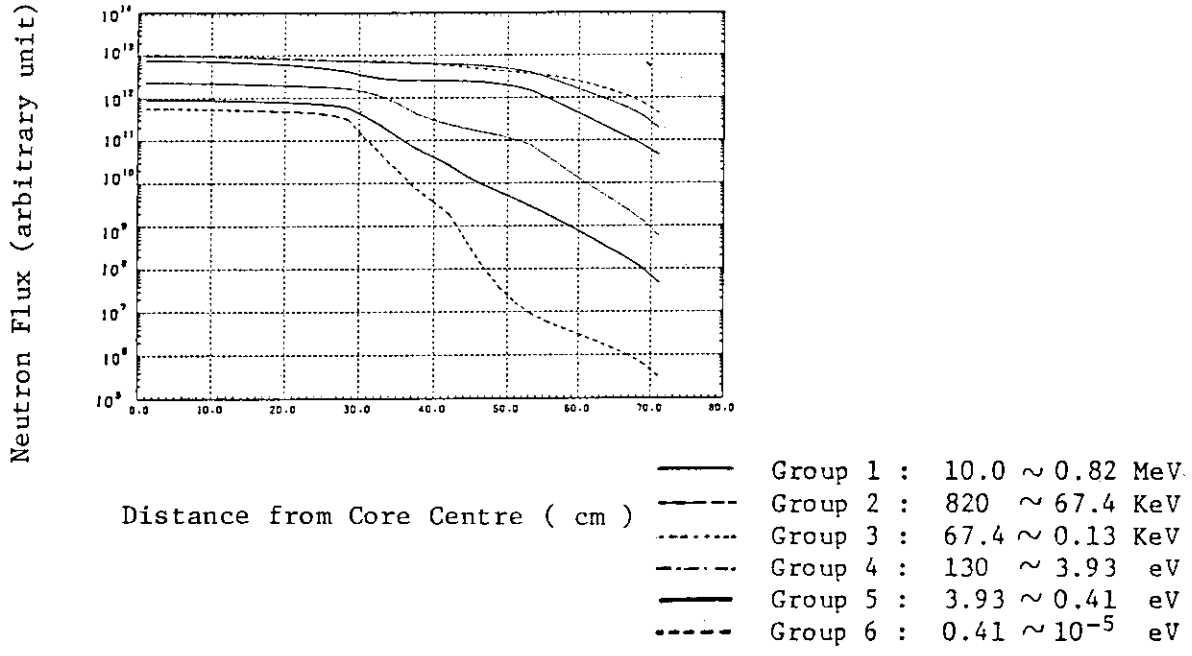

Fig.3.8.3 Few group neutron flux radial distribution for the FCA-XIV core with EU08 test zone and stainless steel buffer zone

3.9 Analysis of Fuel Slumping Experiment at FCA Assembly XII-1

S. Iijima, M. Ōbu, T. Koakutsu, T. Hayase*, N. Tsuji** and K. Satoh

Fuel slumping experiments have been made using FCA Assembly XII-1 in order to study reactivity effects caused by fuel displacement on a core disruptive accident of an axially heterogeneous LMFBR. The experimental results were analyzed in order to examine the reliability of the current data and method for an accident analysis. A fuel slumping zone consists of the nine T2B2 drawers was prepared at the center of the test region of Assembly XII-1. Plate arrangement of the T2B2 drawer is shown in Fig.3.9.1. A unit cell (2inch x 2inch x 2inch) simulating core or blanket fuel was loaded in the T2B2 drawer. First two cells of the T2B2 drawer constitute the internal blanket region and next seven cells the core region. Whole sodium plates of the fuel slumping zone were replaced by stainless steel empty can in order to simulate voided sodium condition.

The reactivity change caused by fuel displacement were measured using the ten core models simulating the fuel slumping condition. In each core model, fuel components (plutonium, uranium and aluminum oxide plates) were moved to different place in the drawers.

Core model (Fuel and aluminum oxide plate movement)

Position		100%	50%
(5Z, 6Z) → (3Z, 4Z)	:	Model-1	Model-6
(5Z, 6Z) → (1Z, 2Z)	:	Model-2	Model-7
(5Z, 6Z) → (7Z, 8Z)	:	Model-3	Model-8
(5Z, 6Z) → (10Z, 11Z)	:	Model-4	Model-9
(3Z, 4Z) → (1Z, 2Z)	:	Model-5	Model-10

Whole fuel were moved in the model-1 through model-5. While 50% fuel were moved in the model-6 through the model-10. Reactivity changes were measured as the difference of the reactivity between the reference core and the fuel slumping core.

* Hitachi, Ltd.

** Fuji Electric, Co.,Ltd.

Experimental results were analyzed using the cross section library JENDL-2[1] and the standard calculation system[2)3)] for fast reactor neutronics. Base calculations of the reactivity changes were made using the first order perturbation method and exact perturbation method based on diffusion theory. Transport correction was applied to the calculation result. The experiment and calculation results for the reactivity changes were shown in Table 3.9.1.

The first order perturbation method is not available in this analysis since there is large discrepancy between the experiment and the calculation result. The calculation values were fairly improved by using the exact perturbation method. It is clear in this analysis that transport calculation is very useful and important. Large differences in C/E values are seen between the 100% and 50% fuel movement models.

References

1) Nakagawa T. : Summary of JENDL-2 General Purpose File, JAERI-M 84-103 (1984).
2) Nakagawa M., Abe J. and Sato W. : Code System for Fast Reactor Neutronics Analysis, JAERI-M 83-066 (1983).
3) Iijima S. : to be published.

Table 3.9.1 Reactivity change in fuel slumping experiment of FCA Assembly XII-1

(unit : ρ)

	Experiment	First order	Exact per.	Corrected by trans.	C/E
Model-1	0.276 ± 0.005	0.018	0.144	0.177	0.641
Model-2	0.192 ± 0.005	0.095	0.174	0.145	0.755
Model-3	-0.045 ± 0.005	-0.414	-0.186	-0.089	1.976
Model-4	-1.051 ± 0.005	-1.391	-1.177	-1.052	1.001
Model-5	0.097 ± 0.005	0.027	0.103	0.082	0.845
Model-6	0.074 ± 0.005	0.034	0.058	0.073	0.986
Model-7	0.073 ± 0.005	0.110	0.118	0.066	0.904
Model-8	-0.077 ± 0.005	-0.161	-0.111	-0.092	1.200
Model-9	-0.555 ± 0.005	-0.630	-0.577	-0.553	0.996
Model-10	0.025 ± 0.005	0.080	0.084	0.036	1.440

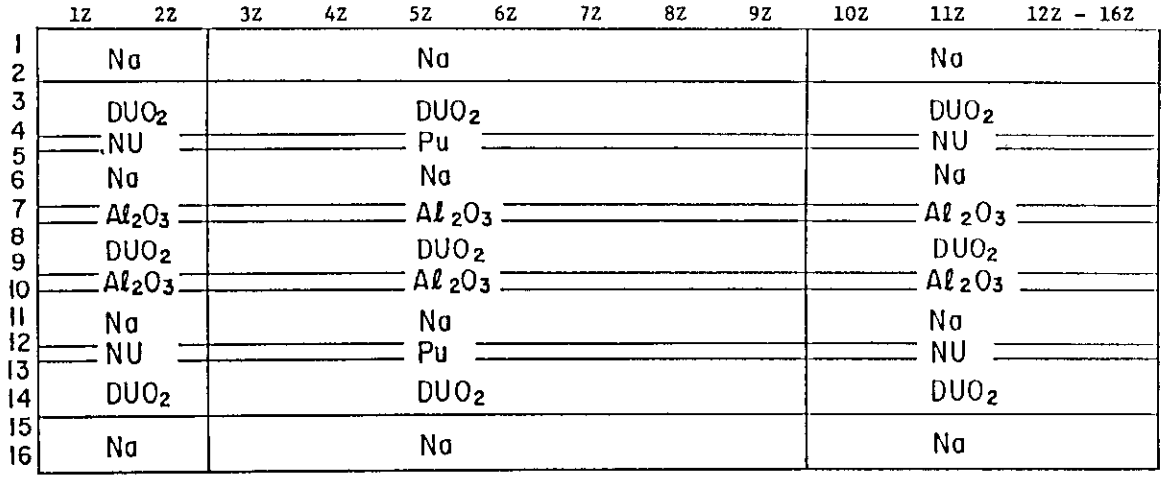

Fig.3.9.1 Plate arrangement of T2B2 drawer in FCA Assembly XII-1

3.10 Experiments on FCA Assembly XII-2 and Their Analysis

S. Okajima, S. Iijima, T. Hayase*, M. Ōbu, T. Koakutsu and N. Tsuji**

The FCA Assembly XII-2, having an internal blanket 30 cm thick,[1] was the third core in the axially heterogeneous core experiment program at FCA.[2] The purpose of the experiment in this assembly was to examine the influence on the nuclear characteristics by increasing the internal blanket thickness from 20 cm to 30 cm. From this point of view, the following were measured : (i) criticality, (ii) reaction rate distribution and its ratio and (iii) sample reactivity worth and sodium void worth.

Assembly XII-2 was a zone type core which is composed of a test region, a driver region and a radial blanket. The core height was 91.4 cm, including the internal blanket 30 cm thick and the total core volume of the test region was 248 liters. The fissile enrichment in the test region was 13.4 w/o. Figure 3.10.1 depicts an R-Z model of this assembly.

In the reaction rate experiment, the axial distributions of fission rate for ^{235}U, ^{238}U, ^{237}Np and ^{239}Pu and capture rate for ^{238}U were measured by using micro fission counters and depleted uranium foils. The sample reactivity worths of ^{239}Pu, depleted uranium, stainless steel and natural B_4C were also measured along the axial direction. In this measurement, plate samples were used and substituted for the appropriate spacer loaded in the core cell. Reactivity was determined from the calibrated control-rod positions. The ^{239}Pu sample worth distribution is shown in Fig.3.10.2.

An analysis of these experiments has been carried out by the use of the JAERI's standard calculation system for fast reactor neutronics analysis and the group constant set JFS-3-J2 with 70 group structure.[3] The transport corrections were applied to obtain the final calculated results.

It is shown in Table 3.10.1 that the calculated value for criticality overestimates the experimental one by 0.7%. The similar tendency is observed in the other assemblies of the program. The calculation of reaction rate distributions shows a good agreement with the experimental results in the core region, but it give underestimates in the internal blanket except for ^{238}U fission rate, and the same situations are

* On leave from Hitachi, Ltd.

** On leave from Fuji Electric, Co., Ltd.

recognized in the other cores. For sample worth and sodium void worth, agreements between the calculated and measured values are poor, and most calculated values are smaller than the measured ones.

References

1) Okajima S., et al. : "Experimental Study of Large Scale Axially Heterogeneous LMFBR Core at FCA (V)," JAERI-M 86-016 (in Japanese) (1986).
2) Iijima S., et al. : "Experimental Study of Large Scale Axially Heterogeneous LMFBR Core at FCA (I)," JAERI-M 84-076 (in Japanese) (1984).
3) Takano H. and Ishiguro Y. : "Production and Benchmark Tests of Fast Reactor Group Constant Set JFS-3-J2," JAERI-M 82-135 (1982).

Table 3.10.1 Calculation results for criticality of FCA Assemblies

Assembly	XII-2 (30cm I.B.*)	XI-2 (20cm I.B.)	XII-1 (20cm I.B.)	XI-1 (0cm I.B.)
Cal. Keff (ref.)**	1.0001	1.0014	0.9993	0.9996
correction				
Transport	0.0103	0.0097	0.0092	0.0089
Mesh	-0.0021	-0.0021	-0.0022	-0.0021
Keff (corrected)	1.0083	1.0090	1.0063	1.0064
Experiment	1.0016	1.0030	1.0009	1.0007
C/E	1.0067	1.0060	1.0053	1.0057

* I.B.:Internal blanket
** 3D(X-Y-Z), 25 Groups

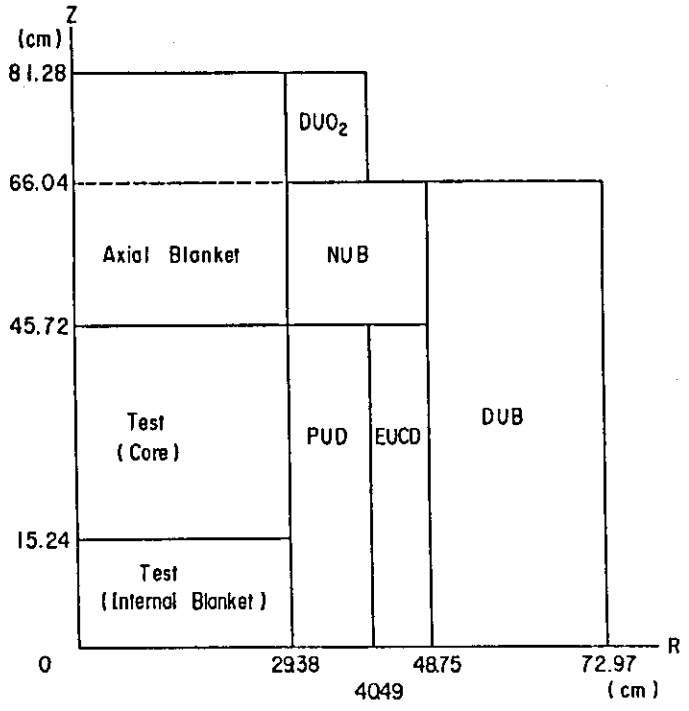

Fig.3.10.1 R-Z model of FCA Assembly XII-2

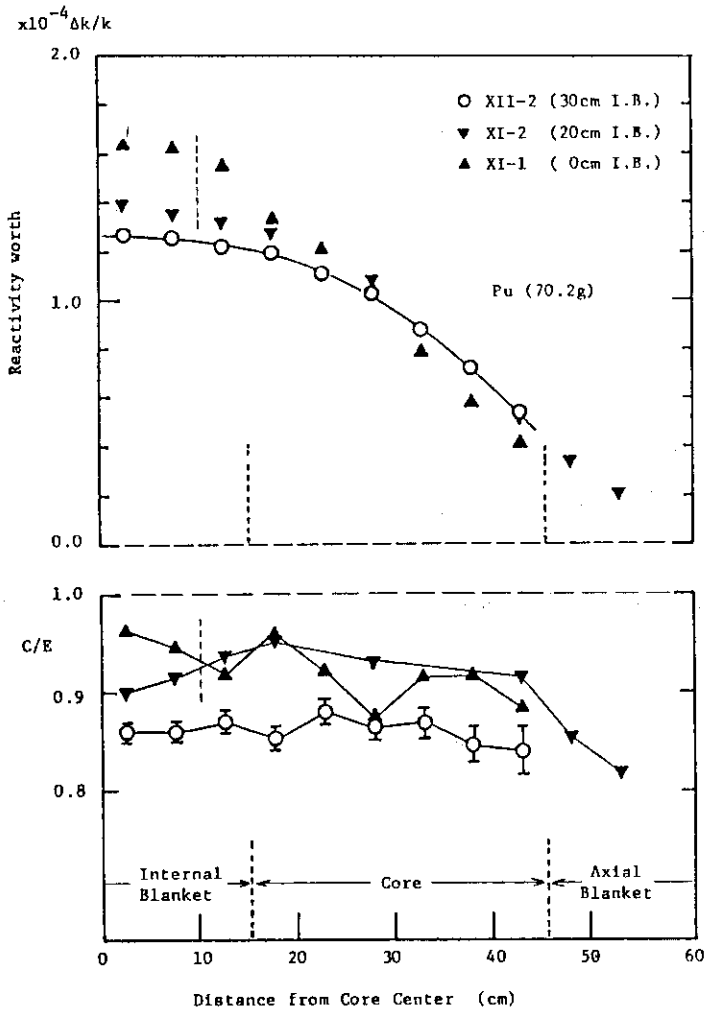

Fig.3.10.2 Axial distributions of Pu sample worths and thier C/Es in FCA Assemblies

3.11 Experimental Study of Large Scale Axially Heterogeneous LMFBR Core at FCA Assembly XIII-1

S. Iijima, S. Okajima, T. Hayase*, M. Ōbu, T. Koakutsu, T. Sakurai, T. Osugi, A. Ohno and K. Satoh

The critical experiment using the Fast Critical Assembly (FCA) of JAERI was planned in order to study fundamental nuclear characteristics of a large scale axially heterogeneous LMFBR and to examine the reliability of the current data and method used on the core design. In the experiment axial and radial nuclear characteristics have been measured using the respective partial mockup cores since enough plutonium fuel is not prepared for the construction of a full mockup core in FCA. Axial nuclear characteristics have been measured on the series of the experiments using Assembly XI and XII. Following those experiments, the radial nuclear characteristics have been measured using Assembly XIII-1 and XIII-2 from July 1985 to February 1986.

Assembly XIII-1 is the standard core in the experiment, (i) criticality, (ii) reaction rates and rate ratios, (iii) power distributions, (iv) material sample worths and (v) B_4C control rod worth have been measured. Experiment of the Assembly XIII-2 was made to examine the influence on the power distribution and control rod worth caused by the modification of the radial boundary shape between the internal blanket and the core. Assembly XIII-1 and XIII-2 have the similar core and blanket region except the radial boundary. The same core and blanket fuel were loaded in both assemblies.

The experimental results were analyzed using the JENDL-2 cross sec tion library and the standard calculation system of JAERI.

Assembly XIII-1 is a sector type partial mockup core and has the test region simulated a core and an internal blanket of an axially heterogeneous LMFBR. The fuel drawers simulating plutonium oxide fuel of an axially heterogeneous LMFBR were loaded in the test region. The disk shaped internal blanket loading the fuel drawers which consists of natural and depleted uranium plates was placed at the middle of the test region. Plutonium enrichment of the core fuel is 18.4 w/o. This value is by about 4% higher than that of the large scale axially heterogeneous LMFBR. The

* Hitachi, Ltd.

core height including the internal blanket is about 81cm and the thickness of the internal blanket is about 30cm. Axial blanket of 35cm thick was placed at upper and lower positions of the core. Cross section view at the midplane of XIII-1 is shown in Fig.3.11.1 and R-Z model is shown in Fig.3.11.2. The test region is surrounded radially by the driver region loading the fuel drawers which consists of 93% and 20% enriched uranium plates. Infinite multiplication factor (K_∞) of the driver region is equall to the value of the core of the test region. A few fuel drawers with lower value of K_∞ were added at the outer boundary of the driver region.

Excess reactivity of the reference core was determined from the calibrated control rod position. The reactivity scale based on the positive period measurement was converted to the absolute unit of $\Delta K/K$ using the calculation value of β_{eff}. The delayed neutron data evaluated by Tomlinson was utilized in the β_{eff} calculation. The basic calculation for K_{eff} was made using anisotropic diffusion calculation in X-Y-Z geometry and 25 energy group constants generated from JENDL-2. Transport and mesh correction were applied to the result. The summary of K_{eff} value is shown in Table 3.11.1. The C/E value for K_{eff} is 1.008 and this value is by about 0.3% larger than that of Assembly XII-1.

The reaction rates and B_4C control rod worth were measured in the experiment of Assembly XIII-2. The experiment and calculation results were compared with those of Assembly XIII-1.

Table 3.11.1 Criticality in FCA Assembly XIII-1

(unit : $\Delta K/K$)

[Experiment]	
Excess reactivity(as built)	0.00142 ± 0.000005
Correction	
Subcriticality	-0.00005 ± 0.000001
Gap effect	0.00092 ± 0.000131
SS effect at midplane	-0.00004 ± 0.000003
K_{eff}	1.0022 ± 0.0001
[Calculation]	
Base calculation(K_{eff})	1.0044
Correction	
Transport	0.0068
Mesh	-0.0010
Corrected	1.0102
C/E	1.0080

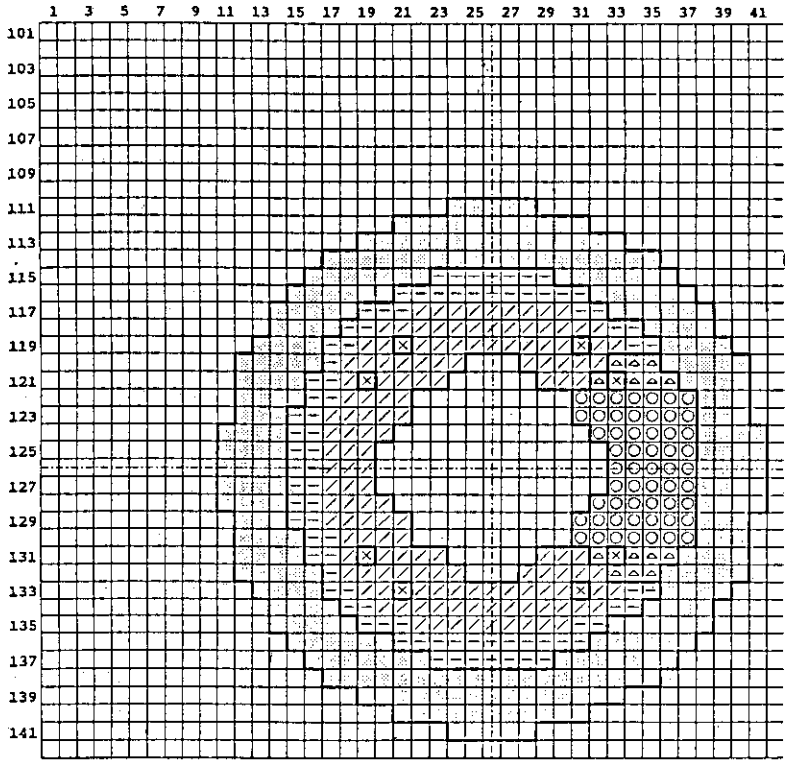

	Drawer	Number
□	T3B3	113
◎	T3	55
△	T3D81	14
▨	HEUCD	145
▤	EUCD	86
⊠	CR	8
□	DUB	308

Fig.3.11.1 Cross section view of reference core of FCA Assembly XIII-1

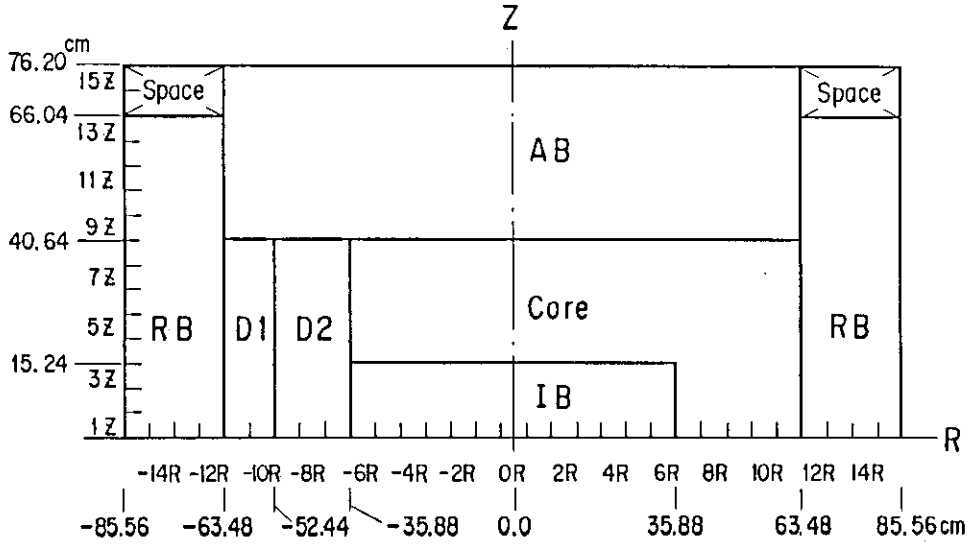

Fig.3.11.2 Vertical cross section of FCA Assembly XIII-1

3.12 Measurement of Sample Worth at FCA Assembly XIII-1

S. Okajima, S. Iijima, T. Hayase* and T. Sakurai

Measurements of small sample worths have been performed at FCA Assembly XIII-1 which is a mock-up core on an axially heterogeneous LMFBR.[1)]

Pu and natural B_4C samples (shown in Table 3.12.1) were used in this measurement. Reactivity change was determined from the calibrated control-rod position. The reactivity scale based on the positive period method was converted to the absolute unit of $\Delta k/k$ using the delayed neutron data evaluated by Tomlinson.[2)] The measured reactivity change was corrected for a drift of the core temperature using the core temperature reactivity coefficient determined experimentally. The experimental error in the measurement of the small reactivity change was estimated to be $\pm 2 \times 10^{-6}$ $\Delta k/k$, except for the uncertainty of the kinetic parameters used in the control-rod calibration. The measurements were carried out as a function of radius and height, being concentrated in the vicinity of the boundary between the internal blanket and the core.

An analysis of this experiment was carried out with the JAERI's standard code system for fast reactor neutronics analysis and the constant set JFS-3-J2 with 70 group structure.[3)] Calculated results for the sample worth were obtained from the first order perturbation method based on three-dimensional diffusion theory. Finally, these results were corrected for the transport effect.

Tables 3.12.2 and 3.12.3 show the measured and calculated values in each cell for ^{239}Pu and natural B_4C sample worths, respectively. The calculation underestimates the measured values for both samples. The C/E values range from 0.88 to 0.95 for ^{239}Pu sample and from 0.90 to 0.98 for natural B_4C sample. The C/E axial distributions for ^{239}Pu sample worth at OR and 6R have the same tendency, in which the values at the edge of the internal blanket and at the middle of the core are larger than those at other positions. On the other hand at 7R and 9R the C/Es have flat axial distribution. These two different trends in C/E were also recognized for the natural B_4C sample worth.

---

* On leave from Hitachi Ltd.

References

1) Iijima S., et al. : "Experimental Study of Large Scale Axially Heterogeneous LMFBR Core at FCA (VI)," JAERI-M 86-065 (in Japanese) (1986).
2) Tomlinson L. : "Delayed Neutrons form Fission," AERE-R 6993 (1972).
3) Takano H. and Ishiguro Y. : "Production and Benchmark Tests of Fast Reactor Group Constant Set JFS-3-J2," JAERI-M 82-135 (1982).

Table 3.12.1 Data of material used on sample worth measurement

Pu(92)	
Dimension(inch)	2-2-1/16
Isotope	Weight(g)
^{239}Pu	32.119
^{240}Pu	2.843
^{241}Pu	0.268
Cr	1.79
Fe	7.51
Ni	1.01
Al	0.52

B_4C	
Dimension	2-2-1/4
Isotope	Weight(g)
^{10}B	4.16
^{11}B	18.56
Cr	7.29
Fe	28.25
Ni	3.40
C	6.36

Table 3.12.2 Experimental Results of Pu(92) sample worth in FCA Assembly XIII-1

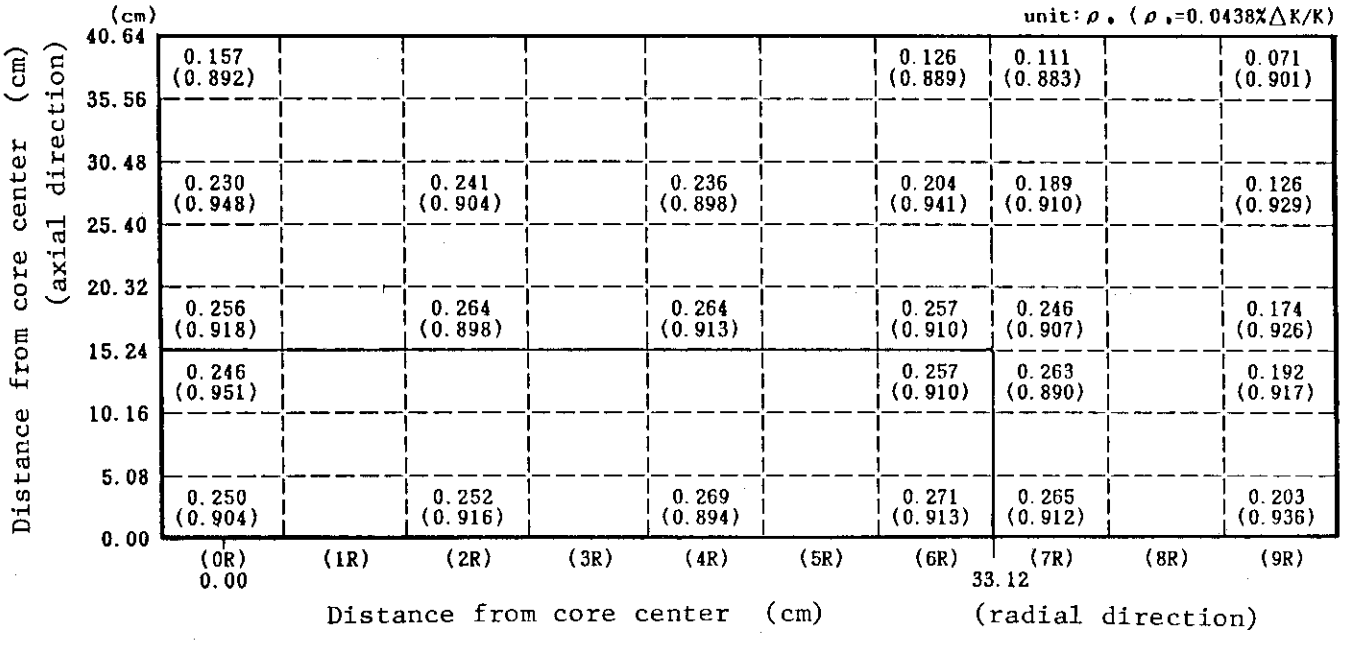

* experimental error:±0.004 ρ$_e$
** Value in parentheses means the C/E value.

Table 3.12.3 Experimental results of Nat. B_4C sample worth in FCA Assembly XIII-1

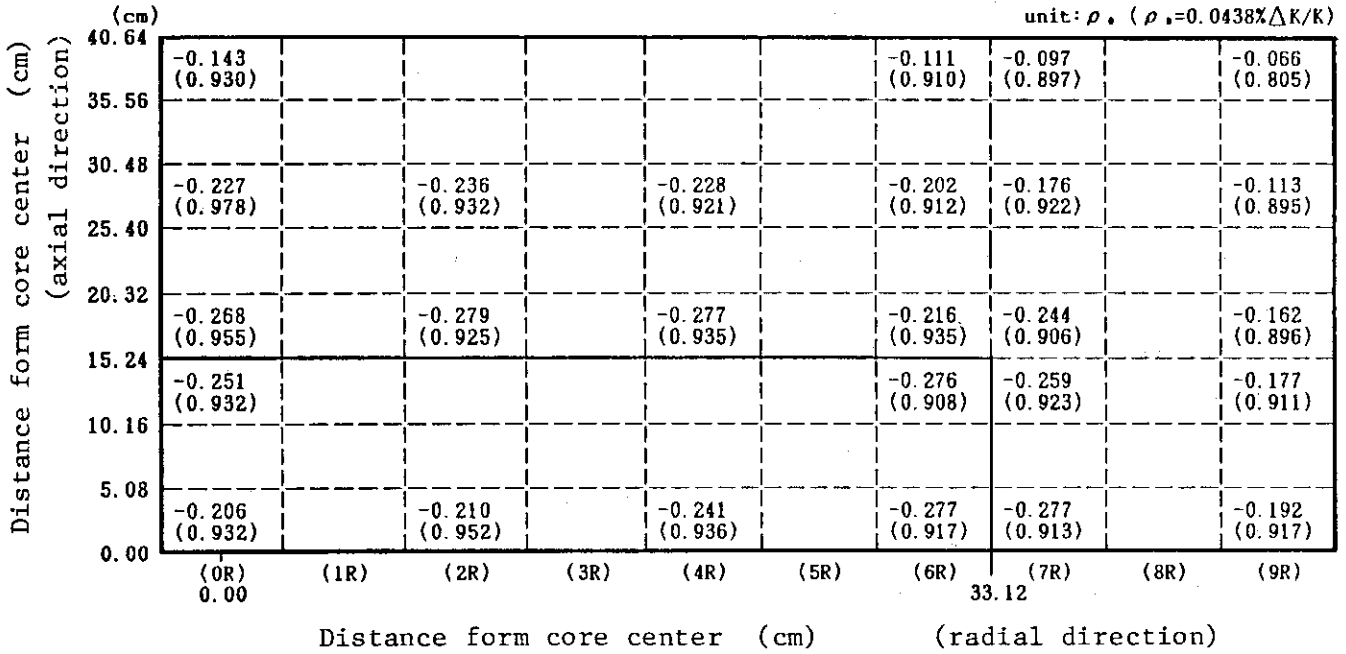

* experimental error:±0.004 ρ$_e$
** Value in parentheses means the C/E value.

3.13 Measurement of Reaction Rates at FCA Assembly XIII-1

M. Ōbu, T. Koakutsu, K. Satoh, S. Iijima and T. Sakurai

Radial reaction rates were measured at the FCA Assembly XIII-1[1] using fission counter and foil techniques. The purpose of this measurement was to clarify radially characteristics of the flat power distribution which occurs in existance of the internal blanket. It is also important to confirm the changes in reaction rates in the vicinity of the internal blanket, since neutron spectrum in the internal blanket is significantly softer than that of the core region.

Micro fission counters with thin aluminum wall were used for the measurement of fission rates of ^{239}Pu, ^{235}U, ^{238}U and ^{237}Np, while depleted uranium foils were used for the measurement of ^{238}U capture rate. Measured positions in the Assembly XIII-1 are illustrated in Fig.3.13.1. The radial traverse measurement was made at three positions along a axial direction : (1) the position 1Z in the internal blanket region (2) the position 4Z in the core region near the internal blanket interface and (3) the position 6Z in the core region far from the internal blanket. The fission pulse rates from the micro fission counters were measured by using a conventional electornic system. For the ^{238}U capture rates, gamma-activities of ^{239}Np produced from the irradiated foils were measured by a gamma-ray spectroscopy system including a coaxial type Ge-detector.

The calculation of reaction rates was based on an anisotropic diffusion theory using the JFS-3-J2 cross section set.[2] The calculation was made initially in 25-group anisotropic diffusion calculation with three dimensional XYZ model and a transport correction was applied to that result.

Fission rate distributions of ^{239}Pu at the position 1Z, 4Z and 6Z of FCA Assembly XIII-1 are shown in Fig.3.13.2, as an example. The distributions, both the measured and calculated results, are normalized to unity at the center of position 6Z to make consistent comparisons. Asymmetrical features appearing in the distributions are due to some structual effect of the enriched uranium driver. As seen in the figure, the ^{239}Pu fission rate distributions become fairly flat. A similar tendency is observed for the ^{235}U fission and the ^{238}U capture rate

results. For the ^{238}U fission and ^{237}Np fission rate distributions, the high energy sensitive materials, more flatter characteristics are obtained in particular in the internal blanket region where neutron specturm is soften.

The calculated values of ^{239}Pu fissions in the core region are in good agreement with the measured ones within 2%. However, they give slight underestimates near the internal blanket interface and about 7% underestimates in the internal blanket region.

References

1) Iijima S., et al. : "Experimental Study of Large Scale Axially Heterogeneous LMFBR Core at FCA Assembly XIII-1," 3.11 in this report (1986).
2) Takano H., et al. : "Production and Benchmark Tests of Fast Reactor Group Constants Set JFS-3-J2," JAERI-M 82-135 (1982) (In Japanese).

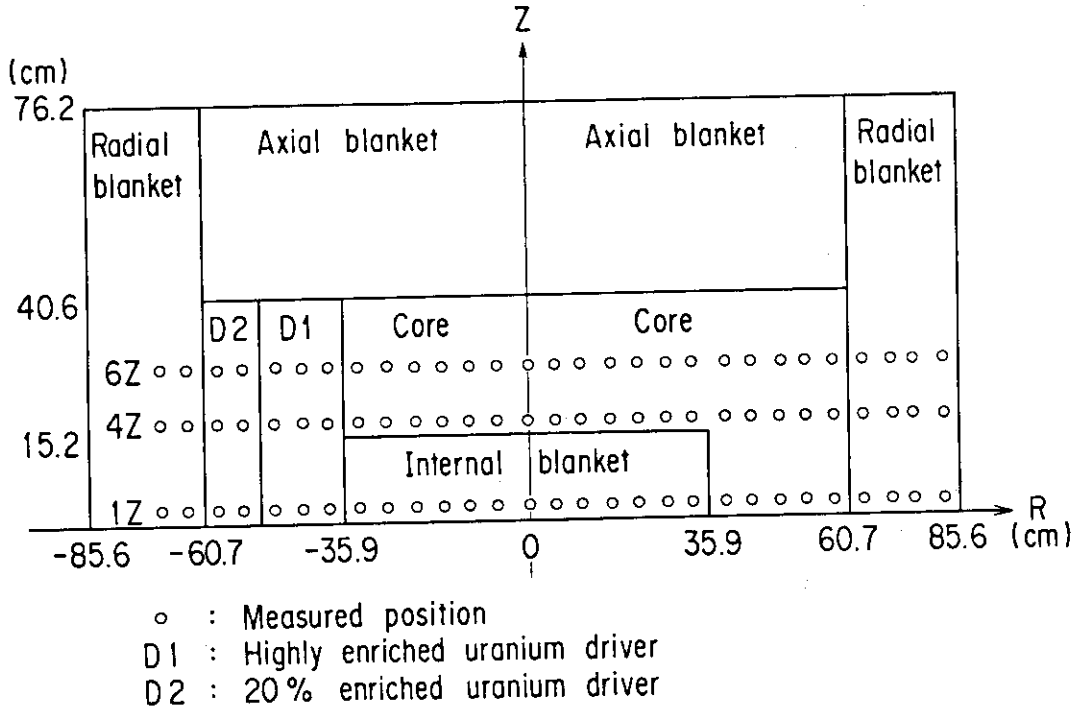

Fig.3.13.1 R-Z configuration and measured positions in FCA Assembly XIII-1

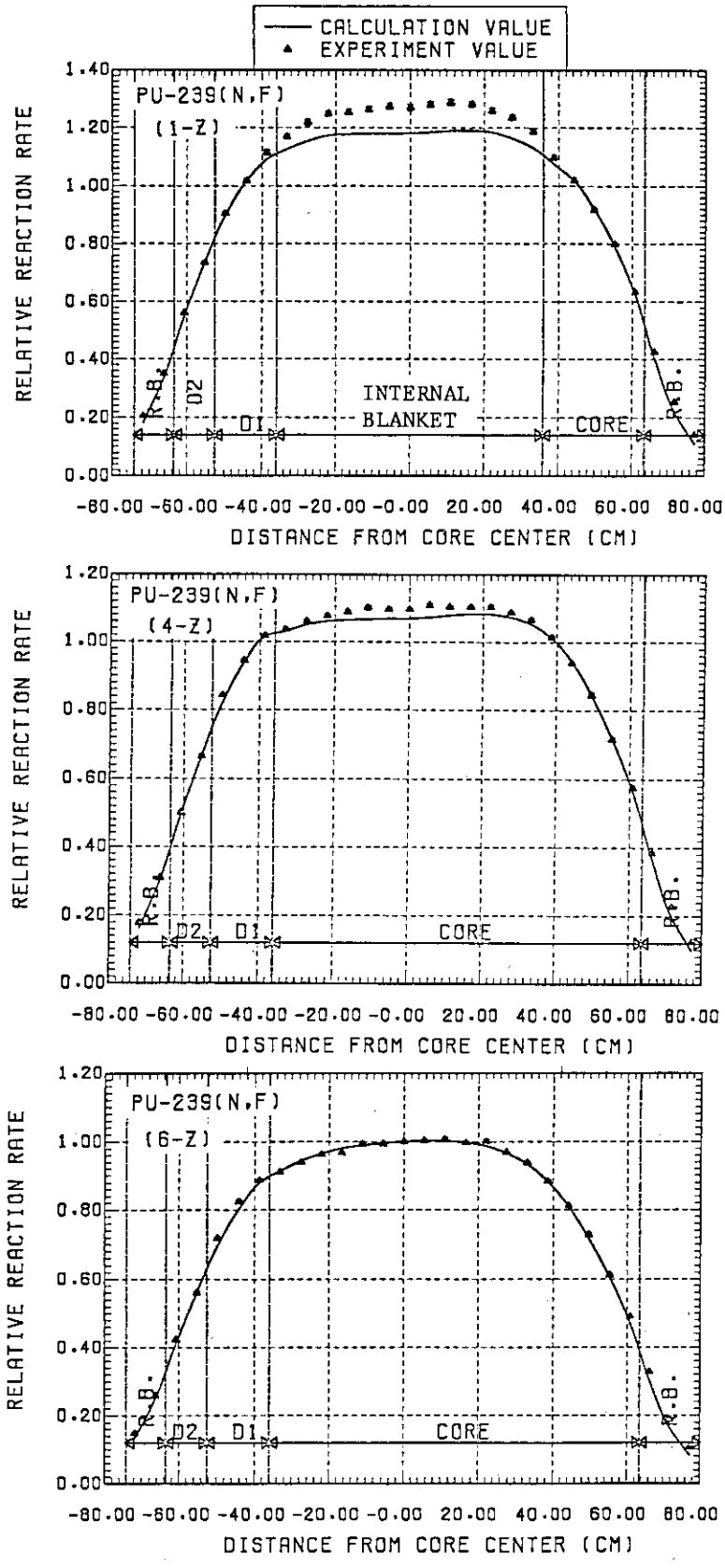

Fig.3.13.2 Radial ^{239}Pu fission rate distributions at position 1Z, 4Z and 6Z in FCA Assembly XIII-1

3.14 Measurement of Power Distribution in FCA XIII Core by γ-Scanning Method

A. Ohno, T. Osugi, K. Satoh and W. Sato*

Measurements of relative power distributions were made on the FCA XIII-1 and FCA XIII-2 core by means of γ-scanning method.[1),2)] Both the cores were the partially simulated cores of the axially heterogeneous FBR, and had the test region of the sector type to simulate the radial characteristics of the core. Figure 3.14.1 shows the R-Z model of the cores. They have the inner blanket at the core midplane. The FCA XIII-1 core has the inner blanket of 30cm thick, while the FCA XIII-2 core has the inner blanket of 30cm and 10cm thick as shown in Fig.3.14.1. The volume of the inner blanket in the FCA XIII-2 core was kept to be equal to that in the FCA XIII-1 core. The relative power of the channels in the test region were measured by the γ-scanning method.

Figure 3.14.2 shows the measured and the calculated channel powers of both cores, of which center channel power is normalized to unity. The almost constant channel powers are observed from OR to 6R in the FCA XIII-1 core, while those are from OR to 5R in the FCA XIII-2 core. The maxium channel power was 1.45 for the FCA XIII-1 at 7R and 1.29 for the FCA XIII-2 core at 6R.

The power peaking factors for both cores were calculated from the measured powers. The definition of the power peaking factor is the ratio of the maxium power to the average power in the core region. In this calculation, the inner blanket is excluded as well as the outer blanket, because the powers in the inner and outer blanket is fairly small. The obtained power peaking factors are 1.39 ± 1.5% and 1.45 ± 1.5%, for the FCA XIII-1 and the FCA XIII-2 core, respectively. The corresponding calculated values are 1.35 and 1.40, and they agreed well with the measured values. From this measurement, following results are obtained :

1) The introduction of the inner blanket at the core midplane is effective to make the power flattening in the core.
2) The change in the shape (thickness) of the inner blanket can bring the flattening of the channel power. In this measurement the maxium

---

* Japan Information Service Co., Ltd.

channel power in the FCA XIII-1 core is decreased by about 12% in the FCA XIII-2 core.

3) The calculated values agreed well with the measured ones.

Reference

1) Ohno, A., Osugi, T. and Satoh, K. : "Measurement of Relative Power Distribution at Fast Critical Assembly using Gamma Counting Method," J. Nucl. Sci. Technol., 22 [1], 76 (1985).

2) Satoh, K., Osugi, T. and Ohno, A. : Measurement of Relative Power Distributions in the Axially Simulated Heterogeneous FBR Cores by γ-scanning Method," JAERI-M 85-207 (1985).

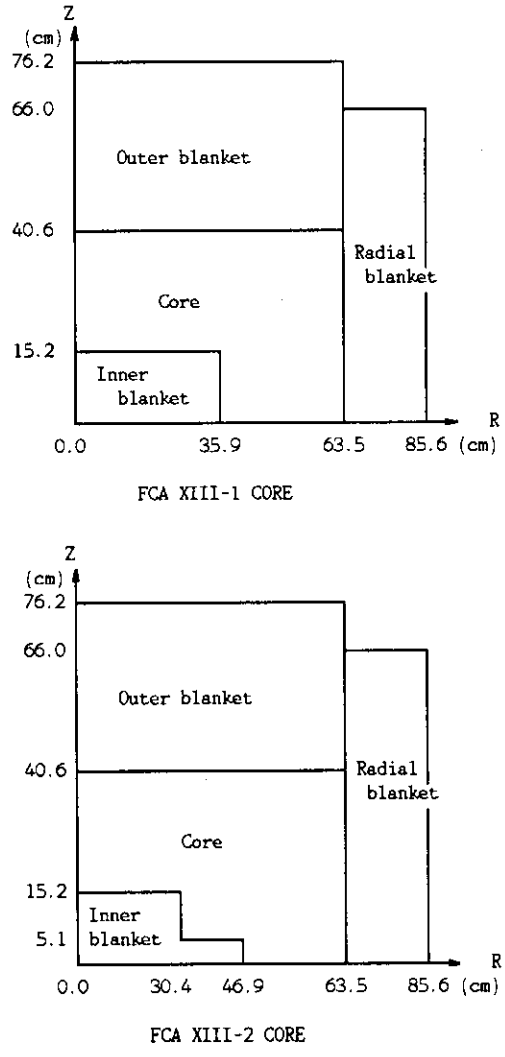

Fig.3.14.1 R-Z model of FCA XIII-1 and FCA XIII-2

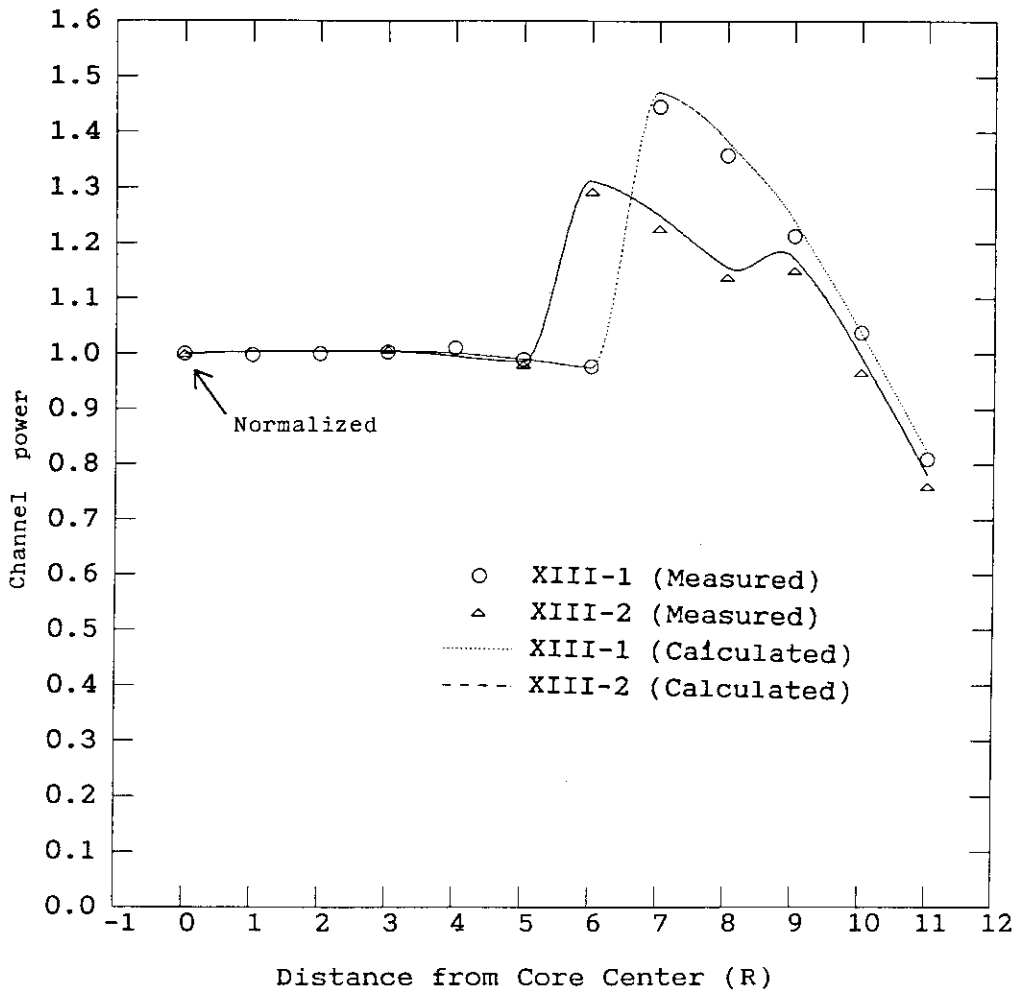

Fig. 3.14.2 Measured and calculated channel power depending on radial position in FCA XIII-1 and FCA XIII-2 core

3.15 Experiment on Fundamental Feasibility of Subcriticality Monitor at FCA

N. Tsuji*, A. Ohno and T. Osugi

Measurements for evaluating the feasibility of a subcriticality monitor were done at FCA. The monitor aims at determining the subcriticality $[1-(1/K_{eff})]$ of multiplying systems such as a spent fuel storage by measuring a change in neutron spectrum depending on the subcriticality. To measure the neutron spectrum change, two detectors called a paired detector, having different sensitivities for neutron energies, were used at the FCA. One was a ^{235}U fission counter and the other was a ^{237}Np fission counter. The ^{235}U fission counter has a high sensitivity to lower energy neutrons. On the contrary, the ^{237}Np fission counter has a high sensitivity to higher energy neutrons and has no sensitivity to neutrons less than 200 keV.

Measurements were done by using the FCA XII-1 assembly. The paired detector was placed in the core region in the half assembly (F-side). The subcriticality of the core was varied from 0 to 17 % $\Delta k/k$ by changing the gap width between the two half assemblies. The subcriticality was determined by the modified neutron source multiplication method. Figure 3.15.1 shows R-Z model of the FCA XII-1 assembly and the position of the paired detector.

The measured count rate ratios R ($^{235}U/^{237}Np$) were plotted against the subcriticality and are shown in Fig.3.15.2. The count rate ratios were normalized by a value at near critical. It is seen in the Figure that the count rate ratio decreases monotonically as the subcriticality of the assembly increases.

From this measurement, the following conclusions were obtained :

(1) The neutron spectrum change was clearly observed depending on the degree of subcriticality of the assembly.

(2) The count rate ratios R ($^{235}U/^{237}Np$) decrease monotonically with increase of subcriticality of the assembly,

(3) It is necessary to develope the detector that has a high sensitivity for higher energy neutrons to achieve high count rates.

(4) To estimate the subcriticality, it is necessary to normalize the count

---

* Fuji Electric Co.,Ltd.

rate ratios R by the value at near critical. In practical cases, however, the value at the near critical can not be determined experimentally. Necessity is to develope the method of estimating the normalization value at the near critical.

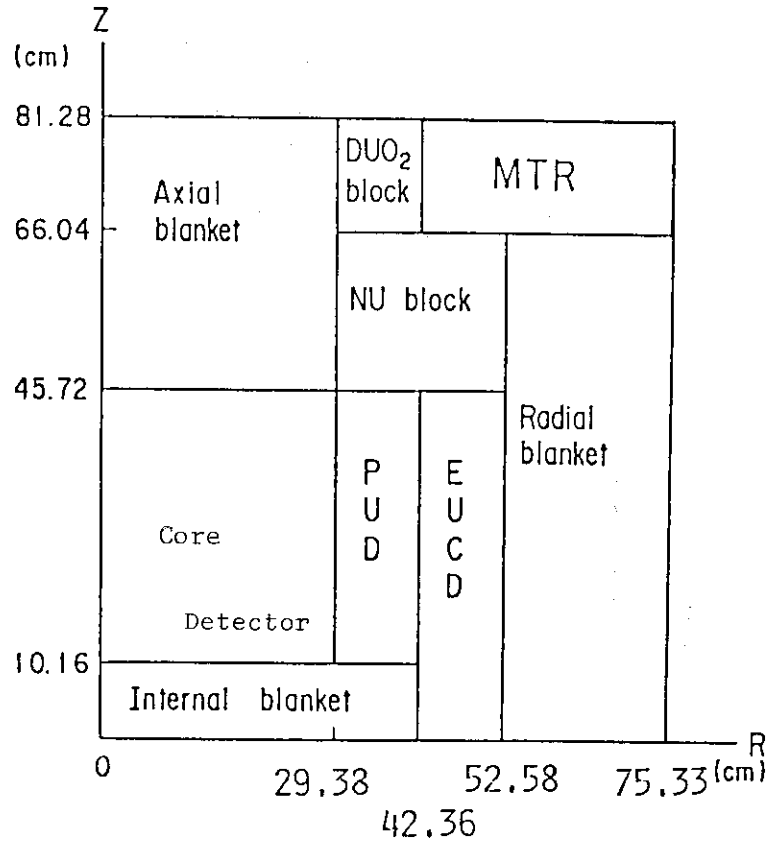

Fig. 3.15.1 R-Z model of FCA XII-1 assembly

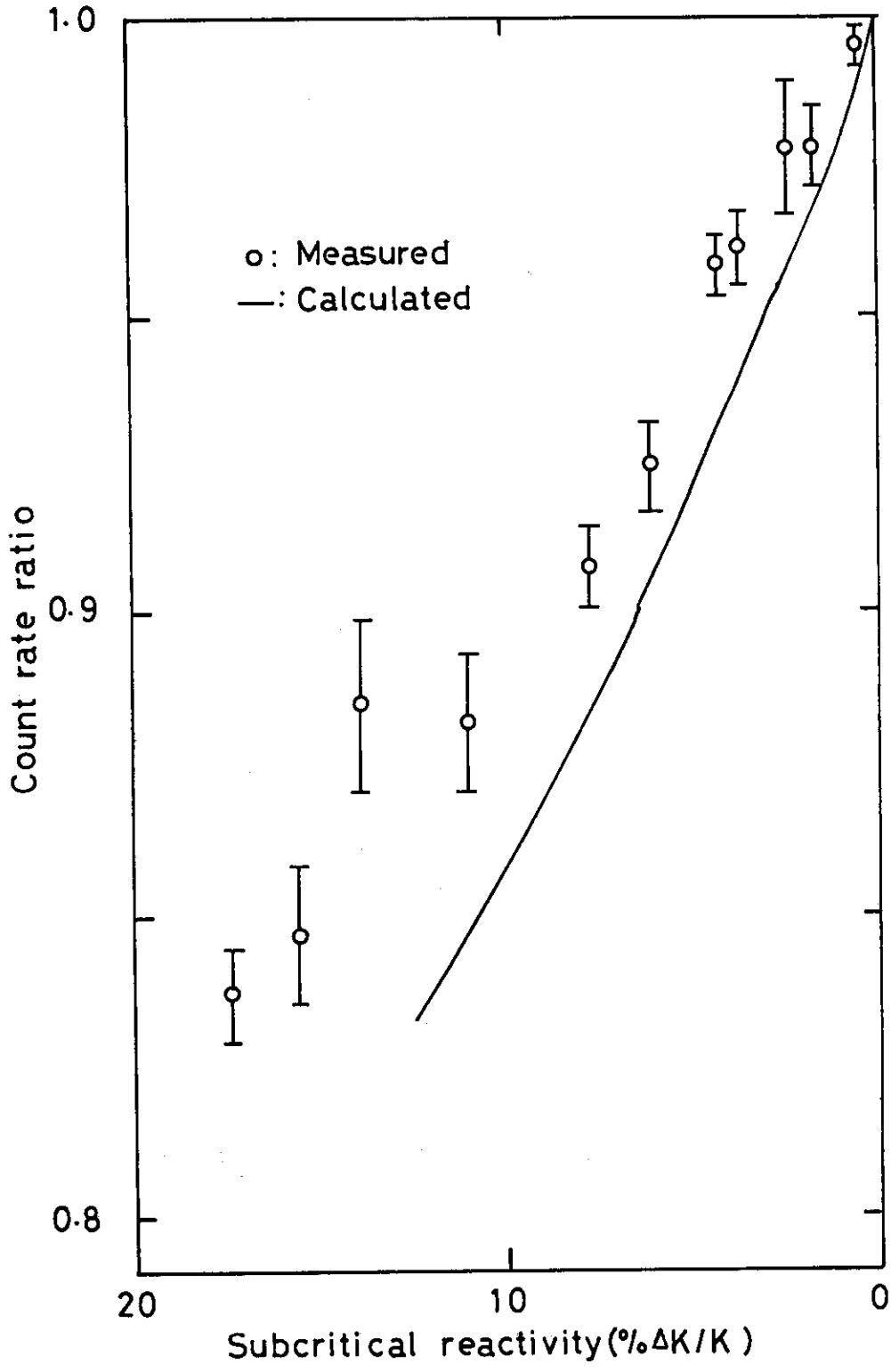

Fig. 3.15.2 Measured and calculated count rate ratio of ^{235}U to ^{237}Np in FCA XII-1 assembly

3.16 Operation Report of FCA

S. Fujisaki, K. Satoh, A. Ohno, R. Kurokawa and M. Nakano

In fiscal 1985, much labor was expended in activities concerning operations and maintenances of the Fast Critical Assembly (FCA), and consequent performance of the operation was achieved in success. The FCA XII and XIII core were assembled to obtain benchmark data on a large axially heterogeneous core. Operations for the above purposes completed as scheduled, without any major problem disturbing the execution of the experiments.

Operations of 192 times were carried out in 112 days to perform the experiments. One scram happened during operations. The operating time was 748 hours and the integrated power 4075 Wh. The total run of 3900 criticality operations has been recorded at the end of this fiscal year since the first achievement of criticality on 29 April 1967. According to the regulation of operations, at FCA 2 days were devoted to the monthly inspection and about 4 weeks to the annual inspection in November. Normal maintenance activity was done in these days to provide maximum operations for the experiments.

The other major activities relating to the maintenance were carried out. First, the Log N channel (CH.3) and the Linear channel (CH.5) were renewed in cooperation with the Electronics Divisition of JAERI. Second, the FCA 2000 mm table position indication system was renewed in this year. The magnetic scale in this system was used to measure precisely the distance between two half assemblies. The scale has the precision of 10 μm. As for fuel management, the defects of coating on the surfaces of natural uranium fuels were repaired for about 3,000 coupons by spraying calloidal solution of fluorocarbon. Weights of coating on the fuel coupons were obtained from measurements of fuel weight before and after coating.

In connection with safeguards, IAEA and NSB carried out every two week inspection under the international treaty. The Physical Inventory Taking (PIT) of the fuels was performed from May 7 to 31 by means of item counting, weighing and non-destructive assay. IAEA and NSB made the Physical Inventory Verification (PIV) from May 23 to 31. No anomaly was

confirmed.

A lot of plutonium and highly enriched uranium fuels were used for various experiments. That causes high radiation doses due to spontaneous fission neutrons and gamma rays from the fuels. Personnel shields were renewed in this year to protect working people from these high radiation exposures. The drive mechanisms for two half assemblies were placed on the overhead track system. The shielding doors were suspended from the drive mechanism. It consists of a movable side and a fixed side. The shields are interlocked with the table movement and are retracted during reactor operations. When the reactor halves are separated, the personnel shields can be driven in front of both half assemblies by the control system placed in the reactor room. The setting time is about 2 minutes. The shields have the safety mechanism which consists of photosensors. When the safety mechanism detects an obstacle as a jutted fuel drawer, it stop quickly the movement of the shields.

Each side of personnel shields are composed of four shielding doors 2.5 m high, 0.63 m wide, and 0.12 m thick. The door are mechanized by AC servo motor and can be separated from 15 cm to 50 cm in 5 cm step. The new system of personnel shields is shown in Fig.3.16.1. The shielding door consisted of the boron-polyethylene sheet (natural boron 5w/o), the cadmium, lead and stainless steel. The geometrical arrangement is shown in Fig.3.16.2. The four door shown in Fig.3.16.3 can cover the whole core. By these shields, radiation dose could be decreased more than one-tenth.

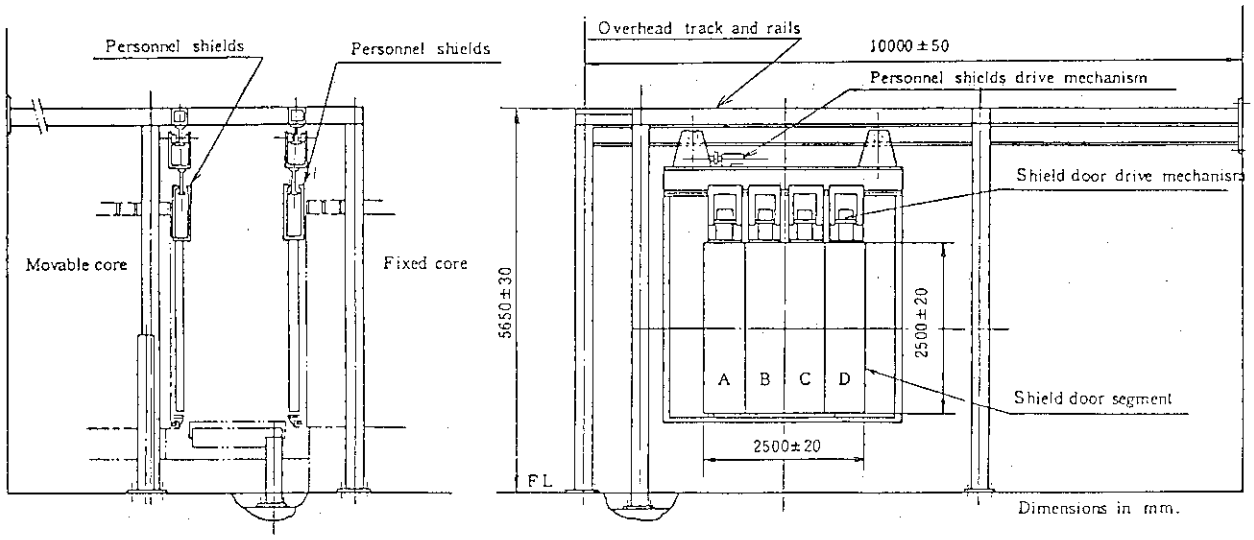

Fig.3.16.1 New personnel shields in FCA

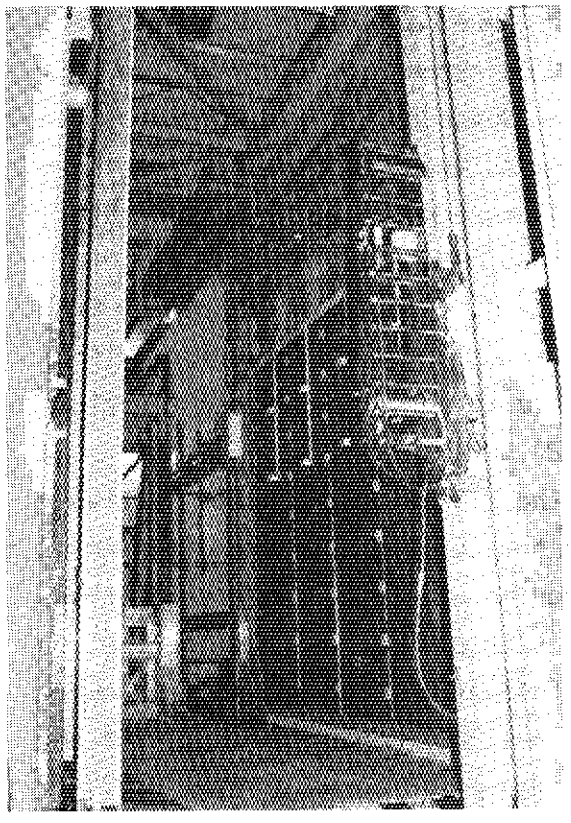

Fig.3.16.3 New Personnel shields

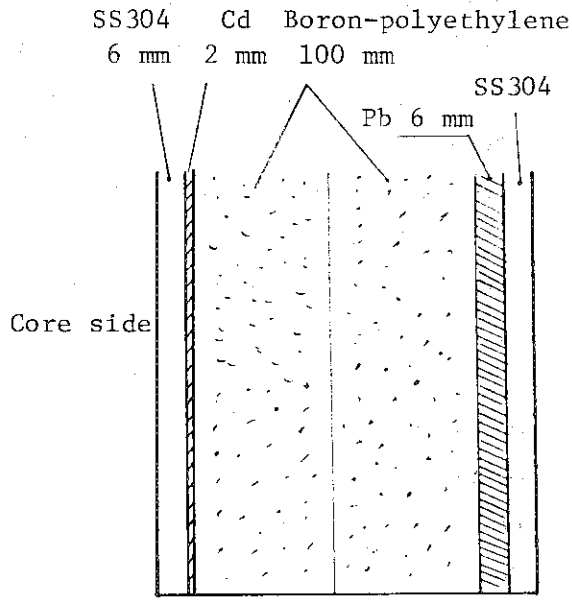

Fig.3.16.2 The geometrical arrangement

3.17 Analysis of PROTEUS Experiments by the SRAC System

Y. Ishiguro , H. Akie , K. Kaneko* and M. Sasaki*

In the previous analysis of PROTEUS experiments by the SRAC system [1] , preferable results were obtained compared with the other codes developed in foreign coutries. But some problems were also pointed out. We analysed the experiments again, because of the two following reasons.

(1) To solve the problems in the previous analysis, several improvements have been made in the SRAC system. These are

a) correction of infinite dilution cross sections of important resonance nuclides (U-238,Pu-239, etc.) in the unresolved resonance region and

b) improvement in the method of Dancoff factor calculation for cells that include different fuel rods [2] .

(2) After the previous analysis, new results of PROTEUS experiments were published [3] .

The test lattices of PROTEUS cores are shown in Fig. 3.17.1. Moderator material of the lattice can be exchanged by Dowtherm or air to simulate moderator void conditions; Dowtherm is a moderator to simulate 42.5% void condition. According to the moderator species there are six test cores, i.e., cores 1 and 6 correspond to H_2O moderator, cores 3 and 4 to Dowtherm, and cores 2 and 5 to air [4] .

To examine the calculation method, we first compared the SRAC system with a continuous energy Monte Carlo code VIM. There are differences in the effective cross sections in resolved resonance region, especially in one of U-238 (Fig. 3.17.2).

In the experimental analysis, the large disagreement between calculation and experiment is found in the two rod heterogeneity factor of C8 (U-238 capture rate). The differences are twice as large as those between SRAC and VIM (Fig. 3.17.3). Although the calculated reaction rate ratios deviate from the experimental values, the k_∞ values agree within the experimental errors (Fig.3.17.4). Comparing SRAC with the other codes, the former results are generally reasonable (Fig. 3.17.4).

---

* Japan Information Service Co.,Ltd.

References

1) Ishiguro Y. et al.: "Physics Problems on Analysis of High Conversion Pressurized Water Reactor (HCPWR) with Tighter Pitch Lattices (An Analysis of PROTEUS-LWHCR Cores by SRAC System)," JAERI-M 84-180 (1984) (in Japanese).
2) Ishiguro Y. et al.: "Generalized Dancoff Factor in Complex Lattice Arrangement," J. Nucl. Sci. Technol., Vol.22, 853 (1985).
3) Chawla R. et al.: "Further Investigation in the PROTEUS-LWHCR Phase I Program," NEACRP-A-636 (1984).
4) Chawla R. et al.: "Reactivity and Reaction Rate Ratio Changes with Moderator Voidage in a Light Water High Converter Reactor Lattice," Nucl. Technol., Vol.67, 360 (1984).

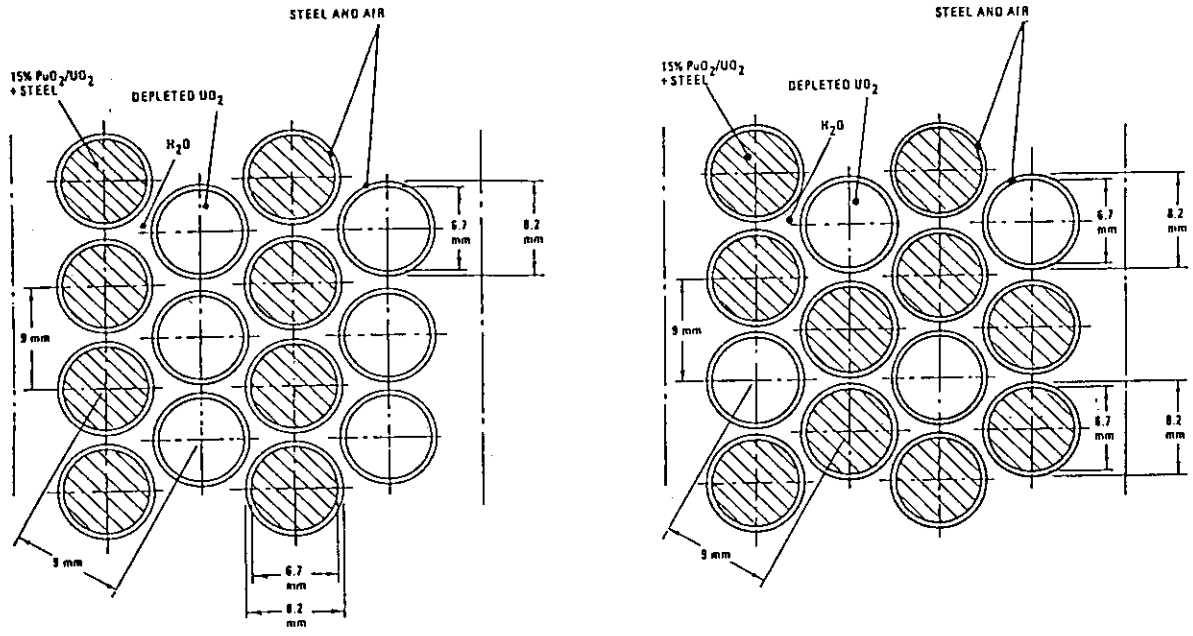

Fig. 3.17.1 Test lattices for PROTEUS-LWHCR cores

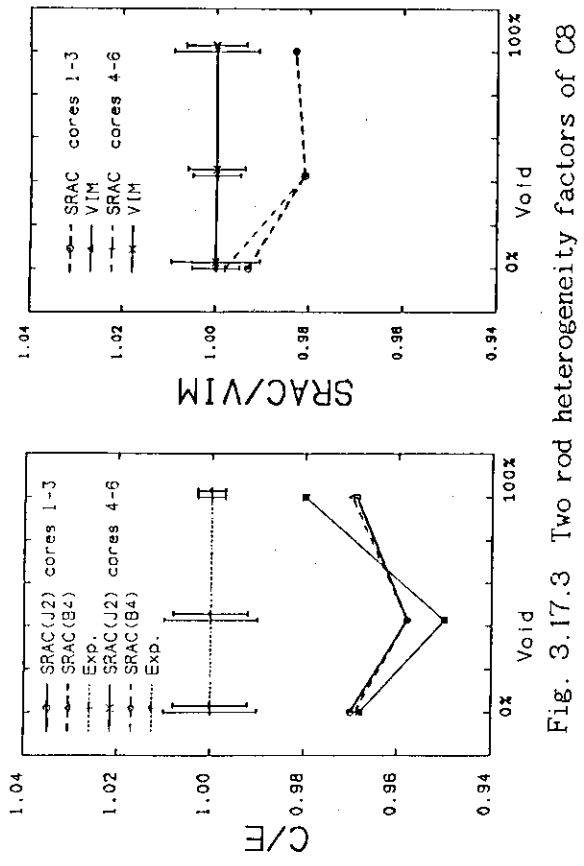

Fig. 3.17.3 Two rod heterogeneity factors of C8

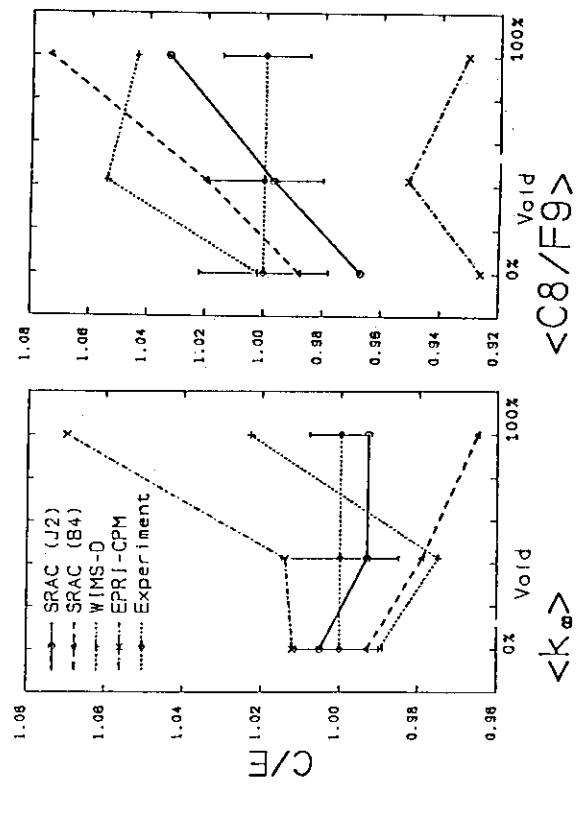

Fig. 3.17.4 k_∞ and C8/F9 reaction rate ratios for cores 1-3

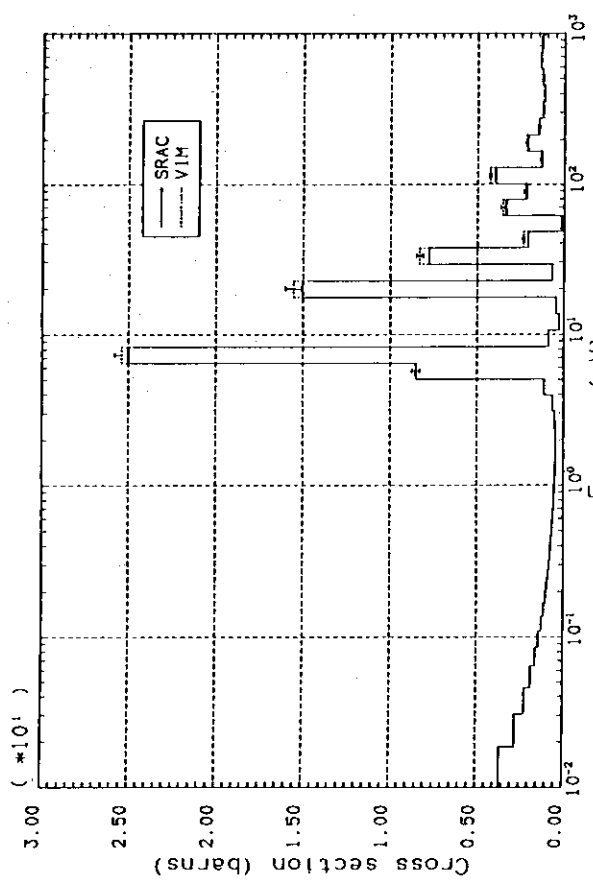

Fig. 3.17.2 U-238 capture cross sections (core 1 , Mox fuel)

3.18 Parametric Survey of Tight Lattice Cell

H. Akie, Y. Ishiguro and E. Doi*

To make a reference data set on burnup characteristics of the high conversion light water reactors (HCLWRs), we made cell burnup calculations by the SRAC system for simple hexagonal tight lattice cells with three regions, MOX fuel, cladding, and H_2O moderator. We parametrically surveyed the relation between cell parameters and burnup characterisics of the cell.

Parameters surveyed here are as follows:

D : fuel rod diameter,
Rv: moderator/fuel volume ratio,
E : fissile Pu enrichment and
B^2: geometrical buckling.

Two cladding materials, zircaloy and stainless steel, are also considered in our survey.

Some of the results are summarized in Fig. 3.18.1, where k_{eff} values and two kinds of conversion ratios are compared. A conversion ratio is defined as the ratio of fertile capture to fissile absorption at each burnup time, on the other hand an average conversion ratio as the ratio of fissile nuclide number densities at any burnup time to those at the zero burnup time.

As shown in Fig. 3.18.1, k_{eff} s are larger than unity during the most period of burnup in this calculations, while nuclear reactors are operated at k_{eff} =1. If a real reactor system is to be considered, cell burnup calculations should be made by controling absorber materials or buckling to keep k_{eff} =1. A sample result of cell burnup calculation controlled by 1/v absorber is shown in Fig. 3.18.2, in comparison with one for uncontrolled cell. This figure shows that there is little effect between the two cases on burnup characteristics of the tight lattice.

Figure 3.18.3 shows the upper limit of the average conversion ratio at 'possible' burnup. Here the 'possible' burnup is defined as 1.5 times the burnup that k_{eff} s become less than 1.01, based on three batch refueling. The figure is made based on all the calculated results using zircaloy cladding. Figure 3.18.3 indicates that it is difficult to achieve both high conversion and high burnup. A very similar figure was drawn also for the stainless steel cases.

* I.S.L. Inc., Tokyo

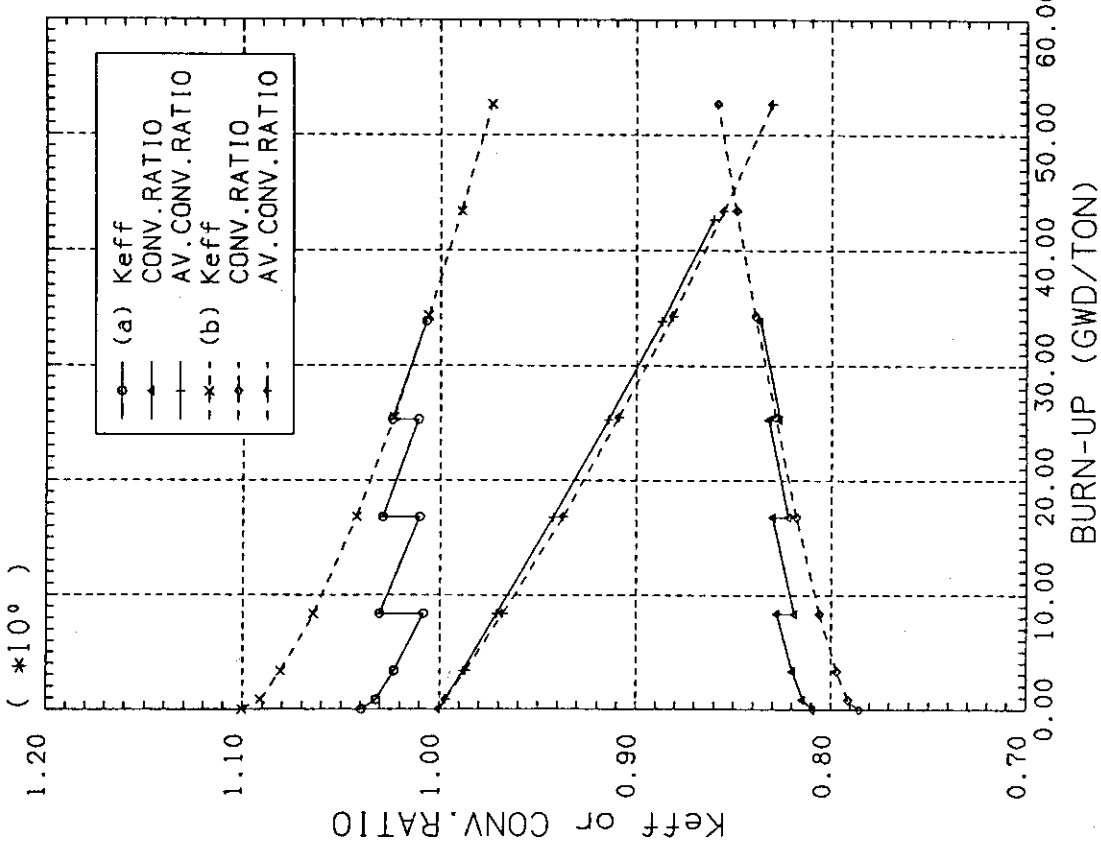

Fig. 3.18.2 Comparison of k_{eff} and conversion ratio obtained by the two models (D=1.0cm Rv=0.8 E=8%)
(a) controlled (b) uncontrolled

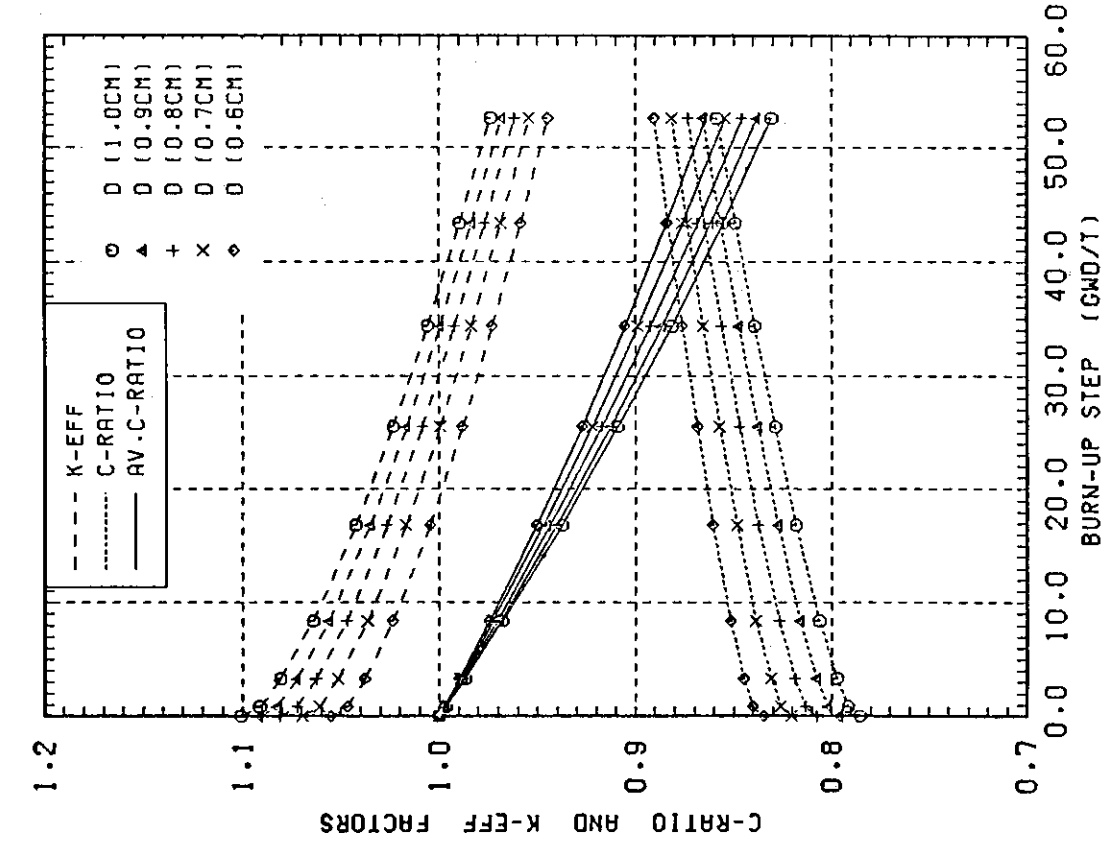

Fig. 3.18.1 Burn up dependence of k_{eff} and conversion ratio (Rv=0.8 E=8%)

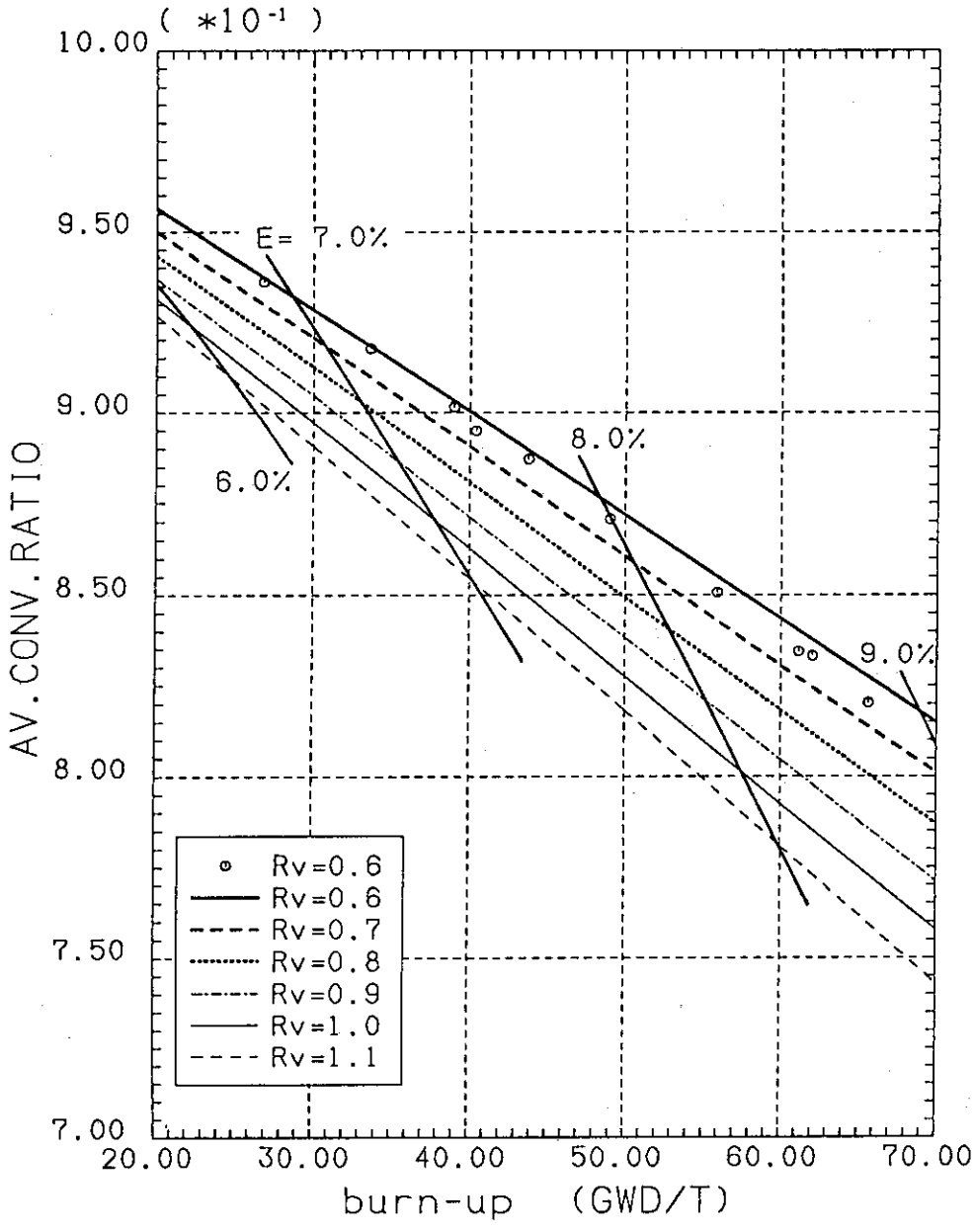

Fig. 3.18.3 Upper limit of average conversion ratio at possible burnup

3.19 Preliminary Benchmarks of Data and Method for Calculating Reactor Characteristics in HCLWRs

H. Takano, H. Akie, Y. Ishiguro, E. Saji* and K. Suzuki*

International comparison of lattice calculations for the PROTEUS-LWHCR experiments has been reviewed by Chawla [1]. Discrepancies between the integral parameters calculated with standard LWR methods and data sets were much larger than those usually encountered for a LWR lattice.

In order to investigate the causes for the discrepancies, preliminary benchmark calculations were performed with the use of the SRAC[2] and WIMS-E codes for the following tight lattice: the fuel is PuO_2-DUO_2, the fuel pellet is a diameter of 8.2 mm and the cladding is zircaloy with the thickness of 1.1 mm. Cell burn-up calculations were performed for the 5 cases as follows: the volume ratios of moderator to fuel pellet are 0.8, 1.1, 1.4 and 2.0, and the Pu fissile enrichments 8.0, 7.0, 7.0 and 4.0 wt% corresponding to these volume ratios, respectively.

Figures 3.19.1 and 2 show the comparison of the k_{eff}, conversion and average conversion ratios as a function of burn-up calculated for the volume ratios of Rv=0.8 and 2.0, respectively. The discrepancies between the k_{eff} calculated with SRAC and WIMS-E are 0.0142 and 0.00317 k for the cases of Rv=0.8 and 2.0, respectively, at the zero burn-up stage. The discrepancies are reduced with increasing volume ratios. It is observed from these figures that the reactivity changes calculated with SRAC are smaller than those with WIMS-E. Furthermore, the conversion ratios obtained with SRAC are larger than those with WIMS-E.

The discrepancies between k_{eff} s are mainly caused by the differences in the absorption rates of U-238 and Pu-239 as seen in Fig.3.19.3. In Fig.3.19.4, microscopic absorption cross sections for U-238 are shown for three energy ranges of the thermal (0.00001 - 4.0 eV), resonance (4.0 - 9118 eV) and fast (9118 eV - 10.0 MeV). Considerable discrepancy is observed in the resonance energy region. This causes in the burn-up calculations that the atomic number density for U-238 obtained with SRAC becomes smaller than that with WIMS-E, and it is inversely for the atomic density of Pu-239. This is one of main reasons for the discrepancies between the reactivity changes obtained with SRAC and WIMS-E. Another reason is due to the differences between capture cross sections of fission product nuclides.

References

1) Chawla R.:" A Review of Lattice Calculations for the PROTEUS-LWHCR Phase I Experiments," NEACRP-A-726, (1985).
2) Tsuchihashi K., et al.,:" SRAC:JAERI Thermal Reactor Standard Code System for Reactor Design and Analysis," JAERI 1285 (1983).

---

* Mitsubishi Atomic Power Industries, Inc. (Tokyo)

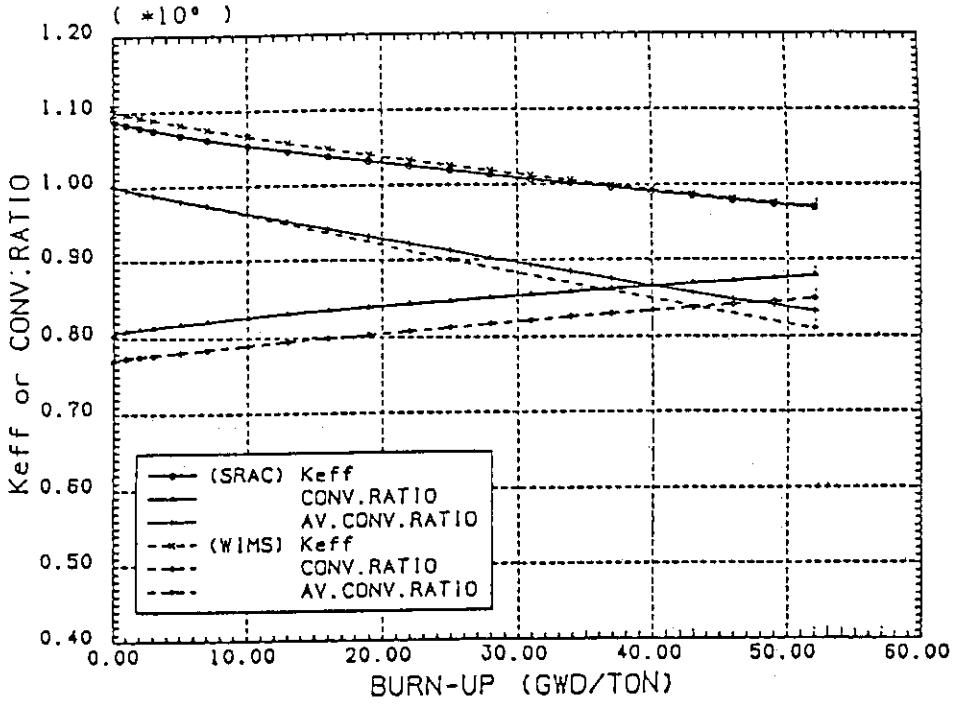

Fig.3.19.1 Burn-up characteristics of Keff and conversion ratio for the case of Rv=0.8

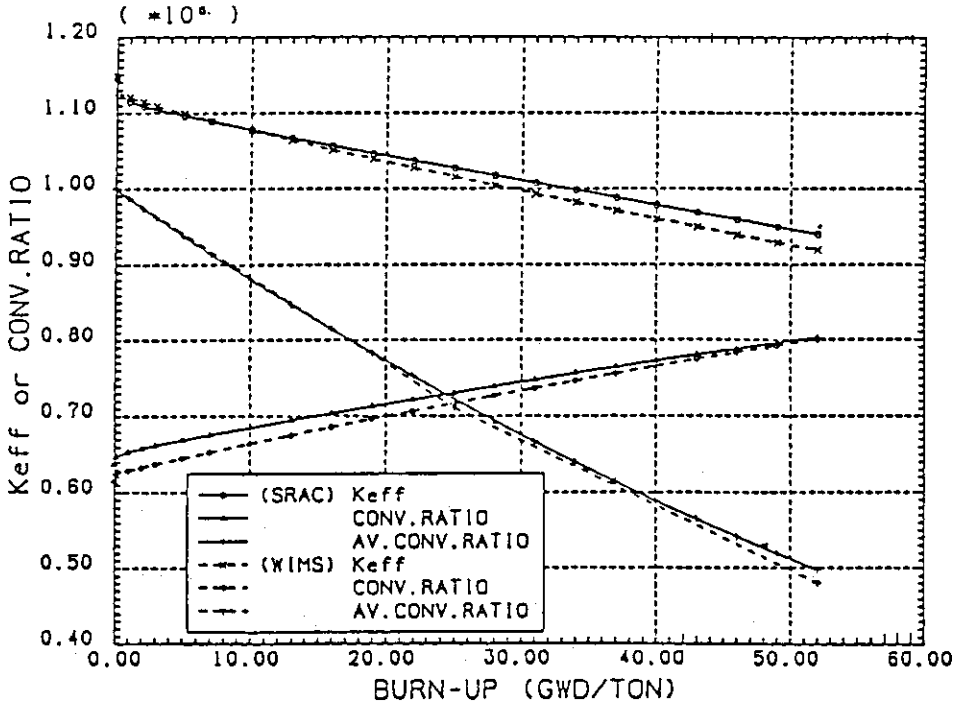

Fig.3.19.2 Burn-up characteristics of Keff and conversion ratio for the case of Rv=2.0

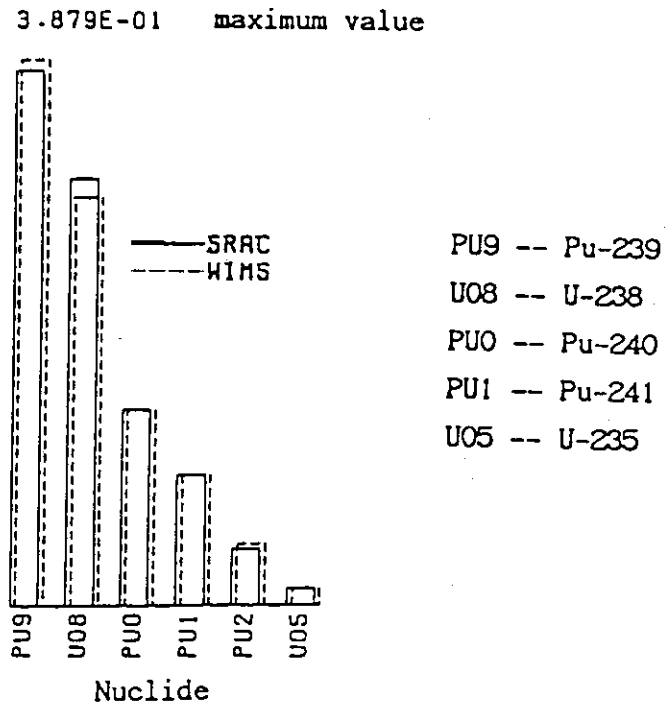

Fig.3.19.3 Comparison of the absorption rate fractions to the total absorptions calculated with SRAC and WIMS-E codes

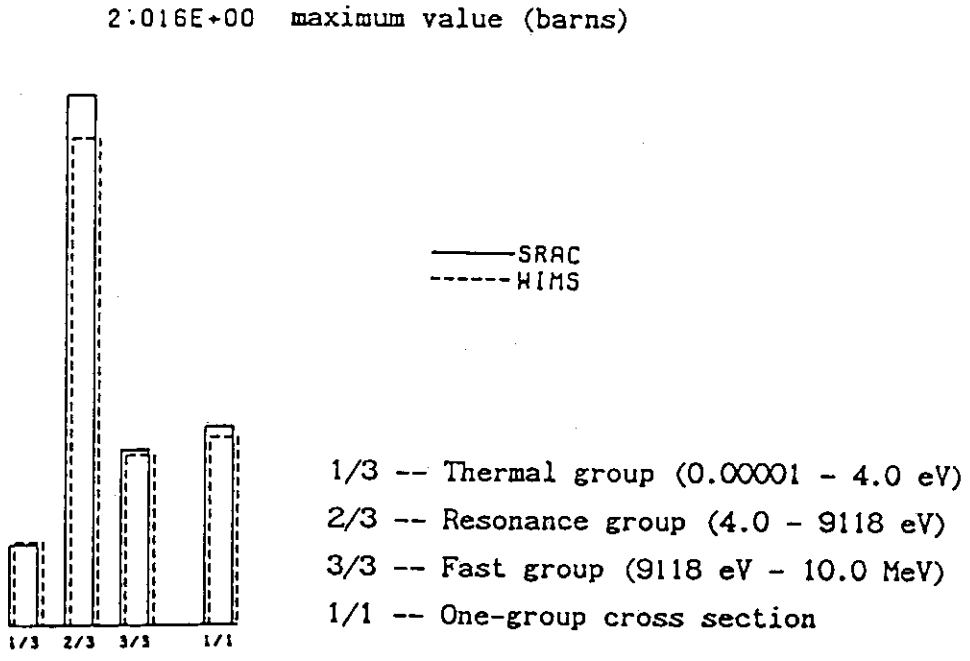

Fig.3.19.4 Comparison of the effective absorption cross sections for U-238 obtained with the SRAC and WIMS-E codes

3.20 Physics Analyses for Design of Cold Neutron Guide

T. Ise, T. Maruo+, M. Isshiki+, and Y. Miyasaka++

Physics analyses have been performed for design of a cold neutron source(see Fig.3.20.1) and neutron guides(see Fig.3.20.2), which are to be installed in a new research reactor.[1)]

To the calculational procedures(see Fig.3.20.3) applied are the Young-Koppel model for liquid hydrogen scattering kernels, the ANISN code for cold neutron source spectra and shielding of neutron guides, and the MORSE code for neutron transport through neutron guide.

The results contain the effect of void ratios in liquid hydrogen on cold neutron spectra, the spatial distributions at the outlets of C_3 guide(see Fig.3.20.4. upper:neutrons;lower: f.s.d. in Monte Carlo calculations;*:read as 7.8×10^{-3}) and the energy spectra at the C_{3-2} outlet(see Fig.3.20.5).

Reference

1) Ise T., Maruo T. et al.: "Shielding Analyses for Design of the Upgraded JRR-3 Research Reactor --- Physics and Shielding of Neutron Guides ---," JAERI-M 86-028(1986)(in Japanese).

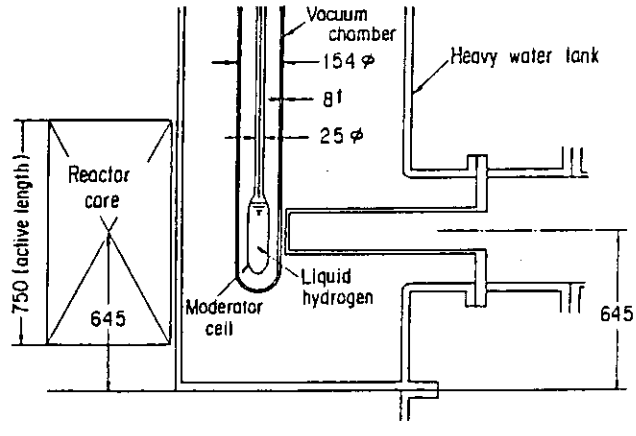

Fig.3.20.1 Cold neutron source device

+ Department of Research Reactor Operation

++ Office of Safety and Control

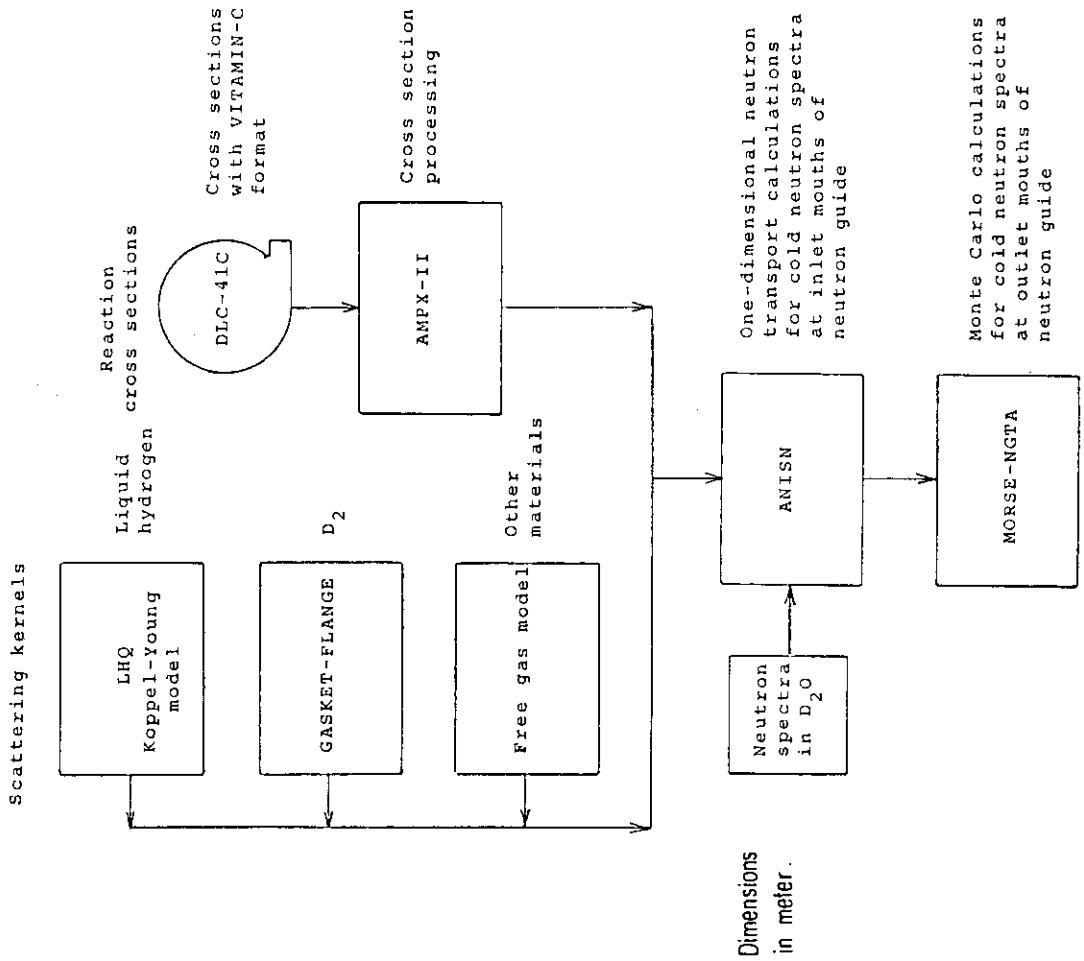

Fig.3.20.3 Flow diagram of physics analyses

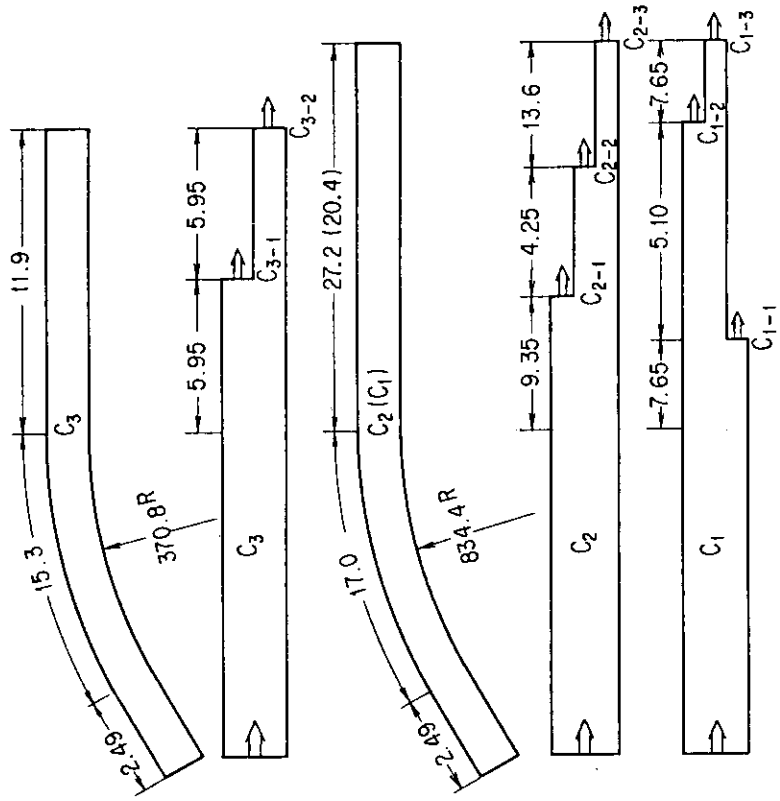

Fig.3.20.2 Longitudinal specifications of cold neutron guides

Top

	7.8-3 *)	4.8-3	3.3-3	2.6-3
	0.02	0.02	0.03	0.03
	7.6-3	4.8-3	3.3-3	2.4-3
Outer	0.02	0.02	0.03	0.03
side	7.4-3	4.4-3	3.4-3	2.4-3
	0.02	0.03	0.03	0.04
	7.6-3	4.8-3	3.5-3	2.7-3
	0.02	0.03	0.03	0.04

Inner side

Bottom

(a) At the end of curved part

Top

	4.4-3	4.4-3	4.2-3	4.2-3
Outer	0.03	0.03	0.03	0.03
side	4.1-3	4.1-3	4.3-3	4.2-3
	0.03	0.03	0.03	0.03

Inner side

Bottom

(b) At the C_{3-1}

Top

	4.0-3	4.0-3	4.1-3	4.3-3
Outer	0.03	0.03	0.03	0.03
side	4.2-3	3 9-3	4.4-3	4.3-3
	0.03	0.03	0.03	0.03

Inner side

Bottom

(c) At the C_{3-2}

Fig.3.20.4 Spatial distributions at the outlets of C_3 guide(relative)

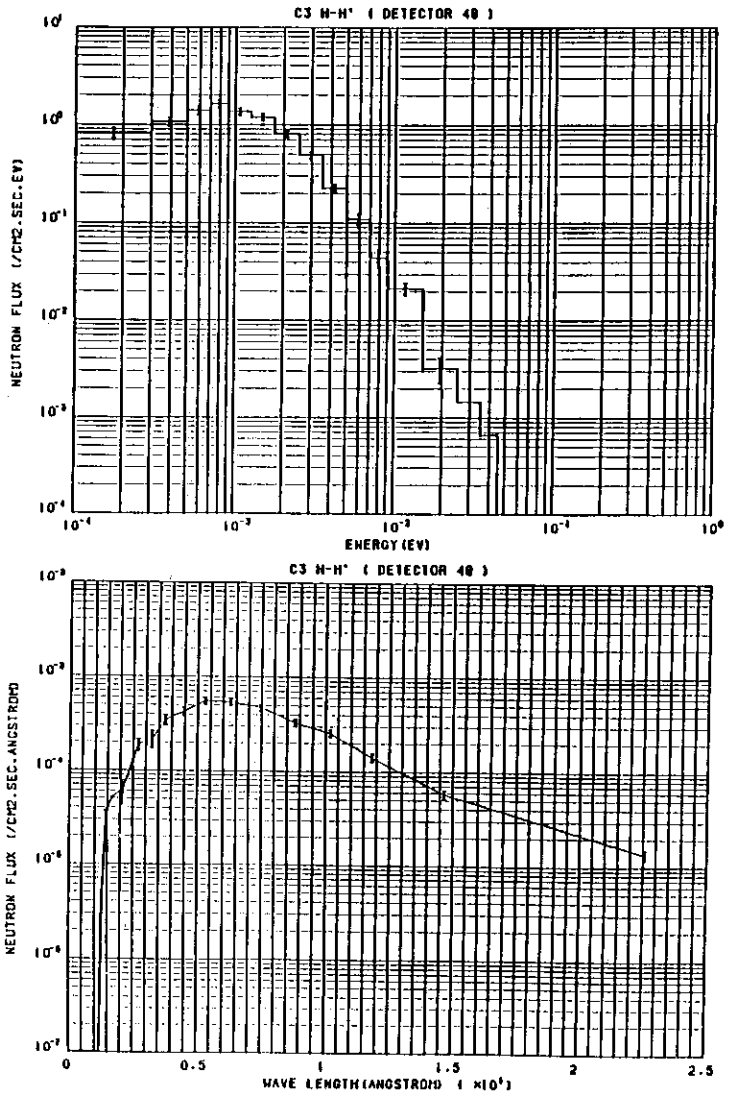

Fig.3.20.5 Neutron spectrum at the C_{3-2} outlet(relative)

3.21 Design Study of a Separate Pebble Bed Type Gas Cooled Reactor

K. Sako

Design studies have been carried out on new type of high temperature gas cooled reactors, SPGR-500 and SPGR-750S.

The SPGR-500 is designed for a thermal utility purpose. The SPGR-750S is designed as a power reactor. These reactors have merits common to both the prismatic and pebble bed reactors as follows.

A. Merit common to prismatic reactor:
   (1) Free arrangement of core (fuel and control rod) and reflector channels, and
   (2) Easy exchange of core and reflector channels.

B. Merit common to pebble bed reactor (mainly related to the use of ball shaped fuel elements):
   (1) Capability of automatic fabrication and inspection of fuel elements,
   (2) Easy transport and storage, and
   (3) Easy fuel exchange.

C. Other merit:
   (1) Capability of higher power density core, and
   (2) Simplified core support structure.

Table 3.21.1 shows the major design parameters.

Figure 3.21.1 shows the concept of SPGR-500. The core consists of many graphite channels filled with fuel balls. The fuel exchanger is fitted to the stand pipe similar to the CRD. Fuel balls are sucked up by differential pressure through a flexible tube. The once-through helical coil type heat exchanger is installed in the lower part of RPV. The helium circulating pumps are attatched to the shell of RPV.

Figure 3.21.2 shows the concept of SPGR-750S. This reactor has bypass slots on the inner surface of the fuel channel in order to obtain higher power density with reasonable core pressure drop. The other parts are similar to SPGR-500.

Figure 3.21.3 shows the core arrangement.

Figure 3.21.4 shows the core support structure.

Figure 3.21.5 shows the fuel exchange system.

Figure 3.21.6 shows the fuel exchanger fitted to the stand pipe. This machine is also used to handle the poison balls.

As a conclusion, this reactor concept will be attractive for modular reactor application. Further studies are under way from a safety point of view.

Table 3.21.1

	SPGR 500	SPGR 750S
THERMAL/ELECTRIC POWER (MW)	500/-	750/285
COOLANT IN/OUTLET TEMP. (C)	350/960	290/760
COOLANT FLOW RATE (T/H)	568	1107
CORE HEIGHT/EQ. DIAMETER (M)	3.6/4.4	3.6/4.4
NO. OF FUEL CHANNELS	180	180
CHANNEL PITCH/DIAMETER (mm)	300/230	300/230
CORE AV. POWER DENS. (W/CC)	9.1	13.6
FUEL NOMINAL MAX. TEMP. (C)	1150	1150
FUEL DIAMETER (mm)	30	25
NO. OF BLOWERS	3	4
IN/OUTLET PRESSURE (ata)	70/73	70/73
TOTAL BLOWER POWER (net,MW)	8.5	15
HEAT EXCHANGER, NO. OF TUBES	1620	800
TUBE IN/OUTER DIAMETER (mm)	24/32	19/25.4
TUBE PITCH (mm)	40	40

Fig. 3.21.1 SPGR-500

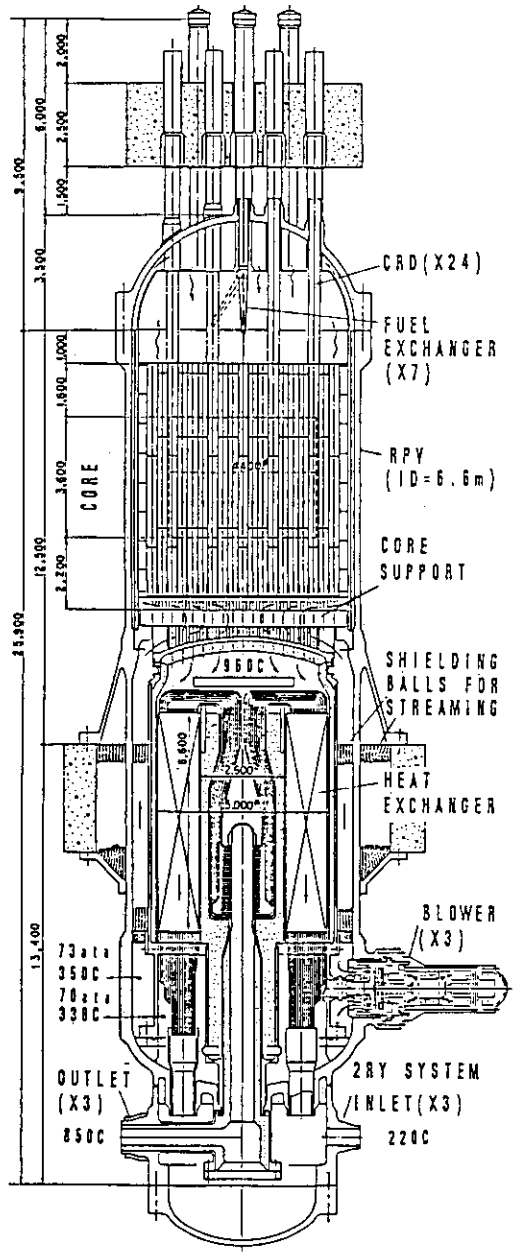

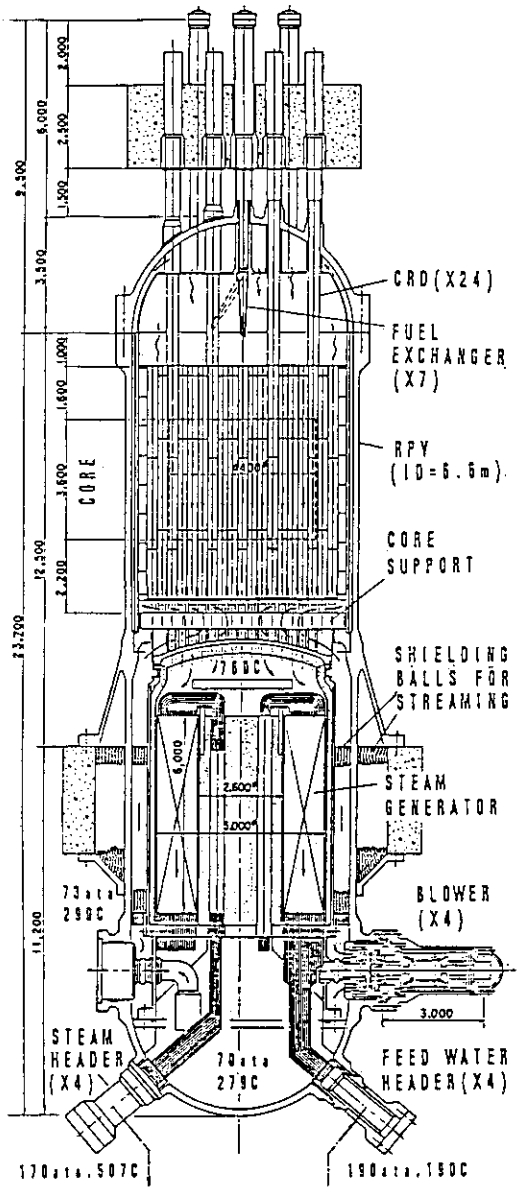

Fig. 3.21.2 SPGR-750S

SPGR (Separate Pebble Bed Type Gas Cooled Reactor)

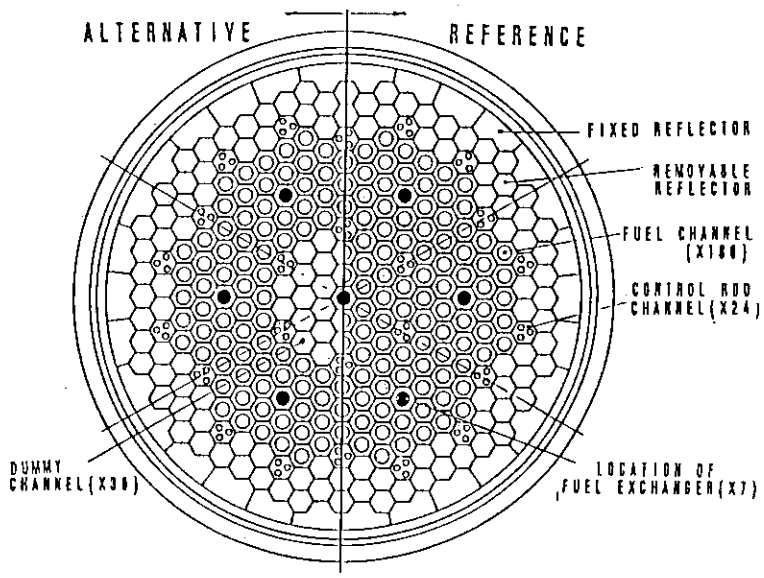

Fig. 3.21.3 Core arrangement

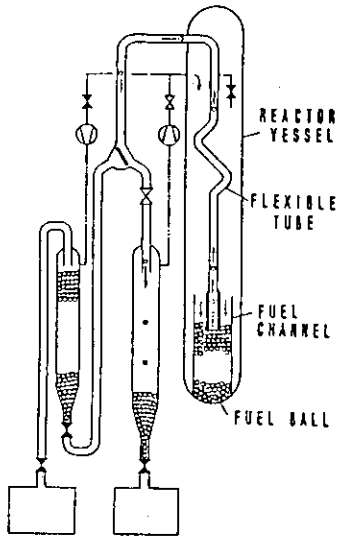

Fig. 3.21.5 Fuel exchange system

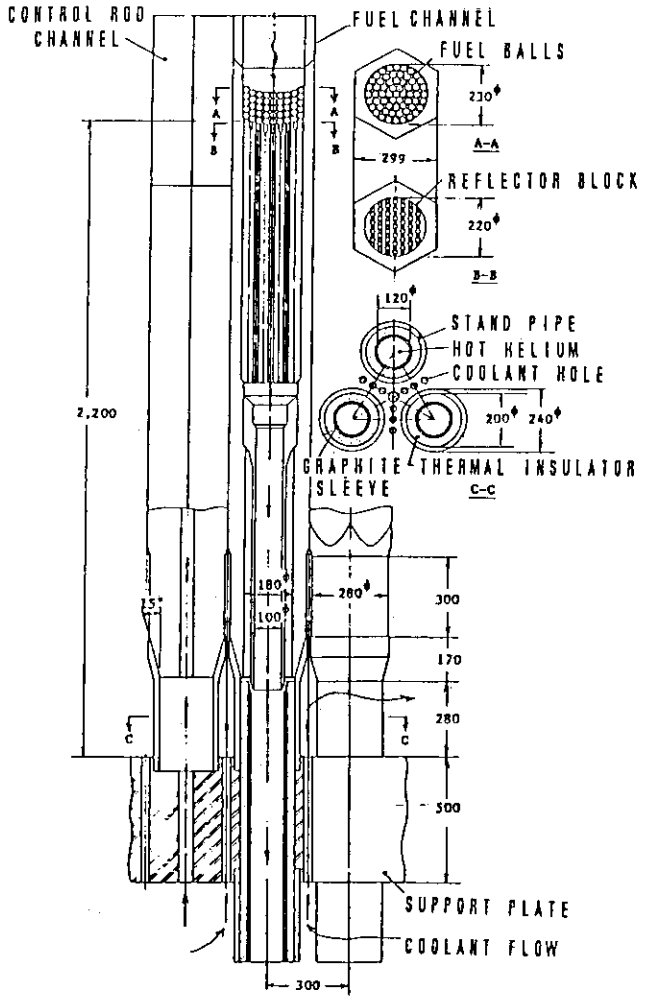

Fig. 3.21.4 Core support

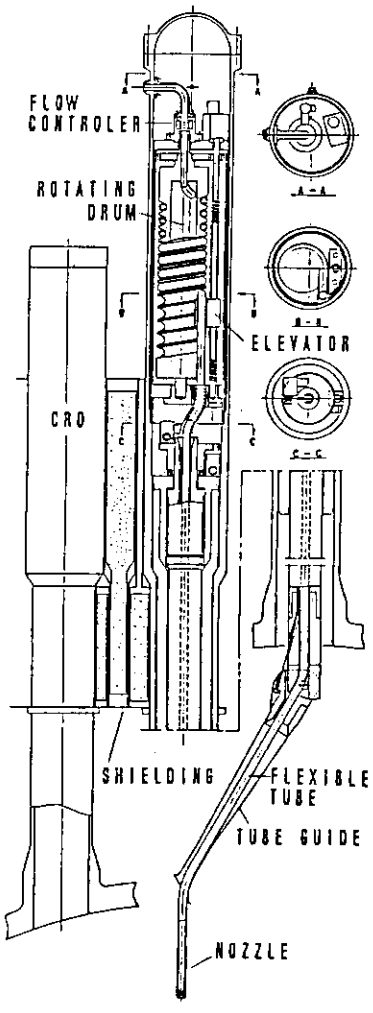

Fig. 3.21.6 Fuel exchanger

3.22 Design Study of a System Integrated Pressurized Water Reactor

K. Sako

Design studies have been carried out on new type of pressurized water reactors, ISER-HV and SPWR.

The ISER-HV has no CRD system with normal core arrangement. The SPWR has CRD system with tight core arrangement to obtain high convertion ratio. Each reactor has an integrated primary cooling system and a poison tank in the reactor pressure vessel. The features of these reactors are as follows:

(1) Reliable reactor shutdown and decay heat removal system,
(2) Simplified reactor system,
(3) Flexible operation,
(4) Easy maintenance and fuel exchange, and
(5) Reactor system suitable for a high conversion reactor (SPWR).

Figure 3.22.1 shows the concept of ISER-HV. The reactor consists of three parts, namely the shell part, a steam generator integrated in the top dome and a poison tank structure which includes core. A single unit pump which includes a pressure riser is fitted to the dome top. Pressure at the pump outlet is 15 MPa.

The once-through helical coil type steam generator is divided into three unit headers.

The poison tank surrounding the core is connected to the core outlet via three hydraulic pressure valves at the upper part. These valves are operated by the pump delivery head. The bottom part of the poison tank is attached to the core inlet plenum through a honeycomb structure which absorbs thermal expansion of poison water. Three coolers are installed in the upper part of the tank to maintain the temperature of the poison water in the tank at 150±5°C during the reactor operation and also to enhance the mixing. The boron concentration in the poison water (borated water) is 8000 ppm. The poison water is injected into the core at the reduced pump head.

Figure 3.22.2 shows the concept of SPWR. This reactor has control rod drive mechanisms at the dome bottom. The other parts are similar to the ISER-HV.

Figure 3.22.3 shows the core and upper core structure.

Figure 3.22.4 shows the pump includes pressure riser.

Figure 3.22.5 shows the hydraulic pressure valve.

Figure 3.22.6 shows the fuel exchange system.

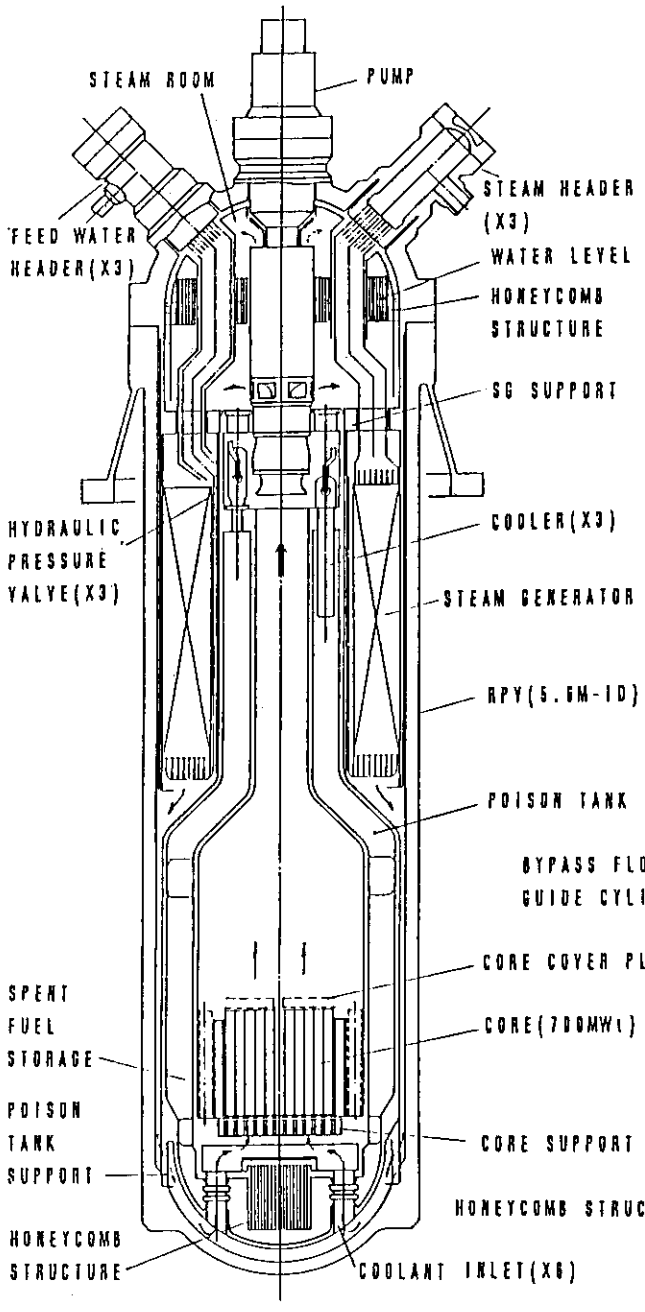

Fig. 3.22.1 ISER-HV

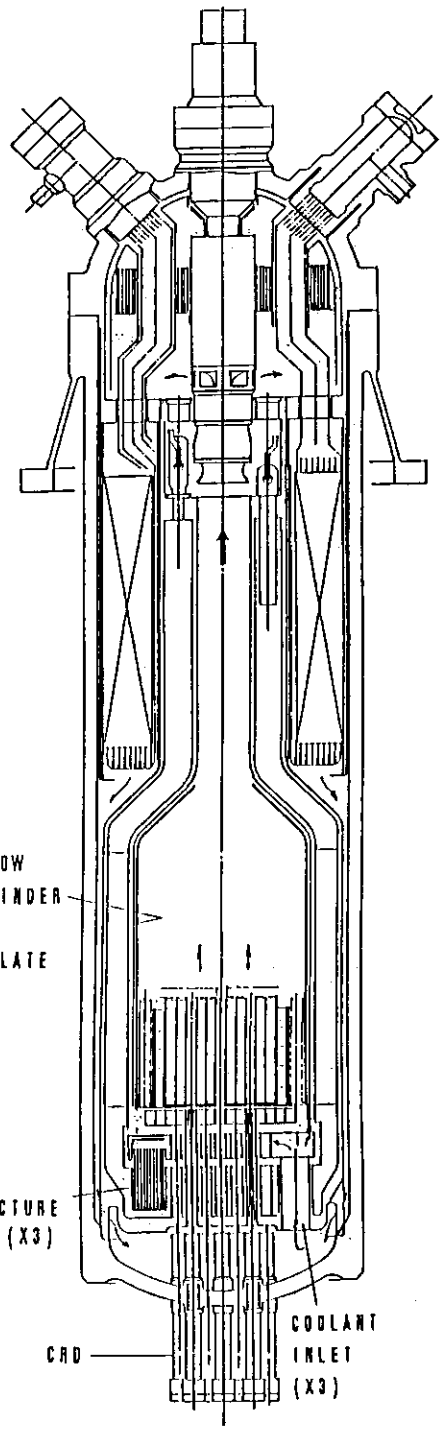

Fig. 3.22.2 SPWR

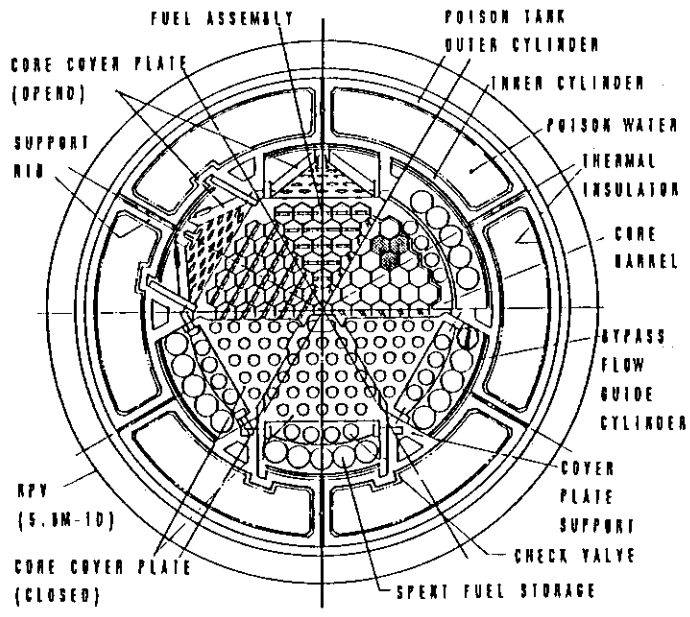

Fig. 3.22.3 Core & upper core structure

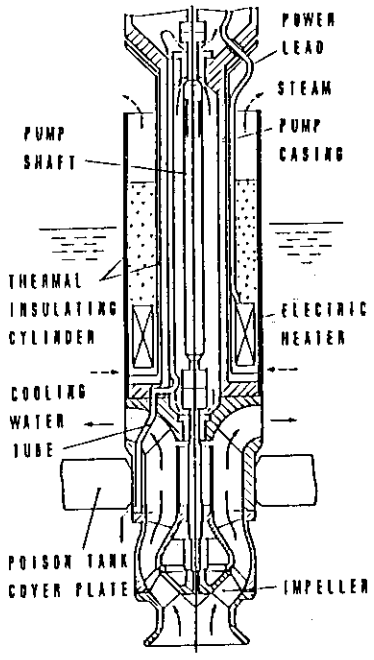

Fig. 3.22.4 Pump includes pressure riser

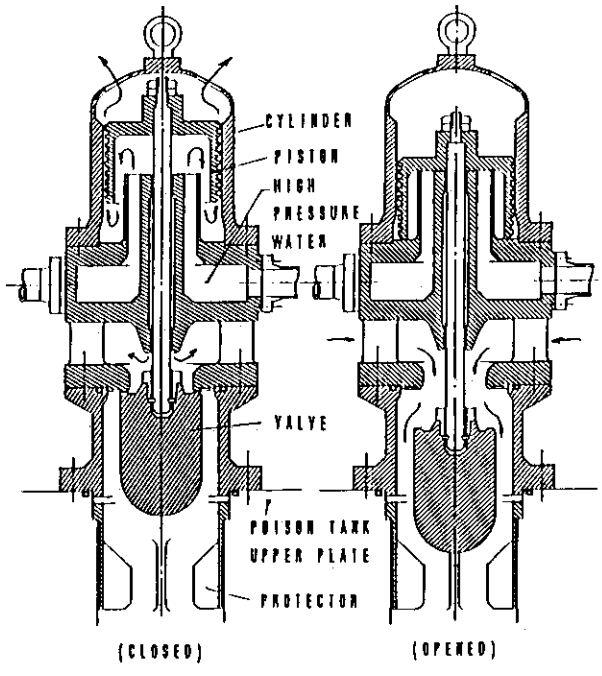

Fig. 3.22.5 Hydraulic pressure valve

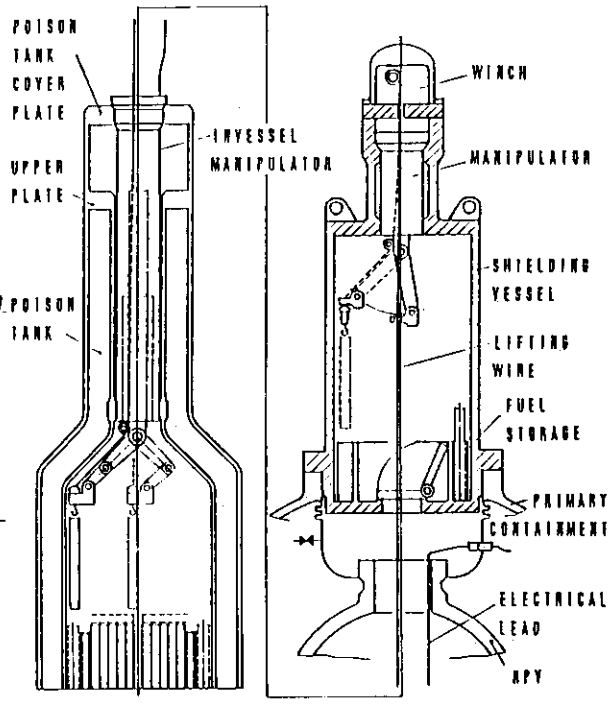

Fig. 3.22.6 Fuel exchange system

4. Fusion Neutronics

Experiments and analyses have been carried out in the area of fusion neutronics.

Self-shielding factors for two kinds of TPR (tritium production rate) measuring techniques using Li-glass scintillator and Li_2O pellet, respectively, were investigated individually by the experimental and calculational methods. The measuring energy range of the neutron time-of-flight system was extended down to 80 keV so as to include the energy region of the resonance cross section of ^{6}Li.

A series of measurements on activation cross section of elements in candidate materials for a fusion reactor was continued by using the FNS facility. The tritium production cross section of ^{7}Li was measured precisely. The measurements on short-lived nuclides has been started by using a pneumatic tube.

The blanket neutronics experiments based on JAERI/US collaborative program was progressed in phase IB period which aimed at obtaining supplementary information of the indirect source term. Also the US participants mesaured the low energy neutron spectra using a recoil-proton proportional counter. The analyses on the previous series of phase IA were performed and compared with the experimental values.

As the other activities of the collaborative program, an international comparison of nuclear data and codes on fusion neutronics was carried out. The time-of-flight experiments were analyzed by using the MCNP code.

Two types of integral experiments on concrete were performed of the activation and the spectrum measurements. The clean benchmark experiments were analyzed to examine the sensitivity of group constant. Four types of 125 group cross section sets were prepared for analyzing the experimental data at FNS.

In maintenance of the FNS facility, the insulated motor generator was replaced by the insulated core transformer. The water-cooled breeder register column of the acceleration tube was also replaced by the air-cooled register column. The electric equipments such as power supply were replaced because of deterioration.

(Yukio Oyama)

4.1 An Experimental Examination of Self-Shielding Effect for Lithium--Glass Scintillator

S. Yamaguchi, Y. Oyama and T. Nakamura

The Lithium-glass scintillator method[1] is used for the measurement of tritium production rate (TPR) in the Fusion Blanket Engineering Benchmark Experiment Program.[2] Since the atomic density of ^{6}Li in the ^{6}Li-glass scintillator (^{6}Li enriched) is four times as large as that in the experimental medium (lithium oxide), the self-shielding effect should be taken into account. Especially in the region where the soft component of neutrons is dominant, the self-shielding factor is considered to be several ten percent. A conventional method[1], in which isotropic incident of neutron and dominance of absorption compared with scattering are assumed and neutron flux obtained by DOT3.5 calculation was used, has been employed to correct the self-shielding effect.

Here, the self-shielding effect is examined experimentally using ^{6}Li-glass scintillator of different thicknesses (see Fig. 4.1.1). The TPR with no self-shielding effect (TPR°) is obtained by extrapolating the thickness of scintillator t to zero:

$$TPR^\circ = \lim_{t \to 0} TPR(t)$$

The self-shielding factor F(t) for the ^{6}Li-glass of thickness t is given by

$$F(t) = TPR(t)/TPR^\circ,$$

where F(t) is unity when t becomes zero.

The measurements were carried out along the central axis of the Be sandwiched system[2] using ^{6}Li-glass scintillator of 0.1, 0.3, 0.6, 1.0 and 2.0 mm thick which were fabricated from the same batch. Measurement in the graphite pile (100 × 100 × 90 cm) at FNS was also performed to examine the self-shielding effect for thermal neutrons. Experimental results at -2.5 cm and 40 cm in the Be sandwiched system and the graphite pile are shown in Fig. 4.1.2 with the calculated result of the coventional method. Self-shielding effect of ^{6}Li-glass of 2 mm thick, F(2.0) in the Be sandwiched system is only few percent at 40 cm but comes up to 40 % at -2.5 cm. Estimation by the conventional method agreed with experimental results within experimental

error. This fact shows that the conventional method is useful for the correction of the self-shielding effect.

References

1) Yamaguchi S., et al.: "A Method for Measuring Tritium Production Rate by Lithium-Glass Scintillators," JAERI-M 85-086 (1985)
2) Makamura T., et al.: JAERI-M 84-138(1984) 105.

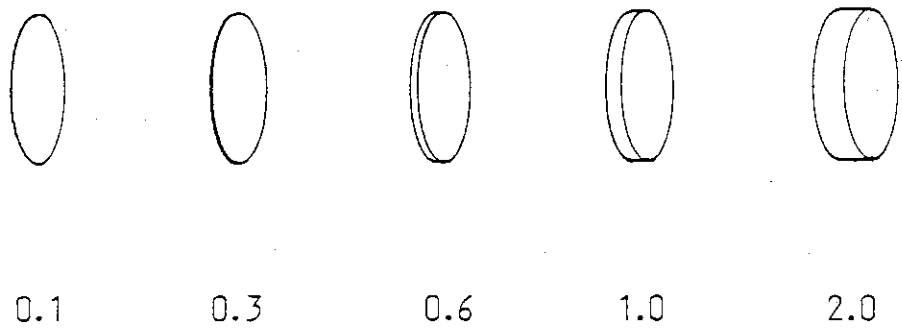

Fig. 4.1.1 ^{6}Li-glass scintillators of different thicknesses

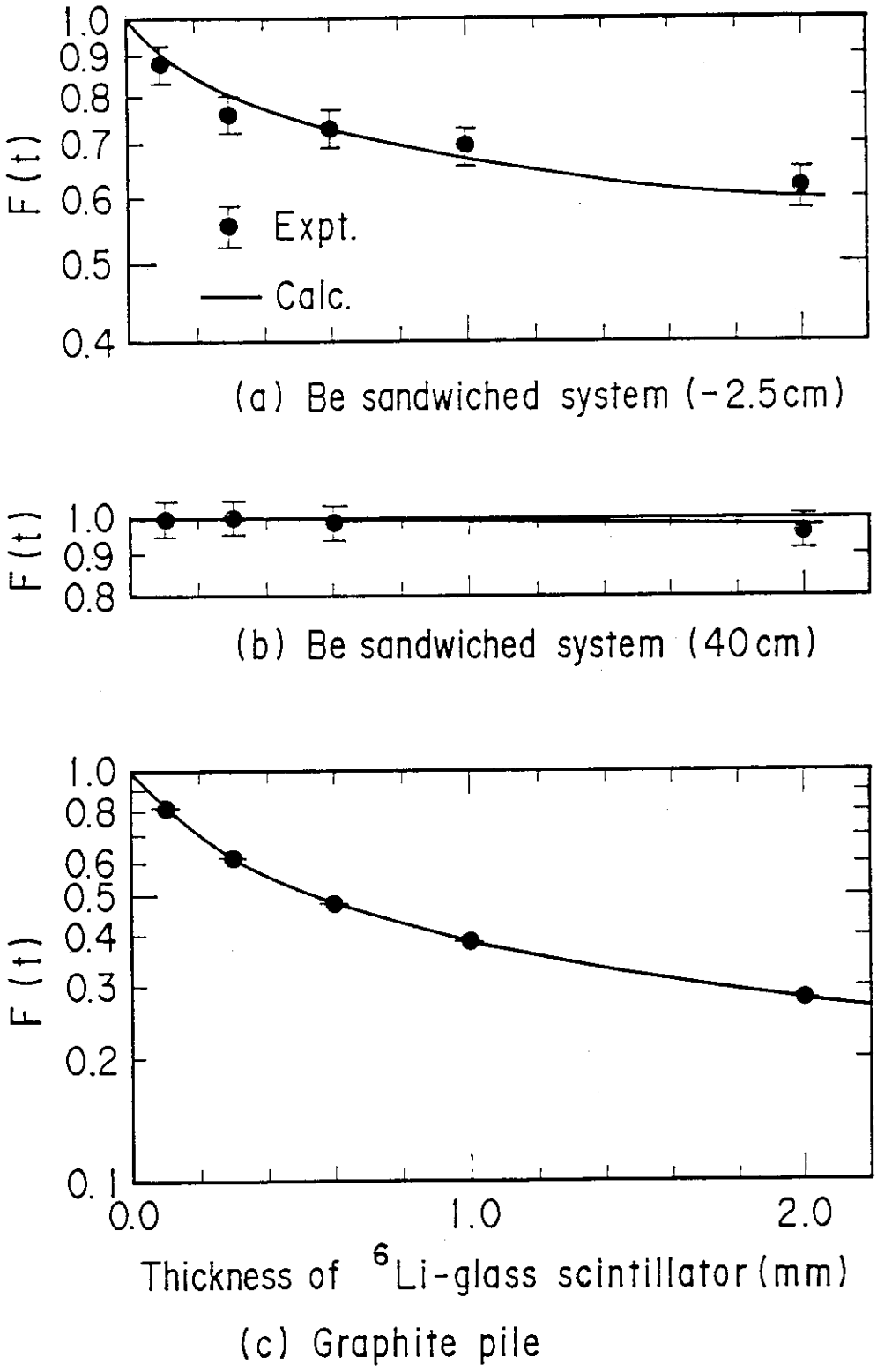

Fig. 4.1.2 Self-shielding factor of ^{6}Li-glass scintillators of different thicknesses; (a) Be sandwiched system (-2.5 cm), (b) Be sandwiched system (40 cm),(c) graphite pile

4.2 Estimation of Self-Shielding Factors Associated with $^{6}Li_2O$ Pellets in the Fusion Engineering Benchmark Experiments

K. Tsuda, K. Kosako, H. Maekawa and T. Nakamura

A ^{6}Li-enriched type of Li_2O pellet detectors, which have the advantage of having high sensitivity, were used to measure the tritium production rates (TPR) from $^{6}Li(n,\alpha)^{3}T$ reactions in the fusion engineering benchmark experiments.[1),2)] In spite of high sensitivity, the neutron spectrum being so soft, the effect of self-shielding should be taken into account. However, as a general rule, accurate correction for it is difficult in fusion blanket systems because the flux of the incident neutrons onto the detector surface is of multi-energy and anisotropy, and moreover the scattering effect in the detectors is not negligible. The authors proposed a calculational method for the self-shielding correction which could cope with the above-mentioned complexities and applied it to the fusion engineering benchmark experiments.

Accurate correction method for self-shielding effect

The fundamental formulation of self-shielding factor, Gr, which can deal with the incident neutrons of multi-energy and anisotropy is given by the equation (1) on the assumption that the incident neutron flux, $F(E,\theta)$, is constant along the surface and that no perturbation occurs.

$$G_r = \frac{\iint T_6'(E,\theta)F(E,\theta)d\omega dE/N'_6}{\iint T_6(E,\theta)F(E,\theta)d\omega dE/N_6} \qquad (1)$$

Where, $T_6(E,\theta)$ is the number of the tritium atoms produced from ^{6}Li atoms in $^{N}Li_2O$ pellets by irradiation of unit flux of uniform neutrons incident onto the surface with an angle θ to the normal and N_6 is the number of ^{6}Li atoms in $^{N}Li_2O$ pellets. The primes denote ^{6}Li-enriched pellets. $T_6(E,\theta)$ and $T'_6(E,\theta)$ were calculated by a Monte Carlo code UMCTP developed for accurate neutronic calculation of tritium production. These functions were devided by the number of ^{6}Li atoms and by the cross section of $^{6}Li(n,\alpha)^{3}T$ to obtain the non-dimensional form that have a physical concept of self-shielding. They were named absolute self-shielding functions, $g_{abs}(E,\theta)$ and $g'_{abs}(E,\theta)$, and are

shown in Fig.4.2.1.

Application to the fusion engineering benchmark experiments

F(E,θ) in equation (1) was calculated by DOT 3.5 with the 42 energy group cross section set GICX40[3] both for the reference system and for the Be sandwiched system. The self-shielding factors calculated are shown in Fig.4.2.2. The comparison between the measured TPRs corrected for self-shielding and the calculated values is shown in Fig.4.2.3. The calculated TPRs were obtained by DOT 3.5 with the 125 group cross section set JACKAS.[4]

Reference

1) Nakamura T.,et al. : JAERI-M 84-138, pp105-107 (1984).
2) Nakamura T.,et al. : JAERI-M 85-116, pp140-143 (1985).
3) Seki Y. and Iida H. : JAERI-M 8818 (1980).
4) Kosako K.,et al. : In this Annual Report 4.15.

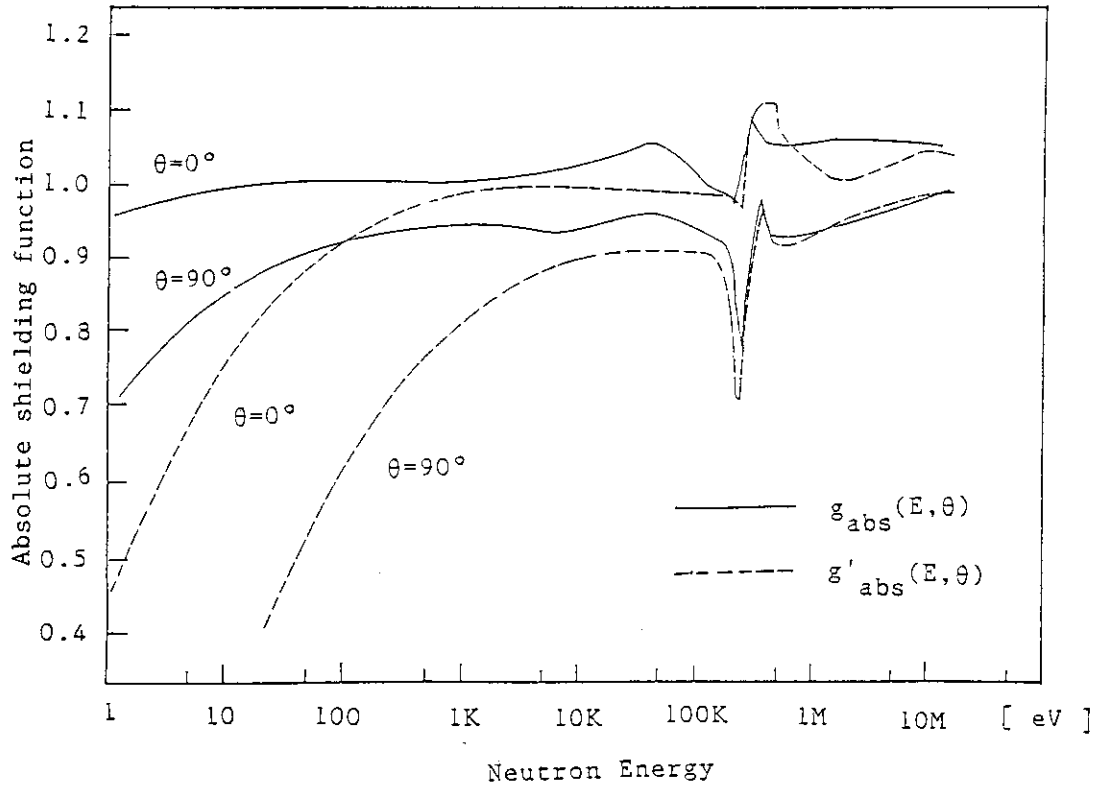

Fig.4.2.1 Absolute self-shielding functions

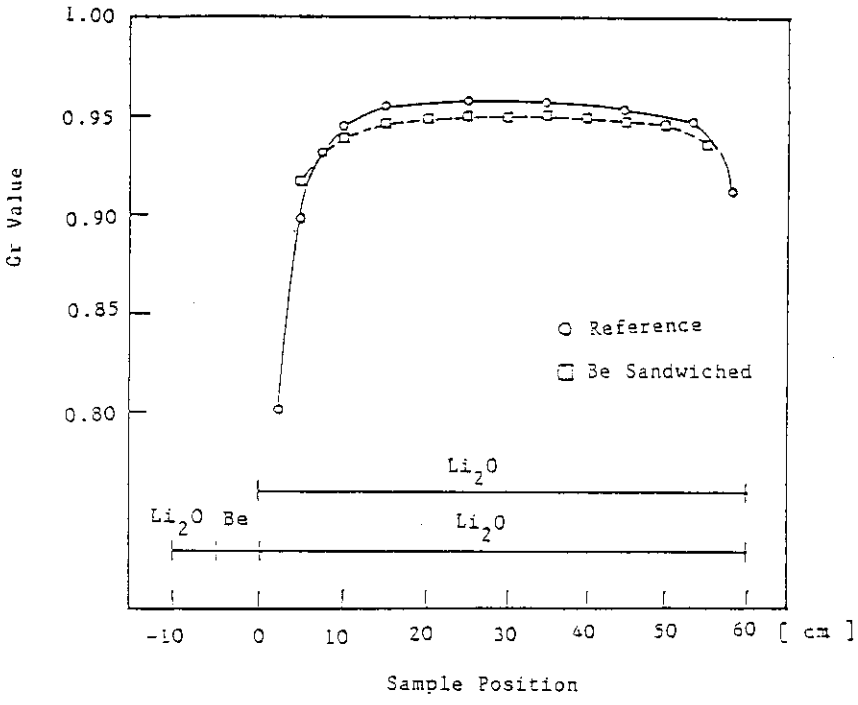

Fig.4.2.2 Self-shielding factors in the fusion engineering benchmark experiments

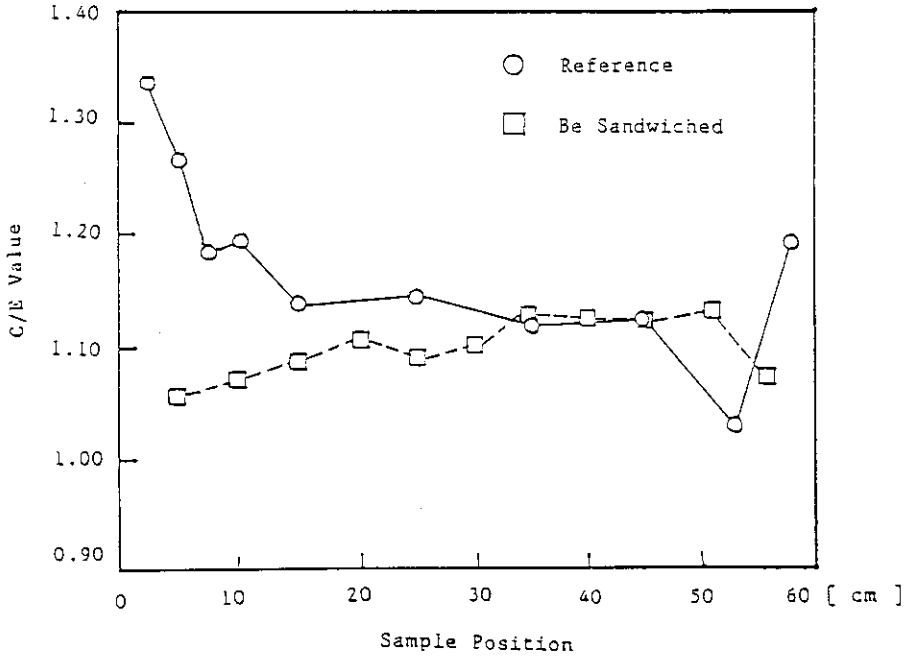

Fig.4.2.3 Comparison between the corrected experimental ^{6}Li-TPRs and the calculated

4.3 Calculation of Gamma-Ray Response Function for NE213 Liquid Scintillator

S. Yamaguchi, Y. Oyama and H. Maekawa

The measurement of the gamma-ray leakage spectrum is being carried out using a 5.06-cm diameter. by 5.06-cm long NE213 liquid scintillator. The gamma-ray energy spectrum is obtained by unfolding the pulse-height data. The unfolding requires an accurate response matrix. There are some studies of gamma-ray response function of NE213. A response matrix for the same type detector as that used in the present experiment was calculated by Shin et al.[1] However the discrepancy between their calclation and experiment is large due to not taking account of the materials around the scintillator. The present authors have calculated the response function considering the peripheral materials by a Monte Carlo code "MARTHA",[2] which was developed for NaI scintillator.

The computational model of the NE213 detector is shown in Fig. 4.3.1. The gamma-rays were assumed to impinge on the detector parallel to the cylinder axis. The mass attenuation coefficients of photon was refered to Ref. (3). An electron was assumed to move in accordance with the multiple-scattering theory, and to lose its energy only by collisions with carbon atom. The energy loss due to collision with hydrogen and bremsstrahlung were ignored. It was assumed that the scintillation efficiency of the NE213 for electrons is linear with energy.

The comparison of calculated and measured responses for ^{54}Mn and ^{24}Na γ-sources are shown in Fig. 4.3.2 and 4.3.3, respectively. The calculated spectra are broadened by the detector resolution ($(\Delta E/E)^2 = a+b/E$) and normalized to the experimental value. The results of calculation agree fairly well with experimental values.

Calculations of the response matrix were carried out for the incident γ-ray energies of 0.39 $\sim$ 11.51 MeV covering pulse-height range from 0.313 to 9.5 Na light unit. The isometric representation of the obtained response matrix is shown in Fig.4.3.3.

The energy loss by bremsstrahlung and the non-lineality of scintillation efficiency is to be considered in the further study.

References

1) Shin K., et al.: J. Nucl. Sci. Technol. 16 (1979) 390.

2) Saito K. and Moriuchi S.: Nucl. Instr. and Meth. 185 (1981) 299.

3) Storm E. and Israel H.I., LA-3753 (1967).

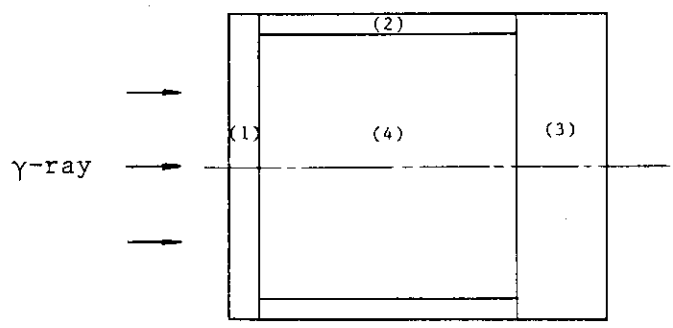

Fig. 4.3.1 Calculational model of the NE213 liquid scintillator
(1),(2),(3) : alminum layer, (4) : scintillator

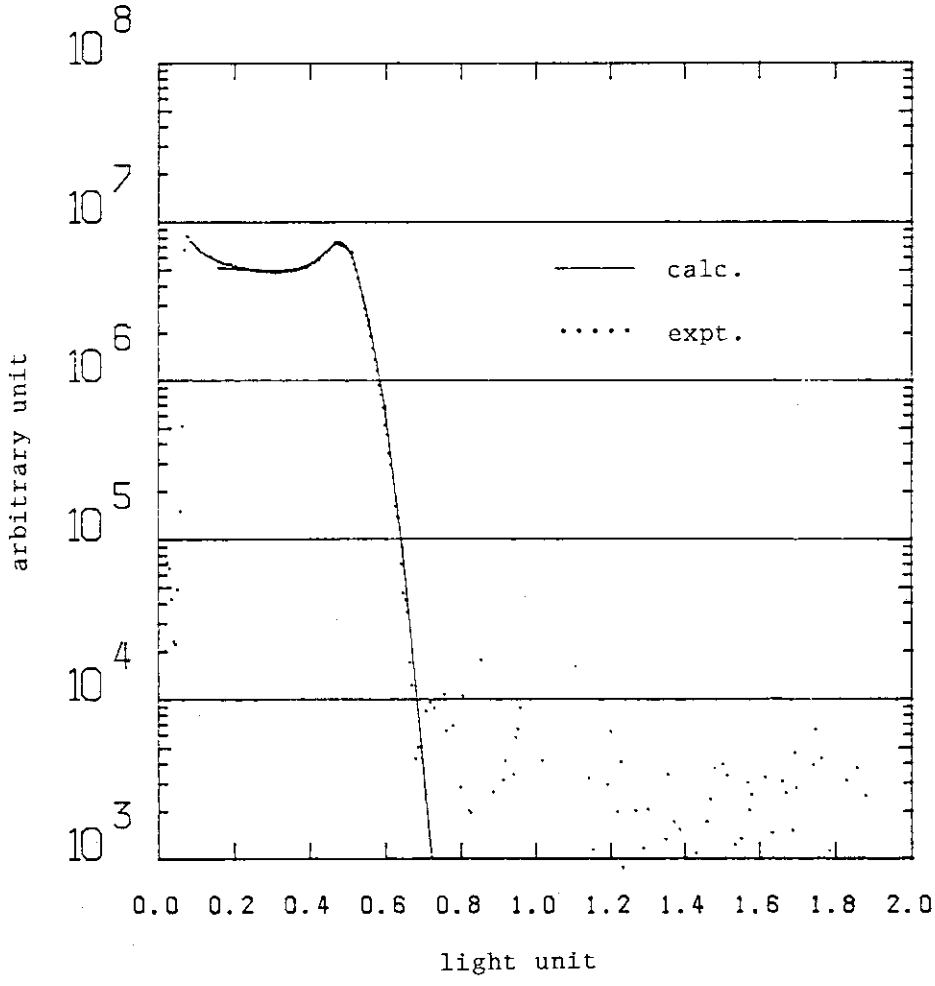

Fig. 4.3.2 Comparison of calculated and measured response functions for γ-rays from ^{54}Mn source

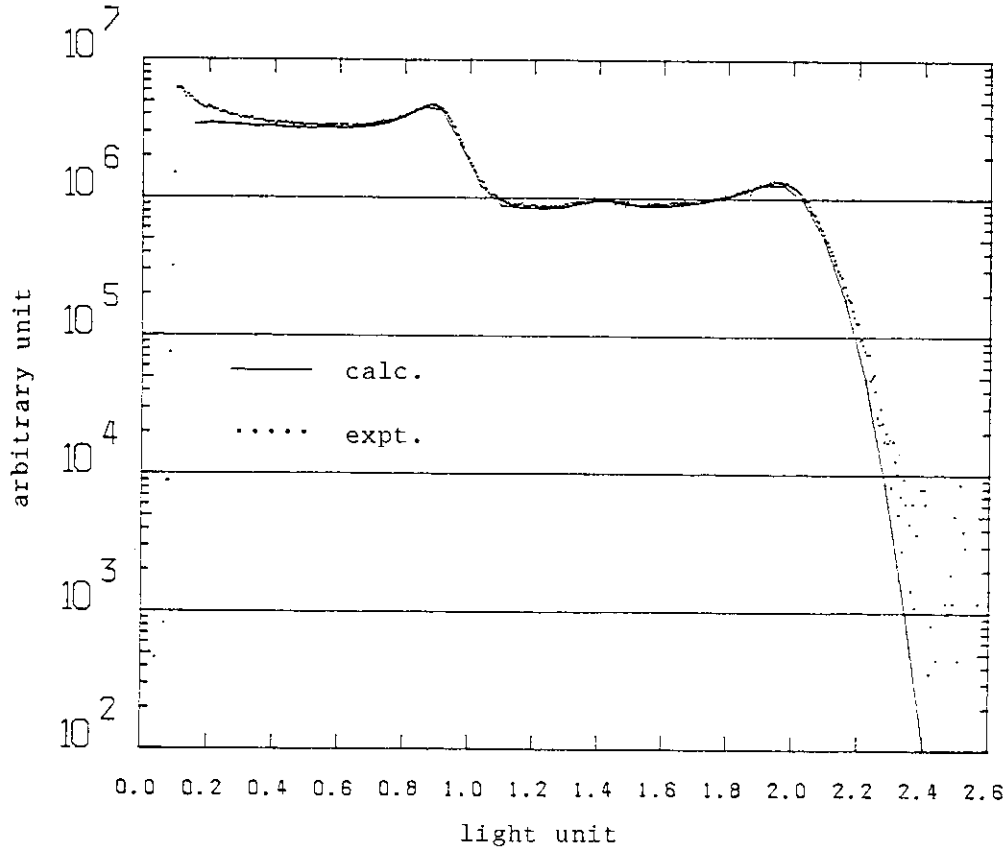

Fig. 4.3.3 Comparison of calculated and measured response functions for γ-rays from ^{24}Na source

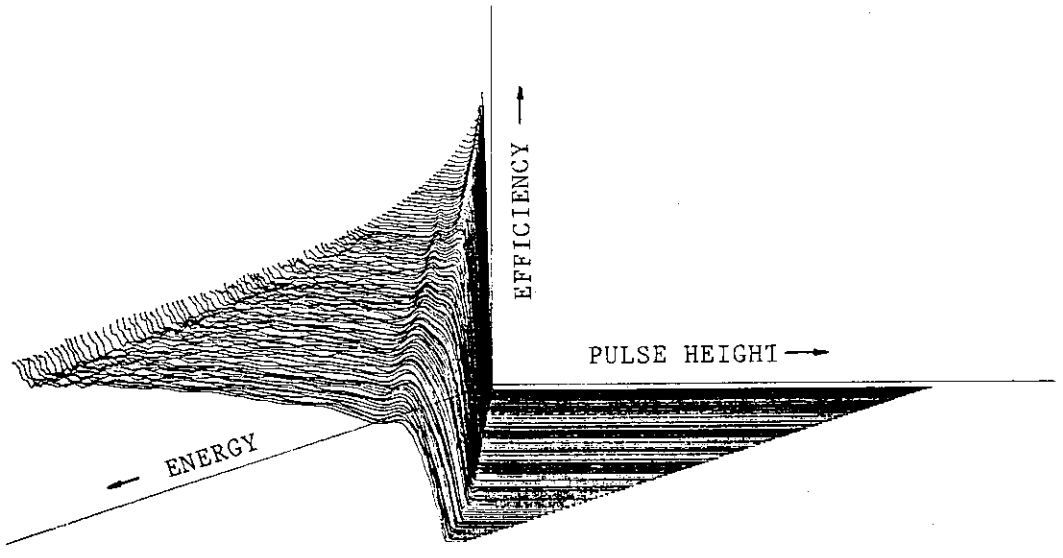

Fig. 4.4.4 Isometric representation of the response matrix for 5.06 cm-diameter by 5.06 cm-long NE213 liquid scintillator

4.4 Modification of the Time-of-Flight System for Extending to Lower Energy Range

Y. Oyama, S. Yamaguchi and H. Maekawa

The time-of-flight system has been modefied to extend the lower energy limit from 500 keV to 80 keV for the leakage neutron spectrum measurement. The new system can measure the resonance region of ^{6}Li which is more interested in fusion blanket neutronics.

The modification of the electronic circuit was performed according to the change of voltage supplied for the photmutiplier tube to extend the measuring energy range as shown in Fig. 4.4.1. The main feature compared with the previous two-bias system[1] is that the energy pulse is feeded to two independent shape discrimination circuits to eliminate the pulse saturation. The one-tenth attenuated pulse is used for higher pulse height signal and the direct pulse was limited to lower pulse height which does not saturate in the circuit. The coincidence scheme of pulse shape discrimination for low bias setting is illustrated in Fig. 4.4.2. The mixed coincidence signals are provided for the low bias measurement. The result of new pulse shape discrimination system is shown in Fig. 4.4.3 for the gated and ungated pulses as two parameter expression.

The other problems related to the lower extension of energy range are on the methods of calibration for setting bias level and determination of efficiency. Since there is no aproppriate gamma-ray source corresponding to the proton energy below 100 keV, the discriminator for bias setting should be calibrated on the pulse height spectrum to ensure the reproducibility of the effeciency for the system. The Americium-241 gamma-ray source was used for this purpose and the discriminator was set to the one-sixteenth of its photo-peak.

The efficiency corresponding to this bias setting is composed by the differential efficiencies calculated by the Monte Carlo method, considering the fraction of neutron loss at each pulse height bin due to the pulse shape coincidence. The efficiency was also determined by the comparison method using a graphite standard neutron field and MORSE-DD[2] calculation. The comparison of both methods shows a good agreement with each other as shown in Fig. 4.4.4.

Reference

1) Oyama Y., Maekawa H. : Nucl. Instr. and Meth. A245 (1986) 173, also JAERI-M 83-195 (1983)

2) Nakagawa M., Mori T.: JAERI-M 84-126 (1984)

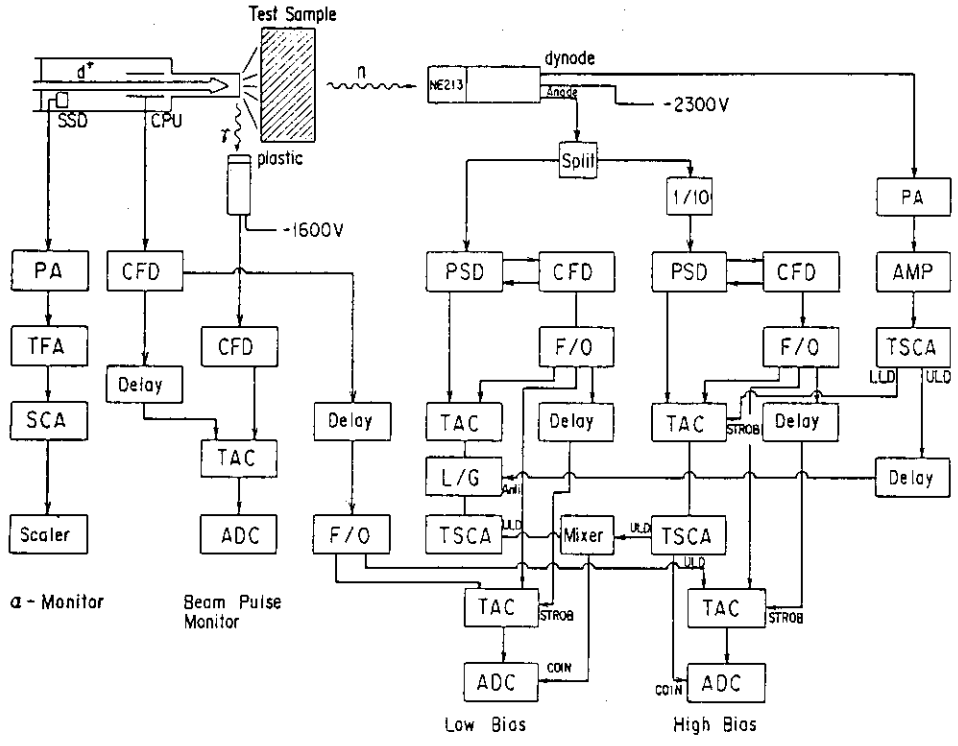

Fig. 4.4.1 New electronic circuit diagram

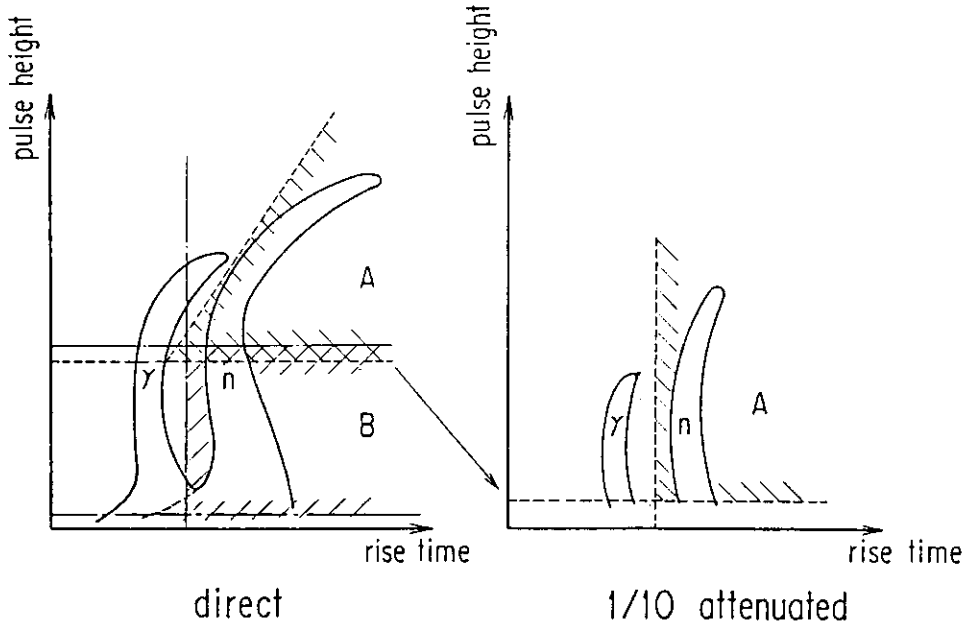

Fig. 4.4.2 Pulse shape coincidence scheme
mixed gate A+B is provided for low bias

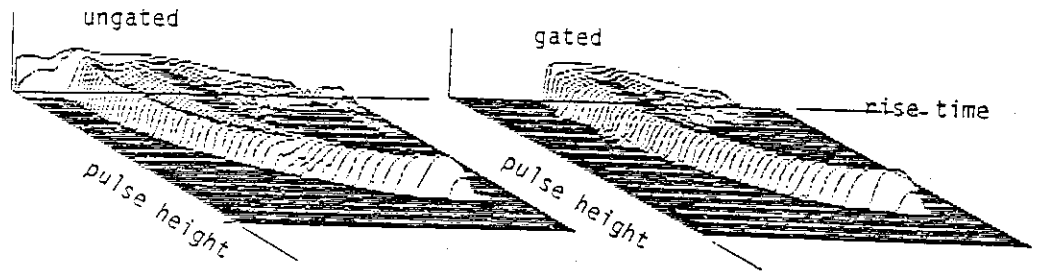

Fig. 4.4.3 Two parameter expression of pulse shape discrimination

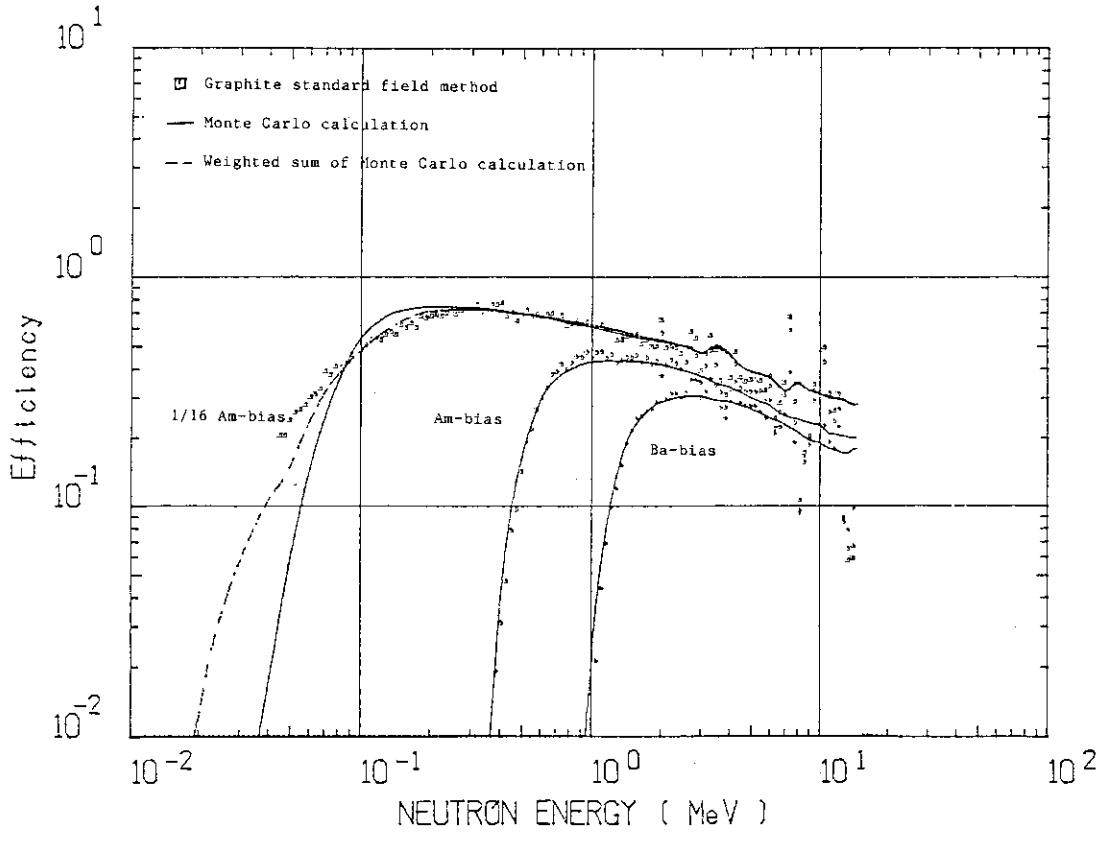

Fig. 4.4.4 Comparison of efficiency determination method
Simbols are the values by graphite standard field method and solid lines are the values by Monte Carlo method for 1/16 Am, Am and Ba bias, respectively. Dotted line is corrected by neutron loss fraction

4.5 Activation Cross Section Measurement of Zr and Cr for 14 MeV Neutrons

Y. Ikeda, C. Konno, K. Oishi**, T. Nakamura, H. Miyade*, K. Kawade*, H. Yamamoto*, and T. Katoh*

The measurement of activation cross section of the elements included in the fusion reactor materials has been conducted for 14 MeV neutrons utilizing the FNS facility since 1984. There has been significant progress in getting data extensively on the elements of Zr, Ti, Cr, Sc, V and so on. In this chapter, the measurements of Zr and Cr are described.

The method and irradiation configurations were the same as the former case reported in the annual report in 1985.(1) The measured reactions and associated nuclear data are given in Table 4.5.1. In order to obtain data as much as possible, the flux monitoring method was improved by applying a technique in which two Nb flux monitor foils were measured simultaneousely by one Ge detector. This method could reduce the overall measuring time. The shape and weight of the two foils, however, should be equal to keep the accuracy of the flux values at the sample position.

In the case of $^{96}Zr(n,2n)^{95}Zr$ measurement, one ^{96}Zr sample was repeatedly used since it is difficult to obtain. The data for each energy was obtained by irradiating the sample in the corresponding angle. The activity remained in the previous irradiation was subtracted from the measured activity correcting the decay.

As mentioned in the previous report there were several adjacent isotopes in Zr and Cr which make it difficult to deduce the actual contribution of the interest reaction from other ones by competing reaction. The measured cross sections were corrected by the abundance of the target nuclei in the sample.

In usual cases, neutron intensity at the D-T target was about 1.5×10^{11}n/sec. The detector efficiency of the Ge detectors was calibrated using the calibrated gamma-ray sources and the directly irradiated sample.

---

* Nagoya University

** Visiting researcher from Shimizu Construction Co.,Ltd.

The obtained cross section for the $^{52}Cr(n,2n)$, $^{90}Zr(n,p)$, $^{91}Zr(n,p)$, and $^{91}Zr(n,np)$ are shown in Figs 4.5.1 to 4.5.4, respectively, with the data measured by other persons and evaluated in JENDL-2 and ENDF. Present data are smooth over the energy and cover a wider energy range. The experimental errors are smaller than those of other data.

We have measured the cross sections on more than fifteen elements and more than fifty reactions already and now planning to extend the number of the data on the Ni, W and Sn isotopes. Those data measured are expected to be useful in the next activation cross section library such as JENDL and ENDF.

Reference

(1) Ikeda Y., et al. : JAERI-M 85-116 (1985) 109

Table 4.5.1 Reactions and the associated decay parameters

Target Nucleus	Reaction	Product	Half-life	Gamma-ray Energy(keV)	Branching Ratio(%)
^{50}Cr	(n,2n)	^{49}Cr	41.9m	152.9	29.1
^{52}Cr	(n,2n)	^{51}Cr	27.7d	320.1	10.2
^{90}Zr	(n,α)	^{87m}Sr	2.81h	388.4	87.0
	(n,p)	^{90m}Y	3.19h	479.5	91.0
^{91}Zr	(n,np)	^{90m}Y	3.19h	479.5	91.0
	(n,p)	^{91m}Y	49.7m	555.6	94.9
^{92}Zr	(n,np)	^{91m}Y	49.7m	555.6	94.9
	(n,p)	^{92}Y	3.54h	934.5	13.9
^{94}Zr	(n,np)	^{93}Y	10.25d	266.9	6.8
	(n,α)	^{91}Sr	9.48h	1024.3	33.0
^{96}Zr	(n,2n)	^{95}Zr	63.98d	756.7	54.6

*Data were taken from Table of Isotopes, 7th Edition

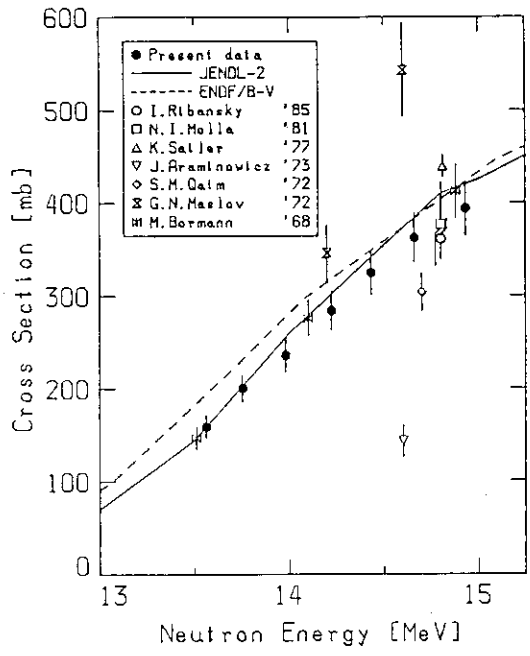

Fig. 4.5.1 $^{52}Cr(n,2n)^{51}Cr$

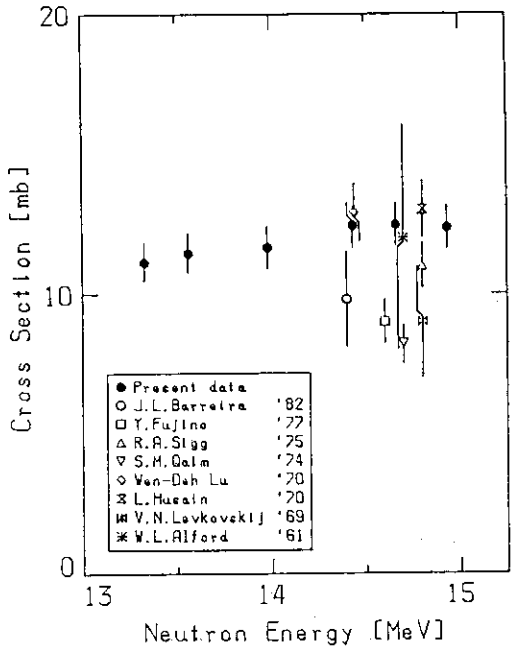

Fig. 4.5.2 $^{90}Zr(n,p)^{90m}Y$

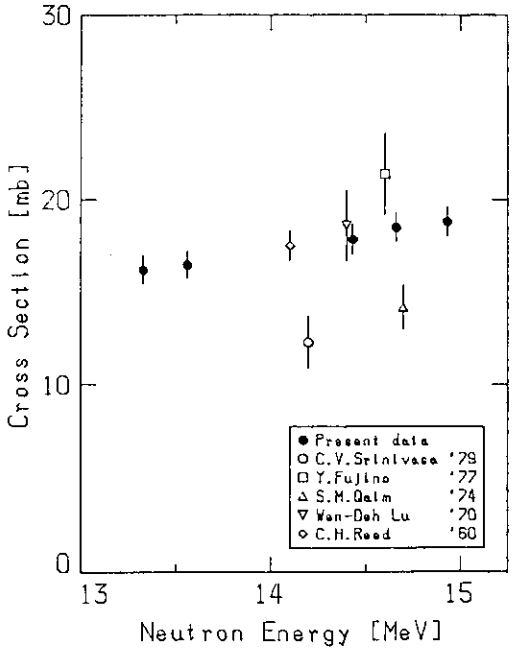

Fig. 4.5.3 $^{91}Zr(n,p)^{91m}Y$

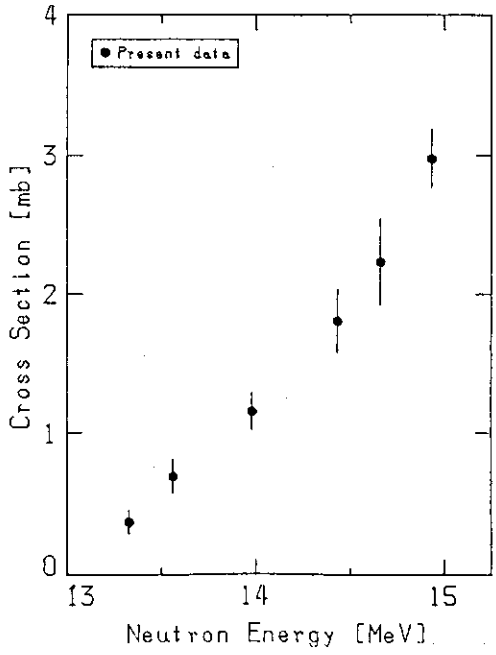

Fig. 4.5.4 $^{91}Zr(n,np)^{90m}Y$

4.6 Measurement of $^{7}Li(n,n'\alpha)^{3}T$ Cross Section Between 13.3 and 14.9 MeV

H. Maekawa, K. Tsuda, Y. Ikeda, K. Oishi[*1] and T. Iguchi[*2]

The cross section of $^{7}Li(n,n'\alpha)^{3}T$ is very important for tritium breeding not only by itself but also by $^{6}Li(n,\alpha)^{3}T$ reaction due to change of spectrum. From the result of simulated fusion blanket experiment, it was pointed out that a calculation using ENDF/B-IV overestimated the tritium production rates by about 15 %.[1] There are large differences among recently measured data. For example, the data of H. Liskien et al.[2] is lower than those of ENDF/B-IV by (8.6 - 18.5) %, those of D. L. Smith et al.[3] by (5 - 20) % and those of M. T. Swinhoe[4] by about 25 %. Therefore, we have measured the cross section of $^{7}Li(n,n'\alpha)^{3}T$ accurately using the new technique of tritium production rate measurement developed recently at JAERI.[5] At the same time, Dierckx's method [6] was also applied to the experiment by the University of Tokyo group.[*3]

Irradiated samples of JAERI were sintered $^{7}Li_2O$ pellets of 12 mm dia. x 2 mm and 85 % T.D. Those of the University of Tokyo were cold-pressed $^{7}Li_2CO_3$ pellets of 12 mm dia. x 3.5 mm. Starting material of both pellets was the same enriched $^{7}Li_2CO_3$ powder (^{7}Li : 99.926 $\pm$ 0.005 atom %). These samples were sandwiched by aluminum and niobium foils, which were used as neutron flux monitors. (See Fig. 4.6.1.) They were placed surrounding the target. The distance from the target to the each sample was about 10 cm. Irradiation time, total D-T neutron yield and average yield rate were 22500 s ($\sim$ 6 h), 4.46×10^{15} and 1.98×10^{11}, respectively.

Irradiated pellets of both groups were treated chemically and the amount of produced tritium was measured by liquid sintillation counting method. In the cases of $^{7}Li_2O$ pellets, some of produced tritium in the pellets was unresolved and remained in the gas-phase during the resolving procedure by water. The tritium in the gas-phase

---

*1 Visit scientist from Shimizu Construction Co.,Ltd.

*2 Faculty of Engineering, The University of Tokyo

*3 Collaborative Program between JAERI and The University of Tokyo

was trapped and measured separately from that in the liquid-phase. The fraction of escaped tritons during the irradiation was estimated by the independent experiment.(7) Then we got total amount of produced tritium in the pellets accurately.

Measured cross section data by $^{7}Li_2O$ pellets are shown in Fig. 4.6.2 with JENDL-3PR1, ENDF/B-IV and -V curves. These data are based on the cross section of $^{27}Al(n,\alpha)^{24}Na$ as the standard. Neutron energy at the each sample position was estimated by use of source spectrum calculated by the Monte Carlo code MORSE-DD.(8) Systematic and accidental errors are 4.1 and 2.3 %, respectively. Measured data by $^{7}Li_2CO_3$ pellets are also shown in Fig. 4.6.2. In this case, the cross section of $^{93}Nb(n,2n)^{92}Nb$ is used as the standard.

Good agreement has been obtained between the results of JAERI ($^{7}Li_2O$) and those of the University of Tokyo ($^{7}Li_2CO_3$). They also agree with those of Liskien et al.(2) and Osaka University.(9) The data of JENDL-3PR1 and -3PR2 are about 7 % lower than the present results.

References

(1) Maekawa H., et al. : JAERI-M 83-196 (1983).
(2) Liskien H., et al. : Int Conf on Nuclear Data, Antwerp (1982).
(3) Smith D. L., et al. : ANL-NDM-87 (1984).
(4) Swinhoe M., et al. : Nucl. Sci. Eng., 89, 261 (1985).
(5) Tsuda K., Maekawa H. : To be published.
(6) Dierckx R, : Nucl. Instr. Meth., 107, 397 (1973)
(7) Kudo H., et al. : To be published.
(8) Nakagawa M. and Mori T. : JAERI-M 84-126 (1984).
(9) Takahashi A., et al. : Private communication.

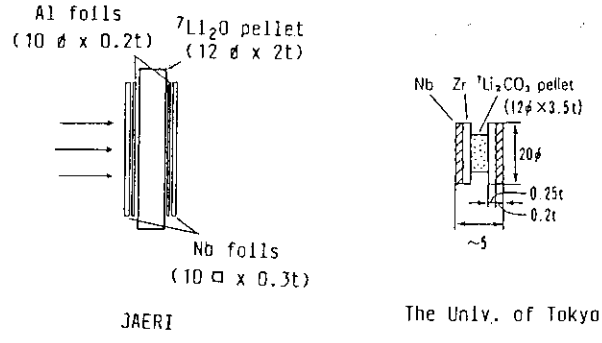

Fig. 4.6.1 Layout of irradiation samples.

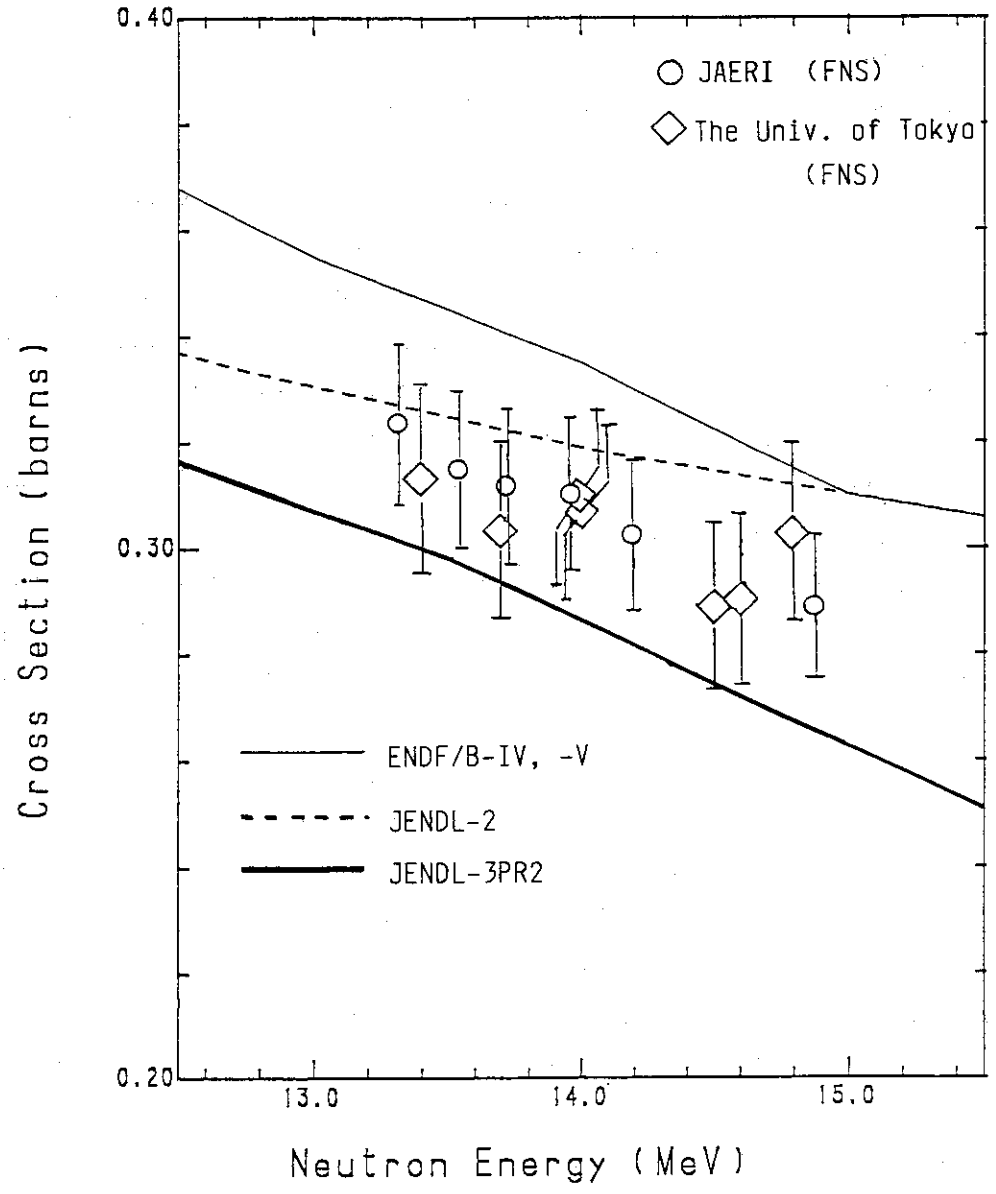

Fig. 4.6.2 Measured and evaluated cross section of $^{7}Li(n.n'\alpha)^{3}T$.

4.7 Measurements of Activation Cross Sections
——— Short-Lived Nuclides ———

C. Konno, Y. Ikeda, K. Oishi**, H. Maekawa, T. Nakamura,
T. Yamada*, K. Kawade*, H. Yamamoto*, and T. Katoh*

The effects of short-lived radioactive nuclei are important for dose estimation after shutdown of the D-T fusion reactor. Measurements of short-lived activation cross sections are rarely performed and the accuracy of them is poor. Therefore the systematic measurements on short-lived activation cross sections were planned of several elements included in the candidates of structural materials for the fusion reactor. This year the cross sections of the reactions shown in Table 4.7.1 have been measured.

Samples were irradiated by D-T neutrons at the end of the 80° beam line at the FNS facility. Since the produced nuclei are short-lived, six temporary pneumatic tubes have been set from the target to the outside of the room. The end of each tube in the target room was placed around the Ti-T target, at the angles of 5°, 45°, 65°, 95°, 135°, and 165°, to the d^+ beam, so as to change the incident neutron energy. Samples (10 mm × 10 mm × 1 mm) wrapped by cartrige papers were put in the sample holders (outer diameter 18 mm, length 40 mm) and were sent to the other end of the tube. The irradiation time was 2 ∿ 10 minutes. Gamma rays emitted from samples were measured using the Ge detector immediately after samples were returned to the outside through the pneumatic tubes. The neutron flux was estimated by reaction rate of the aluminum foil which was irradiated separately at the sample position through α-monitor counts as a relative monitor in both reaction measurements. The data of ENDF/B-V was used as $^{27}Al(n,\alpha)^{24}Na$ cross section. Obtained neutron fluxes were 1.2×10^8 ∿ 2.5×10^7 n/cm²·sec at each sample position. The total errors of cross sections using above method were within ± 10 % except the rare reactions, e.g. $^{94}Zr(n,p)^{94}Y$, $^{94}Mo(n,p)^{94^m}Nb$, $^{97}Mo(n,p)^{97^m}Nb$, and $^{98}Mo(n,np)^{97^m}Nb$.

---

* Nagoya University

** Visiting researcher from Shimizu Construction Co., Ltd.

The obtained results for $^{51}V(n,p)^{51}Ti$ and $^{92}Mo(n,\alpha)^{89m}Zr$ were shown in Fig 4.7.1 and 4.7.2, respectively.

Table 4.7.1 Measured reactions

Reaction	Half-life	Eγ(keV)	Branching Ratio(%)
$^{25}Mg(n,p)^{25}Na$	60 s	975.2	14.7
$^{27}Al(n,p)^{27}Mg$	9.46 m	843.8	73
$^{28}Si(n,p)^{28}Al$	2.24 m	1778.7	100
$^{29}Si(n,p)^{29}Al$	5.56 m	1273.2	89.1
$^{30}Si(n,\alpha)^{27}Mg$	9.462 m	843.8	73
$^{51}V(n,p)^{51}Ti$	5.8 m	319.7	93.4
$^{52}Cr(n,p)^{52}V$	3.746 m	1434.1	100
$^{63}Cu(n,2n)^{62}Cu$	9.73 m	511.0	209.2
$^{90}Zr(n,2n)^{89m}Zr$	4.18 m	587.7	89.5
$^{94}Zr(n,p)^{94}Y$	18.7 m	918.8	56
$^{92}Mo(n,\alpha)^{89m}Zr$	4.18 m	587.8	89.5
$^{92}Mo(n,2n)^{91m}Mo$	64 s	652.9	48.1
$^{94}Mo(n,p)^{94m}Nb$	6.26 m	871	0.47
$^{97}Mo(n,p)^{97m}Nb$	60 s	747	97.9
$^{98}Mo(n,np)^{97m}Nb$	60 s	747	97.9

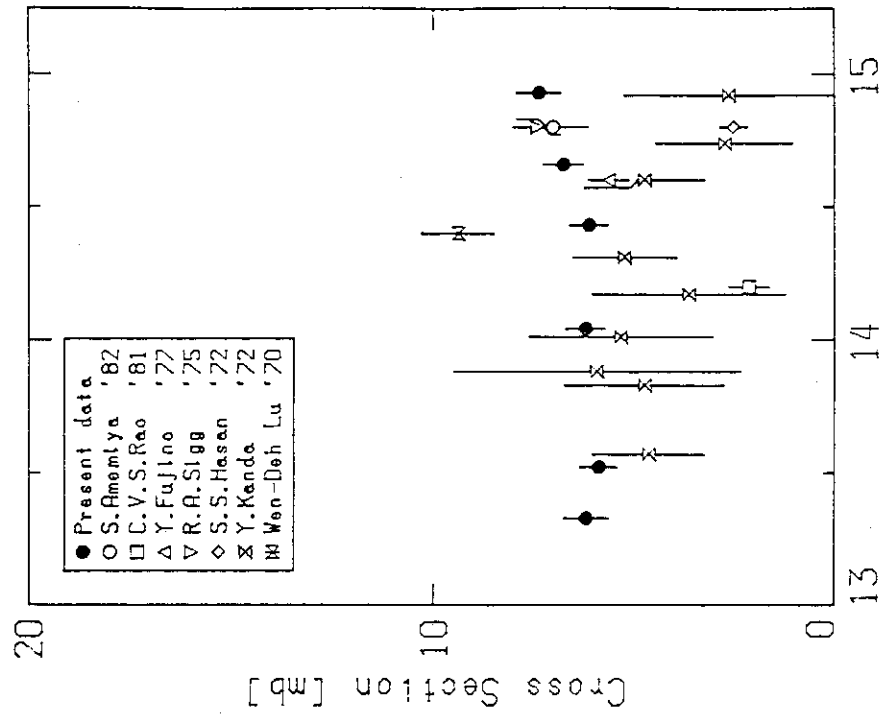

Fig. 4.7.2 Cross section of $^{92}Mo(n,\alpha)^{89m}Zr$

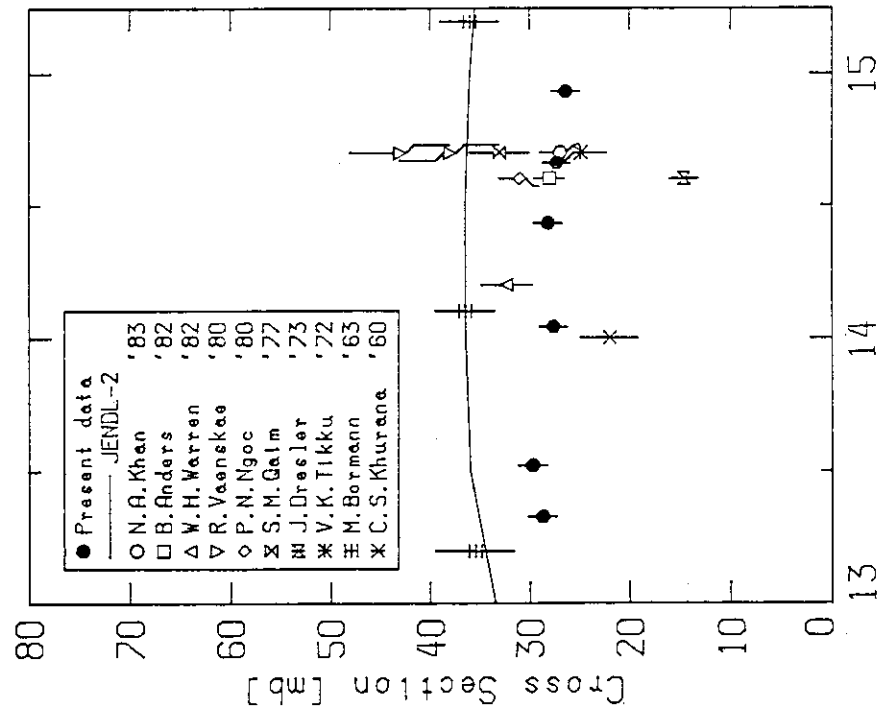

Fig. 4.7.1 Cross section of $^{51}V(n,p)^{51}Ti$

4.8 Experiment and Analysis of Induced Activities in Concrete Irradiated by 14-MeV Neutrons

K. Oishi*, Y. Ikeda, C. Konno, H. Maekawa, and T. Nakamura

Precise estimation of the induced activity of structural materials in fusion facilities is one of the most important issues in the future design of a prototype fusion power reactor. In this study, activation of concrete, one of the structural materials, has been measured experimentally and compared with calculation. From the comparison, the calculational code and the measured cross sections have been verified.

The deuterium-tritium neutrons were generated in the Ti-T rotating target placed at the end of the 0-deg beam line of the FNS facility. Eight samples of the concrete aggregates were selected, and emplaced at the distance of $\sim$ 25 cm from the target in the direction of 45 deg to the d^+ beam line. Each sample, whose dimensions are 16 mm in diameter and, 5 mm thick, was sealed completely in an acrylic case. Niobium foils were used to monitor the neutron flux for each sample. The irradiation time was $\sim$ 43 h, and the measured neutron yield was 3.4×10^{17}. From one day to half a year, after irradiation gamma-rays emitted from the produced activities were measured by Germanium detectors. Reaction rates were deduced from the gamma-ray counts with necessary corrections.

From the results, activation characteristics of each sample were obtained. For this irradiation condition, it was proved that ^{42}K, ^{24}Na, ^{43}K, ^{48}Sc, ^{47}Sc, ^{47}Ca, ^{46}Sc, and ^{54}Mn, in half life order, make an important contribution to the total activity. In addition, the comparison between the experiment and calculation was made. The calculations were performed using the fusion radioactivity calculation code THIDA [1] and its related library CROSSLIB with the input neutron flux generated from the one-dimensional transport code ANISN and the nuclear library GICX-40.[2] For ^{24}Na and ^{54}Mn, whose cross sections were well estimated, agreement between the experiment and calculation was within $\pm$ 10 %, which proved the validity of the calculational code. For reaction rates caused by Calcium and Titanium isotopes,

---

* Visiting researcher from Shimizu Construction Co., Ltd.

however, the calculational results differed from the experimental ones between - 20 % to + 40 % were obtained.(see Fig. 4.8.1) This inconsistency was caused by the uncertainty of cross sections around 14 MeV, because the incident neutron energy was almost 14 MeV.

Cross section measurements around 14 MeV were performed at the FNS and listed in Table 4.8.1. Samples, except ^{48}Ca, were separated isotopes; the abundance of remarkable nuclide was > 90 %. Because the same radioactive products are sometimes produced by different reactions, e.g., $^{46}Ti(n,p)^{46g}Sc$ and $^{47}Ti(n,np)^{46g}Sc$ reactions, different constituents of separated isotopes were irradiated simultaneously to isolate the individual reaction cross sections. Six to eight samples were wrapped by each isotope, of $\sim$ 50 mg, in a cartridge paper, the effective area being 1 cm^2. The samples were positioned at 10 cm in the radius, centered the target from 2.8 to 165 deg to the d^+ beam. The incident neutron energy was from 13.3 to 14.9 MeV. The neutron fluxes were monitored using Niobium foils. The neutron source intensity was $\sim 2 \times 10^{11}$ n/s at the target. Consequently, calculations were performed again using the measured cross sections (see table 4.8.2), and then the agreement between experiment and calculation was improved within ± 10 %. (see Fig 4.8.1)

References

(1) Iida H. and Igarashi M. : JAERI-M 8019 (1978)

(2) Seki Y., et al. :JAERI-M 8818 (1980)

Table 4.8.1 Nuclear parameters for reactions to be measured

Reaction	$T_{1/2}$	Eγ(MeV)	Iγ(%)
$^{42}Ca(n,p)^{42}K$	12.36 h	1.5247	17.9
$^{43}Ca(n,p)^{43}K$	22.4 h	0.3729 0.6178	86.7 80.0
$^{44}Ca(n,np)^{43}K$	"	"	"
$^{48}Ca(n,2n)^{47}Ca$	4.536 d	1.2971	76.0
$^{46}Ti(n,p)^{46g}Sc$	83.8 d	0.88925 1.12051	100.0 100.0
$^{47}Ti(n,np)^{46g}Sc$	"	"	"
$^{47}Ti(n,p)^{47}Sc$	3.35 d	0.1594	68.0
$^{48}Ti(n.np)^{47}Sc$	"	"	"
$^{48}Ti(n,p)^{48}Sc$	43.7 h	0.9835 1.03750 1.31209	100.0 97.5 100.0
$^{49}Ti(n,np)^{48}Sc$	"	"	"
$^{50}Ti(n,\alpha)^{47}Ca$	4.536 d	1.2971	76.0

Table 4.8.2 Comparison between cross sections of CROSSLIB and those of present measurement

Reaction	CROSSLIB σ(mb)	PRESENT σ(mb)	abundance (%)	CROSSLIB / PRESENT
$^{42}Ca(n,p)^{42}K$	152.0	116.0	0.65	0.92
$^{43}Ca(n,np)^{42}K$	30.0	——	0.145	
$^{43}Ca(n,p)^{43}K$	154.0	103.0	0.145	1.36
$^{44}Ca(n,np)^{43}K$	2.6	2.6	2.09	
$^{46}Ti(n,p)^{46g}Sc$	258.36	229.78	7.99	0.94
$^{47}Ti(n,np)^{46g}Sc$	17.60	66.47	7.32	
$^{47}Ti(n,p)^{47}Sc$	112.34	128.60	7.32	0.76
$^{48}Ti(n,np)^{47}Sc$	10.60	15.74	73.99	
$^{48}Ti(n,p)^{48}Sc$	65.40	59.32	73.99	1.10
$^{49}Ti(n,np)^{48}Sc$	6.80	6.78	5.46	
$^{50}Ti(n,\alpha)^{47}Ca$	9.00	9.39	5.25	0.95
$^{48}Ca(n,2n)^{47}Ca$	800.00	843.74	32.43*	

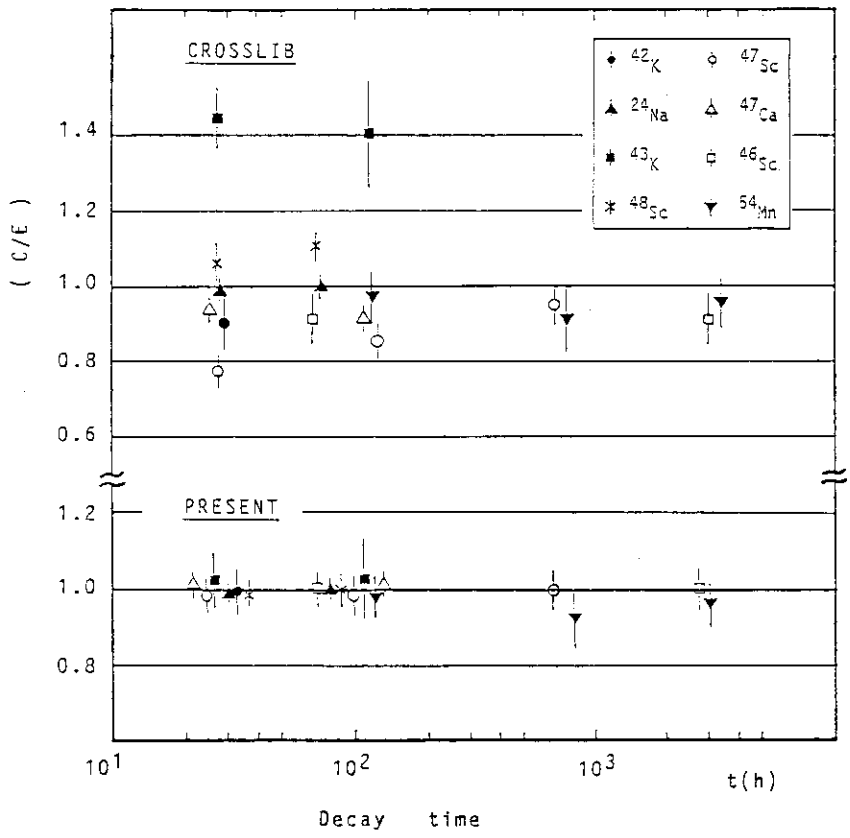

Fig. 4.8.1 The calculation-to-experimental (C/E) value of gamma ray intensity. Calculations were performed with the input cross section of CROSSLIB and present data, respectively.

4.9 Measurements and Calculation of Fast-Neutron Spectra in Concrete Assembly

K. Oishi*, Y. Ikeda, H. Maekawa and T. Nakamura

Measurement of D-T neutron spectra in concrete is a very important issue for fusion facilities ; not only for providing basic data for shielding, but also for estimating activity in concrete, which has become of special interest recently. In this study, neutron spectra in concrete irradiated by 14 MeV neutrons have been measured, and compared to calculations.

Experiment was performed at the first target room of the FNS facility. The 14 MeV neutrons were produced by bombarding the water cooled Ti-T target with the 330 kV deuteron beam. The concrete slab, 60 cm diameter and 60 cm thick, was set at 20 cm apart from the target, in the direction of d^+ beam. Experimental layout is shown in Fig. 4.9.1. Measurements of neutron spectra were done by the two methods :

(1) small sphere NE213 spectrometer,[1)]
(2) multi-foil activation method (MFA) using Fe, In, Al, Ni, Au, Au+Cd, Zr, and Nb foils.

For NE213, neutron spectra were obtained through unfolding the pulse height spectra by the unfolding code FORIST. A typical neutron spectrum obtained using NE213 is shown in Fig. 4.9.2. In case of foil activation method, the result of DOT3.5 calculation was used as a guess spectrum to unfold reaction rates by the code SAND II. The reaction rates for each foil are shown in Fig. 4.9.3.

The change of the peak energy of the spectrum with the detector position in concrete was estimated using the Nb/Zr value and the result is shown in Fig. 4.9.4.

Calculation was performed using DOT3.5 with the 42-group cross section set GICX40. Each experimental result, integrated in the energy range En $\geq$ 10.1 MeV was compared with the calculation. The C/E values are shown in Fig. 4.9.5. From the comparison good agreement

---

* Visiting scientist from Shimizu Construction Co., Ltd.

between two experimental methods was obtained, while the result of calculation was overestimated in comperison with the experimental values as the distance increases from the front suface.

As the further study, a direct method was adopted for estimating the activity of concrete and several concrete samples were set in the assembly. After the irradiation, activities of these samples were measured using Ge detectors. The comparison between measurement and calculation will be performed after all of the measurements have been finished.

References

(1) Oyama Y. et al., "Development of a Spherical NE213 Spectrometer with 14 mm Diameter," JAERI-M 84-12 (1984)

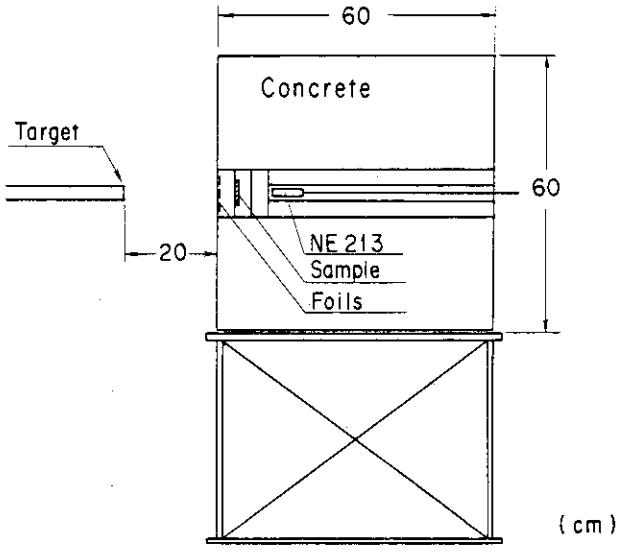

Fig. 4.9.1 Experimental layout

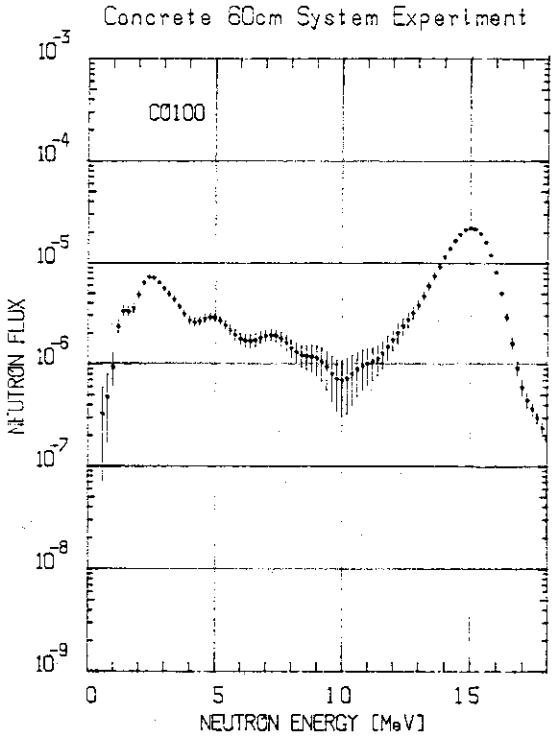

Fig. 4.9.2 Typical neutron spectra obtained using NE213 (d=10cm)

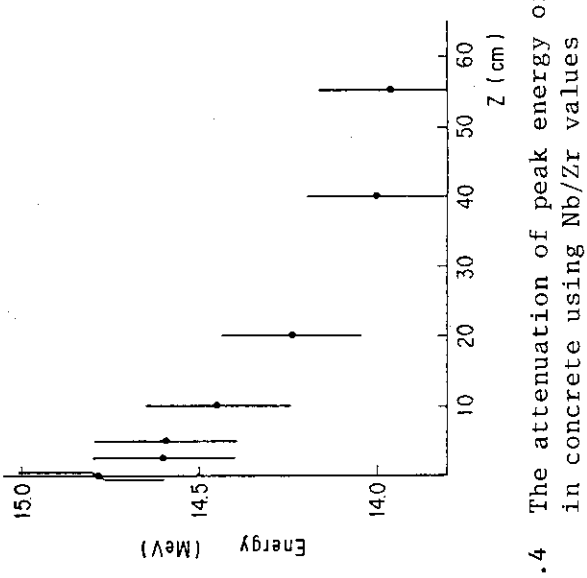

Fig. 4.9.4 The attenuation of peak energy of spectra in concrete using Nb/Zr values

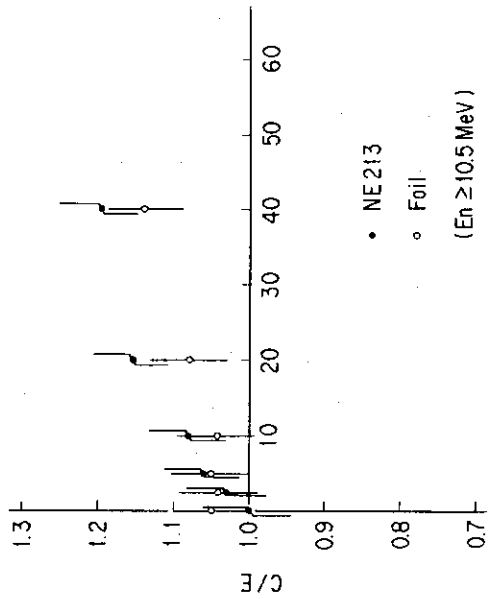

Fig. 4.9.5 C/E values for $E_n \geq 10.1$ MeV

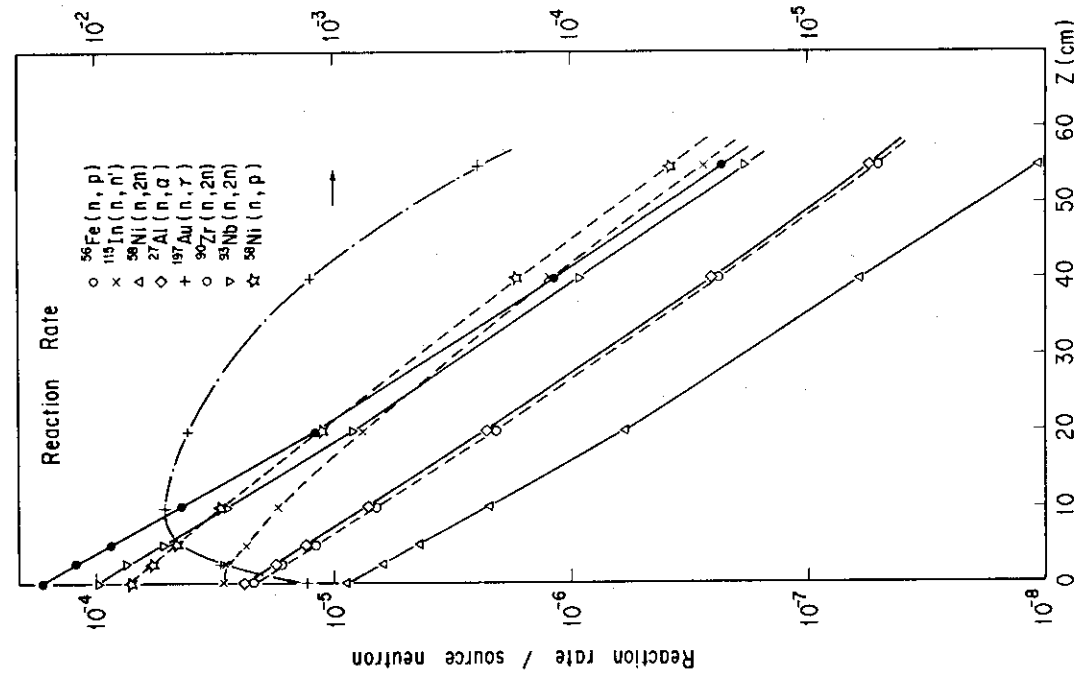

Fig. 4.9.3 Reaction rate for each foil

4.10 Fusion Blanket Engineering Benchmark Experiment - Phase 1
--- Effect of Indirect Source Term ---

T. Nakamura, S. Yamaguchi, Y. Oyama, K. Kosako, K. G. Porges and C. Konno

In the phase 1 series of fusion engineering benchmark experiments at FNS, the neutrons incident to the front face of the test blanket module are of two types: one is 14 Mev neutrons direct from the target and the other is reflected ones on the room wall with degraded energies by the scatterings with the wall materials. In the experimental analysis, the evaluation of the latter is much complicated, since the calculation involves the room itself as a component. It is required, therefore, to obtain an experimental evidence to examine the accuracy of the evaluation method.

An experiment was carried out to meet this requirement. The basic idea of the experiment is to measure the neutronic parameters by inserting a cone-shaped shadowing shield for the direct neutrons between the neutron source and the test module as is shown in Fig. 4.10.1; thus, the contribution of the reflected neutrons can be separated from the sum of two components in the ordinary arrangement without the shadowing shield. The shadowing cone consists of 40 cm long-mild steel in the front and 60 cm long polyethylene behind it. It is designed so as to shadow the front face of the test assembly keeping a distance of 100cm from the rear end of the cone to the front end of the assembly to minimize the interaction between them.

The experiment was conducted on the reference system[1], single-regioned Li_2O assembly, of the phase 1 series. This system is most sensitive to the soft component of indirect source term at the front surface. The measured parameters were: (a) neutron spectrum at the center on the front end of assembly by means of the small spherical NE213 liquid scintillator spectrometer[2] and the hydrogen-containing gas proportional counter spectrometer[3] and (b) the tritium production rates of ^6Li -(T6)- along the central axis of the assembly by Li-glass scintillator method[4]. Here, the result on T6 is reported. As for the neutron spectrum, preliminary results
are given in 4.12.

The measured T6 distributions are shown in Fig.4.10.2 for the present arrangement and the one previously performed without the shodowing shield as well as the difference between two, that corresponds to the contribution of the direct source term. In Fig. 4.10.3 is shown the fraction curve of T6 due to the indirect source term to the total along with that of the calculated. The calculation was conducted by DOT 3.5 transport code in R-Z geometry with cross section set JACKAS (see 4.14). The reflected component which is rich in slow neutrons have large contribution in the front end of assembly, but rapidly decreases the fraction with going deep in the breeder region. From about 10 cm on, the fraction of the direct neutrons is dominant.

The present results provide a good means to examine the accuracy of the indirect source term evaluated in the analysis. A reasonable agreement between the experimental and DOT- calculated curves on the franction of indirect source term shows that the evaluation of the source neutron spectrum and the modeling of the target room in the analysis are adequate.

References

1) Nakamura T., et al.: JAERI-M 84-138 p105 (1984).
2) Oyama Y., et al.: JAERI-M 84-124 (1984).
3) Bennett E., et al.: this report 4.12.
4) Yamaguchi S., et al.: JAERI-M 85-116 p118 (1985).

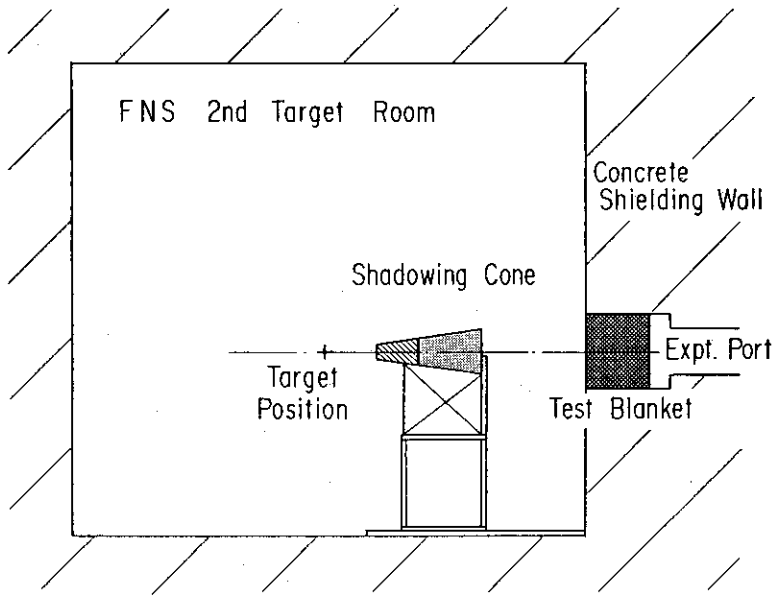

Fig. 4.10.1 Experimental Arrangement for Indirect Source Term

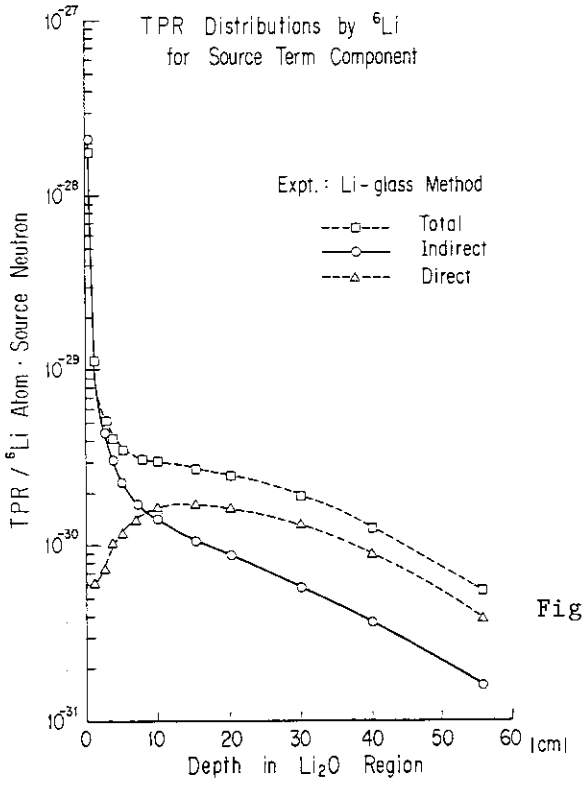

Fig.4.10.2 TPR distributions from ^{6}Li for source term components

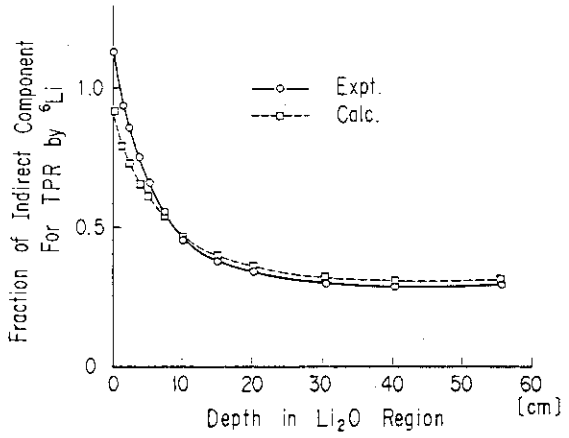

Fig. 4.10.3 Fraction of indirect component to the total TPR from ^{6}Li

4.11 Comparison Between Experiments and the Analyses by DOT 3.5 for Phase 1A Program of Fusion Blanket Engineering Benchmark Experiments

T. Nakamura, K. Kosako, S. Yamaguchi, K. Tsuda, K. Oishi*
Y. Oyama, H. Maekawa, Y. Ikeda, and C. Konno

As one of the post-experiment analyses of Phase 1A program[1,2], the measured parameters were analyzed by the two-dimensional transport code DOT3.5 in R-Z geometry using a newly prepared 125 group cross section set JACKAS[3] which is explained in section 4.15. The DOT calculation have been conducted for all of the experimental systems in the program - the reference, the first-walled and Be neutron multiplier series listed in Table 4.11.1. The present analysis is aimed to choose the cases for analyses by different neutron transport calculational methods such as MORSE-DD to make detailed comparison.

The measured parameters are: a) tritium production rates(TPRs) from ^{6}Li(T6) by the Li-glass scintillation method[4] and neutron spectra above 1MeV by the small NE213 scintillation spectrometer[5], for all assemblies; and b) TPRs by liquid scintillation counting method for lithium-containing samples[6] and reaction rates by activation foils as spectral indices, for the reference and Be sandwiched assemblies in addition to a). The experimental data have been corrected for factors such as self-shielding effect and normalized to unit source strength so that the results is compared in the ratio of the calculated-to-experimental values(C/E).

Representative cases of the results are given in Fig. 4.11.1-6. The figures 4.11.1 and 4.11.2 show the distributions of T6 and T7 for the reference and the 1st-walled systems by on-line counter methods, respectively. The T7 was derived from the measured neutron spectrum and the cross section data of ^{7}Li(n,n'α) reaction. The C/E results for the effect of Be layer to T6 distribution are shown in Fig.4.11.3. The figure 4.11.4 shows the comparison of T6 in different measuring method for the reference and the Be-sandwiched systems. The spectral

---

* Visiting researcher from Shimizu Construction Co.,Ltd.

change with position in the assembly is shown in Fig. 4.11.5 for the reference. The figure 4.11.6 shows the results for the reaction rates of activation foils.

It is concluded from this comparison that the present DOT calculations reproduce the spatial distributions of various reaction rates fairly well, as a whole. Near the region boundaries, however, the agreement is generally not good. As for T6, the calculational values are larger than the measured one for all configurations. The closer examination is necessary to explain the difference in T6 over the breeder region.

References

1) Nakamura T., et al.: JAERI-M 84-138, p105 (1984)
2) Nakamura T., et al.: JAERI-M 85-116, p135 (1985)
3) Kosako K., et al.: this report 4-15
4) Yamaguchi S., et al: JAERI-M 85-086 (1985) (in Japanese)
5) Oyama Y., et al: JAERI-M 84-124 (1984) (in Japanese)
6) Tsuda K., et al: JAERI-M 85-116, p121 (1985)

Table 4.11.1
Experimental assembly

* Reference System

One-regioned Li_2O breeder zone
60cm Li_2O

* First Walled System

No first wall	/60cm Li_2O*
0.5cm SS+	/60cm Li_2O
0.5cm SS/0.5cm PE++	/60cm Li_2O
1.5cm SS	/60cm Li_2O
1.5cm SS/0.5cm PE	/60cm Li_2O

* Be Neutron Multiplier System

5cm Be	/60cm Li_2O
10cm Be	/60cm Li_2O
5cm Li_2O/5cm Be	/60cm Li_2O**
10cm Li_2O	/60cm Li_2O

*: Identical with the reference system
**: Be sandwiched system
+: Type 316 stainless steel
++: Polyethylene as the simulant of water

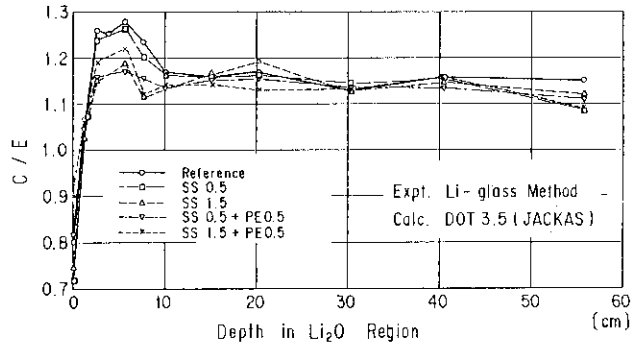

Fig. 4.11.1 C/E values of TPR from ^6Li for 1st wall experiment

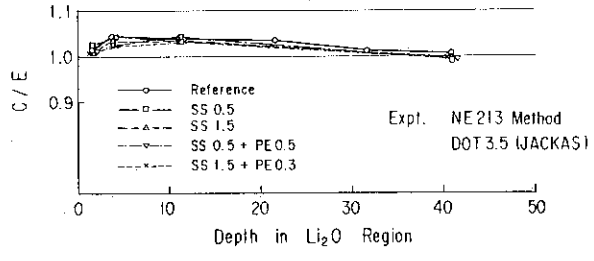

Fig. 4.11.2 C/E values of TPR from ^7Li for 1st wall experiment

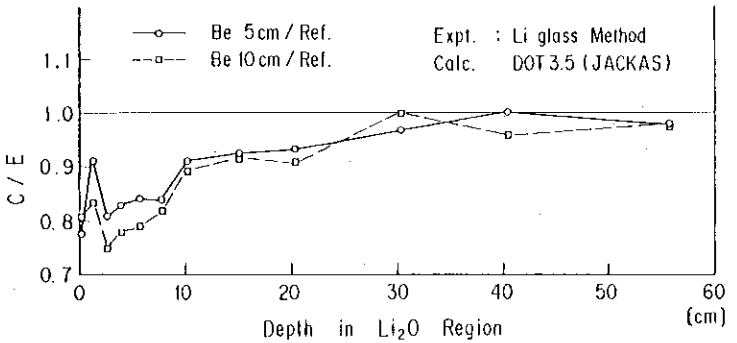

Fig. 4.11.3 C/E values of Be multiplier effect for TPR from ^6Li

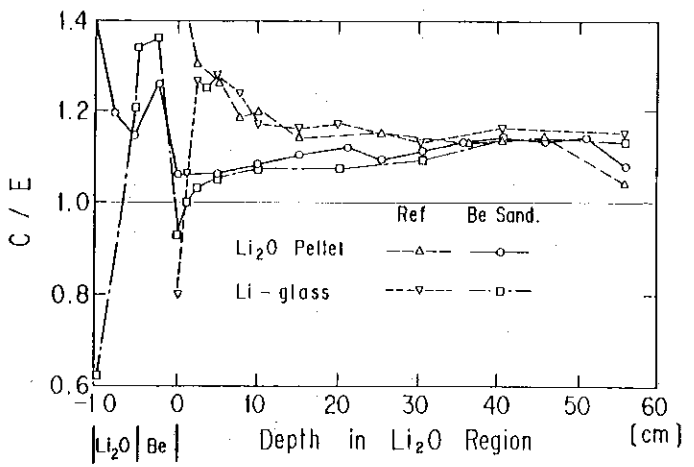

Fig. 4.11.4 C/E values of TPR from ^6Li in different configurations

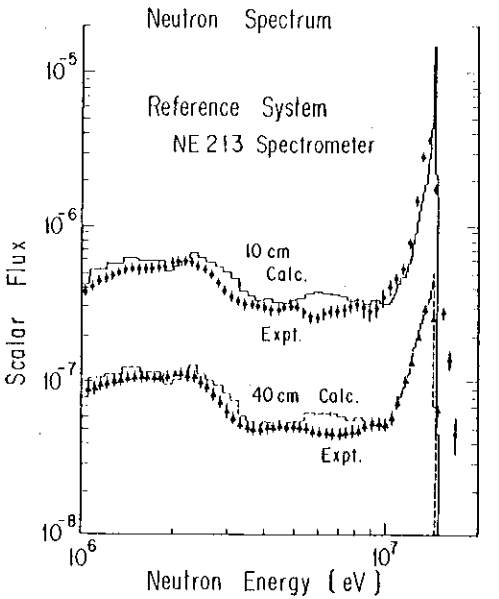

Fig. 4.11.5 Neutron spectra in the reference assembly

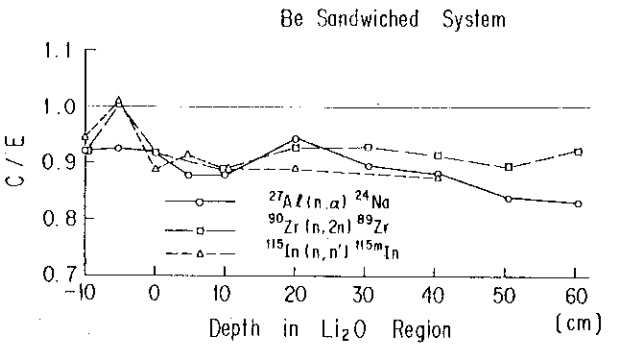

Fig. 4.11.6 C/E values of reaction rate for activation foils

4.12 Neutron Spectrum Measurement Below 1 MeV at the Mouth of Phase-I Experimental Port

E. F. Bennett*, T. J. Yule*, Y. Oyama, H. Maekawa and T. Nakamura

As a part of neutron source characterization in Phase I experiment which is conducted by JAERI-US collaborative program, a proton-recoil proportional counter has been applied by US participants. The measurement was performed at the mouth of expeimental port in the target room 2. There is a significant low-energy component in the incident spectrum because of neutron interactions in the structual material of the target assembly and because of room-returned neutrons. In the series of Phase I experiments, several experiments were conducted to characterize the source. These experiments included; measurements of the source neutron spectrum with an NE213 spectrometer and time-of-flight technique. Those experiments are limited down to 1 MeV. The measurement of spectra with the proton-recoil proportional counter technique allows the low-energy component of the spectrum to be determined with moderate resolution on an absolute basis.

The experiment was carried out for four configurations by the usage of the shadow cone and the lithium oxide assembly loaded in the port. The structure of the counter used [1] is shown in Fig. 4.12.1. The hydrogen-filled detector was used to measure the spectrum from about 2 keV to 300 keV. To cover this range, four voltages were used : 3300, 3600, 3900, and 4200 V. The hydrogen-filled detector cannot be used at higher energies because the range of the proton recoils is such that significant distortion occurs. The methane-filled detector was used to measure the spectrum from about 50 keV to 2.5 MeV. To cover this range, three voltages were used: 3400, 3900, and 4300 V. The methane-filled detector was used for the higher-energy measurements because of the increased stopping power of methane.

Figure 4.12.2 shows neutron spectrum for the configuration with the Li_2O assembly, and with shadow cone that eliminates the most part of direct component from the target. This spectrum is normalized to provide flux per source neutron. All measured neutron flux spectra tend to flatten out and remain relatively fixed in amplitude above

---

* Argonne National Laboratory

about 1 MeV. Flux spectra decrease with decreasing energy; the proton-recoil technique is not reliable below about a few keV. This figure also includes the result by a 14 mm-diameter spherical NE213 scintillation counter.[2] The agreement between both counters around 1 MeV is excellent. This fact ensures the reliability of both counters on the absolute basis.

Reference

1) Bennet E.F. and Yule T. J. : ANL-7763 (1971), see also Nucl. Instr. Meth 98 (1972) 393, and Nucl. Sci. and Eng. 27,16 (1967).

2) Oyama Y., et al. : JAERI-M 84-124 (1984) (in Japanese).

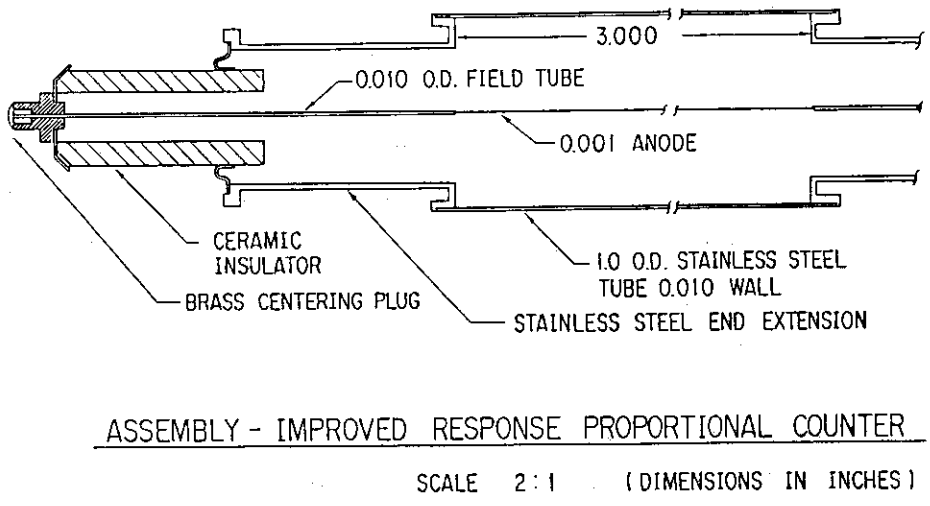

Fig. 4.12.1 Schematic drawing of proton recoil proportional counter

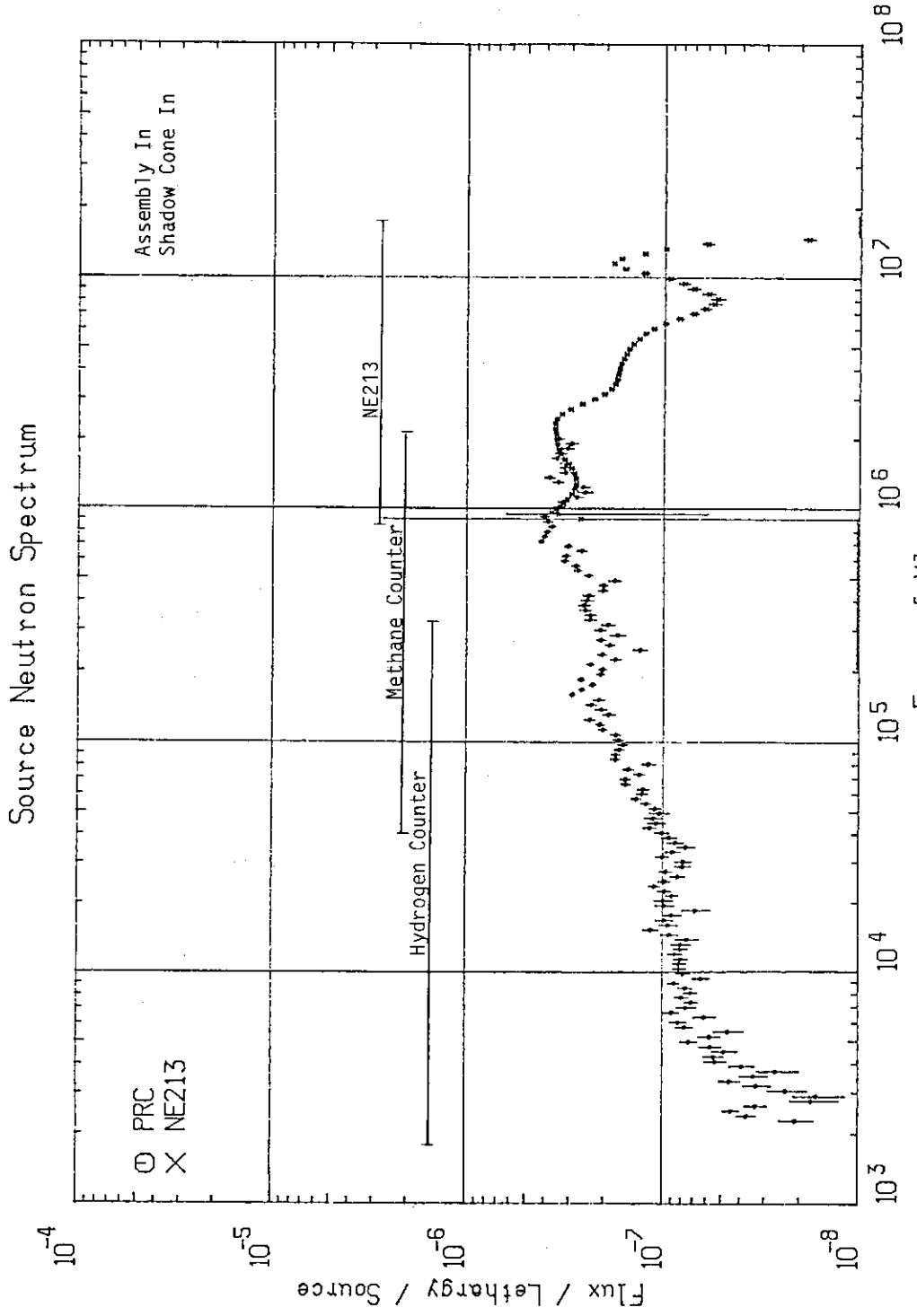

Fig. 4.12.2 Measured neutron spectrum by proton recoil counter
Also shown is the result by NE213

4.13 Analysis on the FNS Clean Benchmark Experiments

Y. Oyama, K, Kosako* and H. Maekawa

Three kinds of benchmark experiments were performed on the lithium oxide, graphite and graphite-reflected lithium oxide slab assemblies.(1) These data are compared with the calculated results for the verification of calculation code system. The uncertainties in those comparison should be examined. Those uncertainties are generally caused by the following parameters.

(1) Group constant : nuclear data, group structure, process code, weighting method, etc.
(2) Modeling : spatial mesh size, density homogenization, etc.
(3) Solution method : discrete ordinate, direct integration, Monte Carlo method, etc.

In this work, the sensitivity of group constant has been examined for possible variations of the parameters.

A variety of cross section sets were prepared to obtain the sensitivity for each parameter in the group constant. The calculations were performed by using DOT3.5 with P_5-S_{16} approximation as a reference code. The sensitivity was expressed by the ratio between the results of the reaction rates calculated by using each cross section set. The parameters for these calculations are summarized in Table 4.13.1.

The result for weighting method is shown in Fig. 4.13.1 for the graphite-reflected lithium oxide assembly. The reaction rates which are sensitive to lower energy neutrons, are much influenced by difference of weighting function as seen in the figure. Also shown is the nuclear data sensitivity in Fig. 4.13.2. In this case, the calculations by JENDL-3PR2 over estimate the reaction rates larger than the others at the deep positions.

The results for each calculation are summarized in Table 4.13.2. The nuclear data file is sensitive to the calculated results but the weighting function is more sensitive to the capture reaction like ^{6}Li for these group structures. It is necessary to check the weighting function for evaluation of the capture reactions. After the

---

* Present address: Century Research Center Corp.

examination, a standard cross section set for a fusion neutronics calculation has been provided[2].

Reference

1) Maekawa H., et al.: To be published in JAERI-M reports, see also JAERI-M 85-116 (1985) pp125-131

2) Kosako K., et al.: this report 4.15

Table 4.13.1 Parameters for the sensitivity calculations of group constant

Parameter	Variation
Process code	NJOY, PROF-GROUCH-G/B
Group structure	42, 125, 135 groups
Weighting function	1/E, E-constant
Nuclear data	ENDF/B-IV, JENDL-3PR1, -3PR2

Table 4.13.2 Summary of results

Parameter	Sensitive energy region	Sensitivity
Process code	general	2 - 3 %
Group structure	high threshold reaction	2 - 5 %
	low energy reaction	5 -10 %
Weighting function	low energy	20 -30 %
Nuclear data	general	∿10 %

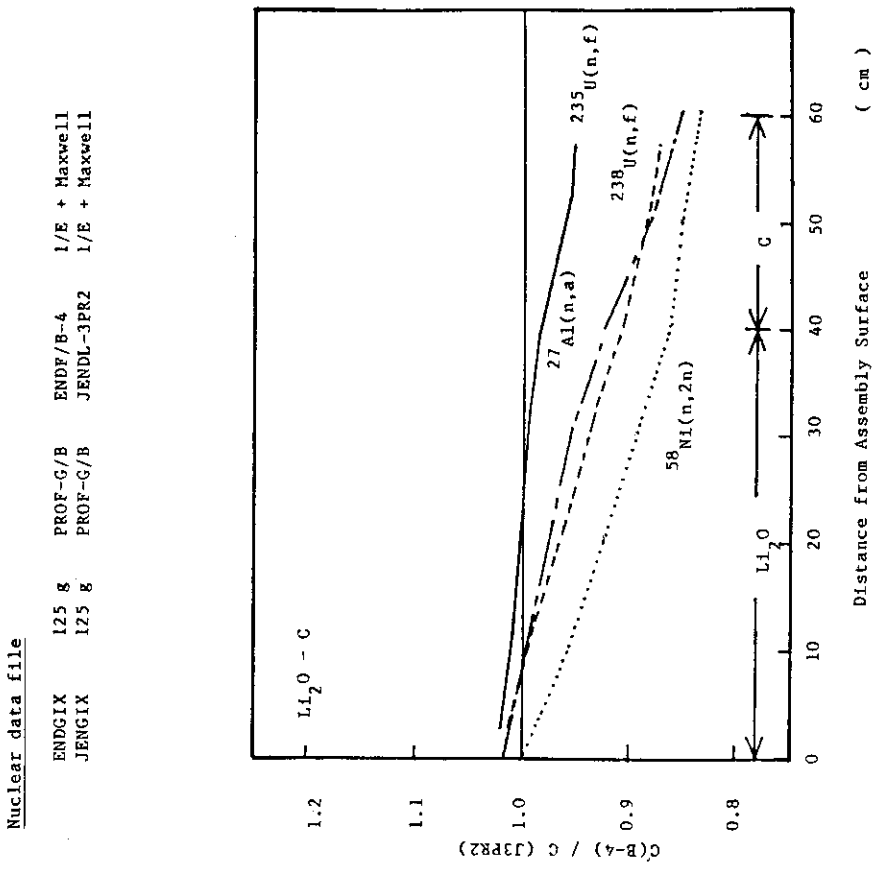

Fig. 4.13.2 Sensitivity for nuclear data file

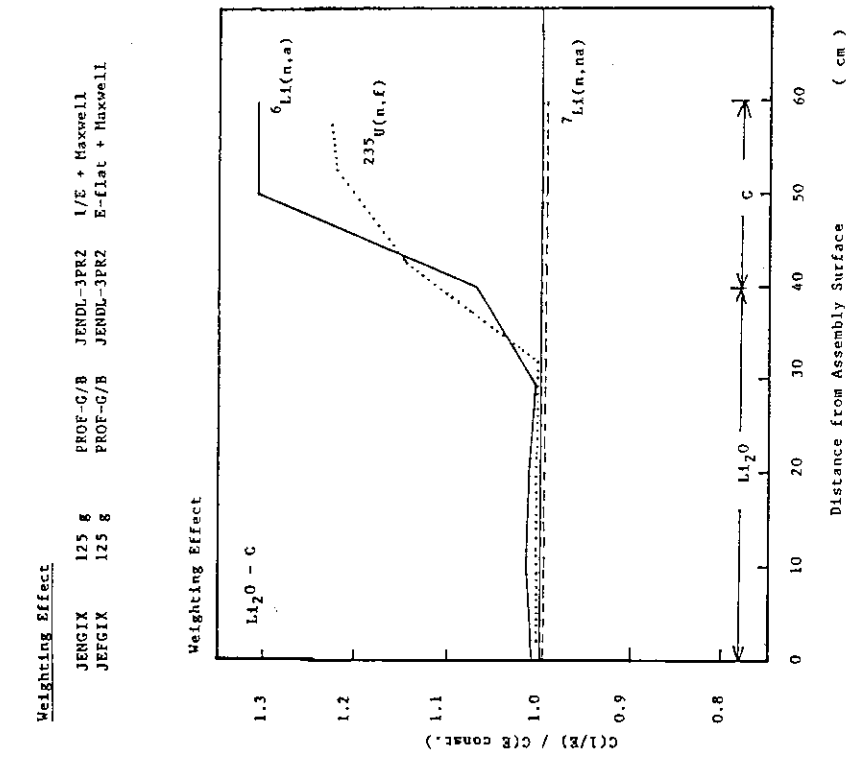

Fig. 4.13.1 Sensitivity for weighting function

4.14 Pre- and Post-Analyses of TOF Experiments Using the MCNP Code with ENDF/B-V

H. Maekawa, Y. Oyama, S. Yamaguchi and J. Jung*

Angle-dependent leakage spectra from lithium-oxide(Li_2O),[1),(2)] graphite[3] and lithium metal[3] slabs have been measured by the time-of-flight (TOF) method. The same type of measurement on beryllium (Be) is planned as the next TOF experiment. As part of JAERI-USDOE Collaborative Program on Fusion Blanket Neutronics, these experiments were analyzed by making use of the MCNP code[4] with the ENDF/B-V data.

The computational model was made precisely taking into account of the geometory of collimator, detector size and position, and their configuration. The collided and uncollided neutron spectra were separately calculated for all measured angles at the same time in a job. The data on experimental assemblies, nuclide densities, layout and neutron source spectra were the same as those used previously in the analyses based on DOT-3.5[5] with JENDL-3PR1, -3PR2, ENDF/B-IV and -V (for graphite assembly only). The calculation was carried out for the 5.06 cm thick slabs of lithium-oxide (Li_2O), graphite and Be. Total number of histories generated in the calculation was 5×10^5, resulting in a standard deviation of a few % to over 10 % depending on angle and energy.

In Fig. 4.14.1, one of the calculated results of the Li_2O slab is shown and compared with that by DOT3.5 with JENDL-3PR2, and measured spectrum. The result of MCNP with ENDF/B-V agrees very well with the experiment except for the elastic peak, while the calculation by DOT3.5 with JENDL-3PR2 underestimates the experiment by about 5 % between 700 keV and 3 MeV.

The results for the graphite slab are shown in Fig. 4.14.2. There is a small difference between the MCNP and DOT3.5 results, even though the ENDF/B-V data were used for both calculations. At the inelastic peak of third level ($\sim$ 5 MeV), all of the calculations based on ENDF/B-IV, -V and JENDL-3PR2 underestimate the flux compared with the experimental value.

---

* Argonne National Laboratory

The calculated results for the Be slab are shown in Fig. 4.14.3. There exist large differences among the nuclear data files used. As the accuracy of Be cross section is important for the selection of fusion blanket concept, it appears that the future TOF experiment on Be is critical to resolve these discrepansies.

References

1) Oyama Y. and Maekawa H. : "Measurement of Angle-Dependent Neutron Spectra from Lithium-Oxide Slab Assemblies by Time-of-Flight Method," JAERI-M 83-195 (1983).
2) Oyama Y., Yamaguchi S. and Maekawa H. : "Analysis of Time-of-Flight Experiment on Lithium-Oxide Assemblies by a Two-Dimensional Transport Code DOT3.5," JAERI-M 85-031 (1985).
3) Oyama Y., Yamaguchi S. and Maekawa H. : To be published.
4) "MCNP : Monte Carlo Neutron and Photon Transport Code," CCC-200, Oak Ridge National Laboratory (1983).
5) Rhodes W. A. and Mynatt F. R. : "The DOT-III Two Dimensional Discrete Ordinates Transport Code," ORNL/TM-4280 (1981).

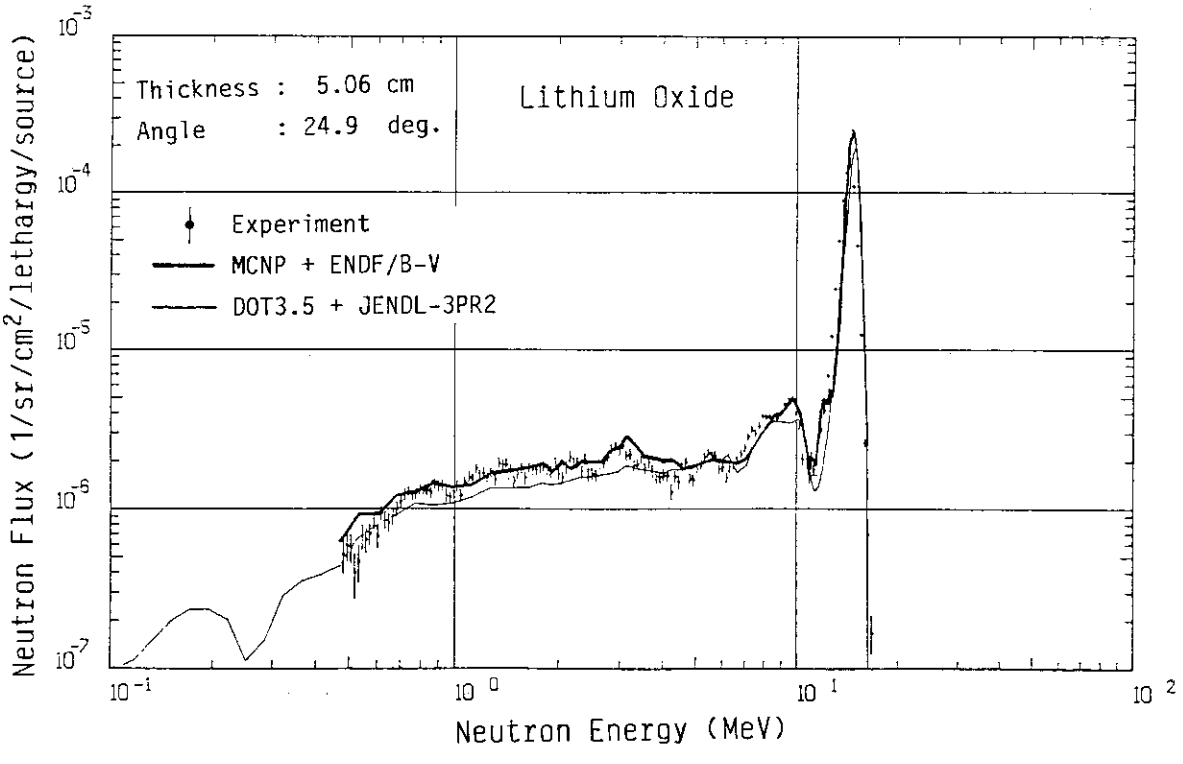

Fig. 4.14.1 Angle-dependent leakage spectrum from lithium-oxide slab.

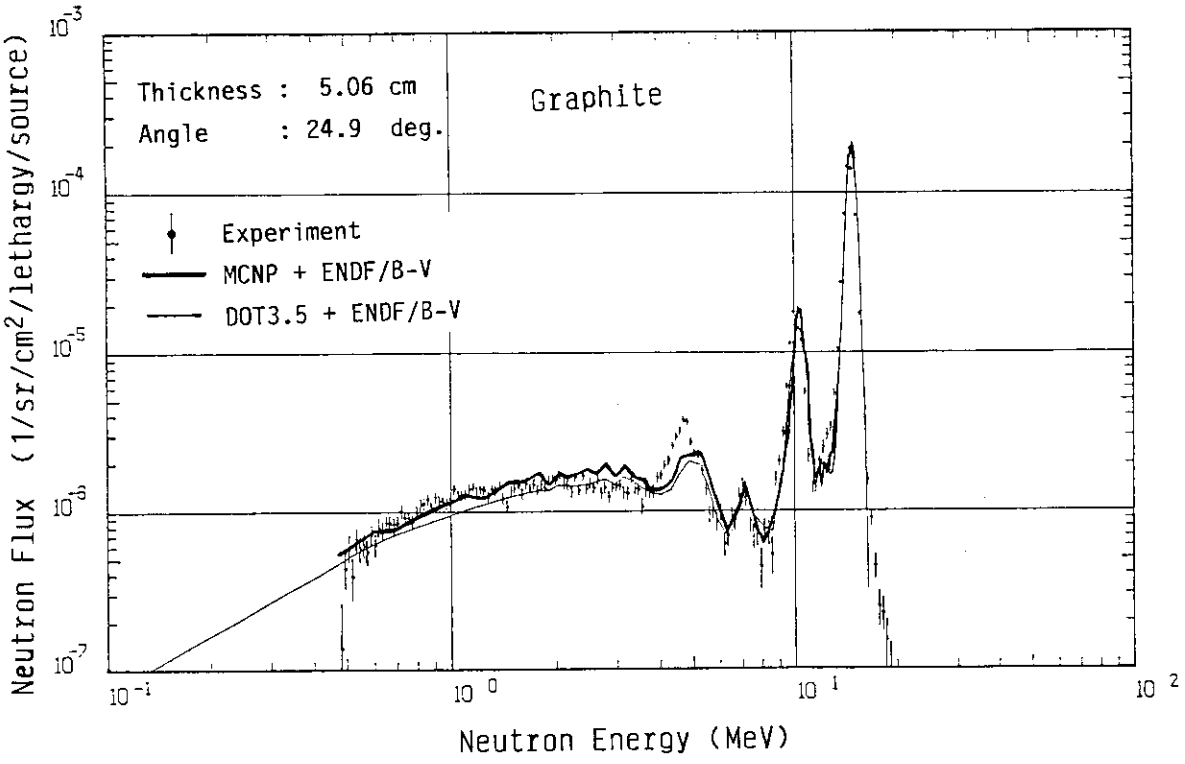

Fig. 4.14.2 Angle-dependent leakage spectrum from graphite slab.

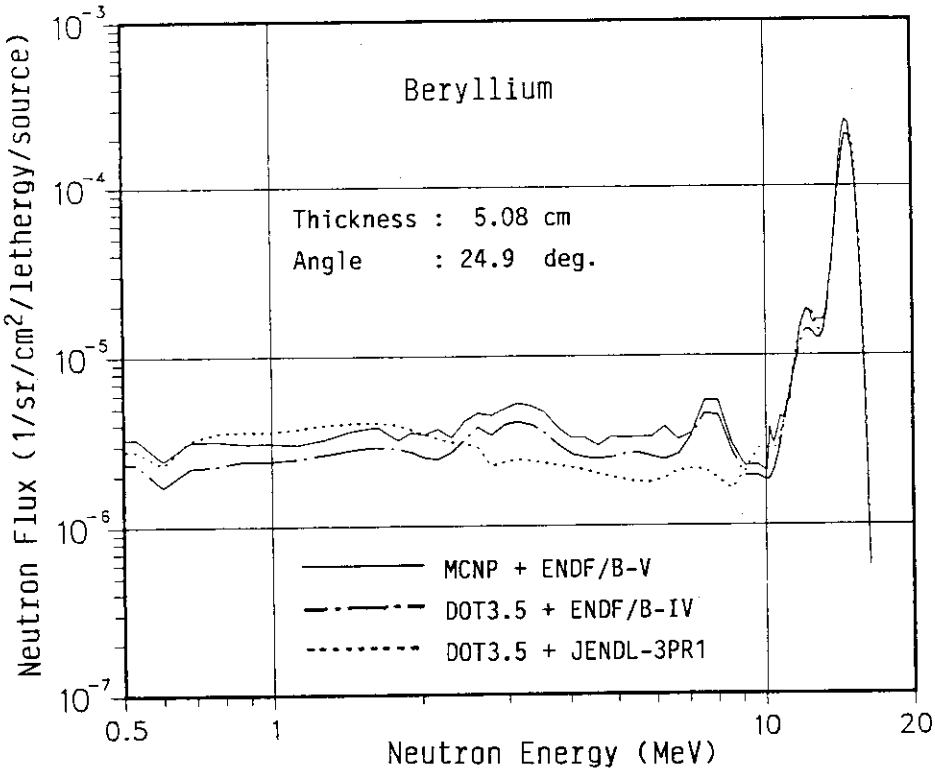

Fig. 4.14.3 Angle-dependent leakage spectrum from beryllium slab.

4.15 Neutron Cross-Section Sets of 125-group for Fusion Neutronic Calculations

K. Kosako, H. Maekawa and T. Nakamura

Neutron cross-section sets of 125-group have been prepared at FNS for analysis of blanket benchmark experiments. Backgrounds of this work are as follows:

1) The widely used GICX40 cross-section set[1] has small group number of 42-group neutron and is based on nuclear data of the ENDF/B-IV.
2) The preliminary version of JENDL-3 for fusion neutronics is produced.
3) New cross-section sets are required for analysing the benchmark experimental data obtained at FNS.

The general features of 125-group cross-section sets provided are shown in Table 4.15.1. The group structure conformed to Ref. (2). First steps of the procedure were linear-linear interporation in energy and cross-section, reconstruction of energy dependent neutron cross-section from a combination of resonance parameters and tabulated floor cross-sections, and generation of doppler broadened cross-sections. Second, the group constant was generated from above result with the process code, PROF.GROUCH-G/B.[3] Finally, the group constant for each nucleus was converted into the ANISN format and was collected into a cross-section set. The present cross-section sets were named as JACKAS, JENGIX, ENFKAS and ENDGIX, respectively, as shown in Table 4.15.2.

In order to examine the characteristics of the cross-section sets, the following calculations were carried out and thir results of tritium production rates (TPRs) were compared with each other: 1) ANISN calculations simulated the one-dimensional infinite cylindorical geometry of FER,[4] and 2) DOT3.5 calculations of the blanket benchmark experiments performed at FNS.[5] The data of JENDL-3PR2 were commonly used as reaction cross-sections. Table 4.15.3 shows the tritium breeding ratio in the breeder region of calculation 1). Both TPRs of ^{6}Li and ^{7}Li calculated with these 125-group sets differ by 10 $\sim$ 13 % from those with GICX40 set. The followings were found from the ratio of the calculated-to-experimental value (C/E) for the TPR of

calculation 2) : a) the TPRs with 125-group sets were larger than those with GICX40 set in the Li_2O region by 4 % (See Fig. 4.15.1), b) the difference of weight functions affected largely on the calculated flux for lower energy neutrons (See Fig. 4.15.2) and c) the TPRs obtained with JENDL files were systematicaly less by about 5 % than those with ENDF/B files (See Fig. 4.15.3).

References

(1) Seki Y., et al.: "Coupled 42-Group Neutron and 21-Group Gamma-ray Cross Section Sets for Fusion Reactor Calculations," JAERI-M 8818, (1980).

(2) Nakagawa M., et al.: "MORSE-DD a Monte Carlo Code using Multi--group Double Differential Form Cross Sections," JAERI-M 84-126, p7-8 (1984).

(3) Hasegawa A.: To be published.

(4) Fusion Reactor System Laboratry: "Conceptual Design of Blancket Structures for Fusion Experimental Reactor (FER)," JAERI-M 83-216, p158 and p168 (1983).

(5) Nakamura T., et al.: "Reactor Engineering Department Annual Report," JAERI-M 85-116, p 140-143 (1985).

Table 4.15.1 The general features of 125-group cross-section sets

items	description
group number	125-group for neutron
Legendre scattering terms	P-5
data format	group independent type cross--section for ANISN code
process code	PROF.GROUCH-G/B
weight functions 1.001E-5 ~ 3.2241E-1 (ev) : maxwell distribution 3.2241E-1 ~ 1.6487E+7(ev) : 1/E or E-flat	
nuclear data files	JENDL-3PR1&2, JENDL-2 ENDF/B-IV&V
nuclide number	13
nuclide name	H-1,Li-6,Li-7,Be-9,C-12, O-16,Na-23,Al-27,Si,Ca,Cr, Fe,Ni

Table 4.15.2 125-group cross-section sets

name	weight function		nuclear data files
	thermal*	others**	
JACKAS	Maxwell	E-flat	JENDL2 + JENDL3PR1 & 2
JENGIX	Maxwell	1/E	JENDL2 + JENDL3PR1 & 2
ENFKAS	Maxwell	E-flat	ENDF/B-IV & V
ENDGIX	Maxwell	1/E	ENDF/B-IV & V

* 1.0010E-5 < E < 3.2241E-1 eV ** E > 3.2241E-1 eV

Table 4.15.3 Tritium breeding ratio in the Li_2O blanket

name	Tritium breeding ratio		
	Li-6	Li-7	total
GICX40	0.84727	0.32072	1.1680
JACKAS	0.95599	0.28699	1.2430
JENGIX	0.94675	0.28693	1.2337
ENFKAS	0.99200	0.30024	1.2922
ENDGIX	0.98497	0.29989	1.2849

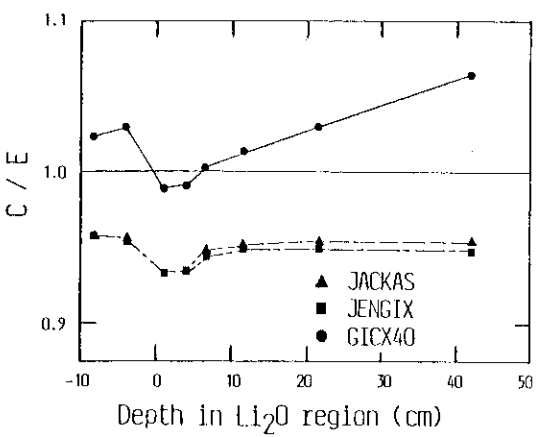

Fig. 4.15.1 The C/E value of TPR of ^{7}Li in the Be multiplier system with Li_2O and Be 10cm thickness

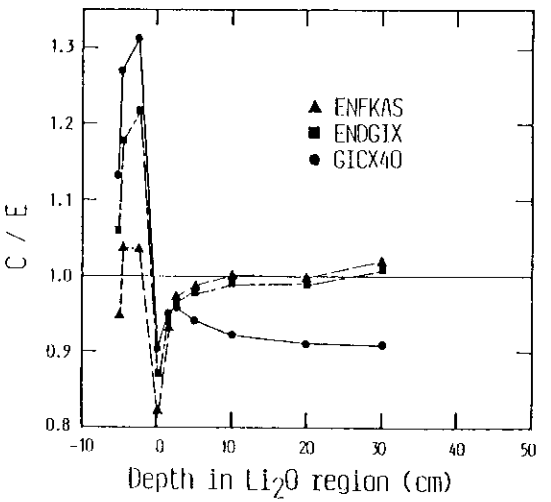

Fig. 4.15.2 The C/E value of TPR of ^{6}Li in the Be multiplier system with Li_2O and Be 10cm thickness

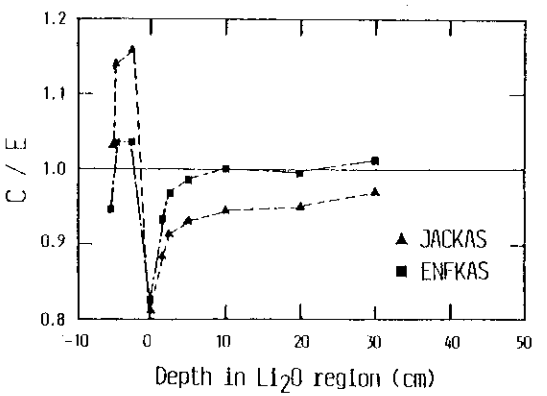

Fig. 4.15.3 The C/E value of TPR of ^{6}Li in the Be multiplier system with Li_2O and Be 10cm thickness

4.16 Operation Report of FNS

J.Kusano, C.Kutsukake, S.Tanaka, Y.Abe and M.Nakano

Operations and maintenances of the FNS facility were performed almost as schedule. Also the related tritium handling was carried out safely. The electrical failure in the high voltage system including the insulated AC power source, which was observed in FY-1984, was cleared by a replacement of the insulated motor-generator by the insulated core transformor at the biginning of FY-1985. The ion beam production ability of 820 type ion source decreased to 70% of full rate by deterioration in spite of the replacement for some related electrodes.

The integrated operation time of the FNS accelerator was 736 hours except the operation for the beam diagnosis.

0° beam line operation

The experiments were carried out mainly using the experimental port at the 2nd target room. They are the 14 Mev neutron streaming experiment through a multi-layered slit of 304SS assembly, the experiment of the bent duct made of concrete and the phase I-B experiment of the JAERI/US-DOE collaborative program. To measure the tritium production rate in the Li_2O blanket assembly planned in the collaborative program, a 60 hour continuous irradiation operation was performed successfully under the full rate condition of beam 20 mA of FNS accelerator.

80° beam line operation

The bunched pulse beam operations were performed for the neutron spectrum measurements on a Lithium slab assembly, on a Graphite slab assembly and on a Berylium slab assembly using a time-of-flight technique. The nominal operating conditions of the pulsed beam for each experiment were 2 ns for pulse width and 36 mA for peak current. The new air cooled type target assembly with pulse pickup unit was used in these operations. In the DC beam operation, the examinations of a lithium-glass scintillation counter utilizing a few micro-ampere beam and the measurements of the activation cross section for the short-lived nuclies utilizing mili-amperes beam were carried out.

Maintenance

To check the reliability of the control systems of the accelerator, the maintenace for the electrical instruments of the accelerator was executed every two monthes. Three equipments of the accelerator were replaced in this fiscal year to improve the ion beam condition. They were the vacuum chamber at the 90° bending magnet for mass separation, the breeder resistor column of the acceleration tube and the DC power supply for the arc discharge in the ion source. Figure 4.16.1. shows the new type breeder resistor column installed.

New rotating target assembly

The new rotating target assembly, which has a large size rotating vacuum seal fabricated in the last year, has been tested to take the vacuum characteristics. The life of the rotating vacuum seal and the behavior of the out-gas in the chamber were studied for three magnetic fluid with different viscosities for the magnetic vacuum seal assembly. This benchmark test will be continued for a year. One of the data of the out-gas behavior is shown in Fig. 4.16.2.

Tritium handling

The accumulated amount of 44 Ci tritium in the exhaust gas from the vacuum system of the accelerator was processed and trapped in the tritium adsorption system. The work for exchanging the tritium target was performed frequently, required by the experiments of the foil activation.

To measure the absolute amount of tritium in the target of 10 Ci to 1000 Ci, the micro calorie meter was specially fabricated. The relation of the absolute value of tritium to the neutron yield for each target will be investigated using this micro calorie meter.

The overhaul of oil rotary vacuum pumps was carried out, and the contaminated oil by high concentration tritium was observed in the pump of the cryo pump system near the rotating target assembly. The level of the tritium contamination was several hundreds $\mu Ci/cm^3$. That pump was not overhauled to avoid the internal exposure for the working personnels.

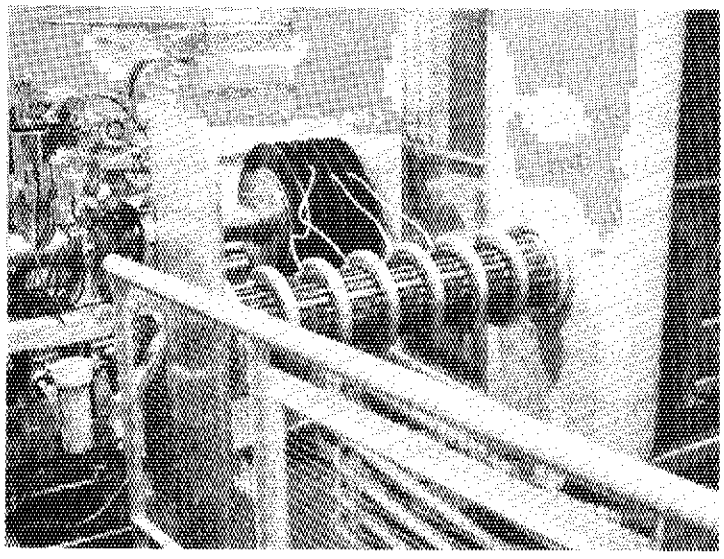

Fig. 4.16.1 Photo of the air cooled type breeder resistor column and the H.V terminal of FNS accelerator.

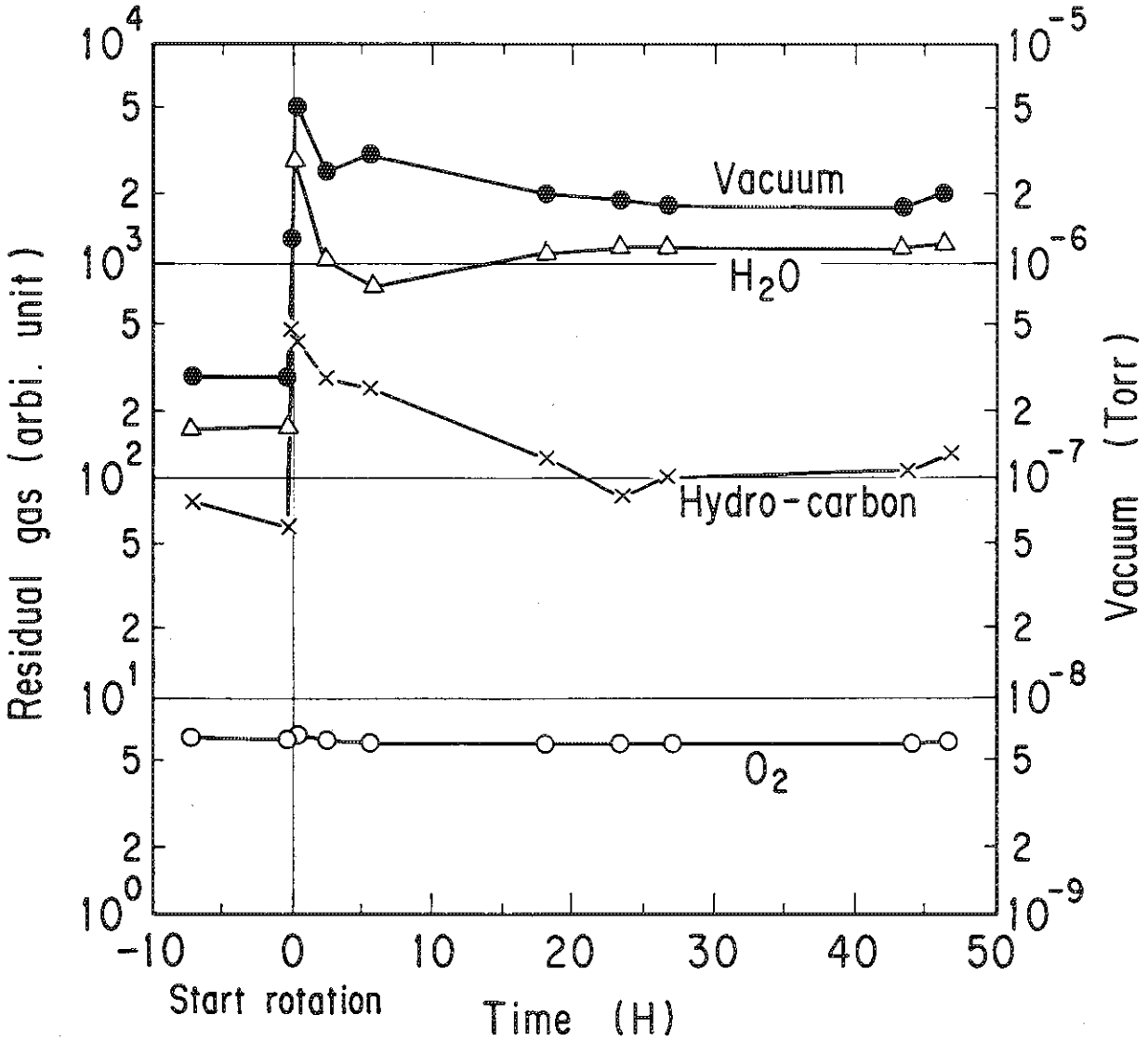

Fig. 4.16. 2 The time dependence of concentration of the residual gas in the vacuum chamber of the new rotating target assembly.

4.17 JAERI/US Fusion Neutronics Calculational Benchmarks for Nuclear Data and Codes

M. Nakagawa T. Mori, K. Kosako,
M.Z. Youssef*, J. Jung** and M. Sawan***

The JAERI and U.S. collaboration program on fusion neutronics is in progress using the FNS facility at JAERI. The program is focused now on measurements of tritium production rates and associated neutronics parameters. Experimental analysis is basically performed by using nuclear data and transport codes developed individually by both countries. The intercomparison of experimental analysis would provide useful information on a prediction accuracy of fusion blanket neutronics.

Prior to examining the accuracy of calculational methods and nuclear data in comparison with integral experiments, both JAERI and U.S. analysts have agreed upon to individually perform calculations on benchmark problems using a common nuclear data file and codes, and also those developed individually in each country. The main objective of this intercomparison includes 1) validation of cross section processing methods, 2) confirmation of common transport codes, 3) intercomparison of individual data and transport codes, 4) estimation of uncertainties in predicting integral parameters due to data and codes and 5) investigation on sources of descrepancy in C/E values between both JAERI and U.S.

The detail of problem specification is given in reference 1 and a brief description is shown in Table 4.17.1. The transport codes used are also shown in the last row in the table.

The nuclear data files adopted are ENDF/B4 as a common one and JENDL3-PR1 by JAERI and ENDF/B5 by U.S. as individually developed ones. These data files have been processed into several different type cross section sets.

Some results are discussed in the following. Figure 4.17.1 compares the ratios of ^{6}T (tritium production rate by ^{6}Li) and ^{7}T (tritium production rate by ^{7}Li) calculated in both countries for problem 1. In all the cases the differences between JAERI and U.S. are within 5% in the lithium oxide region which has closed geometry.

In problem 2 calculations were made for the angular neutron spectra leaked from slab materials composed of Li, O, 316SS, Be, C or lead. In Fig.4.17.2 the neutron angular spectra at $\mu = 0.75$ from beryllium are compared where the results of U.S. using the MATXS5 set(coarse group structure) and of JAERI using the DDL/J3(fine one) are shown. A significantly large difference can be seen in the energy region 10 MeV - 700 keV. This will be mainly attributed to the processing methods and (n,2n) cross sections. In other materials such as lithium, some differences are observed.

The values of ^{6}T and ^{7}T calculated in problem 3 are compared in Figs. 4.17.3 and 4.17.4, respectively. With respect to ^{6}T, the U.S. results using both 30 and 80 group structures are presented and their

---

* UCLA, ** ANL, *** U.W.(University of Wisconsin)

discrepancy is about 8%, that is, the group effect is fairly large for ^{6}T in open geometry. Even if the same nuclear data are used (number of groups is different) the difference between both countries is beyond 5% in the back location. In the cases using ENDF/B5 and JENDL3-PR1, it is several percent through the whole region. On the other hand ^{7}Ts using ENDF/B4 agree well between both countries as shown in Fig.4.17.4. However, if the nuclear data are replaced by ENDFB/5 and JENDL3-PR1 the difference increases up to more than 10% and its space dependency is remarkable.

A comparison using Monte Carlo codes has been made for ^{6}T and ^{7}T in problem 4. The results based on ENDFB/4 show a good agreement between MORSE-DD and MCNP in the zone with small statistical errors. The differences in zone integrated tritium production rates are only 2% for both ^{6}Li and ^{7}Li when ENDF/B4 is used but amount to 13% for ^{7}Li and 2% for ^{6}Li when ENDF/B5 and JENDL3-PR1 are used. Therefore the difference in the nuclear data of ^{7}Li will be significantly affect ^{7}T. The detailed results of both countries and discussion are given in reference 1.

Table 4.17.1 Specification of Problems

Prob. No.	1	2	3	4
Geometry	Sphere	Slab	Cylinder	Cylinder
Material	Li_2O + C	Li,Be,O 316SS,Pb,C	Li_2O	SUS + Li_2O
Dimension (cm)	r = 22.4 46.77 71.77	10 or 20	D = 60 H = 60	D = 60 H = 4 + 56
Main edit	Reaction rate Flux	Angular flux	TPR Fission rate	TPR Fission rate
Code(JAERI) (U.S.)	ANISN-DD ONEDANT	ANISN-DD ONEDANT	DOT3.5 DOT4.3	DOT3.5, MORSE-DD DOT4.3, MCNP,VIM

References

1) Nakagawa M., Mori T. Kosako K. Youssef M. Jung J. and Sawan M.: "US/JAERI Fusion Neutronics Calculational Benchmarks for Nuclear Data and Codes Intercomparison", JAERI-M 85-201, also PPG-900, UCLA-ENG-85-37 (1985)

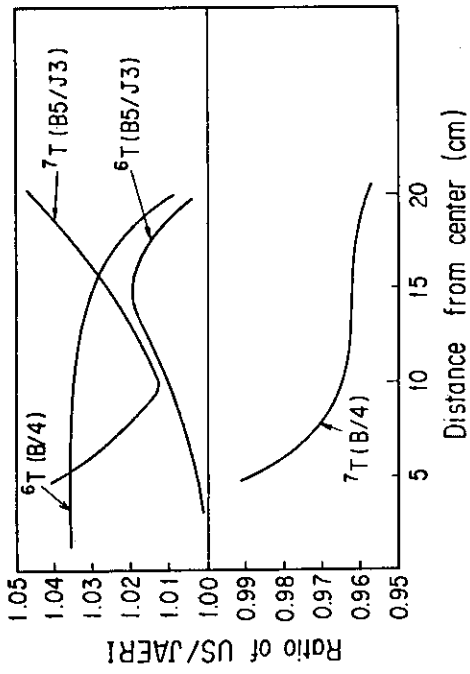

Fig.4.17.1 Comparison of tritium production rates in problem 1

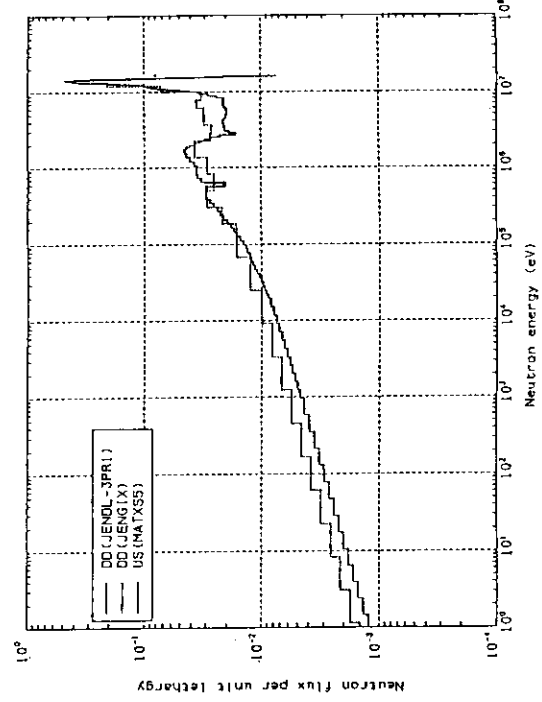

Fig.4.17.2 Comparison of neutron spectrum from beryllium

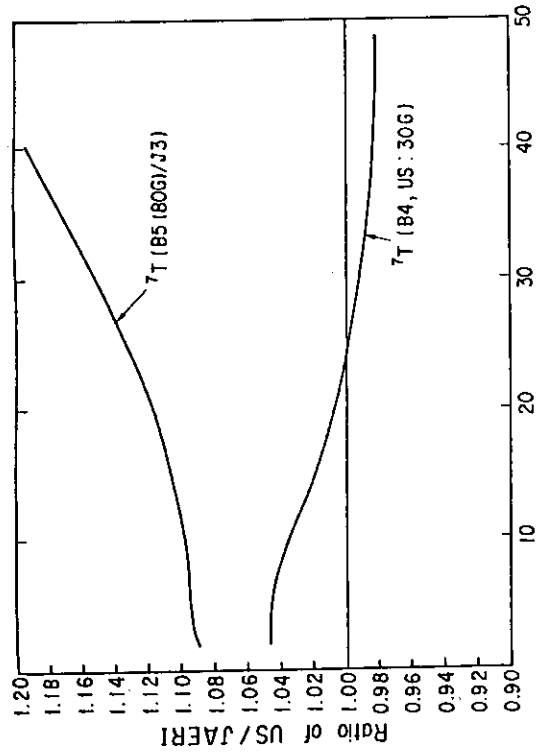

Fig.4.17.3 Comparison of ^{6}T in problem 3

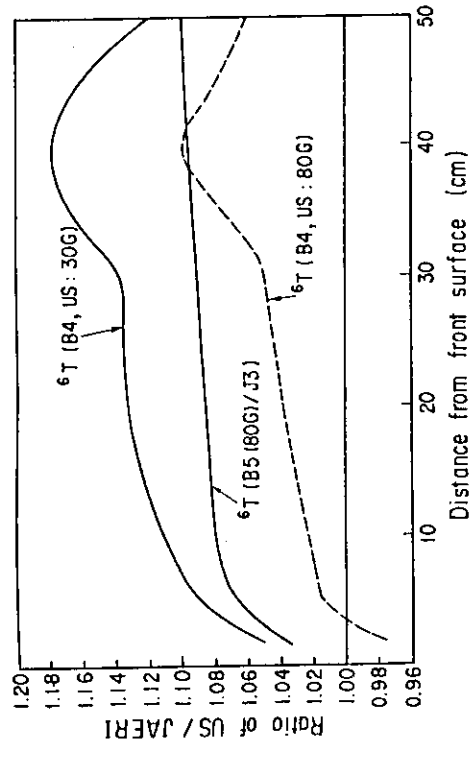

Fig.4.17.4 Comparison of ^{7}T in problem 3

5. Shielding

The activities on shielding presented here are related to an experimental study of neutron streaming, development of a radiation transport code, studies of analytical procedure and design.

To investigate neutron streaming through the neutron beam injector of a fusion reactor, a fast neutron experiment has been carried out using d-T neutrons of Fusion Neutron Source facility. The measurements were compared with Monte Carlo calculations.

Continuous efforts have been made for development of a radiation transport code system BERMUDA: Adjoint neutron transport codes have been completed; A new technique was presented for the particle rebalancing; To analyse practical problems, a bootstrap method has been implemented into the two-dimensional transport code; And the overestimation has been mitigated by adopting an angular quadrature set.

A NEACRP benchmark problem about neutron penetration in graphite was analysed using a Monte Carlo code MCNP. The result was compared with another Monte Carlo calculation and the measurement for verification of its calculational accuracy.

Extensive shielding analyses have been presented for design of neutron beam holes installed in a new reasearch reactor. Some useful comments were presented on calculational procedure and shielding design.

(T. Ise)

5.1 Experiment and Calculation of 14 Mev Neutrons Streaming Through a Multi-Layered Slit Assembly

H. Nakashima, S. Tanaka and H. Maekawa

A streaming experiment using a d-T neutron source of Fusion Neutronics Source Facility (FNS) has been carried out to examine the calculational technique for neutron transport in an assembly simulating the beam port of neutral beam injector (NBI) in a fusion reactor, which is composed of multi-layered beam paths and shields.[1)]

The experimental assembly is composed of the central part including three layered slits and the surrounding mortar shield. The size of the central part of 304 stainless steel is 400 mm high, 400 mm wide and 1450 mm long, in which three layered slits of about 40 mm x 320 mm are provided. The mortar 180 mm thick covers the cental part except for the inlet and outlet sides of the neutrons. This assembly is located at the outlet of the experimental port of FNS.

Reaction rate distributions and energy spectra of fast neutrons were axially measured in the slits of the beam port and the surrounding mortar shield region, using a small spherical NE213 liquid scintillation counter.[2)] Thermal neutron flux distributions were also measured in the mortar shield with use of thermoluminescence dosimeters (TLDs).

The measured reaction rates and energy spectra are compared with the calculations using the continuous energy Monte Carlo transport code MCNP with several different kinds of estimators, in which the built-in cross section library was used.[3)] To reduce the variance and CPU-time, the source biasing and weight window methods were employed. The comparison shows that the option of the once more collided flux estimator (OMCFE) is not adequate for the calculation of streaming neutrons in the slits.

Comparisons between the measured and calculated reaction rates of fast neutrons are made along the lines E and F in the slits as illustrated in Fig. 5.1.1 and along the lines B, C and G in the surrounding mortar as drawn in Fig. 5.1.2. The calculated reaction rates in the slits using the track length estimator having the same volume as the detector's used in the measurements agree with the measurements within the range of experimental errors, while the

calculations in the mortar shield using the OMCFE agree with the measurements within a factor of 2. As shown in Fig. 5.1.1, the two calculated values at each position of F6M, F7M and F8M, where a part of the detector does not look at the d-T neutron target directly, represent the deviation of the reaction rates due to the variation in the detector efficiencies, where the influence of the variation in the detector efficiency is assigned to the calculation.

The neutron energy spectrum above 2.0 MeV at the point of F8M is compared with the measured one as shown in Fig. 5.1.3. The calculated spectrum is consistent with the measured one within the experimental errors above 6 MeV, while it is slightly low at 6.0 MeV and below. This figure shows that a variation of the detector efficiency is assigned to the experiment.

Figure 5.1.4 shows the thermal neutrons attenuate with the distance, of which the tendency is different from that of the fast neutrons. Such a calculation has never been performed for the thermal neutrons, since it is impossible to obtain the meamingful value within the reasonable computation time.

References

1) "Conceptual Design Study of Quasi-Steady State Fusion Experimental Reactor (FER-1) Part 2," Department of Large Tokamak Research, JAERI-M 85-178 (1985) (in Japanese).

2) Oyama Y., et al.: " Development of a Spherical NE213 Spectrometer with 14 mm Diameter," JAERI-M 84-125 (1984) (in Japanese).

3) "MCNP - A General Purpose Monte Carlo Code for Neutron and Photon Transport," LA-7396-M (Rev.) Version 2B, Los Alamos Monte Carlo Group, Los Alamos National Laboratory (1981).

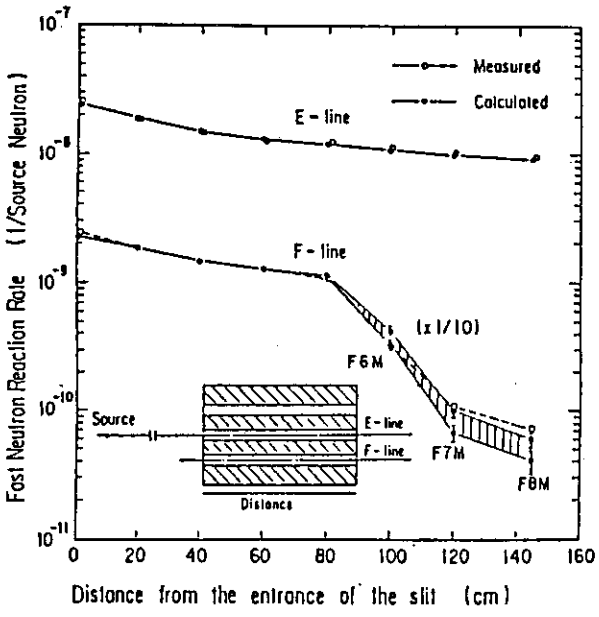

Fig. 5.1.1 Comparison between the calculated and measured fast neutron reaction rate distributions on the E and F lines

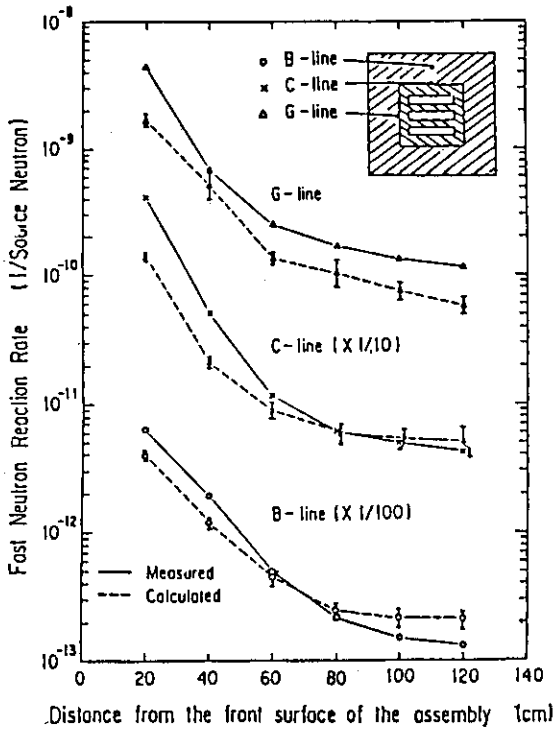

Fig. 5.1.2 Comparison between the calculated and measured fast neutron reaction rate distributions on the B, C and G lines

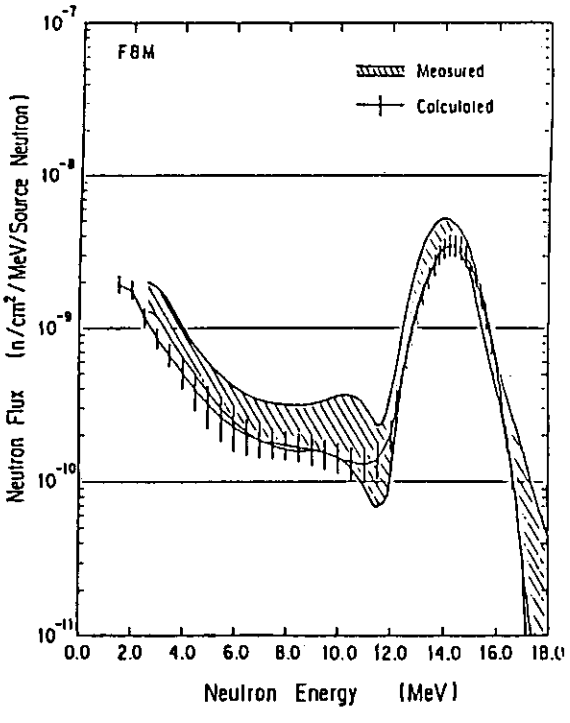

Fig. 5.1.3 Comparison between the calculated and measured neutron energy spectra at F8M

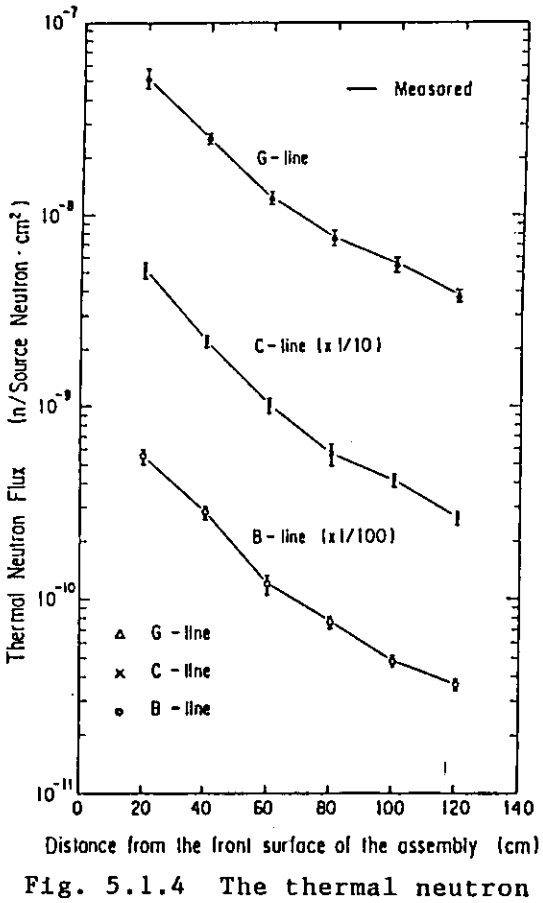

Fig. 5.1.4 The thermal neutron flux distributions measured by TLDs on the B, C and G lines

5.2 Status of the BERMUDA Code System Development

T. Suzuki, A. Hasegawa and T. Ise

Development work of the BERMUDA code system in FY-1985 is summarized in the follwings:

(1) A one-dimensional adjoint neutron transport code BERMUDA-1DNA has been completed. In order to accomplish the numerical equality[1] of $(\phi,S^*)=(\phi^*,S)$, it was necessary that the renormalization factor F for particle balance[2] should be unity in each group for both forward and adjoint calculations. To force the value of F to be unity, we have proposed a new technique to evaluate $\phi(x_{p-1})$ or $\phi^*(x_{p-1})$ either of which is the initial value for direct integration along the characteristic line and is prepared by interpolation with respect to spatial or angular variable from the flux values already solved at the around x_{p-1}.

First, prepared are two interpolated values ϕ_m and ϕ_M at the point x_{p-1}, either of which values is obtained by a concave or convex(to the upper) functions,respectively. Then, the value of $\phi(x_{p-1})$ lies between them, that is;

$$\phi_m(x_{p-1})<\phi(x_{p-1})<\phi_M(x_{p-1})$$

Next, we research a value "ζ" for

$$\phi(x_{p-1})=\zeta\phi_m(x_{p-1})+(1-\zeta)\phi_M(x_{p-1}),$$

so that the "particle balance" would maintain(F=1) for each energy group over the whole spatial region. This procedure resembles that of a "criticality adjustment" starting with the initial value $\zeta=0.5$. The ζ is commonly used in the energy group for all the spatial and angular meshes, and also obtaining scattering source term $q(x_{p-1})$ and $q(x')$ over the integral range$[x_{p-1}, x_p]$. Thus, the equality of $(\phi, S^*)=(\phi^*,S)$ numerically attains within the error of a few percent. Similarly, two- and three-dimensional codes, BERMUDA-2DNA and 3DNA have also been completed.

(2) A kind of the bootstrap method has been implemented into the z-coordinate of the two-dimensional(r,z) forward neutron transport code BERMUDA-2DN. This procedure can calculate separately the second target room and the beam port for streaming experiments of the FNS. In the first step, the second target room is treated using appropriate mesh sizes (not too large) on both the r and z coordinates, and the angular flux distributions are obtained over a fictitious z-plane at the inlet(or inner) point of the beam port. In the second step, the source term is given as the sum of the distributed boundary fluxes obtained above and the direct beam fluxes from the point source at the center of the second target room.

(3) In the BERMUDA-2DN, the overestimation of neutron fluxes in the low energy region, where anisotropy is not so remarkable, were found to be caused by our inappropriate selection of an angular quadrature set. So we chose the "completely symmetric S_8 set[3)] and accordingly the overestimation of reaction rates(dominant in the low energy region) has been mitigated. It is shown that the diffusion theorem condition,

$$\sum_m p_m \Omega_{x_m}^2 = \sum_m p_m \Omega_{y_m}^2 = \sum_m p_m \Omega_{z_m}^2 = \frac{1}{3}$$

is important rather in the neutron field where the anisotropy is not large.

References

1) Department of Reactor Engineering:" Reactor Engineering Department Annual Repott(April 1, 1984-March 31, 1985)," JAERI-M 85-116, p165(1985).

2) Suzuki T. et al.:" BERMUDA-2DN: A Two-Dimensional Neutron Transport Code," JAERI-M 82-190(1982)(in Japanese).

3) Radiation Shielding Information Center:" RSIC Computer Code Collection, DOT3.5, Two Dimensional Discrete Ordinates Radiation Transport Code," CCC-276, pp177-288 " Common Symmetric Quadratures and the DOQDP Computer Code," by J.P. Jenal(1975).

5.3 Calculation of Neutron Penetration Through Graphite Medium with Monte Carlo Code MCNP

H. Kotegawa, N. Sasamoto and S. Tanaka

A benchmark problem of fission neutron penetration into graphite medium proposed by NEACRP[1] was analysed[2] with a continuous energy Monte Carlo code MCNP.[3] The problem is based on an experiment which measured the reaction rate of fast neutrons penetrated into graphite up to 70 cm in depth.

For deep penetration calculation, a combination of the Weight-Window and Exponential Transform methods implemented in MCNP were employed in order to reduce the variance. The MCNP library used in the present calculation involves the pointwise cross sections which were processed with NJOY code based on the ENDF/B-IV files.

The neutron spectra calculated with MCNP are seen to agree relatively well with the calculated ones by another continuous energy Monte Carlo code McBEND[1], although MCNP's calculations slightly underestimates McBEND's ones. As example, Figure 5.3.1 gives the penetraion spectra at 70 cm in depth calculated with MCNP and McBEND. On the other hand, Figure 5.3.2 shows the comparison between the reaction rate distributions calculated with both MCNP and McBEND, and the measured ones.

The reactions of $^{27}Al(n,a)$, $^{32}S(n,p)$, $^{103}Rh(n,n')$ and $^{115}In(n,n')$, are all sensitive to fast neutrons. The reaction rates on a front surface of the graphite calculated with MCNP agrees well with the measured ones. For penetrations larger than 20.0 cm, the MCNP calculations agree with the measurement for the reaction rates of $^{27}Al(n,a)$ and $^{32}S(n,p)$ but underestimates the measurement for the reaction rates of $^{103}Rh(n,n')$ and $^{115}In(n,n')$. Further, it was found that the underestimation has a tendency to increase with penetration. On the other hand, the reaction rates of $^{103}Rh(n,n')$ and $^{115}In(n,n')$ calculated with McBEND are in better agreement with the measurments than those with MCNP for all penetrations except the front surface of graphite.

In addition to the analysis of NEACRP benchmark problem, the fast neutron penetration experiment into graphite sphere by Profio et al.[4]

was analysed with MCNP in order to verify its calculational accuracy through comparison of calculated and measured angular fluxes. The angular fluxes obtained by MCNP without any help of the variance reduction techniques agree fairly well with the measured ones, reproducing precisely spectral peaks and dips around 3.5 MeV, which characterize penetration neutron spectra in graphite.

The above analysis comfirmed the validity of the MCNP calculations of fast neutron penetration in graphite and then the effectiveness of the Weight-Window method was shown for deep penetration problem.

References

1) Carter M.D., et al.:private communication
2) Kotegawa H.,Sasamoto N. and Tanaka S.:"Calculation of Neutron Penetration through Graphite Medium with Monte Carlo Code MCNP," JAERI-M 86-055(1986)
3) LASL Group TD-6:"MCNP-A General Monte Carlo Code for Neutron and Photon Transport," LA-7396-M (1978)
4) Profio A.E.,Antunez H.M. and Huffman D.L.:Nucl. Sci. Eng.,35, 91(1969)

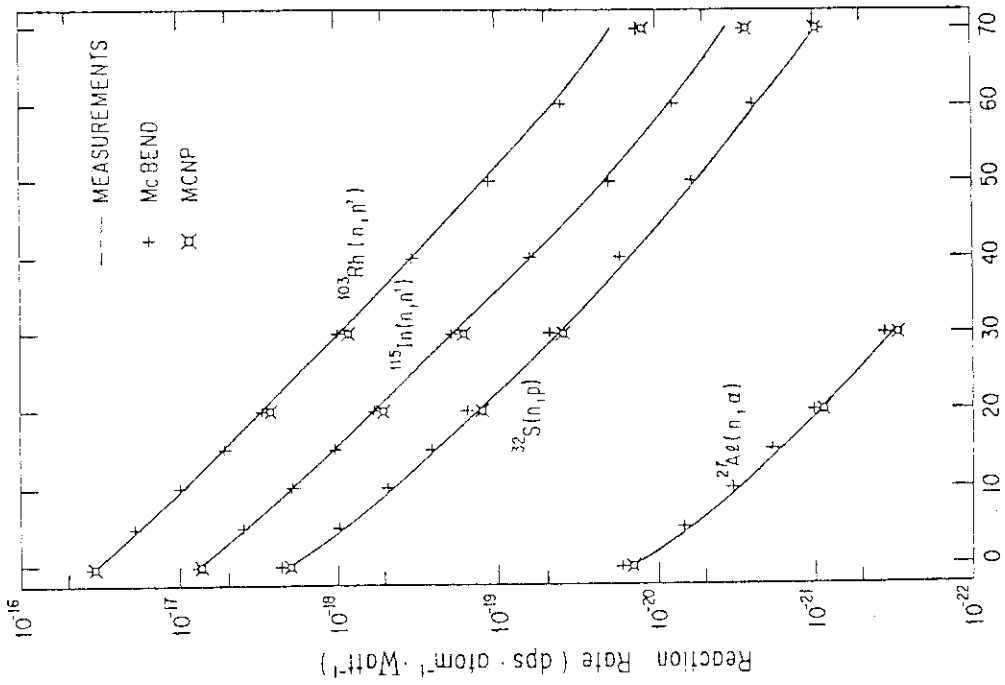

Fig.5.3.2 Comparison between calculated MCNP, McBEND and measured reaction rate distributions.

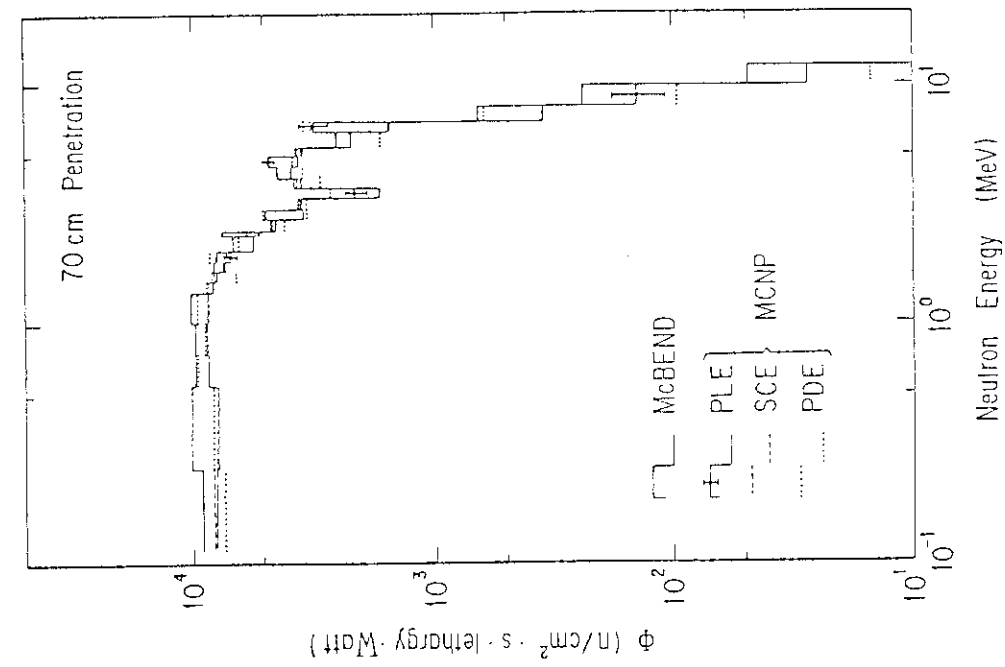

Fig.5.3.1 Comparison between calculated MCNP and McBEND spectra after 70 cm penetration through graphite. A combination of W-W and exponential transform methods is applied to MCNP calculations.

5.4 Shielding Analyses for Design of Neutron Beam Holes in a New Research Reactor

T.Ise, T.Maruo,[+] Y.Miyasaka[++] and M.Isshiki[+]

Extensive shielding analyses have been presented for design of neutron beam holes which are to be installed in the upgraded JRR-3 reactor.[1] Description is given about the standard beam hole, beam hole for neutron radiography and guide tunnel.

As shown in Figs.5.4.1(flow diagram for shielding analyses) and 5.4.2(computational model for beam hole), the Monte Carlo and two-dimensional Sn calculations have been performed mainly for analyses of the duct streaming since the beam holes are arranged so that they do not look at the reactor core(that is, tangential beam tube). In the present analyses, Sn calculations have been carried out with angular meshes finer than those for the reactor shielding.[2]

One of the computed shielding analyses is shown in Figs. 5.4.3(DOT computational geometry) and 5.4.4(neutron and gamma -ray dose rate distributions).

Engineering design has been being performed on the basis of these results.

References

1) Ise T., Maruo T. et al.:"Shielding Analyses for Design of the Upgraded JRR-3 Research Reactor·2 --- Shielding of Neutron Beam Holes --- ," JAERI-M 85-105(1985)(in Japanese).

2) Ise T., Maruo T. et al.:"Shielding Analyses for Design of the Upgraded JRR-3 Research Reactor·1 --- Shielding of Reactor --- ," JAERI-M 85-050(1985)(in Japanese).

+ Department of Research Reactor Operation

++ Office of Safety and Control

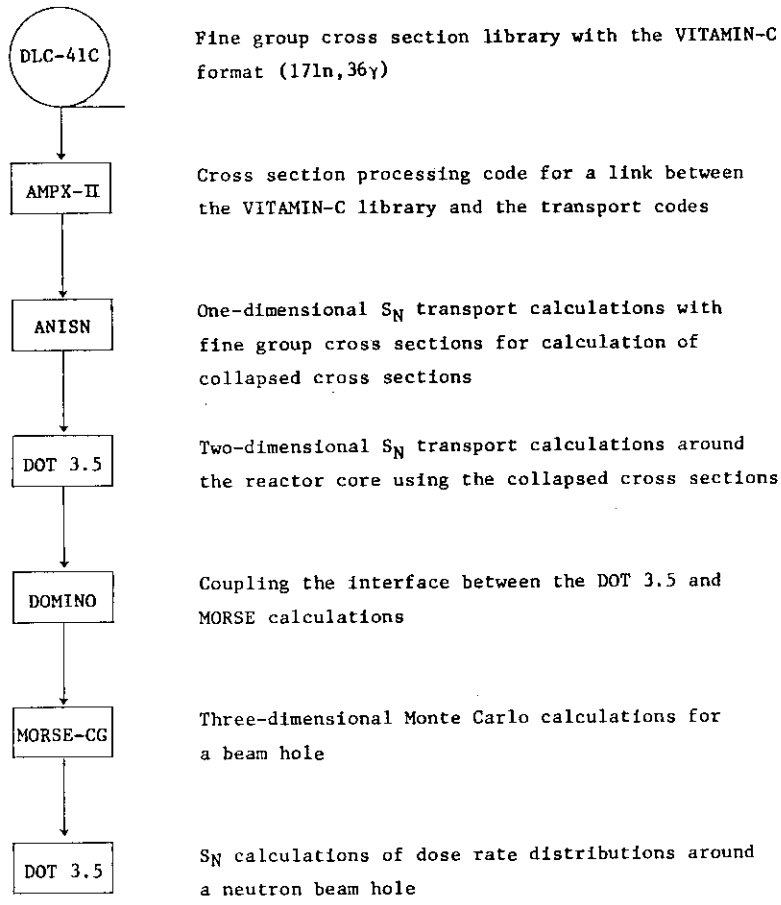

Fig.5.4.1 Flow diagram for shielding analyses

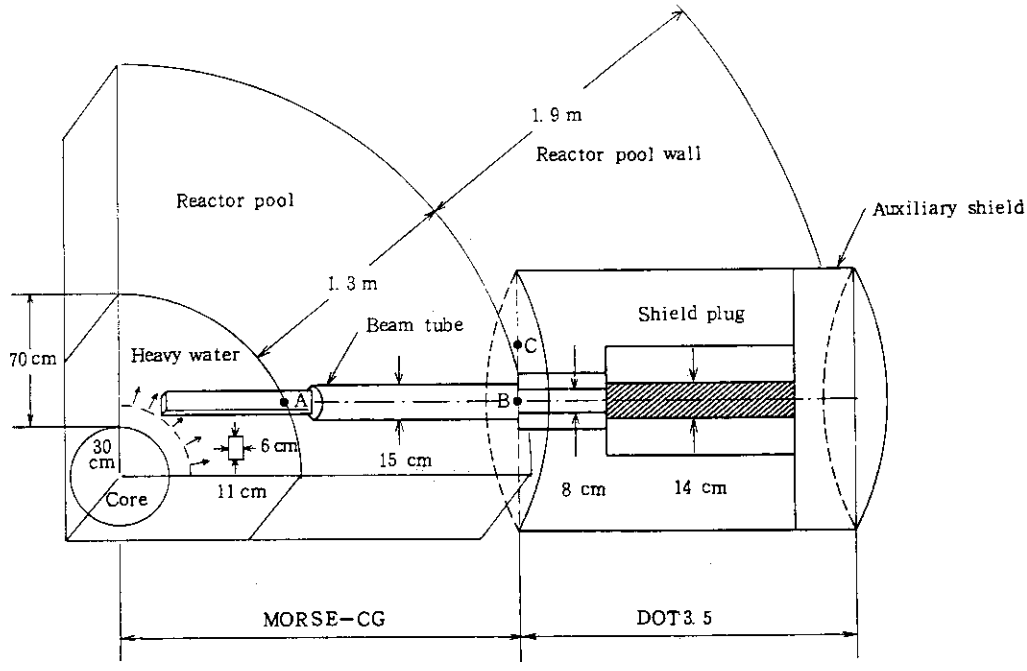

Fig.5.4.2 Computational model for a beam hole

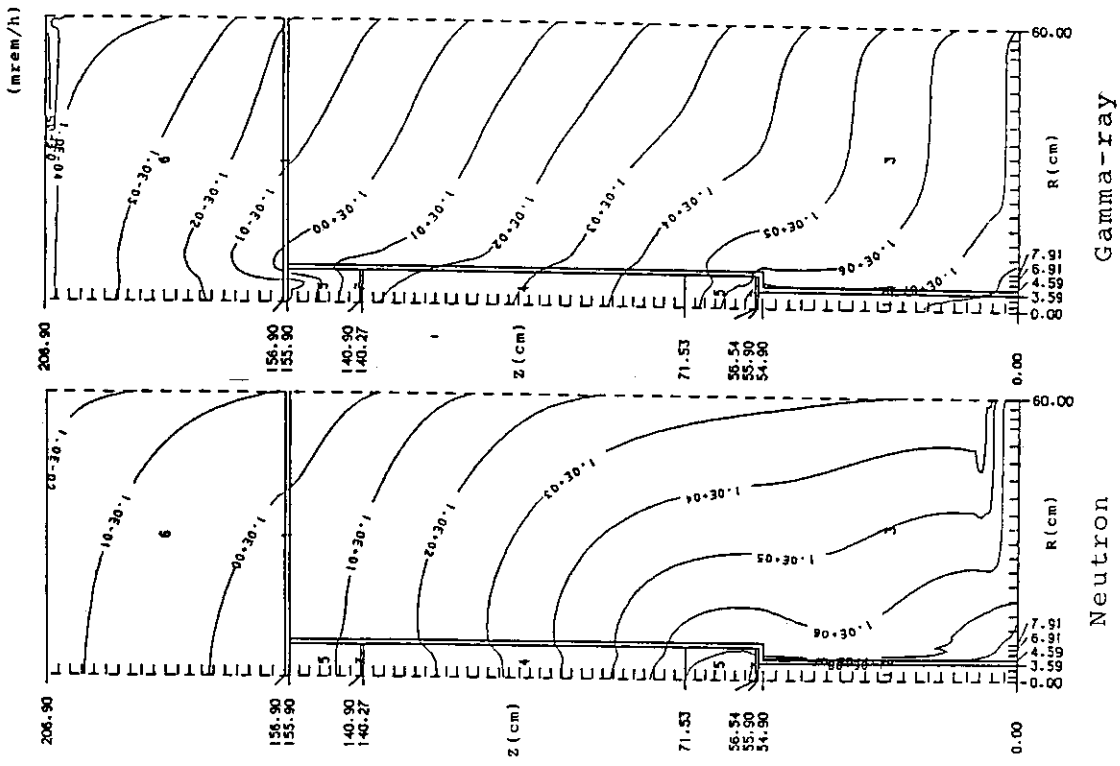

Fig.5.4.4 Computed dose rate distributions

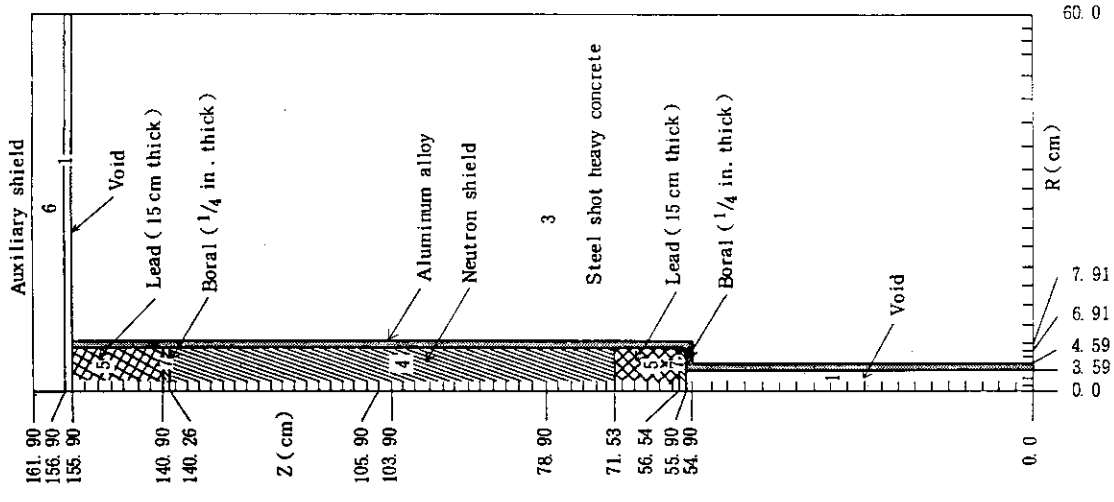

Fig.5.4.3 A DOT computational geometry

6. Reactor and Nuclear Instrumentation

There are two major themes in the Reactor Instrumentation Laboratory. One deals with studies on general nuclear and reactor instrumentation and the other relates to the reactor instrumentation for the High-Temperature Gas-Cooled Reactor.

In the field of the general reactor instrumentation, various kinds of investigations have been carried out such as measurements of transient response of BICOTH type in-vessel water level gauge, radiation resistance of a graded index type optical fibers developed, and video, force and proximity sensors.

In the area of the nuclear instrumentation and method, an in-situ nondestructive measurement system for the radioactivity and a telescopic measuring system for the specific radioactivities of structural components in a reactor vessel were successfully developed for the evaluation of the residual inventories of radioactivities in decommissioning plants. An instrumentation system and a pulse neutron generator were provided for the development of a sensitive and nondestructive measuring techniques for the transuranic materials in waste drums. Characteristics of various kinds of gamma-ray detectors and effects of irradiation were also actively studied and a calculation method was improved for determination of the peak area of gamma-ray spectra.

In the field of HTGR instrumentation, a high temperature fission counter-chamber developed was tested in the HFR in Petten, the Netherlands as a cooperative experiment with the Institut fur Reactorentwicklung of KFA-Julich, Germany and a good operating performance was verified through the test. The period of irradiation life test of two gamma-compensated ionisation chambers in the JRR-4 reached about 4.5 years. The test is continued with the ambient temperature of 600 C. An extensive effort has also been made on development of a reliable and neutron-irradiation resistant in-core thermo-couple comprising Pt-Mo alloys and TZM sheath, and having a operating temperature range between 850 and 1350 C. A study for developing a fuel failure detection method for thecoated particle fuels (CPFs) for HTGRs was carried out in the JMTR using a gas-sweeping irradiation rig with two kinds of fuel compacts, one of which contains only normal CPFs and the other contains some artificially failed CPSs, respectively. The diffrences of behaviour of FP release between these fuel compacts were observed as a function of the temperature, reactor power and the lapse of time.

(N. Wakayama)

6.1 Development of High-Temperature Neutron Detectors

N. Wakayama, H. Yamagishi, H. Itoh, K. Sakasai
T. Tomoda* and S. Fukakusa*

High-performance and high-temperature fission counter-chambers and gamma-compensated ionization chambers were developed to be used as in-vessel neutron sensors for VHTR, HTGR and large scale LMFBR.

The performance and the result of irradiation life tests of the high-temperature fission counter-chambers has been reported.(1)-(4)

As concerns the high-temperature gamma-compensated ionization chamber(CIC), the accelerated life tests for two CICs(#12, #16), (the electrodes of CIC#12 and #16 were made of nickel base super alloy and titanium, respectively), has been being continued in the research reactor JRR-4 since October 1980. The irradiation tests at 400°C were carried out for about 2.5 years and the irradiation tests at 450-500°C tests for about 2 years.

At the end of December 1984, the total neutron fluence and the gamma-ray fluence reached 1.2×10^{18} cm^{-2} and 3.6×10^{6} C/kg, respectively.(5)-(7)

After the irradiation tests at 450-500°C, the test temperature was incleased up to 600°C for the CIC and the initial detailed inspection of 600°C-irradiation-test was carried out. The plateau characteristics were measured at 600°C for the various levels of neutron flux with the compensation voltage of 400V DC. Figure 6.1.1 shows a results of measurement of the plateau characteristics of the CIC. The figure shows a good plateau characteristics in the neutron flux range of 4×10^{7} to 4×10^{11} cm^{-2} s^{-1}. Figure 6.1.2 shows the output current linearity of the CIC with the reactor power(neutron flux). A temperature effect on the linearity was observed at 600°C only in the very low neutron flux range below 2×10^{7} cm^{-2} s^{-1}.

After these tests, the CIC is under irradiation at 600°C in JRR-4 since middle of March 1985 to investigate the irradiation life of the chamber at the temperature.

---

*Mitsubishi Electric Corp.

References

1) Wakayama N., Yamagishi H., Tomoda T., Kawashima K. : "Development of Fission Chambers for High-Temperature Reactors," Symposium proccedings on Nuclear Power Plant Control and Instrumentation, Vol.II, IAEA-SN-226/32, 243 (1978) IAEA

2) Wakayama N., Yamagishi H., Itoh H., Tomoda T., Fukakusa S. : " Reactor Eng. Div. Annual Report (Apr. 1978 - Mar. 1979)," JAERI-M 8393, 77 (1979)

3) Wakayama N., Yamagishi H., Itoh H., Tomoda T., Fukakusa S. : " Reactor Eng. Div. Annual Report (Apr. 1979 - Mar. 1980)," JAERI-M 9032, 98 (1980)

4) Wakayama N., Yamagishi H., Itoh H., Tomoda T., Fukakusa S. : " Reactor Eng. Div. Annual Report (Apr. 1980 - Mar. 1981)," JAERI-M 9672, 90 (1981)

5) Wakayama N., Yamagishi H., Itoh H., Tomoda T., Fukakusa S. : " Reactor Eng. Div. Annual Report (Apr. 1981 - Mar. 1982)," JAERI-M 82-114, 78 (1982)

6) Wakayama N., Yamagishi H., Itoh H., Tomoda T., Fukakusa S. : " Reactor Eng. Div. Annual Report (Apr. 1983 - Mar. 1984)," JAERI-M 84-138, 168 (1984)

7) Wakayama N., Yamagishi H., Itoh H., Sakasai S., Tomoda T., Fukakusa S. : " Reactor Eng. Div. Annual Report (Apr. 1984 - Mar. 1985)," JAERI-M 85-116, 182 (1985)

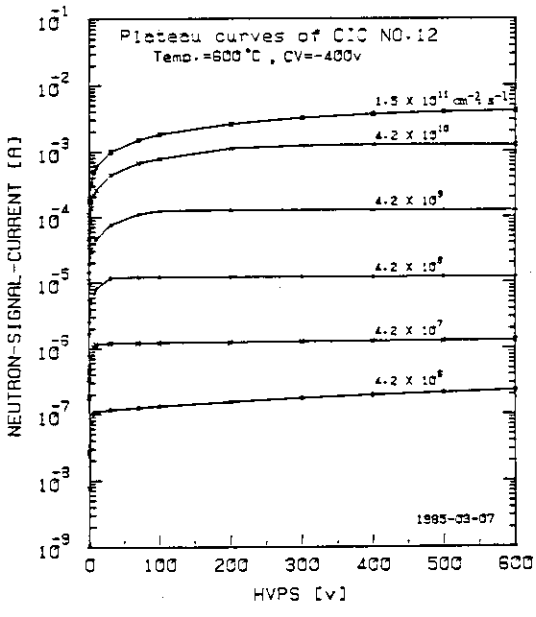

Fig. 6.1.1
Plateau curves of gamma-compensated ionization chamber at 600°C

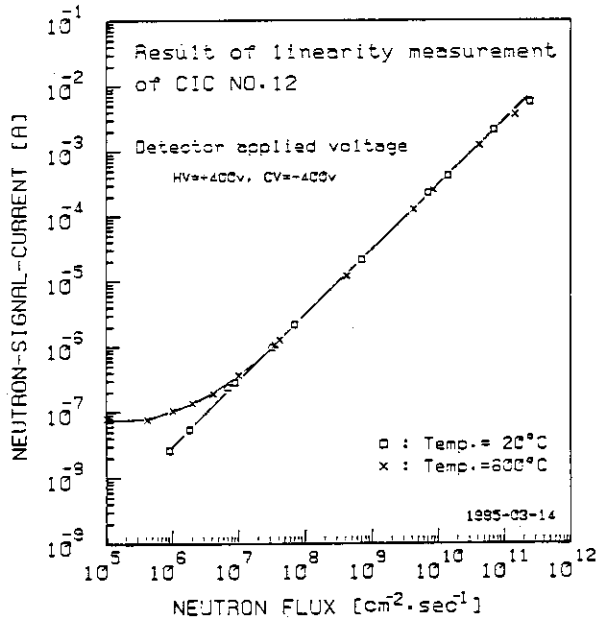

Fig. 6.1.2
Linearity of gamma-compensated ionization chamber at 20°C and 600°C

6.2 Development of Fuel Failure Detection System for a High Temperature Gas Cooled Reactor

H. Terada, N. Wakayama, M. Obata[+], I. Gotoh[++],
I. Yokouchi[+++], T. Tobita[++++], H. Yoshida and Y. Tomiyama

A high sensitive fuel failure detection (FFD) method for the very high temperature gas-cooled reactor (VHTR) under designing in the JAERI has been studied using an irradiation rig of the JMTR (Japan Material Testing Reactor) as shown in Fig. 6.2.1. Two reconstructed precipitators were used in the FFD system, which are aimed at detecting only short-life noble-gas fission-products selectively. Gamma-ray spectra of the sample gas were monitored simultaneously by a Ge spectrometer. In the experiment, a specially designed irradiation-capsule which can include two different types of coated particle fuel samples was used. One included artificially failed particles in a fuel compact as shown in Fig. 6.2.2, the other was made up only intact particles. The fuel temperature under irradiation can rise up to around 1400 °C independently of the reactor power. The primary helium gas with fission products released from the fuel samples in the reactor core was led to our FFD system. The response of the FFD system the each sample gas was monitored during the irradiation cycle about a month. The behaviors of the fission products released from the intact fuels and the failed fuels were compared in the various fuel temperatures.

Figure 6.2.3 shows a result obtained in the JMTR No. 71 operation cycle. The fuel temperatures of the failed sample and the intact sample were changed from 1200 °C to 1350 °C and from 1125°C to 1275 °C, respectively. In the experiment, the power of the JMTR (the neutron flux level at the fuel samples) was kept constant. In the figure, precipitator counting rates due to the intact sample shows slight dependence on the fuel temperature. On the other hand, the results of the failed fuel samples show significant dependence on the temperature. Moreover, the counting rate of the precipitator increased day by day, as shown by arrow signs in Fig. 6.2.3, at the constant temperature of 1350 °C.

By gamma-ray spectrum monitoring, it was made sure that the FP-nuclides released from the intact samples are almost same as those from the failed samples. Shorter life nuclides such as ^{89}Kr (half life 3.1 min) and ^{90}Kr (32.3 s) gave large contributions to the counting rate of the precipitator. Table 6.2.1 shows the concentrations of each FP-nuclide released from the intact samples and the failed samples.

+ Irradiation Division II, Department of JMTR Project
++ Irradiation Division I, Department of JMTR Project
+++ Irradiation Division III, Department of JMTR Project
++++ Fuel Irradiation and Analysis Laboratory, Department of Fuels and Materials Research

Table 6.2.1 Concentrations of FP-nuclides released from the intact fuels and failed fuels

Nuclide	Concentration(μCi/ml) intact sample*	failed sample**
^{85m}Kr	1.31×10^{-4}	5.66×10^{-3}
^{87}Kr	$5,13\times10^{-4}$	2.76×10^{-2}
^{88}Kr	2.88×10^{-4}	1.43×10^{-2}
^{89}Kr	1.93×10^{-3}	4.0×10^{-2}
^{133}Xe	1.01×10^{-4}	7.0×10^{-3}
^{135m}Xe	6.69×10^{-4}	3.12×10^{-2}
^{135}Xe	2.62×10^{-4}	1.60×10^{-2}
^{137}Xe	8.06×10^{-4}	7.1×10^{-3}
^{138}Xe	1.03×10^{-4}	3.72×10^{-2}

Graphite sleeve temperature of fuel samples
* 1100 °C
** 1195 °C
in the JMTR No. 71 operation cycle

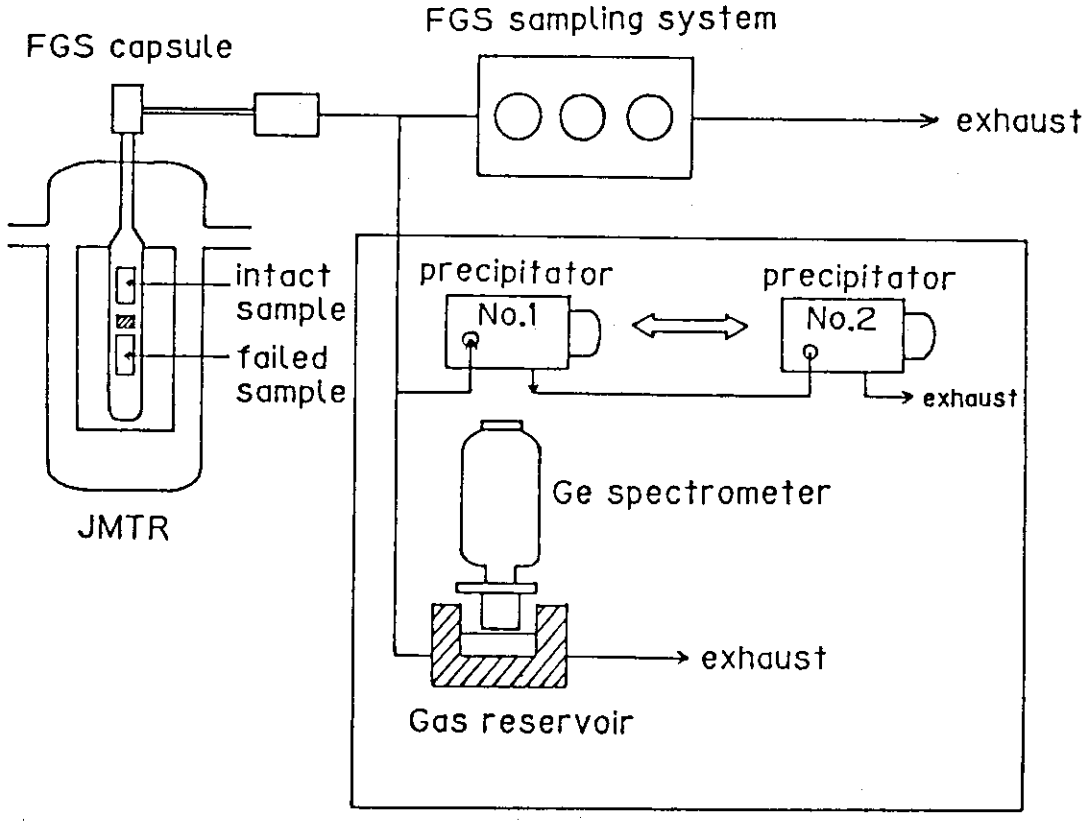

Fig. 6.2.1 FFD experimental system

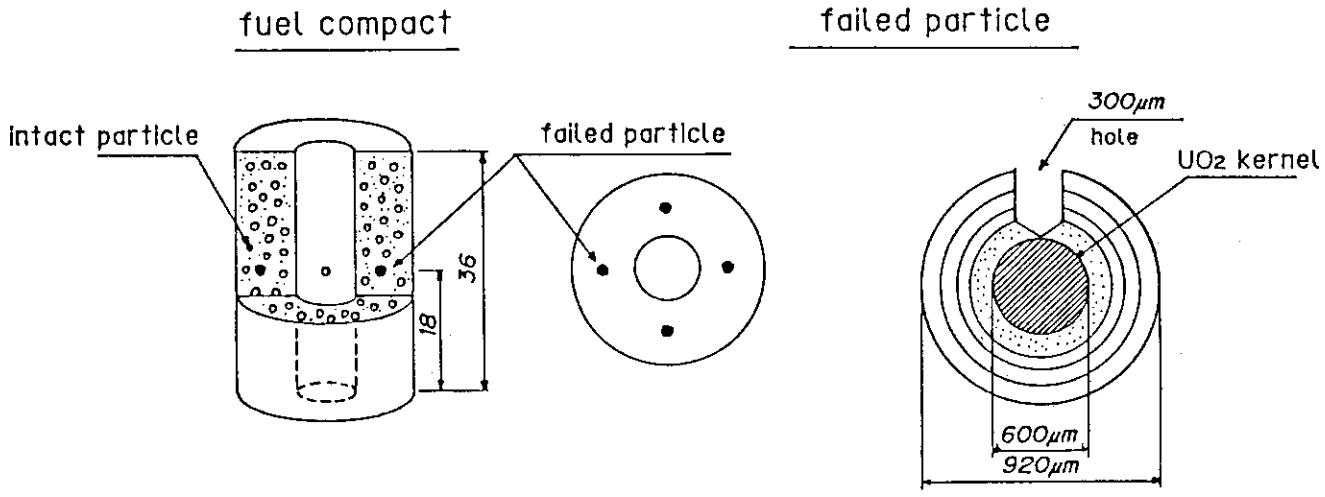

Fig. 6.2.2 Fuel sample of coated particles used in the experiment

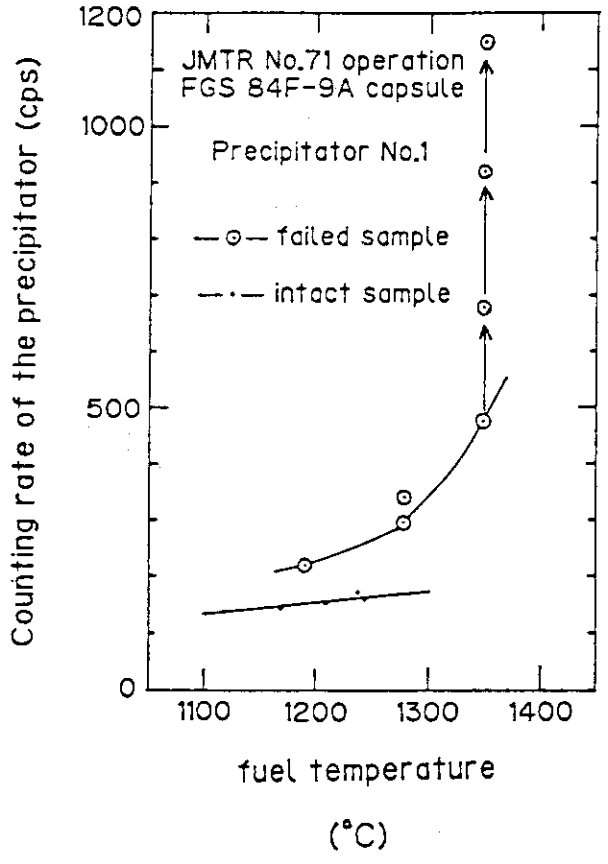

Fig. 6.2.3 Comparison of the precipitator response for the fuel temperature with intact fuels and failed fuels

6.3 Transient Response of BICOTH Water Level Sensor

K. Ara and N. Wakayama

A new type of water level sensor, named BICOTH (Binary Coded Thermocouple-array with Heater), was developed and its tests have been proceeding. Figure 6.3.1 shows the structure of fabricated sheathed-wire type BICOTH, where a DTCT wire and a heater wire are encased with MgO insulator in a stainless-steel sheath with a diameter of 1.6 mm. Five sets of DTCT's with heaters are arranged around a stainless-steel support rod to make a binary-coded thermocouple array.

After measurement of static characteristics of the sensor[1], its transient responses for movement of water level were examined at room temperature. The results are shown in Figs. 6.3.2 and 6.3.3. Figures 6.3.2(A) and 6.3.3(A) show the responses of DTCT TH5 for step increasing and decreasing water level, respectively. Figure 6.3.2(B) shows the ramp response of DTCT TH1 for continuous increase of water level with a speed of 47.2 cm/min, and 6.3.3(B) for continuous decrease with a speed of 19 cm/min. The difference in time response between the cases of increasing and decreasing water level comes from the difference in thermal conductance between the conditions of "sheath to water" and "sheath to air (steam)". This can be explained by use of a simple model, shown in Fig. 6.3.4, of heat transfer from the heater to the water and the air. During increase of water level, the small thermal resistance R_1 is switched on at the "newly water-immersed" surface of the sheath; and as a result, the time constant of heat transfer circuit becomes small. In case of decreasing

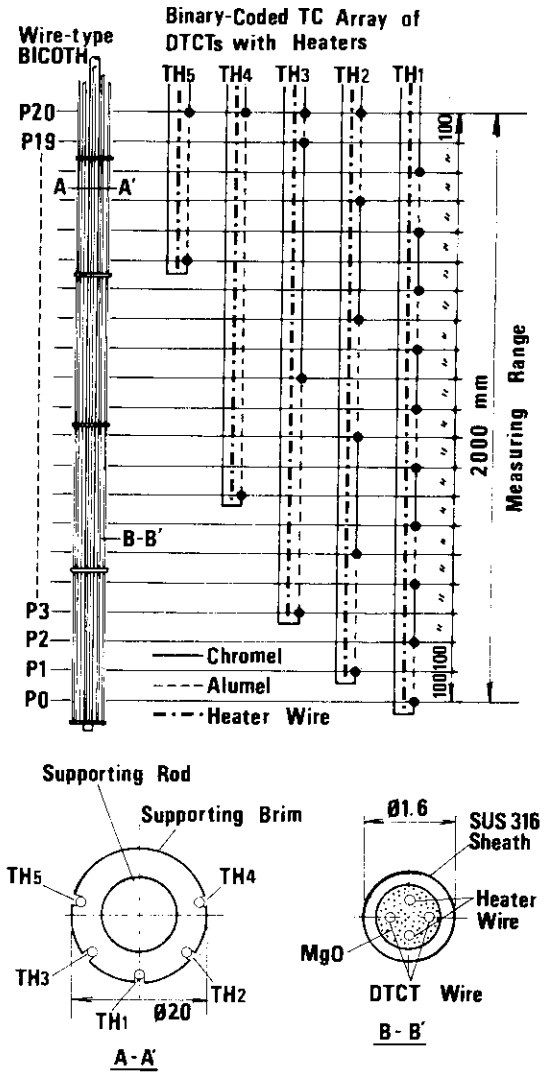

Fig. 6.3.1 Sheathed-wire type BICOTH

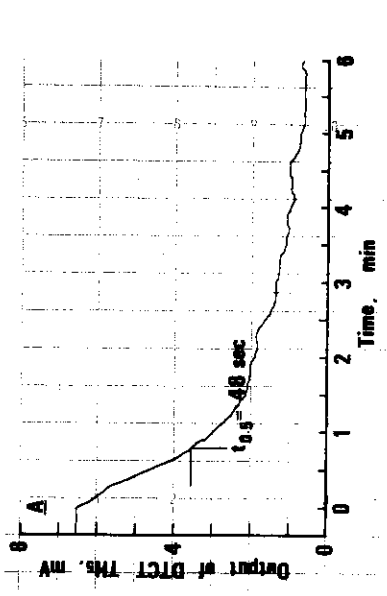

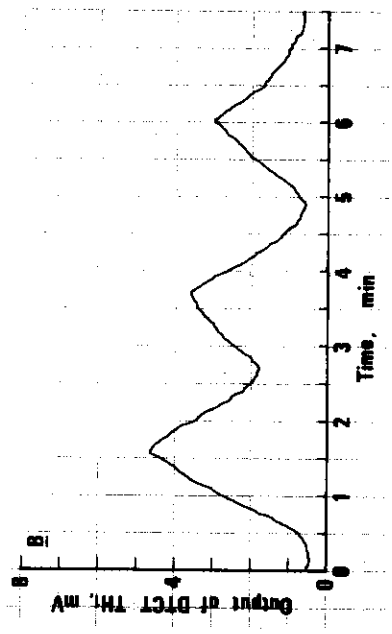

Fig. 6.3.3 Transient responses of sheathed-wire type BICOTH for decreasing water level

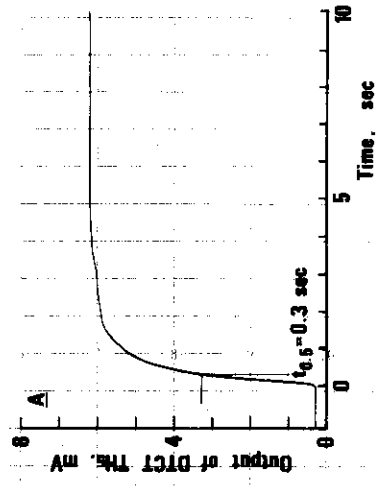

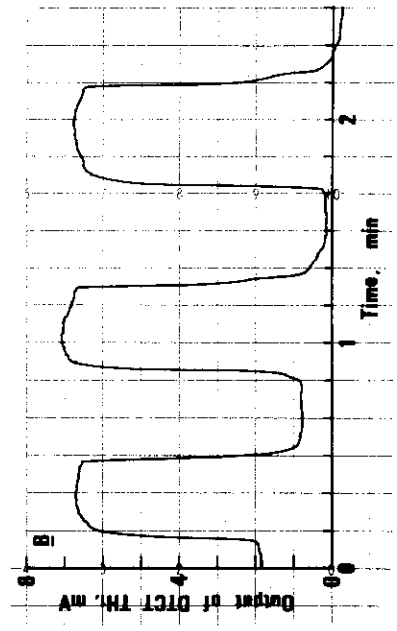

Fig. 6.3.2 Transient responses of sheathed-wire type BICOTH for increasing water level

water level, on the contrary, R_1 is switched off and the large resistance R_2 is switched on, resulting in a large time constant. It has been made clear through experiments that the time delay due to vaporization of water film on the sheath surface during decrease of water level does not play a dominant role in the cause of the slow time responese.

Reference

1) Ara K., Wakayama N.: JAERI-M 83-129, pp. 155 - 157 (1983)

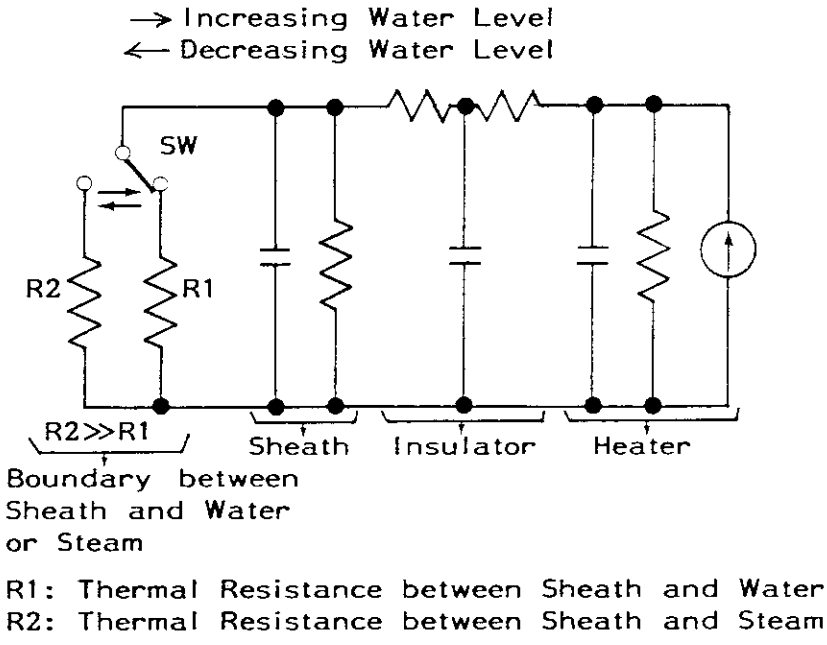

Fig. 6.3.4 Heat transfer model for explanation of step responses for increasing and decreasing water level

6.4 Development of Nondestructive Measuring Techniques of Transuranic Elements in Waste Drums

H. Gotoh, N. Wakayama, M. Haruyama, H. Yamagishi, K. Sekine and M. Suzuki

A neutron generating machine, a neutron moderation chamber and a data analyzing apparatus for the neutron differential die-away technique were built as the second year work of the five year program for the development of nondestructive measurement system of transuranic elements in radioactive waste drums coming from abroad. Kaman A-801 D-T neutron generators were adopted for the neutron generating machine. The neutron moderation chamber was built of 20cm thick graphite walls and 10cm thick polyethylene reflectors. The data analyzing apparatus was constructed of microprocessor-based computers. A system control program was manufactured for the measurement system. The goal of detection limit of transuranic content is set at 100nCi/g.

A new project, NUCEF(Nuclear Fuel Cycle Safety Engineering Research Facility) project, started to study the back-end technology of fuel cycle. The first year budget for building construction was obtained for the fiscal year 1986. Budgets of instruments for the first period of research program will be requested in the fiscal years 1987 through 1988 parallel with those for building construction.

A differential die-away system and a computed tomography system will be built in the first period of the program. The former will be equipped with a new D-T neutron generator and will act as an experimental tool for the development of the detection techniques corresponding to the special discrimination level. The latter will act as an experimental tool for the development of the diagnosis technique of the soundness of waste drums.

The second period of the program will contain the development of a high sensitivity detection system of transuranic contents in waste drums equipped with an electron linear accelerator and the development of a new type scanner for surface transuranic contamination.

6.5 Development of Radiation Resistant Electronic Devices

T. Kakuta, H. Yagi, K. Ara and K. Sanada*

Radiation Resistace of Boron and Fluorine Doped Graded Index Type Optical Fiber

Boron and Fluorine(B-F) doped Graded Index(G.I.) type optical fiber has been developed and radiation resistance characteristics were tested at the Co-60 irradiation facility of the Tokai Research Establishment.

The optical fiber with B_2O_3 and F doped silica core, was fablicated by MCVD method using BBr_3 and SF_6 as a starting materials of the dopants. The initial signal transmission loss and the bandwidth of B-F doped optical fiber were 2.83dB/km, 540MHz-km at wave length of 850nm and 4.77dB/km, 950MHz-km at 1300nm, respectively. Table 6.5.1 shows the initial characteristics of B-F doped optical fiber used for the experiment. The refractive index profile of the fiber is shown in Fig. 6.5.1.

A measurement of the signal transmission loss induced by radiation was conducted in-situ with the light power being monitored through the optical fiber using LED. The exposed fiber length was 100m.

Figure 6.5.2 shows the result of a high exposure under conditions of a exposure-rate of 6.5×10^5 R/h and an input optical power of 1.4uW. The radiation induced loss grew with increase of the exposure up to exposure of 1MR. However, the induced loss tended to saturate at a higher level of exposure. From this result, it has been found that there is a radiation hardening phenomena in the case of the high exposure radiation. This trend is similar for the pure silica core optical fiber which have much higher radiation resistivity reported in our previous paper[1),2)] and is different for the other G.I. type fibers containing GeO_2/P_2O_5. The radiation induced loss of the B-F doped fiber was 250dB/km at the exposure of 10^8 R.

Irradiation Test of Radiation Resistant Sensor Devices

Radiation resistant sensors were developed to make a smart remote manipulation system. These sensors consist of three parts for the viewing, force detecting and proximity sensing. The radiation hardened properties of these sensors were tested.

---

* Fujikura Ltd.

A single tube color camera of a frequency separation type and a divided camera control unit was tested. The camera head was irradiated up to 10^7 R at the exposure rate of 2.2×10^5 R/h and its radiation hardened properties were confirmed. A torque sensor of the eddy current type was developed and its radiation resistivity was confirmed up to 10^8 R. A photo-proximity sensor which makes use of radiation hardened optical fiber was tested up to 10^7 R.

References

1) Kakuta T., Sanada K., Inada K. et al.; "Radiation Resistance of Pure Silica Core Optical Fibers," CEIDP, Oct.21-24, (1984) pp.101-107.

2) Kakuta T., Sanada K., Yamashita R., et al.; "Radiation Resistance of Cl-free OD-exchanged Pure Silica Core Optical Fibers," ECOC, Sept. 3-6, (1984)

Table 6.5.1 Initial characteristics of B-F doped G.I. type optical fiber

△n (%)	Core o.d. (μm)	Clad o.d. (μm)	Silicone o.d. (μm)	Trans. loss (dB/km) 0.85μm	1.3μm	Band width (MHz·km) 0.85μm	1.3μm
0.9	50	125	400	2.83	4.77	540	950

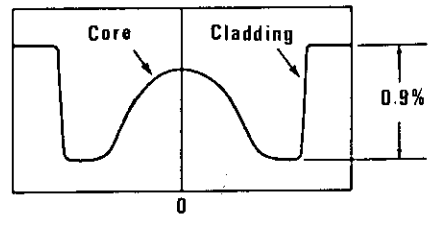

Fig. 6.5.1 Refractive index profile of B-F doped fiber

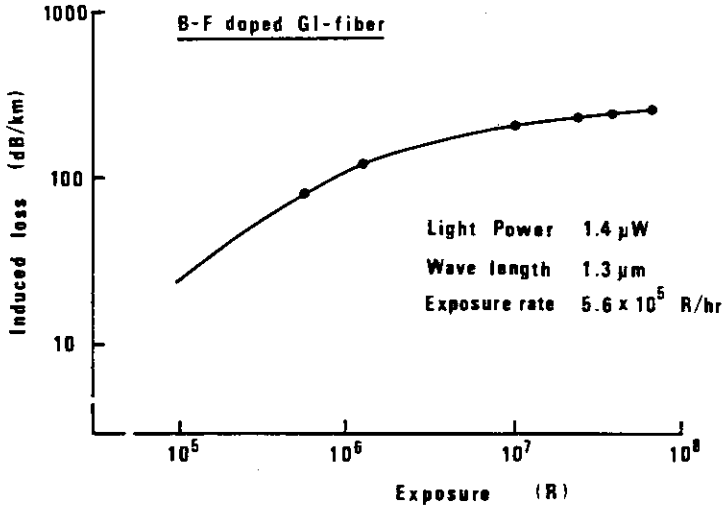

Fig. 6.5.2 Radiation induced loss obtained at the high exposure

6.6 Development of an In-situ Nondestructive Measurement System for Measuring Radioactivities Inside Contaminated Pipings

M. Katagiri, N. Wakayama, H. Yamauchi, Y. Tabe and H. Itoh

Before decomissioning of nuclear power plants, testimation of the residual radioactive inventories is necessary. However, it is difficult to estimate the activities inside pipings in the primary cooling system using calculations. Therefore, we have developed an in-situ nondestructive measurement system which can perform the determination of nuclides, the quantities and states (that is, plateout or liquid) of radioactivities inside the contaminated pipings.

Figure 6.6.1 shows a block diagram of the proposed measurement system. This system consists of a field-side equipment and a data-analysis-side equipment. The former is arranged with a mini-size gamma-ray detector with a collimator, an electronic circuit with a signal amplifier, a microcomputer controller and a telemeter; This instrument is used for measuring the gamma-rays emitted from the inside of pipings. The latter is composed of a telemeter, a signal processing device, a data analysis device and a display board; This instrument is used for analyzing the quantities of radioactivities of each nuclide inside pipings. These instruments are connected to each other with a set of the wireles telemeters.

We have developed a gas-cooled germanium gamma-ray detector to make a field-side equipment portable. Then, we designed a system which can operate with a battery and by remort control.

Moreover, we have developed a control and analysis program for this measurement system. Hardware devices are controlled automatically by the computor program so that a gamma-ray spectrum can be measurd at each scanning point. Then, from the results of the gamma-ray spectra analysis, the quantity and the state of radioactivities of each nuclide are calculated by computations.

Using this system, evaluation tests of the developed measurement system were performed for the test pipings which imitated the contaminated pipings in a primary cooling system. Figure 6.6.2 shows an example of gamma-ray peak counting rate distributions plotted for comparison between the measured and calculated values obatined under the conditions such as gamma-ray energy, sizes of the piping, geometics etc. From these results, the quantities of the plateout radioactivities and the radioactivities of the liquid containing Co-60 were obatined by separation of both states using the computer program. In each

state, the difference between the measured and the already-known values of Co-60 radioactivities was found to be below 10 %. Table 6.6.1 shows the measured results of Co-60 and Eu-152 inside the test pipings. These results exhibit that the measured values agree well with already-known ones.

As the effectiveness of this measuring technique was confirmed, a prototype measurement system was made for mesurments of contaminated pipings in JPDR.

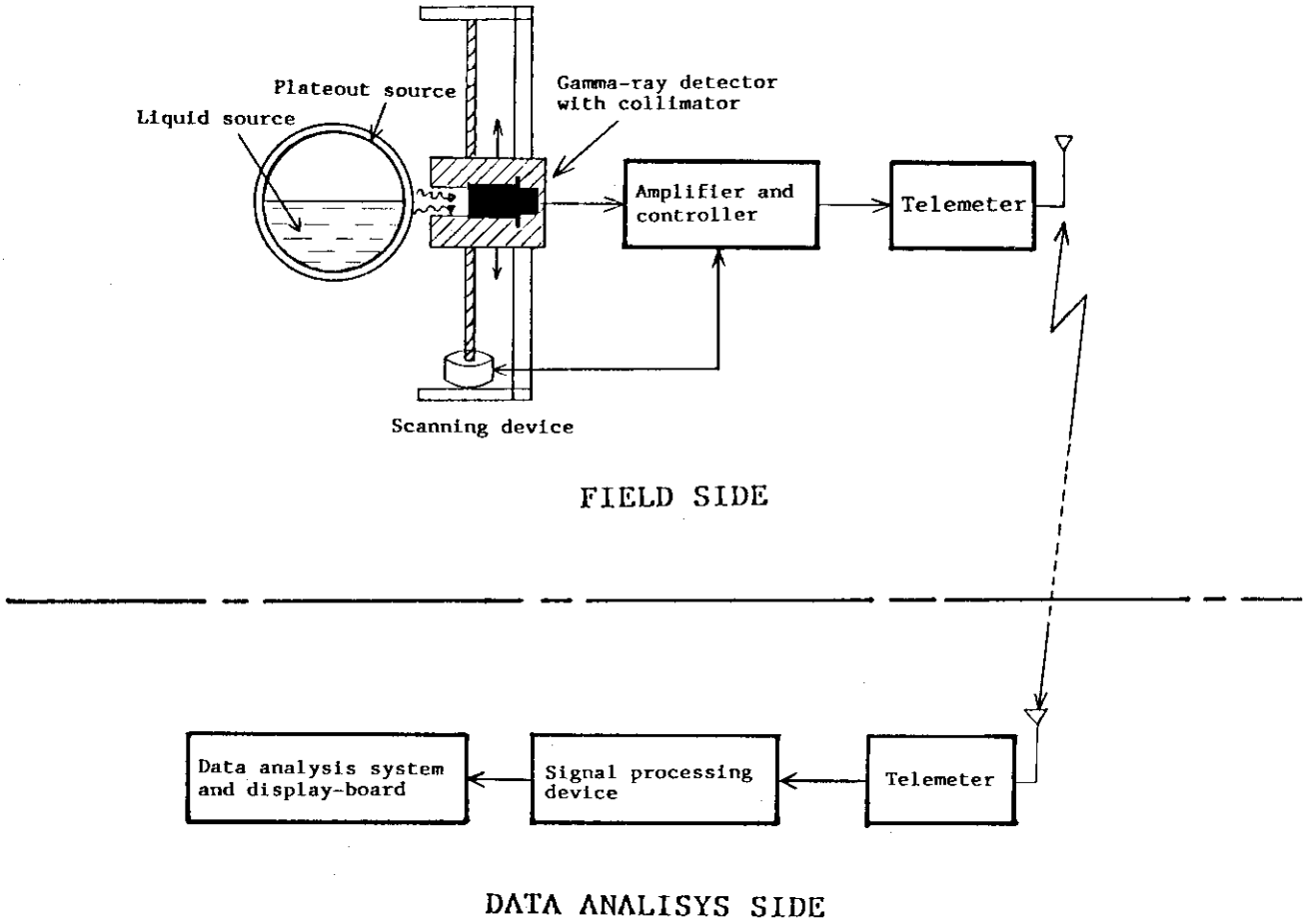

Fig. 6.6.1 A block diagram of a developed measurement system

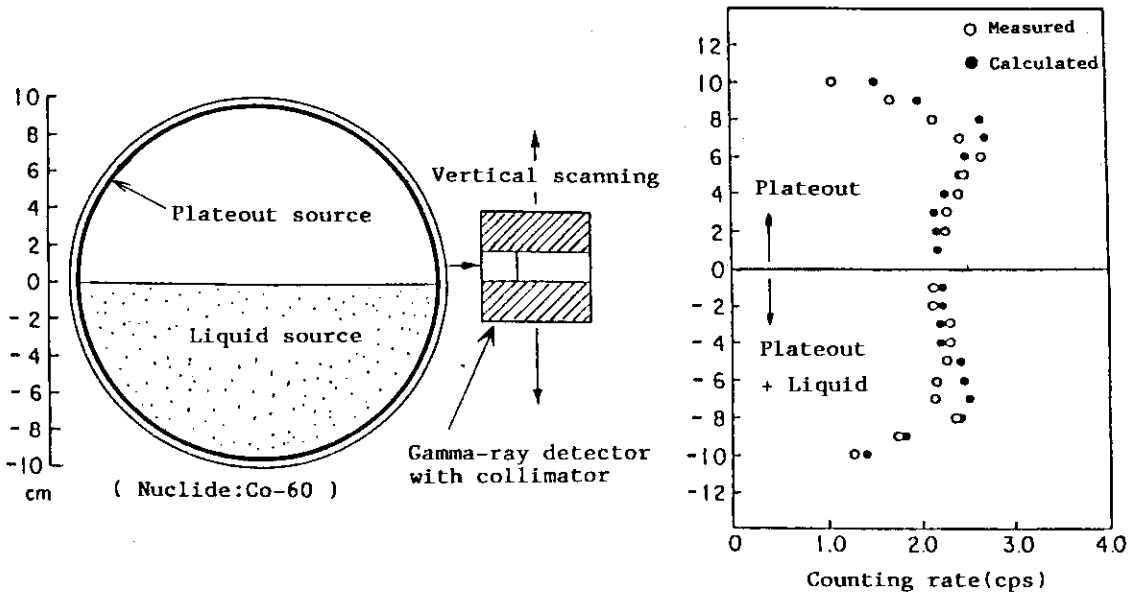

Fig. 6.6.2 Outline of test experiments, and counting rate distributions of the measured values and calculated values

Table 6.6.1 Comparison with measured quantities and already-known qantities of Co-60 and Eu-152

Nuclide	Gamma-ray energy (keV)	Plateout (μCi/cm^2)		Liquid (μCi/cm^3)	
		Measured	Known	Measured	Known
Eu-152	122	0.230	0.233	0.0086	0.0102
	344	0.224		0.0124	
	779	0.252		0.0111	
	964	0.270		0.0113	
	1408	0.209		0.0117	
Co-60	1173	0.075	0.085	0.0066	0.0075
	1332	0.076		0.0063	

6.7 Development of a Telescopic Measurement System for Nondestructively Measuring Radioactivities of Activated Structural Components in RPV

M. Katagiri, N. Wakayama, M. Hatakeyama+, F. Satoh+, H. Yamauchi
Y. Tabe and H. Itoh

In decommissioning of nuclear power reactors, it is very important to measure the radioactivity distributions in stractural components and inner walls of a reactor pressure vessel (RPV) for estimation of the residual radioactive inventories.

Therefore, we have developed a telescopic measurement system which can non destructively measure these radioactivity distributions for each nuclide at a high level of radioactivities. Figure 6.7.1 shows the principle of telescopic measuring system. The straight piping was installed in the primary coolant water in RPV, aiming at the object component: The collimator is made with this piping and water. Gamma-rays transmitted through this pipe are measured by a germanium gamma-ray detector. Background gamma-rays scattered by other materials can be removed by means of gamma-rays spectroscopy using this detector. Then, the specific radioactivities are calculated through the spectrum analysis results by taking account of absorption loss, detection efficiencies, etc.

This system was applied to the radioactivity measurements of activated structural components, such as core shrouds, grids and inner walls in RPV of JPDR. Figure 6.7.2 shows an example of measurements at a core shroud. At the center of the core shroud, the specific radioactivities of Co-60 were 1.2×10^{3} μCi/g. the measured results at upper, middle and lower coreshroud agreed with the specific radioactivities measured by the sampling method within an error of 10 %. The measued results at inner walls, which range from 10^{-1} μCi/g to 30 μCi/g, agreed with the results measured by the sampling method within the error of 30 %.

These results confirm the effectiveness of the telescopic measurement system developed by us.

+ Decommissioning Technolgy Laboratory, Department of JPDR

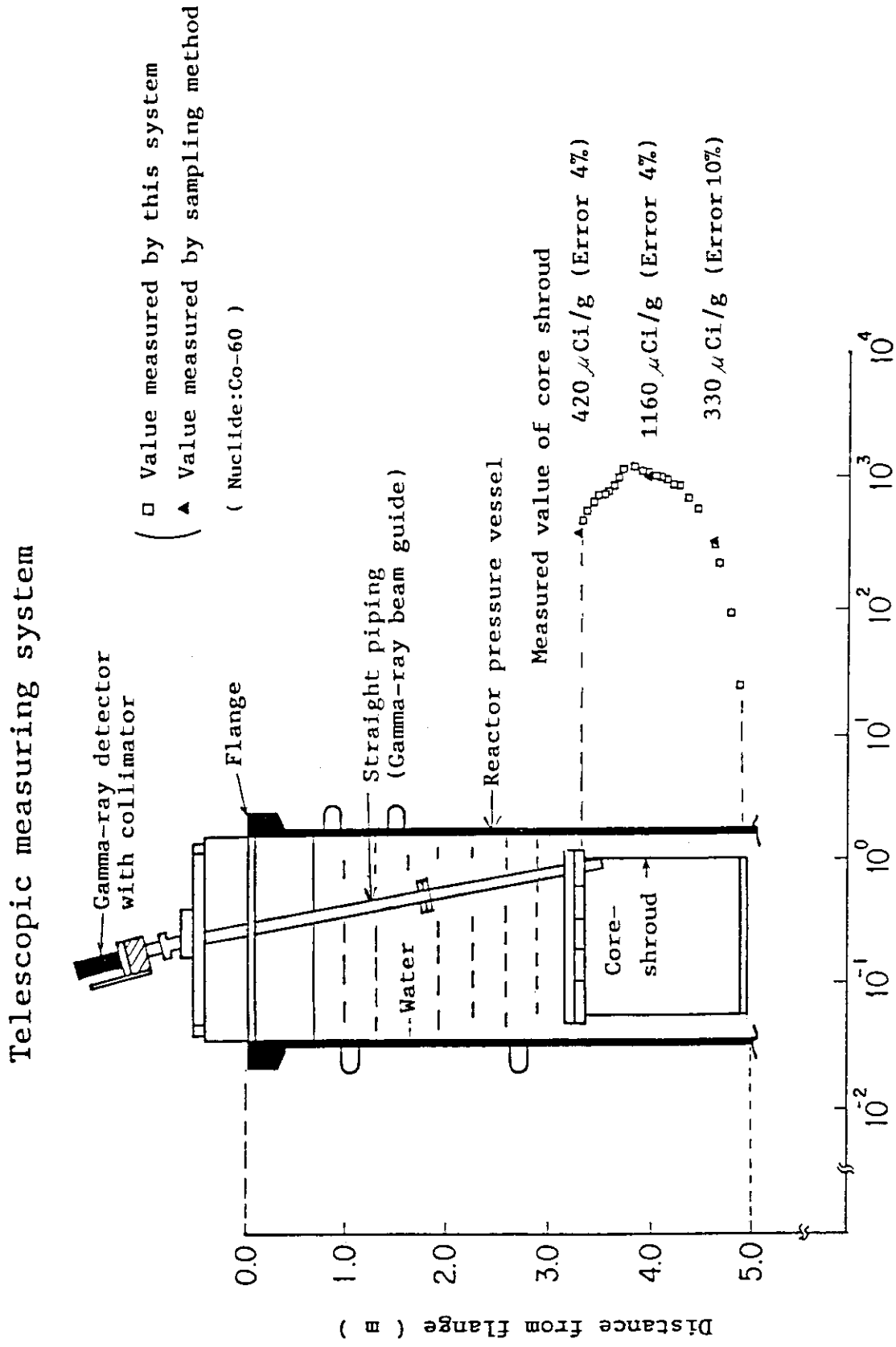

Fig. 6.7.1 Principle of telescopic measurements and an example of measurements at core-shrouds in RPV

6.8 Further Measurements of Induced Radioactivities in Silicon and Germanium Irradiated with High-Energy Heavy Ions

E.Sakai

Semiconductor detectors are known to be sensitive to radiation damage which may be annealed by heating at an elevated temperature. In high-energy heavy-ion detection with semiconductor detectors, nuclear reactions in the semiconductor materials themselves are expected to introduce radioactive nuclides which increase background counting rates of the detectors during and after the irradiation. These radioactive nuclides can not be removed by heating and the only method to remove these nuclides is etching. The production of radioactive nuclides is also important in manufacturing dopant layers buried deep into semiconductor materials by the ion implantation since the radioactivities may result in noisy devices and also the nuclides with their daughters may change the type of the materials.

In order to evaluate the amount of background counting rate increase in semiconductor heavy-ion detectors, the author started measuring the induced radioactivities in Si and Ge after the irradiation with various high-energy heavy-ions. Gamma-ray spectra from irradiated Si and Ge wafers were measured using a high-purity Ge spectrometer to determine the induced gamma-ray-emitting nuclides, their radioactivities, their numbers of atoms at the end of the irradiation and the numbers of atoms per incident heavy-ion. Some of the results were already published[1)2)].

In this fiscal year(1985), irradiations with 90 MeV $^{79}Br^{6+}$, 120 MeV $^{19}F^{7+}$, 165 MeV $^{32}S^{10+}$, 66 MeV $^{10}B^{4+}$, 150 MeV $^{32}S^{9+}$, 50 MeV $^{32}S^{7+}$ and 100 MeV $^{32}S^{8+}$ were carried out and some of the results are summarized in Table 6.8.1.

References

1) Sakai E.: IEEE Trans. Nucl. Sci., NS-31(1984) pp. 316 - 319.
2) Sakai E.: IEEE Trans. Nucl. Sci., NS-33(1986) pp. 651 - 654.

Table 6.8.1 Residual gamma-ray-emitting nuclides induced in Si and Ge irradiated with heavy ions, their radioactivities at the end of irradiation, corresponding numbers of atoms, numbers of atoms per incident ion, resultant stable daughter nuclides and the calculated threshold energies for compound nucleus formation

(Table 6.8.1 continued)

Heavy ions (Range)	Number of particles	Irradiated materials	Residual nuclide	Radioactivity(nCi)	Number of atoms	Number of atoms per particles	Stable daughter nuclide	Threshold energy(MeV)
120MeV $^{19}F^{7+}$ (61.8 μm)	6.21E14 /3.14cm^2	Ge	Ga-67(78.9h)	22.6	3.41E8	5.56E-7	Zn-67	50.06
			Ge-69(39.0h)	118	8.81E8	1.46E-6	Ga-69	
			As-71→Ge-71(11.2d)				Ga-71	
			As-71(61h)	121	1.42E9	2.32E-6	Ga-71	
			As-74(17.78d)	38.8	3.18E9	5.14E-6	Ge-74,Se-74	
			As-76(26.3h)	417	2.11E9	3.54E-6	Se-76	
			Se-75(118.5d)	4.9	2.66E9	4.28E-6	As-75	
			Br-77(57.0h)	136	1.49E9	2.44E-6	Se-77	
			Kr-79(35.0h)	333	2.24E9	3.72E-6	Br-79	
			Sr-83→Rb-83(86.2d)				Kr-83	
			Sr-83(32.4h)	1800	1.12E10	1.87E-5	Kr-83	
			Y-87→Sr-87m(2.80h)				Sr-87	
			Zr-86→Y-86(14.74h)				Sr-86	
			Y-87(80.3h)	1560	2.40E10	3.92E-5	Sr-87	
			Zr-88→Y-88(106.6d)				Sr-88	
			Zr-86(16.5h)	1970	6.25E9	1.07E-5	Sr-86	
			Zr-88(83.4d)	33.0	1.27E10	2.05E-5	Sr-88	
			Zr-89(78.4h)	736	1.11E10	1.81E-5	Y-89	
			Nb-90(14.6h)	1070	3.01E9	5.21E-6	Zr-90	
50MeV $^{32}S^{7+}$ (15 μm)	~5.29E13 /0.72cm^2	Si	None					70.74
100MeV $^{32}S^{8+}$ (29.3 μm)	~4.46E14 /0.72cm^2	Si	Cr-51(27.7d)	6.1	7.74E8	~1.74E-6	V-51	70.74
			Mn-52(5.59d)	5.0	1.29E8	~2.93E-7	Cr-52	
			Co-55→Fe-55(2.7y)				Mn-55	
			Co-55(17.5h)	112	3.76E8	~9.45E-7	Mn-55	
			Ni-56→Co-56(77.12d)				Fe-56	
			Ni-57→Co-57(271.77d)				Fe-57	
			Ni-56(6.10d)	1.8	5.10E7	~1.16E-7	Fe-56	
			Ni-57(36.0h)	221.5	1.53E9	~3.63E-6	Fe-57	
150MeV $^{32}S^{4+}$ (47.4 μm)	~8.56E14 /0.3cm^2	Si	Cr-48(15.976d)→V-48(15.976d)				Ti-48	70.74
			Cr-48(21.56h)	66.7	2.77E8	~3.74E-7	Ti-48	
			Cr-51(27.70d)	25.3	3.24E9	~3.80E-6	V-51	
			Mn-52(5.59d)	143.7	3.70E9	~4.43E-6	Cr-52	
			Co-55→Fe-55(2.7y)				Mn-55	
			Co-55(17.54h)	265.6	8.95E8	~1.25E-6	Mn-55	
			Ni-56→Co-56(77.12d)				Fe-56	
			Ni-57→Co-57(271.77d)				Fe-57	
			Ni-56(6.10d)	8.0	2.24E8	~3.13E-7	Fe-56	
			Ni-57(36.0h)	124.6	8.62E8	~1.10E-6	Fe-57	
165MeV $^{32}S^{10+}$ (54 μm)	1.05E14 /0.98cm^2	Si	Sc-44m(2.44d)	3.4	3.78E8	3.72E-7	Ca-44	70.74
			Sc-44m→Sc-44(3.93h)				Ca-44	
			Cr-48→V-48(15.976d)				Ti-48	
			Cr-48(21.56h)	69	2.86E8	2.97E-6	Ti-48	
			Cr-51(27.70d)	18	2.31E9	2.20E-5	V-51	
			Mn-52(5.59d)	102	2.62E9	2.53E-5	Cr-52	
			Co-55→Fe-55(2.7y)				Mn-55	
			Co-55(17.54h)	130	4.39E8	4.65E-6	Mn-55	
			Ni-56→Co-56(78.8d)				Fe-56	
			Ni-57→Co-57(271d)				Fe-57	
			Ni-56(6.10d)	1.8	5.10E7	4.92E-7	Fe-56	
			Ni-57(36.0h)	93.8	6.49E8	6.51E-6	Fe-57	

(Table 6.8.1 continued)

Heavy ions (Range)	Number of particles	Irradiated materials	Residual nuclide	Radioactivity(nCi)	Number of atoms	Number of atoms per particles	Stable daughter nuclide	Threshold energy(MeV)
50MeV $^{32}S^{7+}$ (10.9 μm)	~1.96E14 /3.0cm^2	Ge	None					94.25
100MeV $^{32}S^{4+}$ (20.6 μm)	~1.38E15 /2.88cm^2	Ge	As-71→Ge-71(11.2d)				Ga-71	94.25
			As-71(61h)	1.0	1.18E7	~8.86E-9	Ga-71	
			Y-87→Sr-87m(2.80h)				Sr-87	
			Y-87(80.3h)	0.4	5.56E6	~4.15E-9	Sr-87	
			Ru-97(2.88d)	0.8	1.02E7	~7.64E-9	Mo-97	
			Pd-100→Rh-100(20.8h)				Ru-100	
			Rh-101m(4.34d)	4.5	9.03E7	~6.69E-8	Ru-101	
			Pd-100(3.63d)	2.0	3.43E7	~2.55E-8	Ru-100	
150MeV $^{32}S^{4+}$ (30.9 μm)	2.46E15 /2.15cm^2	Ge	Ga-67(78.3h)	6.3	9.53E7	3.97E-8	Zn-67	94.25
			Ge-69(39.0h)	50.4	3.77E8	1.62E-7	Ga-69	
			As-71→Ge-71(11.2d)				Ga-71	
			As-71(61h)	34.4	4.03E8	2.65E-7	Ga-71	
			Se-72→As-72(26.0h)				Ge-72	
			As-74(17.8d)	53.7	1.82E8	8.26E-8	Ge-74,Se-74	
			As-76(26.32h)	33.4	1.69E8	7.42E-8	Se-76	
			Se-72(26.0h)	102	5.10E8	2.24E-7	Ge-72	
			Se-75(118.5d)	0.85	4.66E8	1.90E-7	Ge-75	
			Br-77(57.0h)	10.5	1.15E8	4.84E-8	Se-77	
			Zr-89→Y-89m(16.1s)				Y-89	
			Zr-89(78.4h)	3.3	4.90E7	2.04E-8	Y-89	
			Tc-95(20.0h)	430	1.65E9	7.43E-7	Mo-95	
			Tc-96(4.35d)	11.0	2.21E8	9.16E-8	Mo-96	
			Tc-99m(6.0h)	4178	4.82E9	2.71E-6	Ru-99	
			Ru-97(2.88d)	238	3.17E9	1.32E-6	Mo-97	
			Rh-99(15.0d)	2.3	1.61E8	6.56E-8	Ru-99	
			Pd-100→Rh-100(20.8h)				Ru-100	
			Pd-101→Rh-101m(4.34d)				Ru-101	
			Pd-100(3.63d)	43	7.25E8	3.02E-7	Ru-100	
			Pd-101(8.47h)	1294	2.11E9	1.08E-6	Ru-101	
165MeV $^{32}S^{10+}$ (35.6 μm)	3.56E14 /3.14cm^2	Ge	Ga-67(78.3h)	4.9	7.36E7	2.11E-7	Zn-67	94.25
			Ge-69(39.0h)	48	3.62E8	1.06E-6	Ga-69	
			As-71→Ge71(11.2d)				Ga-71	
			As-71(61h)	29	3.43E8	9.93E-7	Ga-71	
			Se-72→As-72(26.0h)				Ge-72	
			As-73(80.3d)	0.4	1.32E8	3.70E-7	Ge-73	
			As-74(17.78d)	3.0	2.46E8	6.95E-7	Ge-74,Se-74	
			Se-72(8.40d)	6.5	2.5 E8	7.1 E-7	Ge-72	
			Se-75(118.5d)	0.7	3.75E8	1.11E-6	As-75	
			Br-77(57.0h)	12.5	1.37E8	3.97E-7	Se-77	
			Y-87→Sr-87m(2.80h)				Sr-87	
			Y-87(80.3h)	2.2	3.41E7	9.78E-8	Sr-87	
			Zr-89(78.4h)	5.5	8.31E7	2.39E-7	Y-89	
			Nb-95(35.0d)	16.1	2.60E9	7.31E-6	Mo-95	
			Tc-96(4.35d)	10.9	2.18E8	6.22E-7	Mo-96	
			Tc-99m(6.0h)	35600	4.10E10	1.52E-4	Ru-99	
			Ru-97(2.88d)	188	2.50E9	7.20E-6	Mo-97	
			Rh-99(15.0d)	1.8	1.21E8	3.42E-7	Ru-99	
			Pd-100→Rh-100(20.8h)				Ru-100	
			Rh-101m(4.34d)	100	2.01E9	5.75E-6	Ru-101	
			Pd-100(3.6d)	58	9.61E8	2.76E-6	Ru-100	

6.9 Curing of Neutron Damage in Closed-End-Coaxial High-Purity Germanium Detectors

E.Sakai

The author's experience on the complete curing of the neutron damage in a true coaxial Ge(Li) gamma-ray detector was reported in a previous report[1]. The present paper describes the results of the annealing experiments on three neutron-damaged high-purity Ge detectors of a closed-end-coaxial type commercially made of p-type material. The first and the second detectors have room-temperature type preamplifiers and the third has a cooled FET preamplifier. All the three detectors had been damaged by unknown fast-neutron fluences in various accelerator experiments.

The FWHM energy resolution and the peak-to-Compton ratio of the 1332 keV gamma-ray peak obtained from the first detector operated at 2000 V bias voltage degraded to 3.835 keV and 22.87, respectively, with an amplifier shaping time of 4μs as shown in Fig.6.9.1 (a), while the leakage currrent(0.017A), capacitance(30 pF) and relative peak detection efficiency(14.83 %) did not degrade at all. The pulser FWHM was 1.034 keV. The detector was scanned with a collimated ^{60}Co gamma-ray source to find which type of carriers are responsible for the degraded FWHM, as shown in (b) and (c). The outer edge irradiation resulted in a worse FWHM(3.572 keV) than that(2.249 keV) obtained from the central region irradiation: this means a preferential hole-trapping, which is a general consequence of neutron damage in Ge(Li)[1] and high-purity Ge[2)3)] detectors. Firstly, this detector was warmed up in the dipstick whose bottom was dipped in 80°C water for 2.5 hours although no change in the detector performance was found by this treatment. Next, the detector was heated under a continuous operation of vacuum pump in the dipstick whose bottom-copper-rod was heated at 100°C for 2 complete days. The FWHM and the peak-to-Compton ratio improved to 2.327 keV and 34.54, respectively, with 6μs shaping time while the capacitance and detection efficiency stayed almost unchanged. A bias voltage of 2500 V became applicable since the leakage current at this voltage was reduced, and the FWHM and peak-to-Compton ratio improved 2.110 keV and 36.75, respectively. A comparison of the detector performance before and after the 2 day - 100°C annealing is summarized in Fig.6.9.2.

The second detector exhibited an FWHM of 2.849 keV, peak-to-Compton ratio of 30.63 and relative peak detection efficiency of 15.37 % for the 1332 keV gamma-ray peak with 2000 V bias and 4μs shaping time. The collimated ^{60}Co gamma-ray scan gave a FWHM of 2.190 keV at the center and 2.673 keV at the periphery, thus, indicating hole trapping. An annealing was performed at 100°C

for 2 days and 3 hours. The FWHM and peak-to-Compton ratio improved to 2.249 keV and 35.03, respectively, with 6μs shaping time.

The third detector displayed 2.684 keV FWHM, 30.18 peak-to-Compton ratio and 14.97 % relative peak detection efficiency for the 1332 keV gamma-ray peak at 2500 V bias and 4μs shaping. The scan data were 2.154 keV FWHM at the center irradiation and 2.930 keV at the periphery. After the detector was annealed at 100°C for 2 days, the FWHM and peak-to-Compton ratio improved to 2.253 keV and 35.18, respectively, at 6μs shaping time. The leakage current improved significantly, thus, 3500 V could become applicable. At 3000 V and 3500 V the FWHM became 2.178 keV. Before the annealing, there was a fear of

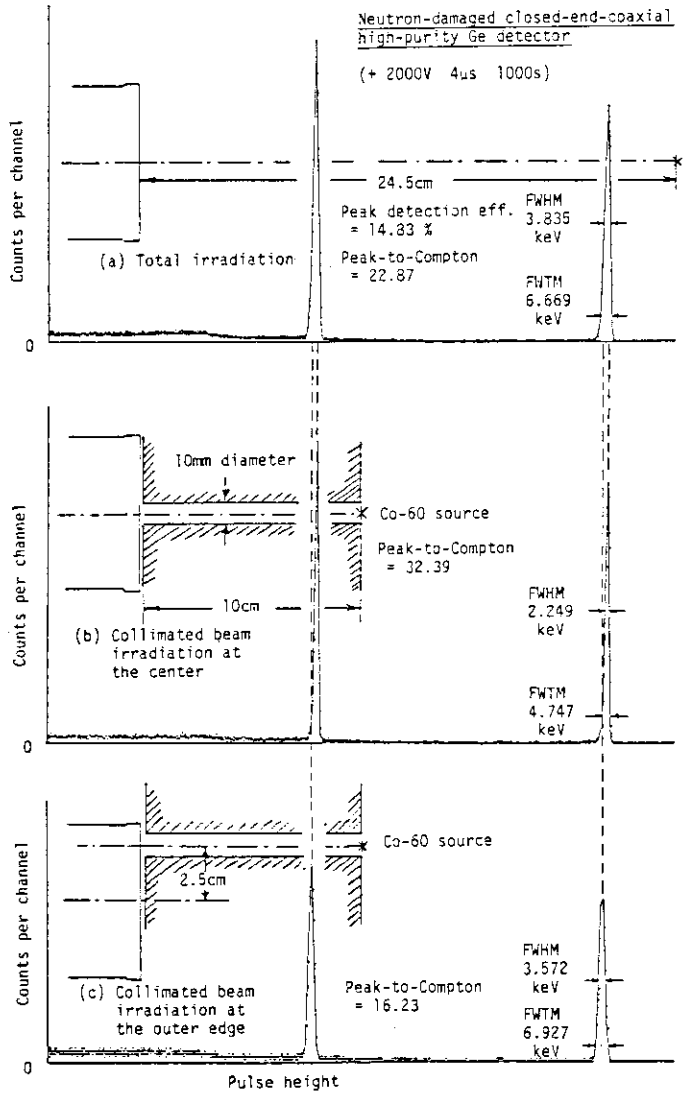

Fig.6.9.1 ^{60}Co gamma-ray pulse height distributions obtained from a neutron damaged closed-end-coaxial high-purity Ge detector at 2000 V bias and 4μs shaping time for three different irradiations. A preferential hole trapping is apparently seen in (c).

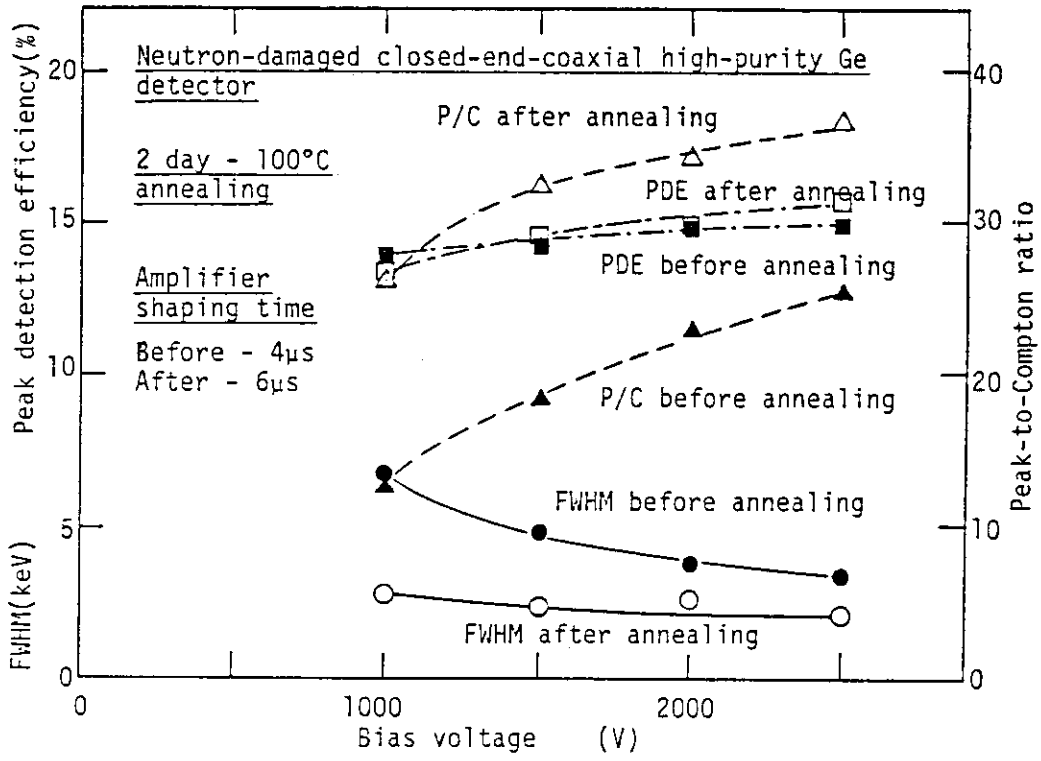

Fig.6.9.2 FWHM energy resolutions, relative peak detection efficiencies and peak-to-Compton ratios for 1332 keV gamma-rays obtained from a neutron-damaged closed-end-coaxial high-purity Ge detector before and after a 2 day-100°C annealing.

possible damage of the input FET in the first stage of the preamplifier, but the fear was found unnecessary.

The author's experience on the three coaxial high-purity Ge detectors described above can be summarized that neutron damage can be cured reasonably and safely by the simple in-dipstick annealing at 100°C for 2 days even for detectors with cooled-FET preamplifiers although more complete curing seems to need annealing at higher temperatures than 100°C, such as 120°C[2] or 150°C[3] where a fear exists to damage some of components in the dipstick.

References

1) Sakai E.: " Curing of Neutron Damage in a True-Coaxial Ge(Li) Gamma-Ray Detector," JAERI-M 85-116(1985) pp. 194 - 196.

2) Kraner H.W., Pehl R.H., Haller E.E.: IEEE Trans. Nucl. Sci., NS-22, No.1 (1975) pp.149 - 159.

3) Darken Jr L.S.,et al.: IEEE Trans. Nucl. Sci., NS-28(1981) pp. 572 - 578.

6.10 Gamma-Ray Energy Dependence of FWHM Energy Resolutions Obtained from a PMT Coupled with Scintillators of Various Kinds

E.Sakai

No literature was found which showed relative pulse height distributions or gamma-ray energy dependence of the full-width-at-half-maximum(FWHM) energy resolutions obtained from scintillators of many kinds plotted together in a single graph. These graphs, if available, will help very much for the users to consider an appropriate use of scintillation counters for their demands. The present report describes the results of the measurements of the pulse height distributions obtained from a photomultiplier(PMT) coupled with eleven kinds of scintillators for gamma-rays of energies between 14 keV and 1836 keV.

The scintillators are mostly of small rectangular parallelepiped(10x10 mm^2 x6 mm, 7 mm, 10 mm or 20 mm) and include NaI(Tl), CsI(Na), CsI(Tl), Ce:Gd_2SiO_5(GSO), CaF_2(Eu), $CdWO_4$(CWO), $Bi_4Ge_3O_{12}$(BGO), CsI(pure), BaF_2, NE 905 and NaI(pure). All the scintillators have one polished face with five ground sides on which white Teflon tape, $BaSO_4$ or MgO powder was lapped as a reflector. The PMT was one of Hamamatsu R 1306(2 in. dia., bialkali photocathode, borosilicate glass window). Each of the scintillators was placed with silicone oil or compound on the PMT window. The anode output pulses were fed to a charge-sensitive preamplifier(Canberra 2005) followed by a spectroscopy amplifier(Canberra 2013(4μs shaping time)) and a multichannel analyzer(Canberra 8100). The anode voltage of the PMT was +825 V.

Figure 6.10.1 shows a comparison of the ^{88}Y gamma-ray pulse height distributions obtained from the eleven scintillators with the same settings of the PMT voltage and the amplifier gain. The CsI(Na) exhibited the largest pulse heights and the pulse heights decreased in the order of NaI(Tl), CsI(Tl), GSO, CaF_2(Eu), CWO, BGO, CsI(pure), BaF_2, NE 905 and NaI(pure). The CaF_2(Eu) and the NE 905 did not produce photopeaks for ^{88}Y gamma-rays because of their small attenuation coefficients and small sizes. The FWHMs of the 898 keV and 1836 keV gamma-ray peaks are indicated in the figure. The FWHMs degrade as the pulse heights decrease. Figure 6.10.2 shows gamma-ray energy dependence of the FWHM energy resolutions(%) of the scintillators. The scintillators except CsI(Na), NaI(Tl), CsI(Tl) and CsI(pure) indicated a $E^{-1/2}$ dependence while the four scintillators deviated significantly from the $E^{-1/2}$ dependence at energies above 100 keV. This deviation is brought by the so-called "intrinsic pulse height broadening"[1] which is caused by a combined effect of the non-linear light outputs with multiple interactions in the scintillators.

Performance of the other kinds and different sizes of scintillators will be studied.

Reference

(1) Narayan G.H., Prescott J.R.: IEEE Trans. Nucl. Sci., NS-15(3), 162 - 166 (1968).

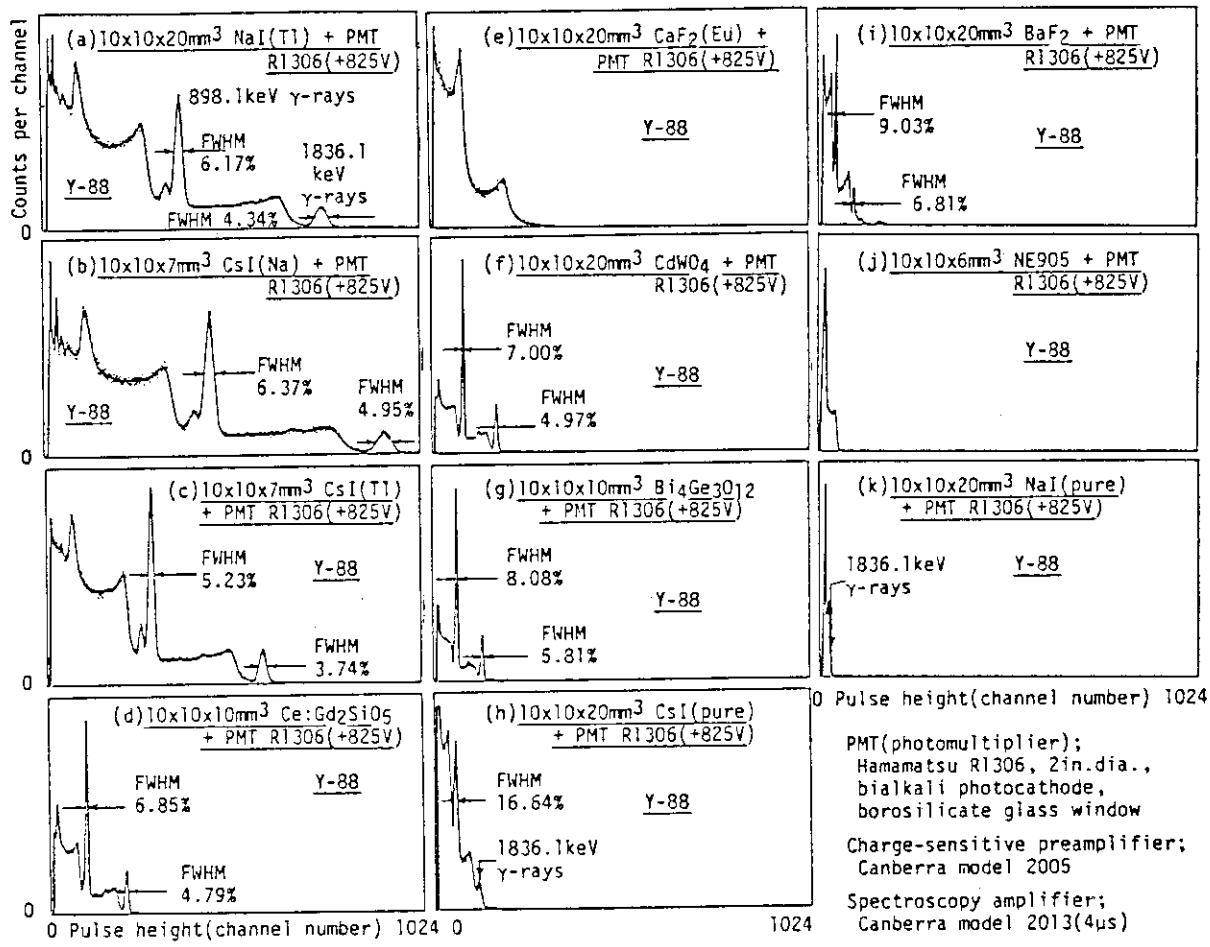

Fig.6.10.1 Comparison of pulse height distributions of ^{88}Y gamma-rays obtained from various scintillators coupled with a photomultiplier Hamamatsu R 1306 - charge-sensitive preamplifier Canberra 2005 - spectroscopy amplifier Canberra 2013(4μs shaping time) system.

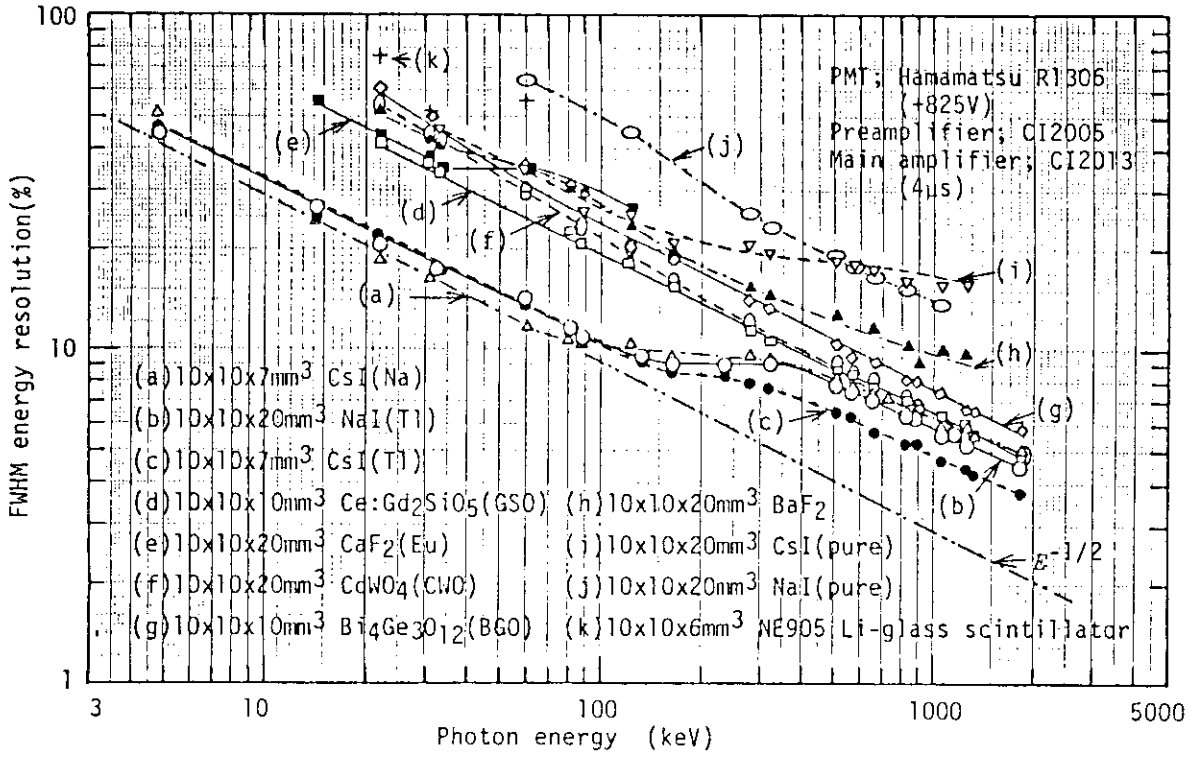

Fig.6.10.2 FWHM energy resolution(%) vs. photon energy characteristics of various small scintillators obtained from a photomultiplier (Hamamatsu R 1306, 2 inch dia., bialkali photocathode, + 825 V) - charge-sensitive preamplifier(Canberra 2005) - spectroscopy amplifier(Canberra 2013, 4μs shaping time) system.

6.11 Measurement of Absolute Numbers of Photoelectrons Emitted from a PMT Photocathode Coupled with Various Scintillators

E.Sakai

Little information is available on the absolute values of the light outputs of scintillators of various kinds although their relative values can be found in manufacturer's catalogs and many standard text books. The absolute values are preferable to relative ones since scintillators of the same kind, for instance NaI(Tl), do not necessarily display the same pulse height and also the relative values listed in the references seem to have an obscure meaning, namely, sometimes simply relative pulse heights, sometimes relative integrated charge outputs, sometimes relative scintillation efficiencies and sometimes wavelength-integrated light outputs. We have measured the absolute numbers of the photoelectrons emitted from the photocathode of a photomultiplier(PMT) Hamamatsu R 1306(2 in. dia., bialkali photocathode, borosilicate glass window) coupled with various kinds of scintillators(10x10 mm^2 x 6 mm, 7 mm, 10 mm or 20 mm, NaI(Tl), CsI(Na), CsI(Tl), Ce:Gd_2SiO_5(GSO), CaF_2(Eu), $CdWO_4$(CWO), $Bi_4Ge_3O_{12}$(BGO), CsI(pure), BaF_2, NE 905, NaI(pure) and 40 mm dia.x15 mm LiI(Eu)jby using the PMT in a photodiode mode[1].

The PMT measurements in the photodiode mode have been made as follows; the grid, the first and the second dynodes of the PMT were connected together with the input of a charge-sensitive preamplifier Canberra 2001(ac-coupled) followed by a spectroscopy amplifier Canberra 2013(4μs shaping time) and a multichannel analyzer Canberra 8100. All the other electrodes of the PMT were connected to the ground. Since the output pulse heights saturate at the voltages above +50 V applied on the first dynode, the measurements have been made with +100 V. The pulse heights were calibrated with a silicon detector, thus the numbers of photoelectrons emitted from the PMT photocathode were obtained using an average energy of 3.6 eV needed to produce one electron-hole pair in silicon.

The results are summarized in the right columns of Table 6.11.1, in which the numbers of photoelectrons emitted from the photocathode for 1 MeV of gamma-ray energy obtained from 1836 keV gamma-ray measurements, the effective quantum efficiencies of the PMT, the numbers of photons emitted from the scintillators per MeV energy of gamma-ray, the average energies of gamma-rays needed to produce one photon and the absolute scintillation efficiencies are listed. The light collection efficiencies in the scintillators and also the collection efficiencies of the photoelectrons in the PMT were assumed as 100 %. The pulse heights of the three NaI(Tl) scintillators differed more than 30

%; this seems to be caused by the difference in light collection and/or crystal quality.It is interesting that the scintillators can be classified into three groups; the first(NaI(Tl), CsI(Na), CsI(Tl)) has the absolute scintillation efficiency of about 0.13, the second(GSO,CaF_2(Eu), LiI(Eu), CWO, BGO, BaF_2) about 0.03 and the third much smaller efficiencies. The left columns list the performance of the scintillator-PMT combinations operated in the ordinary multiplication mode.

This method of the absolute characterization of scintillators and/or PMTs is simple and seems suitable as a standard test procedure of scintillation counters.

Reference

(1) M. Miyajima, et al.; Nucl. Instrum. Meth., 224, 331(1984).

Table 6.11.1 Summary of the measurements on scintillators of various kinds using a photomultiplier Hamamatsu R 1306(2 in. dia., bialkali photocathode, borosilicate glass window) operated in a photodiode mode. The results obtained from the same photomultiplier operated in the ordinary multiplication mode are also listed.

Scintillator	PMT R 1306(+825V)-PMT mode				PMT R 1306(+100V)-Photodiode mode						
	1836keV γ		662keV γ	10-90%	Peak wavelength		Photoelectrons	Eff.q.	Photons	eV-γ	Abs.sci.
(mm^3)	PHR	FWHM(%)	FWHM(%)	risetime	λ(nm)	E(eV)	/MeV-γ(1836keV)	e.[7]	/MeV-γ	/photon	eff.[8]
10x10x10 NaI(Tl)					415[2]	2.988	1.197×10^4	0.265	4.518×10^4	22.13	0.135[9]
10x10x20 NaI(Tl)	100	4.38	7.07	0.5 μs	415[2]	2.988	9.581×10^3	0.265	3.611×10^4	27.69	0.108[9]
10x10x20 NaI(Tl)					415[2]	2.988	1.005×10^4	0.265	3.791×10^4	26.38	0.114[9]
10x10x 7 CsI(Na)	122	4.95	7.37	4 μs	420[2]	2.952	1.118×10^4	0.259	4.308×10^4	23.21	0.127
10x10x 7 CsI(Tl)	78	3.75	5.66	4 μs	540[1]	2.297	7.077×10^3	0.126	5.600×10^4	17.86	0.123
10x10x10 Ce:Gd_2SiO_5	28	4.84	7.82	$<$ 0.1 μs	430[3]	2.883	2.838×10^3	(0.275)	(1.032×10^4)	(96.90)	(0.0298)
10x10x20 CaF_2(Eu)	(27)*	*	*	4 μs	435[2]	2.850	*(2.587×10^3)[6]	(0.270)	(0.958×10^4)	(104.4)	(0.0273)
40dia.x15 LiI(Eu)					470[2]	2.638	2.670×10^3	(0.250)	(1.068×10^4)	(93.63)	(0.0282)
10x10x20 $CdWO_4$	23	4.92	7.97	20 μs	495[1]	2.505	2.278×10^3	0.186	1.222×10^4	81.82	0.0306
10x10x10 $Bi_4Ge_3O_{12}$	17.5	5.81	9.05	0.8 μs	505[1]	2.455	1.859×10^3	0.175	1.061×10^4	94.26	0.0260
10x10x20 CsI(pure)	16	**	17.31	8 μs			1.533×10^3[6]				
10x10x20 BaF_2	13	6.22	11.37	3 μs	310[4]	4.000	1.431×10^3	0.128	1.115×10^4	89.67	0.0446
10x10x 6 NE 905	(6)*	*	*	$<$ 0.1 μs	395[5]	3.139	*(5.750×10^2)[6]	(0.28)	(2.053×10^3)	(487.1)	(0.0064)
10x10x20 NaI(pure)	4	**	16.67	0.4 μs			3.832×10^7[6]				

* No photo-peak. Pulse height ratios(PHR) in parentheses are for 122keV γ-rays. ** Too wide peak to obtain FWHM.
[1] B.C.Grabmair;IEEE Trans. Nucl. Sci.,NS-31(1984)372-376. [2] Harshaw catalog. [3] Hitachi Chemical Co. catalog. [4] M.Laval,et al;Nucl.Instrum.Meth.,206(1983)169-176. [5] Nuclear Enterprises catalog. [6] Calculated from PHR x9.581×10^3. [7] The effective quantum efficiencies of the PMT photocathode calculated from the emission spectra of the scintillators and the response of the PMT except for GSO,CaF_2(Eu),LiI(Eu) and NE 905. The quantum efficiencies for the latter four were taken as those at the peak wavelengths. The quantum efficiency vs. wavelength characteristics of the PMT were those indicated in the manufacturer's catalog.[8] The absolute scintillation efficiencies were calculated from (Photons/MeV-γ)xE(eV)x10^{-6}. [9] An absolute scintillation efficiency of 0.13 was reported by W.J.Van Sciver,et al;Bull.Amer.Phys.Soc.,2(1957)142.

6.12 A Comparison of Gamma-Ray Detection Performance of a Silicon Photodiode Coupled with Various Kinds of Scintillators

E.Sakai and T.Nishihashi*

Although attention has become riveted recently to scintillation light detection with photodiodes(PDs) and avalanche photodiodes(APDs) instead of photomultipliers(PMTs), especially in the fields of computed tomography, high-energy physics as well as general radiation monitoring, no report was found which described the comparative study on the gamma-ray detection performance of PDs or APDs coupled with different kinds of scintillators. The present paper will describe the gamma-ray detection performance of a silicon PD(Hamamatsu S 1790-02(10x10 mm^2)) coupled with each of small scintillators(10x 10 mm^2 x6 mm, 7 mm, 10 mm or 20 mm) of CsI(Tl), CsI(Na), NaI(Tl), $CdWO_4$(CWO), CaF_2(Eu), Ce:Gd_2-SiO_5(GSO), $Bi_4Ge_3O_{12}$(BGO), CsI(pure), BaF_2, NE 905 and NaI(pure).

All the scintillators have one polished face with five ground sides on which white Teflon tape or $BaSO_4$ powder was lapped. The NaI(Tl) and NaI(pure) crystals were encapsulated in aluminum cases with glass windows. The PD has a structure of resin protecting coat(0.8 mm) - SiO_2(0.1 nm) - p^+(less than 1μm) - n(0.2 mm, 4 kohm) - n^+(20μm). The PD response extends from 300 nm to 1100 nm with the maximum quantum efficiency of 79 % at 800nm. The quantum efficiencies are 40 %(350 nm), 51 %(400 nm), 71 %(500 nm) and 75 %(600 nm) according to the manufacturer data. The capacitance and the leakage current of the PD were measured as 85 pF and 1.9 nA, respectively, at a bias of 30 V. Each of the scintillators was placed with silicone oil or compound on the resin window of the PD and the entire unit was lapped with a household aluminum foil. The PD output pulses were fed to a charge-sensitive preamplifier(Canberra 2003T) followed by a spectroscopy amplifier(Canberra 2013, 4μs shaping time) and a multichannel analyzer(Canberra 8100).

Figure 6.12.1 shows a comparison of the pulse height distributions obtained from the PD without any scintillators for ^{57}Co gamma-rays(a) and from the same PD coupled with each of the scintillators of various kinds for ^{88}Y gamma-rays (b) - (l). All the measurements were made with the same settings of the PD bias voltage and the amplifier gain. The CsI(Tl) gave the highest pulse heights and the best energy resolutions among the scintillators. The pulse heights degraded in the order of CsI(Na), NaI(Tl), CWO, GSO and BGO. The CaF_2(Eu) produced rather large output pulses, but did not produce photo-

---

*Summer student from Kobe University of Mercantile and Marine.

peaks due to the small attenuation coefficient and size. The CsI(pure), BaF_2 and NE 905 did produce output pulses, but did not show photopeaks because of their small pulse heights and the system noises. The NaI(pure) produced no observable output pulses. Figure 6.12.2 shows FWHM energy resolutions(%) as a function of gamma-ray energy obtained from the six scintillators exhibited the photopeaks.

Table 6.12.1 summarizes the results of the PD measurements, while in the left columns the pulse height ratios(PHRs) and the FWHMs of 1836 keV gamma-ray peaks, the FWHMs for 662 keV gamma-rays and the 10-90 % risetimes obtained from the PMT measurements are listed. In the right columns, the silicon-detector-equivalent energies(E(Si, keV)) of the 1836 keV gamma-ray peaks, E(Si,keV) devided by 1836 keV(E(Si)/E), the pulse height ratios(PHRs), the FWHMs of 1836 keV peaks, the 662 keV peak FWHMs, the numbers of electron-hole pairs per MeV of incident gamma-ray energy and the gamma-ray energies needed to produce one electron-hole pair obtained from the PD coupled with the scintillators are listed. The numbers of photons emitted from the scintillators for 1 MeV gamma-ray energy, the average gamma-ray energies needed to produce one photon in the scintillators and the absolute scintillation efficiencies were evaluated from the wave-length dependence of the PD quantum efficiency and the scintillation emission.

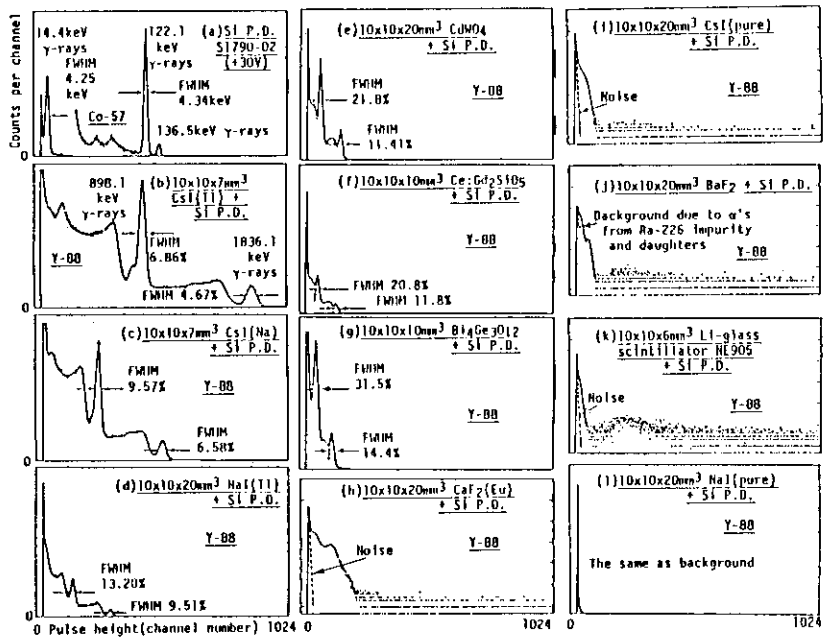

Fig.6.12.1 Comparison of pulse height distributions of gamma-rays obtained from a silicon photodiode(Hamamatsu S 1790-02) only (a) and from the same photodiode coupled to each of CsI(Tl), CsI(Na), NaI(Tl), CWO, GSO, BGO, CaF_2Eu), CsI(pure), BaF2, NE 905 and NaI(pure) scintillators (b)-(l). The main amplifier shaping time was 4 s.

Table 6.12.1 Pulse height ratios(PHR), FWHM energy resolutions and pulse risetimes obtained from various scintillators couled to photomultiplier Hamamatsu R1306(bialkali photocathode, borosilicate glass window) and silicon photodiode Hamamatsu S1790-02. For photodiode measurements, numbers of electron-hole pairs/MeV and gamma-ray energy per electron-hole pair are also listed.

Scintillator	With photomultiplier R1306(+825V)				With silicon photodiode S1790-02(+30V)						
	1836keV γ		662keV	10-90%	1836keV γ				662keV	e-h pairs	γ-energy
	PHR	FWHM	γ FWHM	risetime	E(Si,keV)	E(Si)/E_γ	PHR	FWHM	γ FWHM	/MeV	/e-h pair
10x10x20mm^3 NaI(Tl)	100	4.38%	7.07%	0.5μs	81.6	0.0444	100	9.51%	16.8%[1]	12300[1]	81.0eV
10x10x7mm^3 CsI(Na)	122	4.95%	7.37%	4μs	138.0	0.0752	169	6.58%	22.5%	20900	47.9eV
10x10x7mm^3 CsI(Tl)	78	3.74%	5.66%	4μs	237.5	0.129	291	4.67%	7.64%[2]	35900[2]	27.8eV
10x10x10mm^3 Ce:Gd_2SiO_5	28	4.84%	7.82%	<0.1μs	38.7	0.0211	47	11.8%	29.3%	5860	170.8eV
10x10x20mm^3 CaF_2(Eu)	*(27)	*	*	4μs	*	*	*	*	*	*	*
10x10x20mm^3 $CdWO_4$	23	4.92%	7.97%	20μs	43.5	0.0237	53	11.41%	31.8%	6580	152.0eV
10x10x10mm^3 $Bi_4Ge_3O_{12}$	17.5	5.81%	9.05%	0.8μs	33.5	0.0182	41	14.4%	40.8%[3,4]	5070[3,4]	197.4eV
10x10x20mm^3 CsI(pure)	16	**	17.31%	8μs	*	*	*	*	*	*	*
10x10x20mm^3 BaF_2	13	6.22%	11.37%	3μs	*	0.0065***	*	*	*	1800***	554.6eV***
10x10x6mm^3 NE905	* (6)	*	*	<0.1μs 4μs	*	*	*	*	*	*	*
10x10x20mm^3 NaI(pure)	4	**	16.67%	0.4μs	*	*	*	*	*	*	*

* No photopeak. PHR's in parentheses are for 122keV γ-rays. ** Too wide photopeak to obtain FWHM.
*** Calculated from 7.687MeV α-peak of Po-214 impurity which corresponded to 3.12MeV γ-rays.

[1] J.Markakis, et al, IEEE Trans. NS-32(1985) 559-562; 1 in.x 2in. NaI(Tl), 1in.x800μm HgI_2 PD, 7.8%, 23412 e-h pairs/MeV.
[2] H.Grassmann, et al, Nucl.Instrum.Meth.,A234(1985) 122-124; 10x10x24mm^3 CsI(Tl), Si PD S1790-01, 7.0%, 32000 ± 1000 e-h pairs/MeV.
[3] S.E.Derenzo, Nucl.Instrum.Meth.,219(1984)117-122; 3x3x3mm^3 BGO, Si PD S1722-01, 27%(20°C), 7.2%(-150°C), 4834e-h pairs /MeV(20°C), 11782 e-h pairs/MeV(-150°C).
[4] R.Lecomte, et al, IEEE Trans.NS-32(1985)482-486; 5x5x5mm^3 BGO, Si avalanche PD, 9.5%(23°C), 7.3%(-15°C), 8000 e-h pairs/MeV(23°C), 14955 e-h pairs/MeV(-15°C).

6.13 Development of Room Temperature Semiconductor Detectors

E.Sakai, T.Ishii*, S.Iwai*, Y.Suzui*, K.Taniguchi* and H.Nakatani*

We tested the performance of a-Si:H/c-Si heterojunction detectors at room temperature as well as liquid nitrogen temperature and also continued an effort to develop room temperature semiconductor nuclear radiation detectors made of GaSe and HgI_2.

Performance Test of a-Si:H/c-Si heterojunction detectors

Fuji Electric Research and Development, Ltd.(FERD) developed a new type of silicon nuclear radiation detectors[1] having a construction of evaporated aluminum / amorphous hydrogenated silicon(a-Si:H) film(1μm) / ultra-high purity p-type silicon crystal(c-Si)(300μm) / boron-doped p^+-layer(50 nm) / evaporated aluminum in order to fulfill the requirements of a simple and cheap method of fabrication as well as of lower processing temperature. The a-Si:H film was made by the dc plasma chemical vapour deposition at 200°C while boron-doping was made in a low voltage plasma followed by an argon gas plasma activation at 200°C. The size of the crystal was 3.6 mm x 3.6 mm x 300μm and the area of the top electrode was 1.6 mm^2. We measured the leakage vs. bias voltage characteristics of the four detectors and the pulse height distributions for ^{241}Am X- and γ-rays at room and liquid nitrogen temperatures. The results are summarized in Table 6.13.1.

Table 6.13.1 Summary of the results obtained from a-Si:H/c-Si heterojunction detectors

Temperature	Leakage current	FWHM for 59.5 keV	Preamplifier	Shaping time
Room	1-3 nA at 100 V	1.5-2.0 keV	CI 2001(ac-coupled)	1.5μs
Liquid N_2	2-10 pA at 100 V	1.0-1.5 keV	CI 2001(dc-coupled)	4μs

The leakage currents at room temperature are the same as those of the p-n junction type detectors[2], but those at liquid nitrogen temperature are a bit larger. The pulse heightdistributions for a ^{241}Am source displayed only a Cu $K_{\alpha 1}$ X-rays fluoresced from the copper base plate in addition to ^{241}Am X- and gamma-rays as shown in Fig.6.13.1; this is an improvement in comparison with the canned p-n junction type detectors which emitted fluorescent X-rays of Ni, Sn and Pb used in the can and solder material[2]. The hetero-junction detectors have another merit of thin front dead layers in comparison with 8μm thick n^+-layers in the p-n junction detectors. The size of the present detectors are too small for general X-ray spectroscopy use. We are hoping to test more larger area detectors.

* Summer visitors, Faculty of Engineering, Toyama University, 3190 Gofuku, Toyama, 930. Tel. 0764(41)1271 ext. 737

We are grateful to Mr. Noritada Sato, Fuji Electric Research & Development, Ltd. for supplying the detectors.

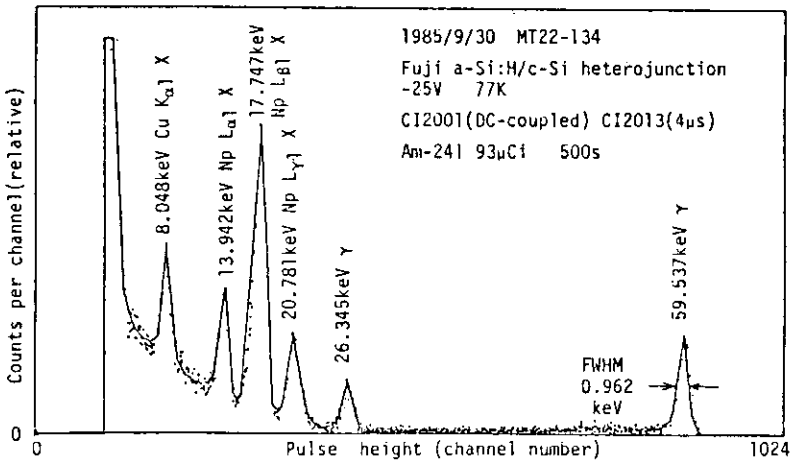

Fig.6.13.1 Pulse height distribution of ^{241}Am X- and gamma-rays obtained from a Fuji a-Si:H/c-Si heterojunction detector(3.6 mm x 3.6 mm x 300$_{\mu}$m, -25 V) at liquid nitrogen temperature.

Development of GaSe detectors

Manfredotti, et al.[3], reported GaSe detectors with evaporated gold electrodes on the crystals or platelets made by Bridgman method or by chemical transport. We started to investigate the possibility of this material as a room temperature detector three years ago. We tested the structures of Au-GaSe-Au, Au-GaSe-Al, In-GaSe-Au, Sn-GaSe-amal-gam(In + Hg)[4], Au-GaSe-Ag, Au-GaSe-Sn and Ag-GaSe-Sn[5] fabricated by evaporating metal films on Bridgman grown GaSe crystals and found that only the latter two structures exhibited better rectifying characteristics and larger output pulses for 5.5 MeV particles.

During the fiscal year 1985, we tested a guard-ring structure on Ag electrodes of Ag-GaSe-Sn detectors and found that the guard-ring did not decrease the leakage current and also that only for α-particles irradiating the Sn-electrode with positive voltages (reverse bias conditions) produced output pulses. The latter fact suggests that the material is of p-type. One of the detectors having the guard-rings on Sn electrodes(#J-57)displayed the largest pulse heights ever observed and the results are summarized in Table 6.13.2. The diameter of the center electrode is 1.5 mm and the inner and outer diameters of the guard-ring were 2.5 mm and 4 mm, respectively. The thickness of GaSe was 85μm. A pulse height of 47 % relative to that obtained from a surface-barrier Si detector was measured at 35 V and a resolution of 9.57 % at 20V. This detector was carefully prepared to have no apparent crease and flaw, which might be a reason of the large pulse heights. An example of

the pulse height distributions obtained for ^{241}Am α-particles(5.486 MeV) is shown in Fig.6.13.2.

Table 6.13.2 A summary of the performance of a Ag-GaSe-Sn detector(#J-57)

Bias voltage(V)	10	15	20	25	30	35
Leakage current(μm)	13	30				
Amplifier shaping time(μs)	0.5	0.5	0.5	0.5	0.5	0.5
Pulse height rel. to Si (%)	16.7	25.7	32.8	38.6	45.7	47.0
FWHM(%)	22.4	14.1	9.57	12.3	12.0	26.9

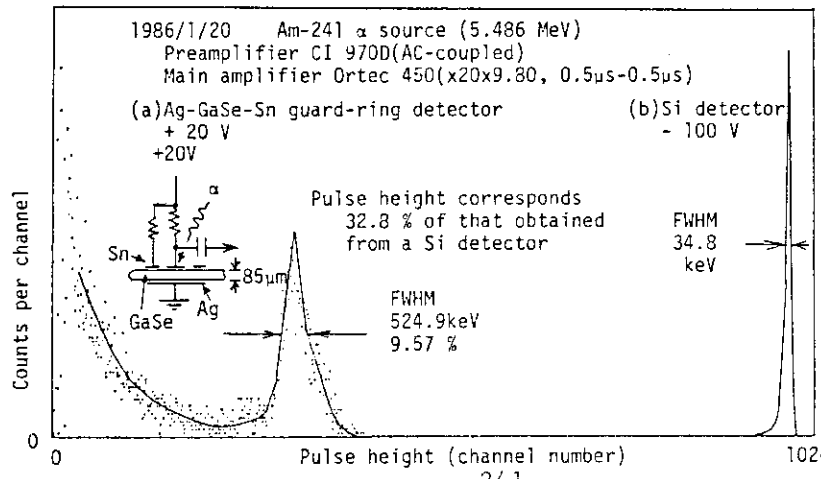

Fig.6.13.2 Pulse height distributions of ^{241}Am α-particles obtained from a Ag-GaSe-Sn detector and a standard surface-barrier Si detector.

Development of HgI_2 detectors

The polymer controlled growth(PCG) method[6] using polystyrene of 2 % and 3 % was tried to make twelve HgI_2 detectors. The best FWHM energy resolution for 59.5 keV gamma-rays was 7 keV, which was obtained from one of the detectors made of the 2 % polystyrene-added crystals, and is poorer than that obtained from the detectors made by the standard vapor growth method. Our experience showed that good detectors are hardly obtained by the PCG method in contrast with the reported[6] and that the appropriate growth conditions of the PCG method are difficult to find. We will try the PCG method using polyethyrene and also the standard vapor growth method using high-purity material.

References

1) Sato N., Seki Y.,Yabe M.: The 21st Annual Meeting on Radioisotopes in the Physical Sciences and Industry, 2p-I-12(1984).
2) Sakai E., et al.: JAERI-M 84-138(1984) pp.150 - 152.
3) Manfredotti C, et al.: Nucl. Instrum. Methods, 115(1974) pp.349 - 353.
4) Sakai E., et al.: JAERI-M 84-138(1984) pp.156 - 158.
5) Sakai E., et al.: JAERI-M 85-116(1985) pp.201 - 203.
6) Fail S.P., et al.: J. Crystal Growth, 50(1980) pp.752 - 756.

6.14 On the Calculation of Peak Area

H. Gotoh and K. Teranishi*

The Quittner method[1] is the most practical one used for peak area determination of a well-separated gamma-ray peak with background regions of different slopes.

The present authors modified this method more precisely estimating the error of the calculated peak area by using the law of error propagation, and made clear the condition of application of the modified method itself.

In the Quittner method, the peak region is set so as it contains the peak to be analyzed and, moreover, the lower and the upper background regions with odd channels are chosen in each side of the peak. These background regions are fitted with second degree polynomials by Savitzky-Golay's coefficients.[2] A baseline is determined with a third degree polynomial with two sets of values of the heights and slopes at two regions. The peakarea is given by $S = T - B$, where T is the total measured counts under the peak area and B is the sum of the counts under the base-line in the peak region. The error of the area is given by $\Delta S \cong (T + 1.3\,B)^{1/2}$ for the typical case.

The points of the modification in our method (Fig. 6.14.1) are as follows :

(1) The fitting curves of the lower and upper background region are straight lines instead of the second degree polynomials, and two sets of values of the heights and slopes (h_1, s_1), (h_4, s_4) are obtained in the background regions.

(2) A baseline is determined so as the extended straight lines in the lower and the upper regions are connected with a step at the channel p which gives the maximum counts in the peak region.

(3) The peak area is determined by the sum of the surplus counts over the baseline from the start channel p_2 to the end channel p_3 in the peak region.

With such modification, it has become easier to obtain the relation between the fluctuation of the counts and the variation of the peak area, and to calculate the peak area S_{net} and the variance of the area V_{net} using some simple matrix representation.

The calculating formula for the area and its error are

* Hitachi Ibaraki Technical College, Hitachi Ltd.

$$S_{net} = \begin{bmatrix} 1 & \cdots & 1 & -\Delta_{p_2} & -\frac{1}{2}\Delta_{p_2}^2 & \Delta_{p_3} & \frac{1}{2}\Delta_{p_3}^2 \end{bmatrix} \begin{pmatrix} C_{p_2} \\ \vdots \\ C_{p_3} \\ h_1 \\ s_1 \\ h_4 \\ s_4 \end{pmatrix} \quad (1)$$

and

$$V_{net} = \sum_{i=p_2}^{p_3} \sigma_i^2 + \begin{bmatrix} -\Delta_{p_2} & -\frac{1}{2}\Delta_{p_2}^2 \end{bmatrix} G_1^{-1} \begin{pmatrix} -\Delta_{p_2} \\ -\frac{1}{2}\Delta_{p_2}^2 \end{pmatrix} + \begin{bmatrix} \Delta_{p_3} & \frac{1}{2}\Delta_{p_3}^2 \end{bmatrix} G_4^{-1} \begin{pmatrix} \Delta_{p_3} \\ \frac{1}{2}\Delta_{p_3}^2 \end{pmatrix}, \quad (2)$$

where $\Delta_{p_2} = p - p_2 + 0.5$, $\Delta_{p_3} = p - p_3 - 0.5$,

$C_{p_2}, \cdots, C_{p_3}$ = counts from channel p_2 to channel p_3,

σ_i^2 = variance of the counts of channel i,

$$G_1^{-1} = \frac{1}{D_1} \begin{pmatrix} \sum_{i=k}^{l} \frac{\Delta_{i2}^2}{\sigma_i^2} & -\sum_{i=k}^{l} \frac{\Delta_{i2}}{\sigma_i^2} \\ -\sum_{i=k}^{l} \frac{\Delta_{i2}}{\sigma_i^2} & -\sum_{i=k}^{l} \frac{1}{\sigma_i^2} \end{pmatrix}, \quad D_1 = \begin{vmatrix} \sum_{i=k}^{l} \frac{1}{\sigma_i^2} & \sum_{i=k}^{l} \frac{\Delta_{i2}}{\sigma_i^2} \\ \sum_{i=k}^{l} \frac{\Delta_{i2}}{\sigma_i^2} & \sum_{i=k}^{l} \frac{\Delta_{i2}^2}{\sigma_i^2} \end{vmatrix},$$

$$G_4^{-1} = \frac{1}{D_4} \begin{pmatrix} \sum_{i=m}^{n} \frac{\Delta_{i3}^2}{\sigma_i^2} & -\sum_{i=m}^{n} \frac{\Delta_{i3}}{\sigma_i^2} \\ -\sum_{i=m}^{n} \frac{\Delta_{i3}}{\sigma_i^2} & \sum_{i=m}^{n} \frac{1}{\sigma_i^2} \end{pmatrix}, \quad D_4 = \begin{vmatrix} \sum_{i=m}^{n} \frac{1}{\sigma_i^2} & \sum_{i=m}^{n} \frac{\Delta_{i3}}{\sigma_i^2} \\ \sum_{i=m}^{n} \frac{\Delta_{i3}}{\sigma_i^2} & \sum_{i=m}^{n} \frac{\Delta_{i3}^2}{\sigma_i^2} \end{vmatrix},$$

$\Delta_{i2} = i - p_2 + 0.5$, and $\Delta_{i3} = i - p_3 - 0.5$.

In Fig.6.14.1, the estimated value for the 122keV peak of ^{152}Eu γ-rays is calculated by using eq. (1) and (2) mentioned above, and the peak area with error 1,570,321±5,448 (0.35 %) is given for this peak.

References

1) P. Quittner, "Precise Peak Area Determination for Ge (Li) Detectors", Anal. Chem., 41 (1969) pp.1504-1506.

2) A. Savitzky and M. J. E. Golay, "Smoothing and Differentiation Data by Simplified Least Squares Procedures", ibid. 36 (1964) pp.1627-1639.

122 keV of Eu-152

K	L	P1	P2	M	N	i'cept	slope	crit.pt.	min.fun.	
446	456	470	513	516	526	8435	14.90	16.92	12.19	(lower background)
						4161	-0.38	16.92	14.45	(upper background)

			area	uncert	relativ
step baseline	1826109	255788	1570321	5448	0.0035
Quittner				1469	0.0009

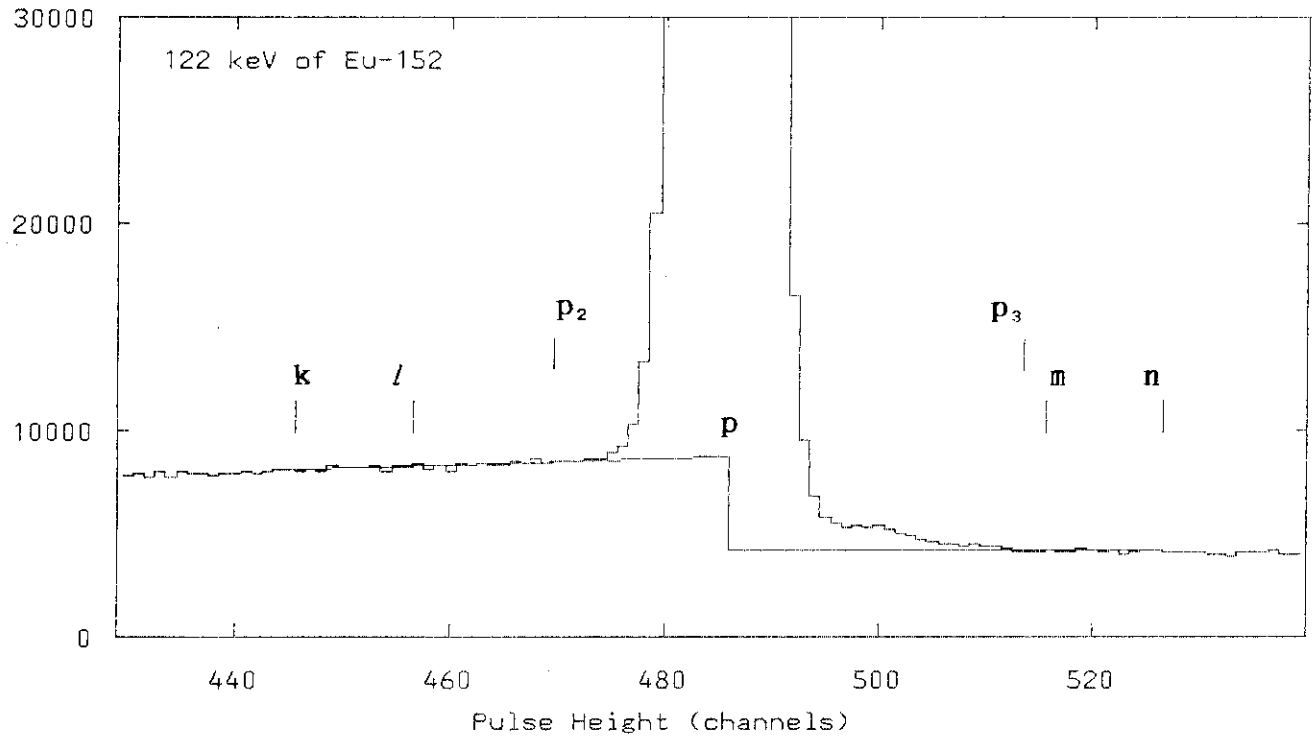

Fig.6.14.1 Principle of the peak area determination using the 122 keV peak of Eu-152, k=start channel number of lower background region, l=stop channel number of lower background region, p_2 = start channel number of peak region, p=channel number which gives maximum counts in the peak region, p_3 =stop channel number of peak region, m= start channel number of upper background region, n= stop channel number of upper background region

7. Reactor Control, Diagnosis and Robotics

As for the reactor control, studies have been made on the Very High Temperature Gas-ccoled Reactor (VHTR) plant with respect to the design of PID-type control systems and optimal setting of trip levels in the protection system. The study of control characteristis using a plant control system consisting of four systems for control of the reactor inlet/outlet temperatures and the steam drum has shown that the parameters of the control systems should be optimized with regard to the flowrate disturbances. With a view to reduce false scrams, a method for determining trip levels has been studied under the assumptions of normal probability distributions for process variables. This method will help to optimize trip settings in a logical way.

As for the diagnostics study, acoustic signals of sodium boiling have been analyzed using noise analysis methods. In order to improve signal-to-noise ratio in boiling detection, a relatively simple nonlinear signal processing method was applied. The result showed s/n ratios improved by several times. Continuous study has been being made on the application of autoregressive model fitting methods for reactor noise analysis. Two algorithms, Marple's and Kitagawa-Akaike's, have been applied to analyze reactor noise data of short time length. The results of this study suggested the applicability of these algorithms for analyzing a certain type of non-stationary reactor noise data.

Much progress has been made in the study of robotics. In the theoretical study on manipulator kinematics, a new algorithm for obtaining rigorous inverse kinematic solutions has been developed for a type of six-joint manipulators. A computer code has also been developed for numerical solution. This algorithm gives very accurate solutions compared with conventional approximation methods such as the inverse Jacobian method. As for the system deveelopment, light-duty (10kg load capacity) and heavy-duty(100kg load capacity) robotic manipulator systems have been developed and tested. Both manipulators can be operated in either a master-slave, a teach-and-playback and a programmed control mode. They can be used in the water as well as in the air.

(Y. Shinohara)

7.1 Control System Design of the VHTR Plant

J. Shimazaki, K. Kudo* and Y. Shinohara

The Very High Temperature Gas-Cooled Reactor (VHTR) is one of advanced future reactors. There are some dynamic charateristics peculiar to VHTR. As the greater part of the reactor core is composed of graphite having a large heat capacity, the thermal response of the reactor is accompanied with a very long time constant. The reactor is connected to a heat sink through two cooling loops which are controlled by the regulation of the flow rates of these loops.

The analysis of the characteristics and the synthesis of PID controllers has been carried out to obtain fundamental data for VHTR design. The controller is based on the concept of turbine slaved to reactor control. The plant control system consists of four control systems for the reacor outlet/inlet temperatures and the steam drum pressure and level. The reactor outlet gas temperature control system forms a cascade control system which regulate the outlet gas temperature by changing the reactor power at the outer loop and the reactor power by control rods. The reactor inlet gas temperature control system is attached to complement the outlet temperature control and keeps the reactor inlet temperature at a set point by manipulating the IHX secondary flow rate. The steam drum control system contains the drum level and pressure control systems. The drum pressure is kept at a set point by means of the control valve while the drum water level is controlled by the conventional type controller which uses the signals of the drum water level, the feed water and the steam flow rate.

The PID control parameters of each control system are shown in Table 7.1.1. The characteristics of the plant with the controllers are summarized as follows.

1. Most of controlled variables settle within a short time for reactivity disturbances. However, the reactor power does not settle quickly for the disturbances caused by a coolant flow rate change.
2. Proper PID parameters of the outlet and inlet temperature control systems vary depending on different type of disturbances. The optimal PID parameters must be chosen taking into consideration the reactor

* Faculty of Engineering, Kyushu University.

responses to the primary flow rate.

3. The control systems for the steam drum pressure and level have shown good behaviors for various disturbances.

Reference

1) Kudo K., et al.: "Dynamics and Control System Design of VHTR," Memoirs of the Faculity of Engineering Kyushu University, Vol.46, No.1, p.105 (1986).

Table 7.1.1 PID control parameters

Control system	PID Parameters			
	K		T_I(1/s)	T_D(s)
Reactor outlet gas temperature control	3.0×10^{-5}	Δk/k/°C	500	300
Reactor power control	7.5×10^{-5}	Δk/k/MW	100	0
Reactor inlet gas temperature control	-5.0×10^{-4}	Kg/s/°C	2000	0
Steam drum pressure control	-0.1	$cm^2/Kg/cm^2$	500	0
Steam drum level control	0.1	Kg/s/Kg	500	0

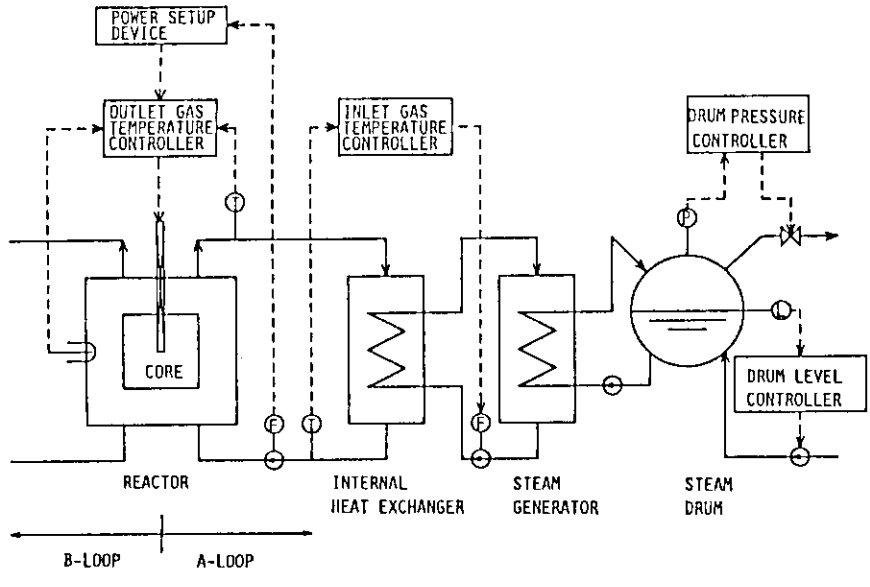

Fig.7.1.1 Schematic diagram of VHTR plant control system

7.2 Spurious Scram Probability in the VHTR Reactor Protection System

J. Shimazaki and K. Suzuki+

In the design of a reactor protection system of a reactor with tight margines between normal operating values and safety limiting ones, it would be necessary to evaluate the spurious scram probability which depends on trip setting points. A probabilistic method is proposed that will permit in the design stage to estimate quantitatively the likelihood with which the trip setting points close to operating values would cause the reactor to sacram falsely due to fluctuations of process variables during normal operation.

One of the explicit formulae for the spurious trip probability is obtained under the assumption of normal probability distributions for a process variable X, a measured signal of instrument channel X_I, and a trip setting point S (its standard variations σ_0, σ_i and σ_s, respectively).

$$P_{st} = \int_{-\infty}^{-(s_0-x_0)/\sigma_T} \frac{1}{\sqrt{2\pi}} \exp(-u^2/2)\, du \qquad (1)$$

where P_{st}: spurious trip probability, x_0 : average value of process variable, s_0 : trip setting point, and $\sigma_T^2 = \sigma_0^2+\sigma_i^2+\sigma_s^2$.
The probability P_{ss} of false reactor scram due to a false trip signal can be given by

$$P_{ss} = \sum_{k=m}^{n} \binom{n}{k} P_{st}^{\,k} (1- P_{st})^{n-k} \qquad (2)$$

for a m-out-of-n coincident scram logic circuit.

In the VHTR, a special aim is to produce helium gas heated up to 950 °C at the reactor outlet for multiple purpose use. One problem faced in the reactor protection system design is that the relatively tight margin between the normal operating values and the safety limiting ones cannot afford the use of conventional methods for the trip setting shown in Fig.7.2.1.

A sample calculation is performed on the probability of a spurious scram event caused by the reactor inlet helium gas temperature signal. In the design of the VHTR, the standard deviations σ_0, σ_i and σ_s are estimated to be 2.67 °C, 1.67 °C and o.67 °C, respectively. Then σ_T = 3.22

+ Department of Power Reactor Project, JAERI.

°C. The probability P_{st} and P_{ss} of spurious trip and scram by the reactor inlet temperature signal can be calculated from equations (1) and (2). The results of the calculations are summarized in Table 7.2.1. From this Table, it can be known that the probability of the spurious scram event by the reactor inlet temperature is kept less than 6×10^{-6} by the trip setting point being set by 10 °C higher than the normal operatiog value of 395 °C.

Table 7.2.1 Spurious trip probability P_{st} and spurious scram probability P_{ss} by the reactor inlet gas temperature signal to VHTR reactor protection system

(s_0-x_0) °C	2	4	6	8	10	15
P_{st}	0.268	0.108	3.10×10^{-2}	6.40×10^{-3}	1.00×10^{-3}	≃ 0
P_{ss}	0.292	6.03×10^{-2}	5.53×10^{-3}	2.44×10^{-4}	5.99×10^{-6}	≃ 0

x_0 : Reactor inlet helium gas temperature (395°C)
s_0 : Trip setting point
P_{st} : Spurious trip probability
P_{ss} : Spurious scram probability

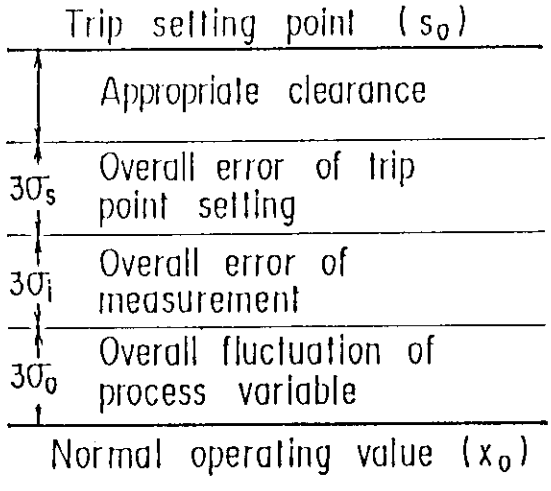

σ : means standard deviation

Fig.7.2.1 Conventional method of trip point setting

7.3 Study on Sodium Boiling Detection Method Based on Noise Analysis

Y. Shinohara and K. Watanabe

A study has been being conducted within the framework of the Coordinated Research Program organized by the International Atomic Energy Agency on Signal Processing Techniques for Sodium Boiling Noise Detection which aims at making a comparative assessment of existing processing techniques used for the noise signal analysis for detection of sodium boiling in a LMFBR core. According to the proposal made for the Program, the acoustic noise signals obtained from an out-of pile experimental sodium loop at KfK, FRG were sent from the Agency .

Based on the results of the preliminary analysis of the auto-power spectral density functions as well as the auto-correlation functions for all noise signal records, the following method of time-domain analysis was chosen.

In the signal processing performed, the raw noise signal was first filtered by a high-pass filter having a cut-off frequency fc and then squared. The squared signal was again filtered by another high-pass filter having the same cut-off frequency as the former and squared. The resultant signal was integrated over a time interval dT to obtain what we call here the "transformed" signal.

The sample mean value M and sample mean deviation D of the transformed signal are calculated over a time interval T to determine a threshold value $L = M + F \times D$, where F is what we call the discrimination factor.

The time of boiling onset Tl was determined on a simulated on-line real-time basis as the time at which the transformed signal exceeded the threshold level L which was calculated for the transformed signal under the non-boiling condition during a preceding period of time T.

In a similar manner as in the case of determining Tl, the time of increasing the boiling intensity T2 was determined as the time at which the transformed signal exceeded the threshhold level L which was calculated for that signal during a preceding period of time T. In this case, however, in order not to detect the time when boiling intensity was increasing at the initial stage of boiling, the calculation was

started 30 seconds after the detection of the boiling onset time Tl.

The signal to noise discrimination was made using a discrimination factor F. The time period T is chosen sufficiently larger than the time interval dT for averaging the squared signal. The choice of the value for F should be made as a compromise between the detection sensitivity and the risk of misjudgement.

From the results obtained it was concluded that the time of onset of boiling as well as the time of increasing boiling intensity could be detected for all test cases using a relatively simple method of signal processing.

Reference

1) Shinohara Y. and Watanabe K.: "Interim Report on the Results of Sodium Boiling Noise Detection Benchmark Test", Paper presented at the IAEA Research Coordination Meeting, Vienna, 1985.

7.4 Study of Autoregressive Model Fitting Algorithms and Their Application to Borssele Reactor Noise Analysis

K. Hayashi and E.Turkcan+

Numerical methods for analyzing reactor noise data of a relatively short length have been being studied in view of applying them to reactor anomaly diagnosis. Two algorithms for univariate autoregressive (AR) model fitting, i.e. Marple's and Kitagawa-Akaike's algorithms which use the least squares method for data fitting, have been evaluated in comparison with other methods.

The results of fitting tests using computer simulated data show that these algorithms are superior to the conventional Yule-Walker's and Burg's algorithms in that they are less numerically ill-conditioned and that they give more stable spectral peak frequencies. However, Kitagawa-Akaike's algorithm requires a fairly large calculation time compared with the convensional or Marple's one.

Both methods have been applied to real reactor noise data obtained at Borssele power plant in the Netherlands. The noise signals used are the secondary loop steam flow rate and the steam temperature measured during reactor shutdown operation. In order to analyze these non-stationary data, 46 sets of data are made as follows. First, the original data recordings for 150 minutes are divided into subsets of 200 seconds each. Then, the first 16 seconds data (1024 sampled points) of each subset which can be considered as locally stationary are used for this analysis. From the AR spectral analysis, both time-independent and time dependent peaks were found, which means that these methods are capable of detecting time dependent feauturs of noise data.

The results of analysis suggest that these algorithms can be applied to reactor diagnostic problems in which nonstationary random processes are involved.

Reference

1) Hayashi K.:"Evaluation of Autoregressive Model Fitting Algorithms Based on Least Squares Method," JAERI-M 84-127 (1984).

2) Hayashi K. and Turkcan E. : to be published.

+ Netherlands Energy Research Foundation ECN, The Netherlands.

7.5 A Study of the Inverse Problem of a Manipulator Arm

S.Sasaki

An understanding of the kinematics of a robot manipulator is fundamental for designing a trajectory planning and control system. Usually, this kinematic problem falls into two categories. Namely, the direct kinematics is easily obtained by calculating a T6 matrix at the end point of the manipulator corresponding to the given joint angles, while the solution procedures of the inverse problem are generally cumbersome and explicit analytical solutions can be derived only for some special arm configurations.

Although a linearization technique is practical for solution of this problem, a new approach has been proposed from a different standpoint :
Its underlying concept is to transform the kinematic relationships into a non-linear polynomial of a joint angle variable at the end point of the manipulator. By close examination of the features of T6 matrix, which consists of twelve scalar equations, (nine dealing with orientations and three with position), these equations were found to be represented as a trigonometric functions of only $\sin\theta_6$ and $\cos\theta_6$.

Defining $\sin\theta_6$ and $\cos\theta_6$ in terms of the tangent of half-angle(and $\tan(\theta_6/2)= t$), we could unify the kinematic description of T6 matrix as a polynomial with a single variable t. In other words, the problem of finding the articular angle of a manipulator was reduced to an algebraic equation with reference to $\tan(\theta_6/2)$. Once the desired solutions t are found from this equation, individual joint angles for a six degree-of-freedom manipulator can be derived straightforwardly. In order to compute real roots of the polynomial as exactly as possible , the Bairstow's method is recommended.

The advantage of the present algorithm is to find out all kinds of arm solutions at the same time (under the mechanical constraints on the range of joint angles), with the consequence that those solutions will contribute to evaluate the mechanical performance or determine the optimum joint angle design as well as to study the topological situations (and redundancies) of a mechanical link moving in the work space.

7.6 Development of Computer Code for Solving the Inverse Kinematics of a Six-Link Manipulator Arm

S. Sasaki

ARM1 is a computer program, written in FORTRAN 77, which was primarily developed to make a transparent geometrical angular description of each joint while the hand of a manipulator moves towards the destination position along some specified trajectory in the cartesian space. So far, joint solutions for manipulator kinematics have been derived using a linearization and iteration technique from a practical viewpoint. Due to shortcomings inherent in this method, however, a rigorous approach to obtain the joint solutions was proposed and programmed.

The program computes the individual joint angles for each position advancement on the trajectory prescribed and also provides graphics information such as plots for polynomial behaviors and individual joint solution curves. The polynomial which plays a central role to solve the inverse problem in the present model is divided into some groups of quadratic equations based on the Bairstow's algorithm and solved with sufficient precision.

From the nature of periodicity of the trigonometric function, every possibility for solutions is taken into consideration within the range of its mechanical constraints imposed for each joint angle.
In addition, these joint solutions are "fed" into the direct kinematic routine in order to obtain the arm matrix T6 and checked to assure the precision or reliability prior to the final solutions.

After completion of the code, the test runs were performed to evaluate its capability. All kinds of feasible solutions latent within kinematic relaionships could be successfully extracted as explicit ones. Concerning the accuracy of solutions, they were of the order of less than 10^{-8} on the average.

References

1) Sasaki S. : "Computer Code ARM1 for Solving the Inverse Kinematics of a Six-link Manipulator Arm," JAERI-M 86-059(1986).
2) Sasaki S. : "A Method of Solving the Inverse Kinematics of a Manipulator Arm," JAERI-M 86-018(1986).

7.7 Development of Light-Duty and Heavy-Duty Underwater Robotic Manipulator Systems

H. Usui, Y. Fujii, A. Kumagai, H. Nakagami, S. Sasaki, J. Shimazaki and Y. Shinohara

Within the framework of the Reactor Decommissioning Technology Development Project, two experimental remote handling systems equipped with a light-duty and two heavy-duty robotic manipulators, respectively, have been constructed and are currently being tested. The manipulators are electrical ones having seven degrees of freedom and can be operated in either a master-slave, a teach-and-playback or a programmed control mode with the assistance of control computers.

The choice of electrical rather than hydraulic manipulator was made from the view points such as the ease of maintenance and broader applicability in various nuclear facilities where hydraulic systems are less favorable.

The light-duty manipulator has a load capacity of 10kg. The slave arm of the manipulator is designed as an amphibious so as that it may be used in the water as well as in the air during the reactor dismantling work. For transport of the slave arm, the present system uses a telescopic boom of triangular cross-section, which is moved in the horizontal plane using a bridge/trolley system. In this system are used several TV cameras of which two are monochromatic underwater cameras and one is three-dimensional color camera. No provision is made for automatic tracking capability of TV camera in this system.

The prototype heavy-duty manipulator system are equipped with two manipulator arms: the main arm having a load capacity of 100kg and the sub-arm of 25kg. Both of them are also amphibious electrical manipulators and have the same kinematic structure with seven degrees of freedom. To transport the manipulators in vertical direction and to fix their base at a position in a reactor vessel, a system consisting of a tripedal support mechanism is used which is suspended by three chaines from a trolley on the bridge instead of using a telescopic tube.

In the man-machine interface system are used two colour graphic display terminals: the one with a touch screen for the control of the

whole system and the other for the display of the system status including graphical presentation of the manipulator posture and alarm indication.

In order to save the time required to operate a three-dimensional underwater TV camera which is mounted on the base of the manipulators, a capability is provided of automatic tracking of the manipulator ends. Other two-dimensional TV cameras can be operated by voice command.

References

1) Usui H. et al.: "Development of Remote Handling Technology for Reactor Dismantling - Light-duty Robotic System for Underwater Test", Fall Meeting of the Atomic Energy Society of Japan, 1985.
2) Fujii Y. et al.: "Development of Remote Handling Technology for Reactor Dismantling - Heavy-duty Robotic System for Underwater Test", Annual Meeting of the Atomic Energy Society of Japan, 1986.
3) Shinohara Y.: "R&D of Robotic Technology at JAERI", Environmental Extremes, CESTA, 1986.

8. Activities of the Research Committee on Reactor Physics

S. Matsuura, Y. Ishiguro, T. Nakamura and T. Suzuki

During this fiscal year, the Research Committee on Reactor Physics held the meetings 2 times, and the Subcommittees on Reactor System, Fusion Reactor and Shielding each held the meetings 2 times. In addition, the Seminar on Software Development in Nuclear Energy Research was held in September 1985, in cooperation with the Nuclear Code Committee.[1]

The Research Committee held the 48th meeting in October 1985 to discuss the following one review paper and 53 technical papers to be presented at the 28th meeting of the NEA Committee on Reactor Physics (NEACRP):

L-285: Reactor Physics Activities in Japan (October 1984 - September 1985) (S. Matsuura and K. Shirakata)

A-705: Three-Dimensional Multi-Group Neutron Transport Calculations by Double Finite Element Method (T. Fujimura et al.)

A-706: BARMUDA-3DN: A Three-Dimensional Neutron Transport Code in (X,Y,Z) Geometry (T. Suzuki et al.)

A-707: Development of a Radiation Transport Code in the Three-Dimensional (X,Y,Z) Geometry for Shielding Analyses. (T. Ida et al.)

A-708: Three-Dimensional Transport Calculation Method for Eigenvalue Problems Using Diffusion Synthetic Acceleration. (M. Bando et al.)

A-709: Discrete Ordinates Transport Code in Hexagonal-Z Geometry (Y. Saito et al.)

A-710: Three-Dimensional Transport Correction in Fast Reactor Core Analysis (T. Takeda et al.)

A-719: Experimental Study of Large Scale Axially Heterogeneous LMFBR Core at FCA Assembly XII-1 (S. Iijima et al.)

A-727: A Generalized Dancoff Factor for Application to HCPWR in Complex Lattice Arrangement (Y. Ishiguro et al.)

A-728: The Study for The Control Rod Worth in High Conversion PWR (E. Saji et al.)

A-729: Experimental Program and Results of Pre-analysis for a High Conversion Light Water Reactor (HCLWR) at FCA
(T. Osugi and H. Yoshida)

A-735: Neutronics Study on Blanket System of High Tritium Breeding Ratio (S. Mori and Y. Seki)

A-736: A Cross-Section Sensitivity and Uncertainty Analysis on Fusion Reactor Blankets with SAD/SED Effect
(K. Furuta et al.)

A-737: Integral Experiments in a 120-CM Lithium Sphere
(K. Sugiyama et al.)

A-738: Clean Benchmark Experiments and Analyses at FNS
(H. Maekawa)

A-744: Characteristics of Plutonium Utilization in ATR
(T. Wakabayashi et al.)

A-746: Burnup Characteristics of JOYO MK-II Core
(T. Ikegami and N. Mizoo)

The 49th meeting of the Committee was held in December 1985 to review the 28th NEACRP meeting where 53 technical papers were presented on 11 topics including 5 new topics: 3-D deterministic transport methods (S_N, FE, etc. status and future role), spatial neutron kinetics application to reactivity measurement, resolution of local geometric heterogeneous effects in FBRs, application of neutron noise in reactor system (to reactivity, kinetics, etc.), special applications of gamma/neutron source modelling (medical therapy, accelerators, beam tubes, etc.), Monte Carlo whole core models, physics problems of tight pitch lattices, physics modelling of neutron source (research reactors, spallation sources, etc.), physics modelling of fusion blankets, calculation of structural reactivity feedback effects such as bowing during the normal operation of reactors, advanced fuel cycles for Th and fast reactors.

The Subcommittee on Reactor System held the 17th meeting in July 1985 to discuss the present status on experimental physics using critical assemblies in Japan. In the 18th meeting held in September 1985, most the discussions were concentrated on the topics related to the 28th NEACRP meeting.

The Subcommittee on Fusion Reactor held the 18th and the 19th meeting in July and December 1985, respectively. Review was made in

the 18th meeting on the topics in the International Conference on Nuclear Data at Santa Fe', and the JAERI/U.S.DOE workshop on fusion blanket neutronics. Discussions were made in the 19th meeting on the topics reported in the 28th NEACRP meeting, the present status of NE213 neutron spectrometer and recent results obtained at FNS experiments. Brief introduction was also made on TPSS at ANL and LBM experiment program at the Lotus facility. In addition, a specialist meeting on nuclear data for fusion neutronics was held in July 1985 by the members from the Working Group on Nuclear Data for Fusion in JNDC and the Subcommittee on Fusion Reactor.

The Subcommittee on Shielding held the 20th meeting in August 1985 to discuss the benchmark problem on a spent fuel transport cask submitted to the NEACRP-CSNI Cask Benchmark Working Group. In the 21st meeting held in February 1986, discussions were made on the NEACRP activities especially on using the JEF-1 shielding group constants library (VITAMIN-J) for the radiation shielding benchmark problems.

Reference

Nuclear Code Committee and Committee on Reactor Physics: "Proceedings of the Seminar on Software Development in Nuclear Energy Research," JAERI-M 86-009 (1986) (in Japanese).

Publication List

2. Theoretical Method and Code Development

(1) Nakahara Y. and Nishida T.: "Spallation Reaction and Nucleon Transport in Macroscopic Medium," Genshikaku Kenkyu (Study on the Nuclear Physics), 29, 121 (1985) (in Japanese).

(2) Nakahara Y. and Nishida T.: "Monte Carlo Simulation of Nuclear Reactions at Intermediate Energies and its Applications in Engineering," Proc. Topical Meeting on Fission, Osaka Univ., RCNP-P-80 (1985).

(3) Ishiguro Y. and Kaneko K.: "Generalized Dancoff Factor in Complicated Lattice Arrangement," J. Nucl. Sci. Technol., 22, 835 (1985), (Short Note).

(4) Ishiguro Y., Akie H., Kaneko K. and Sasaki M.: "Physics Problems on Analysis of High Conversion Light Water Reactor," JAERI-M 86-039 (1986).

(5) Mori T. et al.: "Measurement and Analysis of Neutron Spectra in Lithium Fluoride and Polytetrafluoroethylene Piles," J. Nucl. Sci. Technol., 22, 708 (1985).

(6) Hayashi S.A., Mori T., Nakagawa M. et al.: "Measurement and Analysis of the Neutron Spectrum in a Spherical Pile of Cu," Ann. Nucl. Energy, 13, 131 (1986).

(7) Nakagawa M., Mori T., Kosako K., Youssef Z.M., Jung J. and Sawan E.M.: "U.S./JAERI Fusion Neutronics Calculational Benchmarks for Nuclear Data and Codes Intercomparison," JAERI-M 85-201 (1985).

(8) Abdou M., Nakagawa M. et al.: "Technical Issues and Requirements of Experiments and Facilities for Fusion Nuclear Technology," FINESSE Phase 1 Report, Vol. 1, II, PPG-909 also UCLA-ENG-85-39 (1985).

3. Reactor Physics Experiment and Analysis

(1) Iijima S., Okajima S., Sanda T., Ōbu M., Osugi T., Koakutsu T., Mukaiyama T., Ohno A., Hayase T., Satoh K., Sato W., Kawase Y., Gunji Y. and Nakano M.: "Experimental Study of Large Scale Axially Heterogeneous LMFBR Core at FCA(III) - Experiment of FCA Assembly XII-1 and Their Analysis -," JAERI-M 85-045 (1985) (in Japanese).

(2) Iijima S., Okajima S., Hayase T., Ōbu M., Osugi T., Koakutsu T., Sakurai T., Ohno A., Satoh K., Sato W. and Tsuji N.: "Experimental Study of Large Scale Axially Heterogeneous LMFBR Core at FCA(VI) - Radial Nuclear Characteristics Measerement on FCA Assembly XIII-1 and Their Anlysis -," JAERI-M 86-065 (1986) (in Japanese).

(3) Okajima S. and Mukaiyama T.: "Doppler Effect Measurement in FCA Assembly XII-1," JAERI-M 85-28 (1986) (in Japanese).

(4) Okajima S., Iijima S., Hayase T., Ōbu M., Koakutsu T. and Tsuji N.: "Experimental Study of Large Scale Axially Heterogeneous LMFBR Core at FCA(V) (Experiments of FCA Assembly XII-2 and Thier Anlysis)," JAERI-M 86-016 (1986) (in Japanese).

(5) Satoh K., Osugi T. and Ohno A.: "Measurements of Relative Power Distributions in the Axially Simulated Heterogeneous FBR Cores by γ-Scanning Method," JAERI-M 85-207 (1985) (in Japanese).

4. Fusion Neutronics

(1) Maekawa H., Nakagawa M., Ikeda Y., Oyama Y., Yamaguchi S., Tsuda K., Fukumoto T., Hasegawa A., Mori T., Seki Y. and Nakamura T.: "Integral Test of JENDL-3pr1 Through Benchmark Experiments on Li_2O Slab Assemblies," Proc. Int. Conf. on Nuclear Data for Basic and Applied Science, San ta Fe, May 13-17 (1985).

(2) Ikeda Y., Miyade H., Kawada K., Yamamoto H., Oishi K., Maekawa H. and Nakamura Y.: "Measurement of High Threshold Activation Cross Section for 13.5 to 15.0 MeV Neutrons," ibid. (1985).

(3) Shin K., Oyama Y. and Abdou M. A.: "Analysis of a 14-MeV Neutron Scattering Experiment with Li_2O Assemblies," ibid. (1985).

(4) Kawade K., Yamamoto H., Atsumi H., Miyade H., Katoh T., Ikeda Y. and Nakamura T.: "Activation Cross Section of $^{92}Mo(n,n'\alpha)^{89}Zr$ at 14 MeV," J. Nucl. Sci. Technol., 22, 851 (1985).

(5) Abdou M. A., Oyama Y., et al.: "A Study of the Issues and Experiments for Fusion Nuclear Technology," Fusion Technol., 8, 2595 (1985).

(6) Yamaguchi S., Oyama Y. and Maekawa H.: "A Method for Measuring Tritium Production Rate by Lithium-Glass Scintillators," JAERI-M 85-086 (1985) (in Japanese).

(7) Oyama Y. and Maekawa H.: "Spectral Measurement of Angular Neutron Flux on the Restricted Surface of SLAB Assemblies by the Time-of-Flight Method," Nucl. Instrum. Meth., A245, 173 (1986).

(8) Ikeda Y.: "Dosimetry of Fusion Reactor," RADIOISOTOPES, 34 (7), 49 (1985) (in Japanese).

(9) Maekawa H.: "Clean Benchmark Experiments and Analyses at FNS," Proc. Specialist Meeting on Nuclear Data for Fusion Neutronics, JAERI-M 86-029, 171 (1986).

(10) Nakamura T.: "Fusion Blanket Engineering Benchmark Experiments," ibid., 183 (1986).

5. Shielding

(1) Hasegawa A.: "On the Processing of the Nuclear Data File and the Problems of the JENDL," Proc. of Specialist Meeting on Nuclear Data for Fusion Neutronics, JAERI-M 86-029 p.68-98 (1986).

(2) Hasegawa A.: "Development of EDFSRS: Evaluated Data Files Storage and Retrieval System," JAERI-1295 (1985).

(3) Takeda T., Aoyama T., Hasegawa A. and Kikuchi Y.: "Sensitivity of Sodium Void Worth in Fast Reactors to Cross Sections," J. Nucl. Sci. Technol., 23, 181 (1986).

(4) Aoyama T., Suzuki T., Takeda T., Hasegawa A. and Kikuchi Y.: "Sensitivity Coefficients of Reactor Parameters in Fast Critical Assemblies and Uncertainty Analysis," JAERI-M 86-004 (1986) (in Japanese).

(5) Suzuki T., Hasegawa A. and Ise T.: "BERMUDA-3DN: A Three-Dimensional Neutron Transport Code (x,y,z) Geometry," 28th NEACRP Meet., Madrid, Nov. 4-8, 1985, NEACRP-A-706.

(6) Kotegawa H., Sasamoto N. and Tanaka S.: "Calculations of Neutron Penetration Through Graphite Medium With Monte Carlo Code MCNP," JAERI-M 86-055 (1986) (in Japanese).

(7) Ise T., Maruo T. et al.: "Shielding Design of the Upgraded JRR-3 Research Reactor," JAERI-M 85-065 (1985) (in Japanese).

(8) idem: "Shielding Design of the Upgraded JRR-3 Research Reactor• 2 --- Shielding of Neutron Beam Holes ---," JAERI-M 85-105 (1985) (in Japanese).

(9) idem: Shielding Analyses for Design of the Upgraded JRR-3 Research Reactor•3 --- Physics and Shielding of Neutron Guides ---," JAERI-M 86-028 (1986) (in Japanese).

(10) Takeuchi K. and Tanaka S.: "Point Isotropic Buildup Factors of Gamma Rays Including Bremsstrahlung and Annihilation Radiations for Water, Concrete, Iron and Lead," Nucl. Eng Sci., 90, 158 (1985).

(11) Harima Y. and Tanaka S.: "A Study of Buildup Factors, Angular and Energy Distribution at Small Distances from Three Source Geometries," ibidem, 90, 165 (1985).

(12) Tanaka S. and Takeuchi K.: "Transport Calculations of Energy Spectrum and Buildup Factors for Gamma Rays Including Bremsstrahlung and Fluorescence," 3rd Int. Symp. on Radiation Physics, Ferrara, Italy, Sept. 30 - Oct. 4, 1985.

6. Reactor and Nuclear Instrumentation

(1) Wakayama N.: "Development of high-temperature fission counter chambers," JAERI-M 85-193 (1985) (in Japanese).

(2) Sekiguchi A. and Wakayama N.: "Present Status of In-Core Nuclear Instrumentation System," J. At. Energy Soc. Japan, 27, 325-330 (1985) (in Japanese).

(3) Wakayama N.: "Recent Movement and Some Topics on Nuclear Power Plant Control and Instrumentation in Japan," IAEA, IWG-NPPCI Meeting, Vienna, March, 1986.

(4) Terada H. et al.: "Performance of Fuel Failure Detection for Coated Particle Fuels," IEEE Trans. Nucl. Sci., NS-32(2), 1209-1212 (1986).

(5) Terada H.: "Study on In-situ Measuring Method Using a Portable Ge Gamma-ray Detector," JAERI-M 85-095 (1985) (in Japanese).

(6) Terada H. et al.: "Monitoring Experiment of Gaseous Fission Products in the Primary Coolant Helium of OGL-1," Proc. of IAEA Specialists' Meeting on Fission Product Release and Transport in Gas-Cooled Reactor, Gloucester, Oct. 24, 1985.

(7) Terada H. et al.: "Development of Monitoring System for Gaseous Fission Products in the Primary Helium of HTGR's," IEEE Trans.

Nucl. Sci., NS-33(1), 679-683 (1986).

(8) Ara K., Yamada M., Shimizu K. and Wakayama N.: "Development of High-Reliable Tungsten-Rhenium Alloy Thermocouple for Measuring In-Core Helium-Gas Temperature in Very High Temperature Gas-Cooled Reactor," IEEE Trans. Nucl. Sci., 33(1), 688-693 (1986).

(9) Gotoh H.: "Non-destructive Analysis of Transuranic Elements," Radioisotopes, 34, (8), 57 (1985) (in Japanese).

(10) Kimura T., Kobayashi Y., Akatsu J. and Gotoh H.: "Neutron Yields from Actinide Oxides," Appl. Radiat. Isot. 37, (2), 121-125 (1986).

(11) Sakai E.: "Further measurements of induced radioactivities in silicon and germanium irradiated with high-energy heavy-ions," IEEE Trans. Nucl. Sci., NS-33, 651-654 (1986).

(12) Sakai E.: "Detection of scintillation lights emitted from various scintilators with a silicon photodiode and a comparison with that with a photomultiplier," Hoshasen (A Japanese Quarterly on Ionizing Radiation section of the Applied Physics Society of Japan), 12, No. 3, 22-31 (1986) (in Japanese).

(13) Katagiri M.: "Absolute detection efficiencies of Ge(Li) detector for high gamma-ray energies," JAERI-M 85-190 (1985) (in Japanese).

(14) Katagiri M.: "Development of dead time correction methods for radiation pulse signal measurements," JAERI-M 85-191 (1985) (in Japanese).

7. Reactor Control, Diagnosis and Robotics

(1) Shinohara Y.: "Activities on Computer Application for Nuclear Reactor Operations in Japan," ANS International Topical Meeting on Computer Application to Nuclear Power Plant Operation and Control, Pasco, Washington, USA Sept. 1985.

(2) Yoshida K., Yokobayashi M., Aoyagi T., Shinohara Y. and Kosaka A.: "Development and Verification of an Accident Diagnostic System for Nuclear Power Plant by Using a Simulator," ANS International Topical Meeting on Computer Application to Nuclear Power Plant Operation and Control, Pasco, Washington, USA Sept. 1985.

(3) Kudo K., Tashiro H., Ohta M., Ohsawa T., Nakao Y., Shinohara Y. and Shimazaki J.: "Dynamics and Control System Design of Very High Temperature Gas-cooled Reactor," Memoirs of the Faculty of Engineering, Kyushu University, 46, 105, (1986).

(4) Shinohara Y.: "Present Status of Reactor Noise Analysis," Nuclear Engineering, 31, 45 (1985).

(5) Hayashi K.: "Autoregressive Model Fitting Algorithms Based on Least Squares Method and Its Application to Noise Analysis of Borssele Reactor," 18th International Informal Meeting on Reactor Noise, Budapest, (1985).

(6) Shinohara Y. and Watanabe K.: "Interim Report on the Result of Sodium Boiling Noise Detection Benchmark Test," IAEA CRP Meeting, Vienna, (1985).

(7) Shinohara Y., Usui H., Saito S. and Kumagai A.: "An Experimental Remote Handling System," Advanced Robotics, Vol. 1 (1986).

(8) Shinohara Y.: "R&D of Robotic Technology at JAERI," Environmental Extremes, Proceedings, 93 (1986).

(9) Shinohara Y.: "On Mobile Robots," ELAN, 75, (1986).

(10) Sasaki S.: "A Method of Solving Inverse Kinematics of a Manipulator Arm," JAERI-M 86-018 (1986).

(11) Sasaki S.: "Computer Code ARM1 for Solving the Inverse Kinematics of a Six-Link Manipulator Arm," JAERI-M 86-059 (1986).

8. Activities of the Research Committee on Reactor Physics

(1) Nuclear Code Committee and Committee on Reactor Physics: "Proceedings of the Seminar on Software Development in Nuclear Energy Research," JAERI-M 86-009 (1986) (in Japanese).

Author Index

OBATA+	Masahiro	6.2
OBARA*,	Masami	2.6
ŌBU,	Makoto	3.9, 3.10, 3.11, 3.13
OHNO,	Akio	3.11, 3.14, 3.15, 3.16
OISHI*,	Koji	4.5, 4.6, 4.7, 4.8, 4.9, 4.11
OKAJIMA,	Shigeaki	3.10, 3.11, 3.12
ONO,	Toshihiko	3.1, 3.2, 3.3, 3.4, 3.7
OSUGI,	Toshitaka	3.8, 3.11, 3.14, 3.15
OYAMA,	Yukio	4., 4.1, 4.3, 4.4, 4.10, 4.11, 4.12
		4.13, 4.14
PORGES*,	Kirl G.	4.10
SAJI*,	Etsuro	3.19
SAKAI,	Eiji	6.8, 6.9, 6.10, 6.11, 6.12, 6.13
SAKASAI,	Kaoru	6.1
SAKURAI,	Takeshi	3.11, 3.12, 3.13
SANADA*,	Kazuo	6.5
SAKO,	Kiyoshi	3.21, 3.22
SASAKI*,	Makoto	2.7, 3.17
SASAKI,	Shinobu	7.5, 7.6, 7.7
SASAMOTO,	Nobuo	5.3
SATO*,	Wakaei	3.14
SATOH+,	Fukuji	6.7
SATOH,	Kunio	3.9, 3.11, 3.13, 3.14, 3.16
SAWAN*	Mohamed E.	4.17
SEKINE,	Koji	6.4
SHIMAZAKI,	Junya	7.1, 7.2, 7.7
SHINOHARA,	Yoshikuni	7., 7.1, 7.3, 7.7
SUZUKI+,	Katsuo	7.2
SUZUKI*,	Katsuo	3.19
SUZUKI,	Makoto	6.4
SUZUKI,	Tomoo	5.2, 8
SUZUKI*,	Yasuhito	6.13
TABE,	Yoshinobu	6.6, 6.7
TAJI,	Yukichi	2.9, 2.10
TAKANO,	Hideki	1.2, 1.3, 1.6, 1.7, 3.19
TAKEUCHI,	Motoyoshi	3.1, 3.2, 3.3, 3.4, 3.5, 3.7

TANAKA,	Shigeru	4.16
TANAKA,	Shunichi	5.1, 5.3
TANIGUCHI*,	Kazuyoshi	6.13
TERADA,	Hiromi	6.2
TERANISHI*,	Kazuo	6.14
TOBITA+,	Tsutomu	6.2
TOMIYAMA*,	Yoshimi	6.2
TOMODA*,	Toshimasa	6.1
TSUCHIHASHI,	Keiichiro	2.5
TSUDA,	Koichi	4.2, 4.6, 4.11
TSUJI*,	Nobumasa	3.9, 3.10, 3.15
TSUTSUI,	Tsuneo	2.2, 2.3, 2.4
TURKCAN*,	Edic	7.4
USUI,	Hozumi	7.7
WAKAYAMA,	Naoaki	6., 6.1, 6.2, 6.3, 6.4, 6.6, 6.7
WATANABE,	Koichi	7.3
YAGI,	Hideyuki	6.5
YAMADA*,	Takahisa	4.7
YAMAGISHI,	Hideshi	6.1, 6.4
YAMAGUCHI,	Seiya	4.1, 4.3, 4.4, 4.10, 4.11, 4.14
YAMAMOTO*,	Hiroshi	4.5, 4.7
YAMANE,	Tsuyoshi	3.1, 3.2, 3.3, 3.4, 3.5, 3.6
YAMAUCHI,	Hideshi	6.6, 6.7
YASUDA,	Hideshi	3.1, 3.2, 3.3, 3.4, 3.5
YOKOTA+,	Terufumi	2.10
YOKOUCHI+,	Iichiro	6.2
YOSHIDA,	Hiroshi	6.2
YOSHIDA,	Hiroyuki	3., 3.8
YOSHIFUJI,	Hisashi	3.1, 3.2, 3.3, 3.4, 3.7
YOSHIHARA,	Fumio	3.1, 3.2, 3.3, 3.4, 3.7
YOSHIZAWA+,	Michio	3.5
YOUSSEF*,	Mahmoud Z.	4.17
YULE*,	Thomas J.	4.12

+ Contributors attached to JAERI but not to Department of Reactor Engineering.

* Contributors attached not to JAERI.